CRANFIELD UNIVERSITY

P SODZI

DAMAGE TOLERANT WING-FUSELAGE INTEGRATION STRUCTURAL DESIGN APPLICABLE TO FUTURE BWB TRANSPORT AIRCRAFT

SCHOOL OF ENGINEERING

PhD THESIS

Academic Year: 2008-09

Supervisor: X. Zhang

December 2009

CRANFIELD UNIVERSITY

SCHOOL OF ENGINEERING

PhD THESIS

Academic Year: 2008-09

P SODZI

Damage Tolerant Wing-Fuselage Integration Structural Design Applicable To Future BWB Transport Aircraft

Supervisor: X. Zhang

December 2009

This thesis is submitted in fulfilment of the requirements for the degree of Doctor of Philosophy

Abstract

Wing joint design is one of the most critical areas in aircraft structures. Efficient and damage tolerant wing-fuselage integration structure, applicable to the next generation of transport aircraft, will facilitate the realisation of the benefits offered by new aircraft concepts. The Blended Wing Body (BWB) aircraft concept represents a potential revolution in subsonic transport efficiency for large airplanes. Studies have shown the BWB to be superior to conventional airframes in all key measures. Apart from the aerodynamic advantages, the BWB aircraft also provides a platform for wing-fuselage design changes.

The main objective of this research is to design a damage tolerant wing-fuselage joint with a novel bird's mouth termination for a BWB aircraft that has a similar payload range to the B767 aircraft. The damage tolerance analysis of the proposed BWB wing/fuselage integration structure includes assessments of fatigue crack growth life, residual strength and inspection capability.

The proposed structure includes a bird's mouth termination of the spars that facilitates smooth transfer of loading from the spar web into the root rib and the upper and lower skins and is novel in its application to the blended wing body configuration. A finite element analysis was required to determine local stresses for the prediction of fatigue crack growth life, residual strength and inspection capability and to identify weak spots in the proposed structure. The project aircraft wing comprises of three spars (front, centre and rear) and a false rear spar thus defining a four cell wing box. Wing root shear, bending moment and torque loads were derived and applied to a thin-walled three box idealisation of the proposed structure. The challenges experienced in replicating the loads obtained from the three box idealisation were addressed by modification of the boundary conditions. Checks for compression and shear buckling were also undertaken that confirmed that the applied loads were below the limits of the proposed structure.

The finite element analysis showed very clearly that the stresses in the novel bird's mouth spar termination were significantly lower than in the skin and that the skin remained the more critical damage tolerant component at the wing root when the structure was subjected to ultimate design stresses. The spar web at the bird's mouth termination was shown to have a larger crack growth life compared to the skin. The thickness of the skin requires further investigation as a significant amount of local bending was experienced due to the applied pressure. The skin will sustain a two-bay crack at the design limit load thus proving the proposed wing fuselage integration structure to be damage tolerant.

In conclusion, the main objective of the thesis has been achieved. An integrated wing-fuselage joint with novel bird's mouth spar termination and surrounding structure have been designed and substantiated (evaluated) by damage tolerance requirements.

Acknowledgements

I wish to express my most sincere gratitude to everyone who helped me in my research efforts over the duration of my studies and to acknowledge the initial encouragement received from Mr. Clive Sibley, then General Manager of GKN ENGAGE and now IS/IT Director-Europe, GKN Aerospace, whose support enabled me embark on this flight of discovery.

In particular I wish to thank Dr. Xiang Zhang, my supervisor for her encouragement and constructive suggestions throughout the research. I would also like to thank Professor John Fielding, Dr. Shinjin Guo and Mr. Frank Bamford, VP GKN Aerospace, for their support and encouragement.

I wish to thank my parents, Nathan and Faith Sodzi and Sam and Phyllis Skillen for their support and encouragement.

I will be forever indebted to my family who have experienced the challenge of living with a part-time PhD student, Rosanne my wife and three wonderful children Katrina, Grace and Joel for their patient support and love.

Contents

List of Figures

List of Tables

Nomenclature

a	Half crack length
A	Cross-sectional area
A_R	Aspect ratio
A_{wt}	Total wetted area
b	Wing span
C	Material specific parameter determined by test
C_{Dfric}	Effective friction drag coefficient
C_L	Lift coefficient
C_{Lmax}	Maximum lift coefficient
C_R	Wing root chord
D	Damage per cycle
D	Drag force
d	Fuselage diameter
E	Young's modulus
F	Stress
f	Equivalent parasite area
$F_{s,cr}$	Critical buckling shear stress
G	Critical energy release rate
h	Laminate thickness
I	Moment of area
K	Stress intensity factor
K	Induced drag factor
K_i, K_{ij}	Strength tensors that require off-axis tensile tests to evaluate
K_s	Shear buckling factor
L	Lift force
L	Transverse direction
l_{r_tip}	Distance from wing root to tip
m	Material specific parameter determined by test
N	number of cycles to failure of component
n	number of applications
P	Critical value of contact force below which the damage area is small
q	dynamic pressure
q_s	Shear flow
R	Ration of minimum to maximum stress
S	Wing area
S	Shear force
T	Longitudinal direction
T	Thickness
V_C	design cruise speed (knots equivalent airspeed)

V_D	Dive velocity
V_e	Equivalent airspeed in knots
V_s	Stall speed or minimum flying speed KEAS
W	Aircraft weight
W	Fuselage width
Y	Yield stress or strain
β	Normalised stress intensity factor
γ	Shear strain
σ	Nominal applied stress
υ	Poisson's ratio
Є	Direct strain
FCG	Fatigue crack growth
LT	Long transverse direction
SMT	Shear, Bending Moment, Torque
SU	Ultimate shear strain or stress
UC	Ultimate compression strain or stress
UT	Ultimate tension strain or stress

1 Introduction

1.1 Wing-fuselage integration structure for BWB aircraft

The Blended Wing Body airplane concept represents a potential revolution in subsonic transport efficiency for large airplanes. Studies have shown the BWB to be superior to the conventional configuration in all key measures (Liebeck et al., 1998). The BWB airframe manifests a substantial reduction (in the order of 30 percent) in the number of parts when compared to a conventional configuration: a similar reduction in manufacturing costs is implied (Liebeck, 2002).

Next generation aircraft, including concepts such as the A380 and future concepts such as the Sonic Cruiser, Blended Wing Body and Ramjet powered aircraft, originate from a desire to achieve reduced cycle times. The development of an effective and efficient 21st century global transportation system, of which airplanes must continue to be a key element, remains one of our great challenges in the coming decades (McMasters, 2002). This will be characterised by the requirement for aircraft that are "better, cheaper, faster" (i.e. reduced cycle time).

Blended wing body aircraft research projects have identified several structural integrity issues (Smith, 2002) (Mukhopadhyay, 1996) including:

- Wing/fuselage joints;
- Non-circular fuselage structure (with associated problems of pressurisation) including;
    - Vaulted/non-vaulted structure
    - Double skin structure
    - Honeycomb skin structure
- Temperature differentials between inner and outer skins on the fuselage and the resulting stress issues.

All of the above issues require attention if benefits including reductions in parts count, reductions in manufacturing costs, reduced cycle times and other key efficiency savings are to be realised.

1.2 What has been done, the limitations and constraints

This thesis describes a research project undertaken to identify a configuration for wing fuselage integration structure in the Blended Wing body aircraft that is considered representative of next generation transport aircraft.

The research project commenced with a focus on the "Development of a methodology for damage tolerance substantiation of next generation transport aircraft". This was initially proposed to identify advances in fatigue and fracture technology since the launch of FAA Regulations part 25-571 Amendment 45 and FAA advisory circular AC 25-571-1 "Damage Tolerance and Fatigue Evaluation of Structure" September 28, 1978 and subsequent to work done by Mr T Swift then of the FAA in order to provide further

clarification of the requirements of the above regulations. The main thrust of the research was subsequently expanded to cover the damage tolerance substantiation of next generation transport aircraft. Consequently, a survey of advances in applying fatigue and fracture technology in aircraft design and damage tolerance analysis was considered to form a part of the research project.

The blended wing body aircraft was considered to provide the most suitable platform for research into the damage tolerance substantiation of next generation aircraft. This is because, although of an unconventional configuration, adequate conceptual work has been done to enable the focus of this research to concentrate on damage tolerance substantiation. In addition, it was hoped that this research activity would complement other blended wing body activities.

This research project is novel because it is an assessment of the fatigue and damage tolerance characteristics of a new aircraft configuration – blended wing body aircraft with a novel bird's mouth spar termination and the issues specific to the unique combination of a new configuration.

The research project focused on the identification of structural solutions for wing/fuselage joints and the development of a methodology for damage tolerance substantiation of the specific structural solutions to the issues identified above. The key elements of the project were achieved by detail design of novel features, damage tolerance substantiation using Finite Element Analysis and AFGROW and validation of the proposed methodology by reviewing with airworthiness authorities, aircraft manufacturers and aircraft operators. Dialogue took place with Airbus UK and GKN aerospace on the above.

1.3 Objectives

The objective of this research project is to assess the damage tolerance characteristics of the BWB wing/fuselage joint including the novel bird's mouth spar termination; this includes assessments of fatigue crack growth life, residual strength and inspection capability. A finite element assessment was required to identify local stresses for the fatigue crack growth life, residual strength and inspection capability assessments and to identify potential structural weak spots in the proposed wing fuselage integration structure of a novel damage tolerant design with bird's mouth spar termination for wing fuselage integration that is applicable to future BWB aircraft programmes.

This project was originally intended to focus on the development of a methodology for damage tolerance substantiation of next generation transport aircraft and to be a continuation of work undertaken as part of a Cranfield University MSc course in Air Vehicle Design (AVD) (Smith, 2002) where the design study was for a blended wing body aircraft capable of competing with the Boeing 767 aircraft. However, constraints on access to data from the AVD study meant that this project had to be completed

without access to the results of the MSc study. The Boeing 767 aircraft was maintained as the baseline aircraft for comparison in this project.

This necessitated a change in the direction of the research activity as new structural concepts had to be defined and then assessed. There was, therefore, a change in focus from the development of a "methodology" to the development of a proposal for a structural configuration for "Damage tolerant wing-fuselage integration structural design applicable to future BWB transport aircraft".

1.4 A brief overview of the thesis chapters

The approach adopted was firstly to undertake a review of the existing literature to gain an appreciation of the state of the art. Once the initial review had been completed, a proposal for wing fuselage integration structure including the novel bird's mouth spar termination was made and then assessed using FE and crack growth analysis. A significant amount of iteration was undertaken to obtain the final proposal.

Chapter 2 - Literature review

The review covers damage tolerance and its application, the requirements laid out by the airworthiness authorities that must be complied with and looks at real life application of damage tolerance concepts with a view to meeting the requirements specified by the airworthiness authorities. The use of non-metallic structural material in contrast to metallic material is also explored. Other issues assessed include the two bay crack criterion that provides a basis for demonstrating compliance with airworthiness requirements and is applicable to structure manufactured from metallic and/or non-metallic materials. Existing approaches to aircraft wing root design is explored alongside a review of other work currently ongoing on the BWB concept.

Chapter 3 - Wing root joint: design philosophies and design requirements

Wing joint design is one of the most critical areas in aircraft structures, especially for fatigue consideration of long life structure, the best fatigue design being one with no joints or splices. The different types of joints and the requirements of regulatory bodies are described and discussed.

Chapter 4 - Novel design solution for root joint

Defining the pressurized passenger cabin for a very large airplane offers two challenges. First, the square-cube law shows that the cabin surface area per passenger available for emergency egress decreases with increasing passenger count. Second, cabin pressure loads are most efficiently taken in hoop tension. Furthermore, Wing joint design is one of the most critical areas in aircraft structures. The absence of joints or splices in aircraft structure is preferable where possible. The nature of existing aircraft configurations however means that it is almost impossible to avoid joints at the intersection of the wing and the fuselage. One advantage that blended wing body aircraft appear to have over

existing aircraft configurations is the scope for eliminating the wing fuselage joint altogether. In blended wing body aircraft, the wingbox depth at the wing root is equal to fuselage height making it possible for the wing skin to continue uninterrupted across the wing/fuselage boundary. A proposed wing root design that takes advantage of the issues identified above and that incorporates a novel bird's mouth concept for spar termination is detailed and discussed.

Chapter 5 - Design calculations and load derivation

The reasoning, activities and processes employed to determine the wing geometry and wing loading data are discussed. The project BWB aircraft was designed with a payload-range similar to the Boeing 767 and the AIRBUS A330-200 aircraft. A global load model created to generate loading data for a local finite element model is also discussed. A finite element analysis of a section of the wing root is presented to confirm the integrity of the proposed design and to generate data for the damage tolerance analysis. The approach adopted to generate the required input data and the results of the finite element analysis and the detailed stress analyses undertaken are discussed. Details of the loading derivation and preliminary sizing are presented in the Appendices together with data from the global loads model.

Chapter 6 - Damage tolerance substantiation

The damage tolerance capability of the proposed wing design is assessed by conducting fatigue crack growth assessments of the spar at the novel bird's mouth termination and in the skin by applying the two bay crack criterion to the skin which is demonstrated to be the critical damage tolerant component at the wing root. The fatigue loading required for crack growth is determined together with the required material data and stress intensity factor solutions. The crack growth life of the novel bird's mouth spar termination is determined for a crack in the web and the life of a two bay crack in the skin is determined for three scenarios. A residual strength assessment is also undertaken for the spar web using net section stress. The damage tolerance capability of the skin is demonstrated by applying the two bay crack criterion.

Chapter 7 - Manufacturing Issues

The essential features of the processes applied in the manufacture of aircraft components and their assembly into transport aircraft are explored with a specific focus on wing fuselage integration. The impact of design on operations management and cost control and the relevance of the proposed wing fuselage integration structure in taking advantage of the developments in aircraft manufacture and assembly are explored. An investigation of the manufacturing and assembly issues with respect to the integration of the novel bird's mouth spar termination are also discussed.

Chapter 8 - Conclusions and recommendations for further work

Wing fuselage integration structure has been reviewed in this research project and a novel bird's mouth concept for spar termination has been proposed. The relevant loading has been derived and a fatigue and damage tolerance assessment has been undertaken that has identified the skins as the critical component at the wing fuselage joint.

The novel bird's mouth spar termination has been assessed and shown to be a non critical component of the wing root. The skin has been assessed and shown to be the critical component at the wing root and capable of sustaining a two bay crack under limit loading hence demonstrating the damage tolerant capability of the proposed wing fuselage integration structure.

The assessment has confirmed that skin deflections that, are outside the scope of this project, remain a critical factor and require further assessment

Finally, conclusions are discussed and recommendations for further work made.

2 Literature Review

2.1 Introduction

Fielding (1999) points out that the most crucial stage of any design process is the definition of a correct set of design requirements and specifications for the aircraft. The design specifications are the result of an iterative process and the distillations of decades of design, manufacturing and operational experience.

A review of available literature on damage tolerance and aircraft design has been undertaken in this chapter. This chapter is structured in two parts.

Firstly, sections 2.2 to 2.6 cover damage tolerance and its application, the requirements laid out by the airworthiness authorities that must be complied with and looks at real life application of damage tolerance concepts with a view to meeting requirements of the airworthiness authorities. The use of non-metallic structural material in contrast to metallic material is also explored in this chapter.

Secondly, sections 2.7 to 2.9 explore other issues including the two bay crack criterion that provides a basis for demonstrating compliance with airworthiness requirements and is applicable to structures manufactured from both metallic and non-metallic materials. Furthermore, existing approaches to aircraft wing root design are explored alongside a review of other work currently ongoing on the BWB concept.

2.2 Damage tolerance and its application

Methodologies for damage tolerance substantiation of transport aircraft have evolved over the last 30 years. Damage tolerance is a philosophy used in the design of aircraft structures. At the core of the damage tolerance philosophy is the requirement that any damage sustained by aircraft structure is identified and addressed prior to the structure becoming unstable. The damage may take several forms. The traditional approach being to assess damage in the form of structural cracks (Swift et al, 1969) (Swift, 1971) (Simpson, 1999) (Collins et al, 1997) (Nesterenko, 1997) (Terada, 1997) (Jonge, 1976) (Nagar, 1994) (Hunt et al, 1999) (Petit et al, 2000) (Goranson, 1997). Large crack capability and adequate residual strength are also core requirements while another is design for inspectability.

2.3 JAR/FAR requirements

In December 1978, after several years of discussions with industry and foreign airworthiness authorities, the FAA issued an amendment to the fatigue and fail-safe requirements for commercial aircraft. In Europe, during the same time period, the Joint Airworthiness Authorities Steering Committee issued a set of Joint Airworthiness Requirements (JAR) for the damage tolerance and fatigue evaluation of aircraft structure (Swift, 1981). These requirements and their subsequent revisions have become some of the governing tenets of the damage tolerance philosophy. The extracts from the

FAA regulations, which are virtually similar to the European JAA regulations, are detailed below (FAR 25.571).

"a) General. An evaluation of the strength, detail design, and fabrication must show that catastrophic failure due to fatigue, corrosion, manufacturing defects, or accidental damage, will be avoided throughout the operational life of the airplane. This evaluation must be conducted in accordance with the provisions of paragraphs (b) and (e) of this section, except as specified in paragraph (c) of this section, for each part of the structure that could contribute to a catastrophic failure (such as wing, empennage, control surfaces and their systems, the fuselage, engine mounting, landing gear, and their related primary attachments). For turbojet powered airplanes, those parts that could contribute to a catastrophic failure must also be evaluated under paragraph (d) of this section. In addition, the following apply:

(1) Each evaluation required by this section must include--

(i) The typical loading spectra, temperatures, and humidities expected in service;

(ii) The identification of principal structural elements and detail design points, the failure of which could cause catastrophic failure of the airplane; and

(iii) An analysis, supported by test evidence, of the principal structural elements and detail design points identified in paragraph (a)(1)(ii) of this section."(FAR 25.571)(JAR 25.571)

2.4 Fatigue design philosophies

Fatigue in aircraft components and the mechanisms by which they occur are an integral part of aircraft design philosophies such as safe-life, fail-safe or damage tolerance. The safe-life philosophy assumes that an operating period can be determined for a component whereby the likelihood of failure of the component in service and due to operating conditions is negligible. The fail-safe and damage tolerance philosophies however assume that the possibility of failure is not negligible but that the failure occurs in such a manner that it is detected before the failure becomes catastrophic (Swift, 1985)(Boyd-Lee et al, 2001).

In Carl Osgood's text on fatigue design, it is implied that the terms "fail-safe" and "damage tolerant" are interchangeable. He states further "… fail-safe type of design may be interpreted best in terms of (1) a residual strength after cracking, and (2) redundant load paths." (Osgood, 1982).

The usage of the above terms in sectors of the aerospace industry differs slightly with the fail-safe and damage tolerance philosophies used in different contexts. For the purpose of this report, the fail-safe philosophy is interpreted in terms of the residual strength after complete failure of a primary component whilst damage tolerance is

interpreted in the context of residual strength after cracking. For both approaches, the concept of redundant load paths is assumed to remain valid.

Fatigue forms an essential part of the above philosophies as the point at which failure is assumed to occur is determined analytically by fatigue analysis.

For all the above philosophies, estimation of the fatigue life of a component makes it possible to establish a safe life. For the safe-life component, current practice is to withdraw the component from active service. An example of a safe-life component is undercarriage structure as defined in FAR/JAR part 25.561. For damage tolerant or fail-safe components, the safe life is identified as the period for which no inspection is required. The safe life then identifies the inspection threshold at which inspections commence.

The fail-safe philosophy as used in the context of this report requires that the fatigue life of a secondary component after failure of a primary component, be estimated. The fatigue life of the secondary component is determined in a similar manner to that described above although it is assumed that on failure of the primary component, the secondary component is subjected to a more severe loading spectrum than in its usual operating condition. The secondary component is also assessed for static residual strength after failure of the primary component. This is explored further in the sections below.

2.5 Life prediction methods (metallic structure)

2.5.1 Safe-Life approach

The Palmgren-Miner damage summation rule is one of the means by which the fatigue life of a component can be established (Fatemi, 1998) (Spottswood, 2002) (Kwofie, 2001). The summation rule is based on the assumption that the damage per application of a cycle of a given stress amplitude can be determined for a given mean stress value such that damage per cycle

$$D = \frac{1}{N} \tag{2.1}$$

Where N = number of cycles to failure of component.

The number of cycles to failure is determined by interrogating S-N curves which present the response of the component or material being assessed in number of cycles to failure for a given stress amplitude and mean stress. An example of an S-N curve is presented in Figure 2.1.

The calculated damage then, for n applications of the above cycle

$$n \times D = \frac{n}{N} \tag{2.2}$$

In the case of a component subjected to several repetitions of stress cycles of varying amplitude, Miner's cumulative damage rule states that failure occurs when the linear summation of partial damage reaches unity, as shown below (Miner, 1945);

$$\frac{n_1}{N_1} + \frac{n_2}{N_2} + \frac{n_3}{N_3} + \frac{n_4}{N_4} + ... + \frac{n_i}{N_i} = 1 \tag{2.3}$$

$$\text{i.e.} \quad \sum \frac{n}{N} = 1 \tag{2.4}$$

With Miner's rule, it is possible to estimate the fatigue life of a component N_{Life} as:

$$N_{Life} = \frac{1}{\sum_{n=1}^{i} \frac{n_i}{N_i}} \tag{2.5}$$

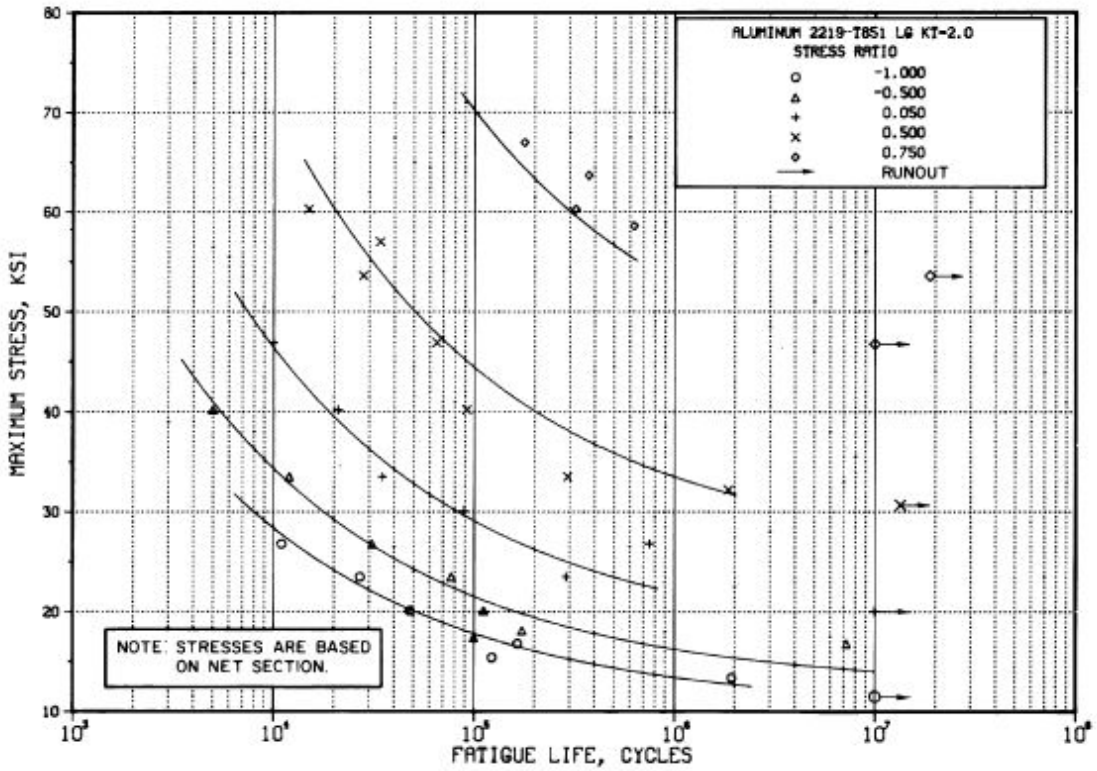

Figure 2.1 Example of SN Curve (MIL-HDBK-5H, 1998)

2.5.2 Fatigue crack growth prediction

The damage tolerance philosophy, which is of most interest in this research activity requires that the crack growth life of the structure be assessed. This then enables an inspection regime to be established such that crack growth can be monitored and assessed so that the component can be withdrawn from service/repaired before the occurrence of catastrophic failure. The process by which crack growth is assessed is described in greater detail below.

"The damage tolerance of a structure is based on the progress of degradation/damage accumulation until a finite crack occurs, and the crack propagates until the failure process culminates in a complete failure of the structure" (Niu, 1990). A typical crack growth analysis process is shown in Figure 2.2.

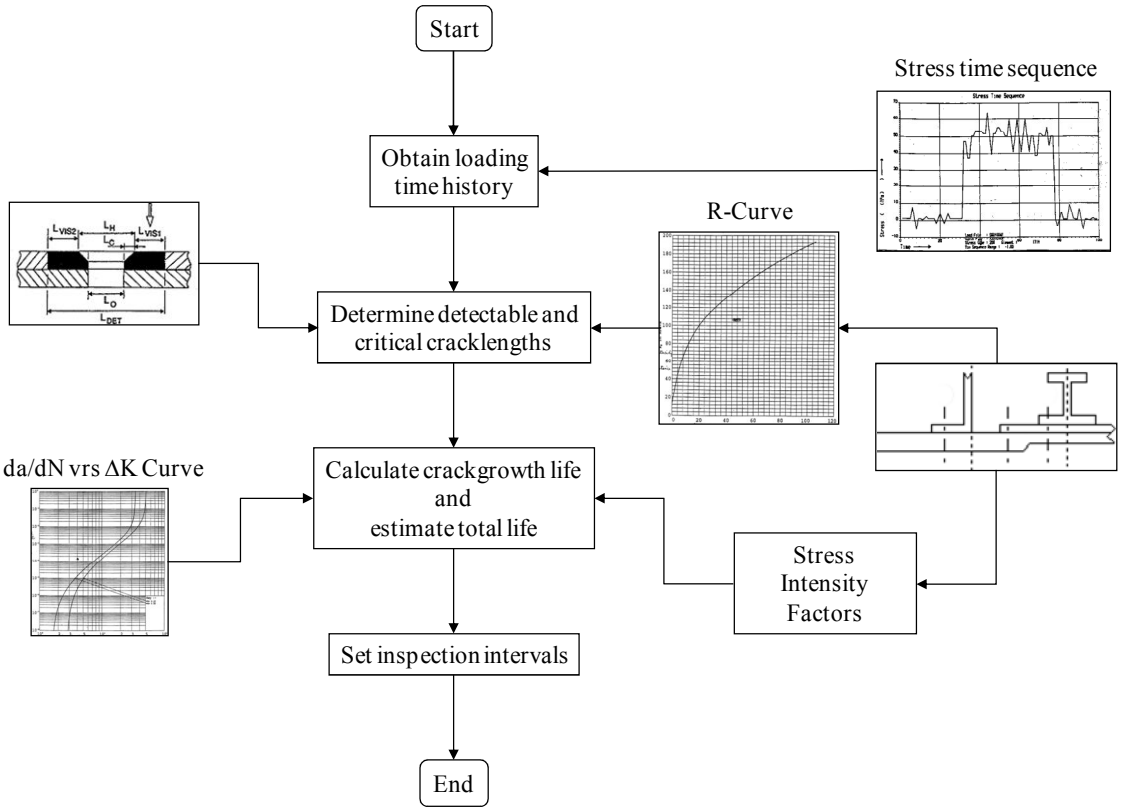

Figure 2.2 Example of crack growth analysis process

For any structure or component with a crack, "the stresses at the crack tip can be described in terms of the stress intensity factor K (Broek, 1991) where,

$$K = \beta\sigma\sqrt{\pi a} \tag{2.6}$$

Where σ is the nominal applied stress, a is the half crack length and β is the normalised stress intensity. When the component is subjected to cyclic loading, it can be assumed that at any given crack length a, a variation in K, (ΔK), occurs with change in stress levels ($\Delta\sigma$) and increases in crack length (a). Crack growth takes place in most instances

as a result of cyclic loading, stress corrosion due to sustained loading or some combination of the two processes. There are other causes, however the two mentioned tend to be the main sources of crack growth (Broek, 1991) (Pidaparti et al, 2002) (Hoffman, 2001) (Wanhill, 2001).

Fatigue crack growth rate $\frac{da}{dN}$ can be described in the form of the Paris law (Paris, 1963);

$$\frac{da}{dN} = C(\Delta K)^m \tag{2.7}$$

Or Forman's law (Forman, 1967),

$$\frac{da}{dN} = f(\Delta K, R) \tag{2.8}$$

C and m are material parameters that are determined by test (Döker, 1997). With the above data it is possible to determine the crack growth life for a component. For complicated time histories, the order in which the load applications occur have a significant impact on the crack growth rate and crack retardation and acceleration effects then need to be taken into account.

The critical crack length and load at which fast or catastrophic fracture of the component occurs, also need to be identified. This again is governed by the stress intensity at the crack tip and the fracture toughness of the material K_{1C}.

The data created by the above analyses enable aircraft designers to set the design lives of safe-life components and together with fail-safe and damage tolerant components, to confirm that the structure has been designed to meet requirements. The key issue for damage tolerant components is the inspection regime required, to ensure that any damage sustained by the component is identified before it becomes critical. By identifying the inspection threshold and a subsequent critical crack length, it is then possible to set intervals that enable inspections to be carried out at the appropriate time.

2.6 Fatigue and Damage Tolerance of composite aircraft structures

The US Federal Aviation Administration initiated a comprehensive study concerned with all aspects of civil aircraft safety in response to the Aviation Safety Research Act of 1998. The major objective of the study by the Committee on New Materials for Advanced Civil Aircraft was to identify issues relating to new materials and the effect that advanced materials would have on the durability and technical risk of future civil aircraft throughout their service life.

The committee chaired by Green (1996) predicted that polymer-matrix composites (e.g., tailored forms; woven and sewn three-dimensional configurations; automated tape and tow placement) and advanced metallic alloys (e.g., tough aluminium; high yield strength aluminium; aluminium-lithium; high strength titanium; and high strength steel) would see increased use in next generation commercial transport aircraft.

Furthermore Paul et al. (2002) amongst many others argued that advanced composites have been in use in military applications for over 30 years and will see increasing application in civil aircraft.

Jones (1999) defines composite materials as a combination of two or more materials on a macroscopic scale to form a useful third material where the individual constituent materials are identifiable to the naked eye. Niu (1992) describes composites as a matrix material reinforced with continuous filaments. The combination or matrix of different materials makes it possible to take advantage of the individual strengths of the constituent materials thus providing novel solutions to complex engineering problems. Four accepted types of composite materials exist including;

1. Fibrous composite materials that consist of fibres in a matrix
2. Laminated composite materials that consist of layers of various materials
3. Particulate composite materials that are composed of particles in a matrix
4. Combinations of some or all of the first three types.

Laminated composite materials currently find the most application within the aircraft industry and the term composites is therefore used to mean laminated materials.

The mechanical behaviour of laminated composites differs significantly from that of most known materials which are homogenous and isotropic in nature. Most metallic materials for example are isotropic as they have uniform mechanical properties in all directions. The measured properties of an isotropic material are independent of the axis of testing.

Laminated composite materials on the other hand tend to be inhomogeneous and non isotropic, their properties being described as anisotropic, orthotropic or quasi-isotropic at best. The mechanical properties of anisotropic materials vary with direction relative to natural reference axes inherent within the material whilst orthotropic materials have three mutually perpendicular planes of elastic symmetry, a basic unidirectional lamina being an example. It is possible to engineer laminated composite materials with quasi-isotropic properties by design of the lay-up sequence of the composite.

The differences in property between metallic materials on the one hand and composites on the other hand means that the failure mechanisms in composites differ significantly from metallic materials thus requiring a different approach to fatigue and damage tolerance in composites.

A thorough understanding of the failure modes of laminated composite materials is required if a fatigue and damage tolerance approach is to be adopted. Niu (1992) identifies the failure modes in laminate composite panels as follows;

- Longitudinal tension;
- Longitudinal compression;
- Transverse tension;
- Transverse compression;
- In-plane shear;
- Delaminate and sub laminate buckling;
- Inter laminar shear, and;
- Inter laminar tension.

It is possible to predict failure in composite materials subjected to static loads. Some of the failure criteria currently in use include the following;

1. Maximum stress theory - no interaction is assumed between stresses. Failure occurs when;

$$F_1 = F_L^{UT} \text{ or } F_L^{UC} \tag{2.9}$$

$$F_2 = F_T^{UT} \text{ or } F_T^{UC} \tag{2.10}$$

$$F_{12} = F_{LT}^{SU} \tag{2.11}$$

Where;

UT = Ultimate tension strain or stress
UC = Ultimate compression strain or stress
SU = Ultimate shear strain or stress
Y = Yield stress or strain
L = Longitudinal direction
T = Transverse direction
LT = long transverse direction

2. Maximum strain theory - no interaction is assumed between strains. Failure occurs when;

$$\epsilon_1 = \epsilon_L^{UT} \text{ or } \epsilon_L^{UC} \tag{2.12}$$

$$\epsilon_2 = \epsilon_T^{UT} \text{ or } \epsilon_T^{UC} \tag{2.13}$$

$$\gamma_{12} = \gamma_{LT}^{SU} \tag{2.14}$$

The sub and superscripts have the same meaning as above.

3. Hill's (Azzi-Tsai) maximum distortional energy theory - based on metallic yielding theory and assumes that interaction between stresses may occur. Yielding occurs whenever;

$$\frac{\left(F_1^2 - F_1 F_2\right)}{\left(F_L^Y\right)^2} + \frac{F_2^2}{\left(F_T^Y\right)^2} + \frac{F_{12}^2}{\left(F_{LT}^{SU}\right)^2} = 1 \tag{2.15}$$

Where:

$$F_1 = F_L{}^{UT} \text{ or } F_L{}^{UC} \tag{2.16}$$

$$F_2 = F_T{}^{UT} \text{ or } F_T{}^{UC} \tag{2.17}$$

$$F_{12} = F_{LT}{}^{SU} \tag{2.18}$$

The sub and superscripts have the same meaning as above.

4. Tsai-Wu strength tensor theory – tensorial so that it is subject to transformation with interaction between stresses. Failure occurs whenever;

$$K_i F_i + K_{ij} F_{ij} = 1 \qquad (i,j = 1,2,6) \tag{2.19}$$

Where Ki, Kij are strength tensors that require off-axis tensile tests to evaluate.

5. Hashin's failure criterion – tensile matrix failure occurs when maximum stress exceeds the tensile strength in a transverse direction such that;

$$\frac{1}{Y_t^2}\left(\sigma_{yy} + \sigma_{zz}\right)^2 + \frac{1}{S^2}\left(\sigma_{yz}^2 - \sigma_{yy}\sigma_{zz}\right) + \frac{1}{S^2}\left(\sigma_{xy}^2 + \sigma_{xz}^2\right) = e_m^2 \tag{2.20}$$

Where;

Y_t = Transverse normal strength in tension
S = Transverse shear strength
z = axis normal to laminate
z – and y – axes are local coordinates parallel and normal to the fibre direction in the layer under consideration.

Whilst the above criteria enable designers to predict the onset of failure in composite material due to static load conditions, a step change in approach is required if the fatigue and damage tolerance of laminate composite materials is to be assessed. The failure modes identified earlier are macroscopic outcomes that are the result of microscopic events due to fatigue and other damage. These are explored further below.

Jones (1999) argues that composite materials undergo a variety of different damage modes during fatigue. Initially, matrix cracking and fibre breaking occurs followed by

coupling of cracks with interfacial de-bonding in addition to fibre breaking. Delamination growth is followed by gross fracture of the entire material with localised fibre breaking occurring throughout the process. This is confirmed by fatigue life assessments of laminate composite materials undertaken by researchers including Schutz and Gerharz (1977) and Roudet et al. (2002).

Despite the extensive amount of test data available, there is still a significant amount of work required in defining models and methodologies for the analytical prediction of fatigue in laminate composites. Himmel (2002) and Schön and Blom (2002) attempt to predict fatigue failure in laminate composites with varying degrees of success. Their work confirms the need for significantly more investigation in order to improve the accuracy of fatigue failure prediction in composites.

Damage tolerance is the ability of a structure to tolerate a reasonable level of damage or defects that might be encountered during manufacturing or while in service which do not result in catastrophic failure. The design of damage tolerant laminate composite structure requires the consideration of impact damage as part of the static ultimate allowables. The failure mechanisms of laminate composite materials are such that it is necessary to consider the effects of large impacts.

Laminated composite structures are more susceptible to impact damage than a similar metallic structure. Experimental work by Ong et all. (1991) and Lauder et all. (1993) confirm that in composite structures, impacts create internal damage that often cannot be detected by visual inspection. This internal damage can cause severe reductions in strength and can grow under load.

For low velocity impacts, damage starts with creation of a matrix crack. In some cases the target is flexible and the crack is created by tensile flexural stresses in the bottom ply of the laminate. This crack which is usually perpendicular to the plane of the laminate is called a tensile crack. Shear cracks also occur and are inclined relative to the normal to the mid plane.

Approaches currently used for damage prediction in laminar composites include;

Estimation of overall size of damaged area based on the stress distribution around the impact point. This method tends to be used for thick laminates and;

Determination of damage initiation using 3D stress analysis of the impact zone and appropriate failure criteria. Subsequent delamination due to in-service loads is then assessed.

When thick laminates are subjected to low-velocity impacts, bending deformations can be neglected and the laminates can be considered as semi-infinite bodies. In order to predict failure, principal stresses and the maximum shear stress can be determined at

each point and the maximum compressive and shear stress distributions then predicted. Maximum shear and compressive stress criteria are also used to determine damage size.

Dobyns (1980) and Dobyns and Porter (1981) proposed a means of predicting overall damage size in thin laminate composites based on the premise that delaminations grow because of high transverse shear stresses in the vicinity of the impactor. Delaminations are assumed to occur when the transverse shear force Qn is such that the average transverse normal stress Qn/h exceeds a specific material property value. This approach makes it possible to predict the damaged zone.

Other proposals deal with the prediction of a threshold contact force that corresponds to damage initiation where if P_c is defined as the critical value of contact force below which the damage area is small and corresponds to the onset of delaminations then delamination occurs when the energy release rate reaches a critical energy release rate for mode II fracture expressed as (Jones, 1999);

$$G_{II} = \frac{9P^2\left(1-\nu^2\right)}{8\pi^2 Eh^3} \tag{2.21}$$

Where E = in plane modulus, υ = in plane poisson's ratio and h = laminate thickness. As P increases, a critical value of G_{IIc} is reached at which the delamination size is indeterminate. When the critical force is reached, delamination increases very rapidly. That critical force threshold is defined as;

$$P_c^2 = \frac{8\pi^2 Eh^3}{9\left(1-\nu^2\right)} G_{IIc} \tag{2.22}$$

Although it is possible to predict fatigue in laminate composites, results have been largely unconservative as demonstrated by Diao et al. (1997) and there is still much work to be done. Gädke (1995) takes the view that the complex interaction between the various strength parameters means that the forecast of damage after impact under tension-compression fatigue loading is difficult to predict. Work done to date also shows that it is possible to estimate the critical force in laminate composites prior to the onset of delamination. Analysis of damage tolerance requires definition of start and finish criteria if a realistic and appropriate assessment is to be made. Damage criteria currently used in laminate composites include the following:

- Scratches – surface scratch 4.0in in length and 0.02in deep
- Delamination – interply delamination of approximately 2.0 in diameter circle (may be more or less depending on location)
- Impact damage – 1.0 in diameter hemispherical impactor with 100 ft-lbs of kinetic energy or with that kinetic energy required to cause a dent

2.7 Next generation aircraft concepts

The development of an effective and efficient 21st century global transportation system of which airplanes must continue to be a key element, remains one of our great challenges in the coming decades (McMasters and Cummings, 2002). This will be characterised by the requirement for aircraft that are "better, cheaper, faster" (i.e. reduced cycle time).

The review of available literature suggests that the term 'next generation aircraft', includes existing 21st century aircraft concepts such as the Sonic Cruiser (Hepperle, 2002), Blended Wing Body and Ramjet powered aircraft. All of these concepts originate from a desire to achieve reduced cycle times. The above definition presents a wide range of aircraft concepts which are all being assessed.

The Blended Wing Body airplane concept represents a potential revolution in subsonic transport efficiency for large airplanes. NASA has sponsored an advanced concept study to demonstrate feasibility and begin development of this new class of airplane. In the NASA study, an 800 passenger capacity BWB and conventional configuration airplanes were compared. The BWB was found to be superior to the conventional configuration in all key measures (Liebeck et al., 1998).

Blended wing body aircraft research projects have identified several structural integrity issues (Smith, 2002) (Mukhopadhyay, 1996) (Liebeck, 2002) (Mukhopadhyay, 2005) including:

- Wing/fuselage joints
- Non-circular fuselage structure (with associated problems of pressurisation) including;
    - Vaulted/non-vaulted structure
    - Double skin structure
    - Honeycomb skin structure
- Temperature differentials between inner and outer skins on the fuselage and the resulting stress issues

All of the above issues were identified as suitable starting points for the work to be done. Other studies include a distributed propulsion concept, applied to BWB aircraft which showed a 5.4% take-off gross weight advantage over a conventional propulsion BWB aircraft (Ko et al, 2003).

The review of reports of BWB research showed a primary focus on wing and fuselage design issues. The issue of wing to fuselage integration does not appear to have received much attention as yet.

2.8 Two-bay crack criterion

Swift (1994) states that, prior to the development of the FAA/JAA requirements for damage tolerance, a two-bay crack criterion had evolved as a means by which aircraft designers could satisfy themselves that, in the event of a crack initiating on aircraft structure, the risk of fast fracture occurring before a predetermined critical crack length was achieved was avoided. Swift (1990) also suggests that the experiences of aircraft designers in the late 1960s confirmed that the pressure cabins of aircraft needed to be designed to sustain a two-bay skin crack with a broken central crack stopper at limit load. A broken central crack stopper was considered, as flat panel cyclic testing had indicated that in the event of a skin crack over a crack stopper a considerable amount of hoop loading was transferred to the crack stopper, creating a high cyclic load and eventual fatigue failure even for small crack sizes. Assessments came to be made for longitudinal and circumferential fuselage skin cracks with broken central stiffeners and chord wise wing skin cracks.

For conventional aircraft structure, the two-bay crack criterion has been applied to the design of fuselage and wing structure since it was first conceived in the late 1960s. Its application has found more use in fuselage design as a stated criterion. Its use in the design of wing structure is also ongoing but not as a named criterion for wing structure design. However, large damage sizes are chosen to allow the opportunity to establish an external visual inspection at reasonable intervals so that the crack can be detected on a walk around inspection. The choice of large damage sizes means that the criterion is best suited to large stiffened panels.

The key success criteria for the two-bay criterion are described by Swift (1994) as follows;

- Limit stress level about the same or a little lower than residual strength capability for two-bay crack thus keeping structural weight to a minimum.
- Visual inspection based on crack growth from detectable crack to crack arresting stiffeners (maximum spectrum load for normal usage is about 60% of limit load and occurs only once in one tenth of lifetime).
- Resulting inspection burden on operator is not excessive.

2.9 Wing root joints

Wing joint design is one of the most critical areas in aircraft structures, especially for fatigue consideration of long life structure, the best fatigue design being one with no joints or splices. Niu (1988) indicates that this is accomplished on modern transport aircraft, which have no joints across the load path except at the side of the fuselage. The wing to fuselage joints currently in use are of three main types, namely spliced plates, tension bolts, shear lugs and a combination of spliced plates and tension bolts. Spliced plates are widely used because they are light weight, more reliable and have inherent fail-safe features. However, they tend to have a higher cost and present more difficulties

in manufacture. Tension bolted joints and shear lug joints are easier to manufacture and assemble but with weight penalties. A combination of spliced plates and tension bolts has the advantages of both methods but also the weight penalty associated with tension bolts.

Matthews (1990) takes the view that mechanically fastened joints have the advantage that they require no special surface preparation, disassembly is easily achieved without damage and there are no special inspection problems. However, the associated holes cause stress concentrations and the joints can incur a large weight penalty. Adhesively bonded joints however have lower stress concentrations and incur smaller weight penalties but disassembly is impossible without causing damage. These joints are also susceptible to environmental effects, require surface preparation and their integrity cannot be confirmed by normal inspection methods.

In-service experience of metallic aircraft structure has revealed ageing aircraft issues including widespread fatigue damage and multiple site damage that have received a significant amount of attention. Swift (1999), Bellinger et al. (2001) and Wanhill and Koolloos (2001) discuss means of assessing the above issues in ageing aircraft structure. They argue that multiple site damage fatigue cracks initiate at faying surfaces near or at rivet hole corners. In some instances however, lap splice secondary fatigue cracks initiate from intergranular cracks due to corrosion and stress corrosion.

Finite element based approaches for determining the strength of composite joints have been proposed by Jones et al. (1999), Pandey et al. (1999) and Bagdanovitch and Kizhakkethara (1999) They show that whist the finite element approach does produce results consistent with test data, great care needs to be taken in the definition of the model and in the assumptions on which the modelling is based. This is because issues such as the spew fillet, residual thermal stresses and the inelastic behaviour of the adhesive material to name a few, can have a significant impact on the integrity of bonded joints.

Schön and Nyman (2002) found that the dominating failure mode in the bolted composite joints they assessed was bolt failure. (Wang et al., 1998) also demonstrate that the finite element modelling technique yielded results in line with expectation although they indicate that further work needs to be done to improve the accuracy of prediction.

Nelson et al. (1983) report that test results have shown that an old NACA formula for the stiffness of bolted joints in metal structures needed only a minor modification to account for the different moduli associated with orthotropic composite laminates. The formula, can be used with confidence to predict the elastic part of the load deflection curve. It appears that the precise definition of the non linear portion of the load deflection curve is not critical, provided that the bearing strength cut-off is reasonable. The explanation of this phenomenon seems to be that tension-through-the hole failures

are associated with the elastic part of the load deflection curve at one particular fastener while if the failure mode is in bearing, the deformations at the bolt hole prior to ultimate failure are so large as to be unacceptable for design practice. Usually, all other fasteners in the joint are less critically loaded and their load deflection characteristic is important only in making the correct determination of the load-sharing between the fasteners.

2.10 Summary

The review of available literature has shown that the design of damage tolerant wing root joint structure requires careful consideration of the constituent material, joint configuration and in-service operating environment. Whilst metallic spliced plates/tension bolts/shear lugs configuration have been the convention, the availability of composite materials provide the opportunity for a step change in the design of wing roots towards achieving the ultimate goal of wing/fuselage interaction structure with a minimum number of joints or splices.

Furthermore, the review shows that there is a requirement for effective and efficient 21st century airplanes where the BWB concept could play a significant role. Wing joint design is a critical area requiring particular attention. This report addresses damage tolerance issues associated with the BWB wing to fuselage joint.

3 Wing root joint: design philosophies and design requirements

3.1 Wing root joints

Wing joint design is one of the most critical areas in aircraft structures, especially for fatigue consideration of long life structure, the best fatigue design being one with no joints or splices.

3.2 Description of existing root joint types

Niu (1988) indicates that this is accomplished on modern transport aircraft, which have no joints across the load path except at the side of the fuselage. The wing to fuselage joints currently in use in aircraft structures are of three main types, namely spliced plates or tension bolts illustrated in figures 3.1 and 3.2, shear lugs illustrated in figure 3.3 and a combination of spliced plates and tension bolts. Spliced plates are widely used because they are light weight, more reliable and have inherent fail-safe features. They however tend to have a higher cost and present more difficulties in manufacture. Tension bolted joints and shear lug joints are easier to manufacture and assemble but with weight penalties. A combination of spliced plates and tension bolts has the advantages of both methods but also the weight penalty associated with the tension bolt solution.

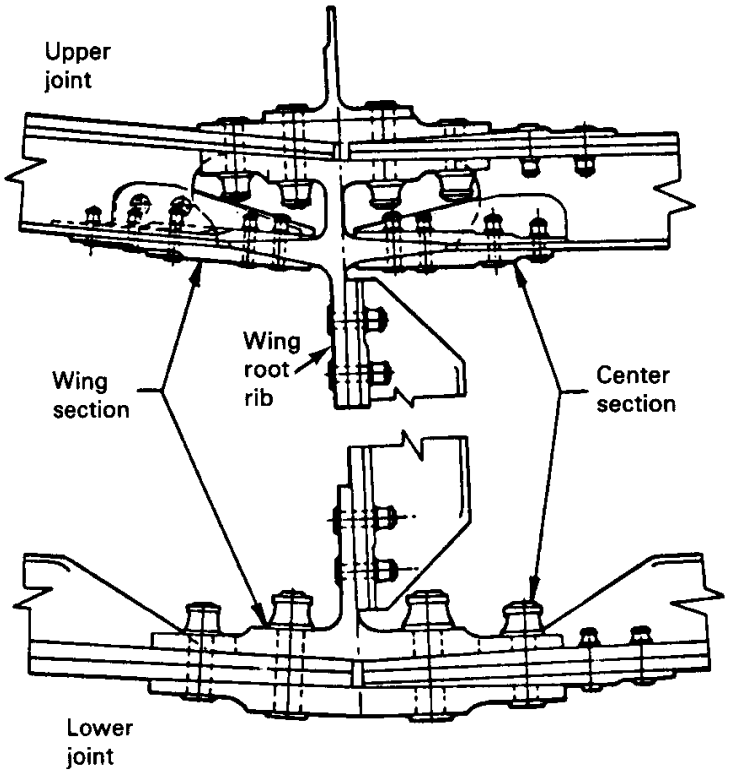

Figure 3.1 Spliced plate wing to fuselage joint (Niu, 1990)

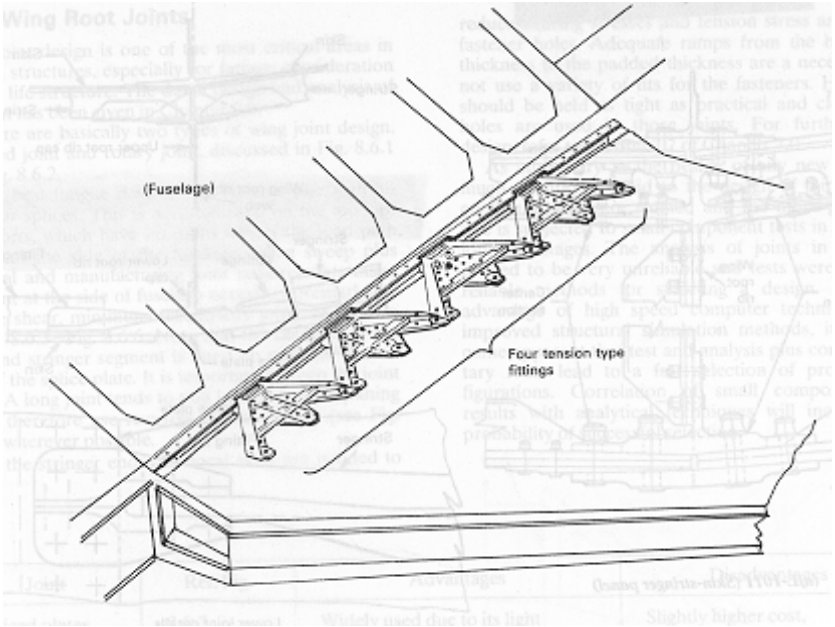

Figure 3.2 Tension bolt wing to fuselage joint (Niu, 1990)

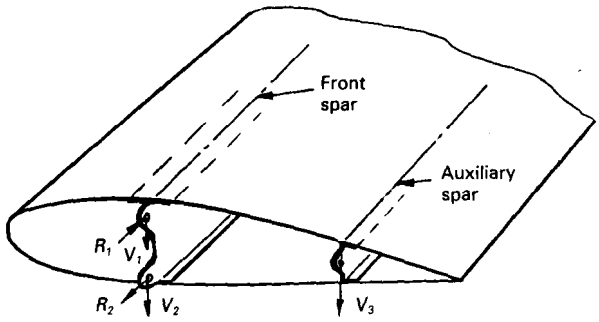

Figure 3.3 Wing lug design (Niu, 1990)

The spliced plate joint is the preferred wing to fuselage joint in transport aircraft. Joints are the most common source of failure for aircraft structure (Niu, 1990). Failures occur due to a variety of factors which all have a significant effect on the fatigue life of the joint and other adjacent structures. Spliced joints generally fail in one of the modes shown in figure 3.4.

A study of the stress variation around holes (in the commonly used aluminium alloys) shows that in the elastic range, the stress at the edge of holes is as much as three times the average stress. This phenomenon is known as stress concentration. Despite careful detail design, the introduction of holes required for assembly of joints result in stress concentrations. The majority of service cracks nucleate in the area of stress concentration at the edge of a hole.

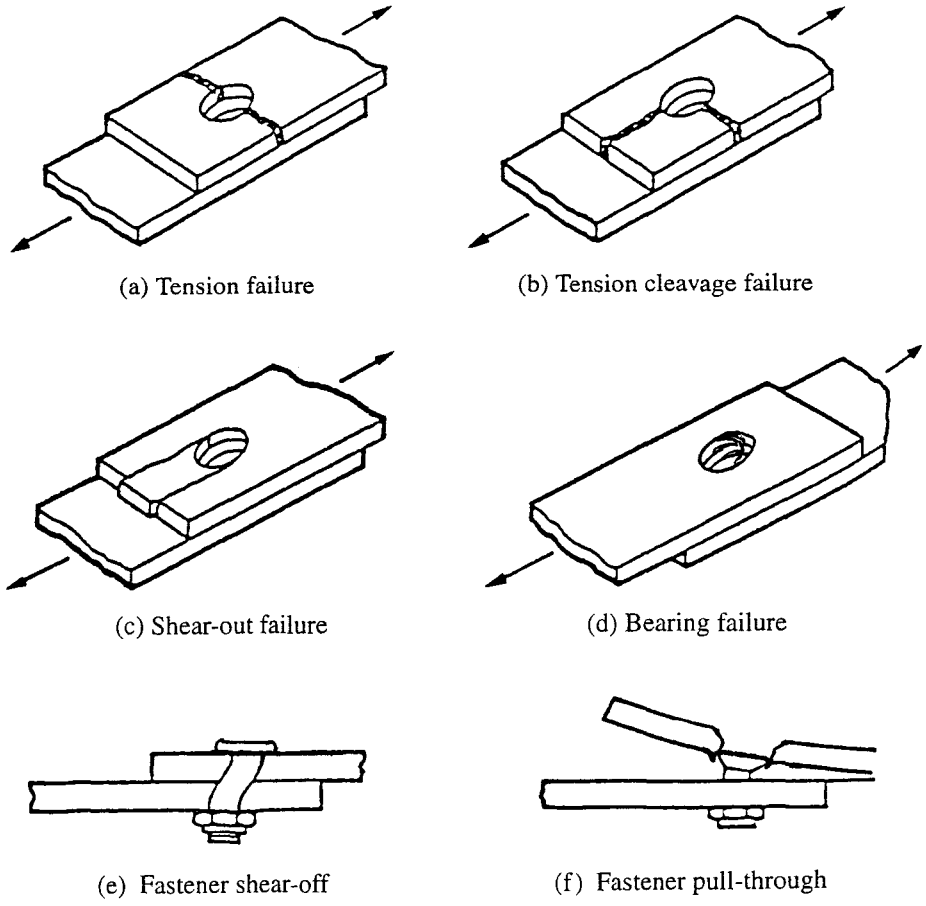

Figure 3.4 Typical failure modes of a splice joint (Niu, 1990)

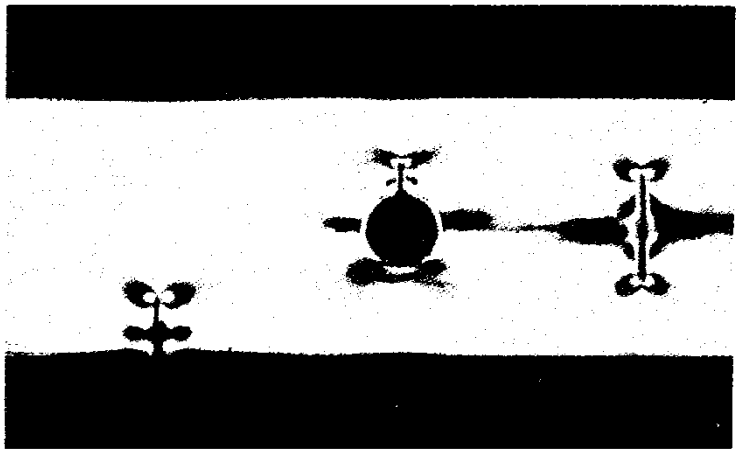

Figure 3.5 Crack emanating from a hole

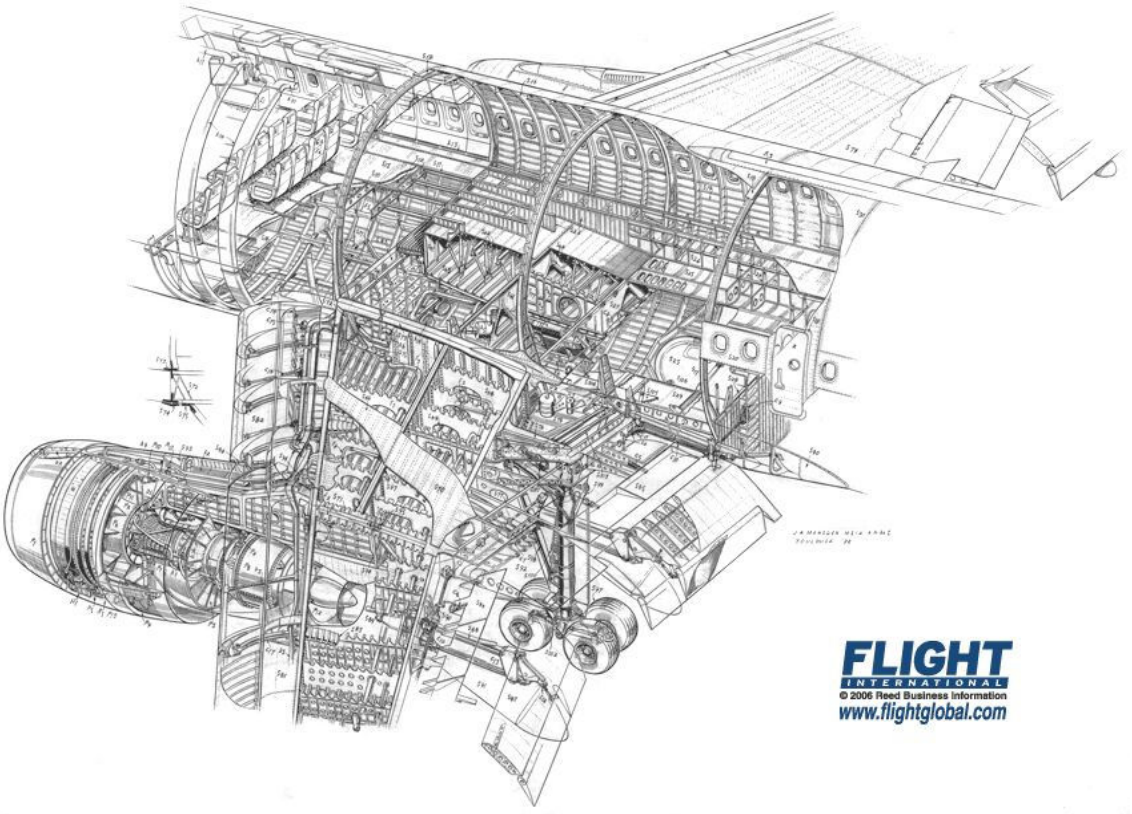

Figure 3.6 Example of aircraft fuselage/wing interface (Flight International 2007)

Figure 3.7 Picture of A380 centre box section (Flight International 2003)

Broek (1991) presents the results of a study illustrated by figure 3.5 that demonstrates that the photo-elastic fringe pattern of a plate with a crack emanating from a hole is similar to that at a central crack of the same total size but also similar to that at an edge crack of half the size. The presence of the hole, therefore, contributes to the total crack size and its associated effect on structure. This emphasises the importance of designing structures with the minimum possible amount of stress concentration features such as holes.

The mid section of the Airbus A300 is shown in figure 3.6 as an example of a typical aircraft fuselage/wing interface and illustrates the complexity of wing to fuselage integration structure. The challenges faced by manufacturers in mating a circular fuselage section to an aerofoil section wing makes the spliced plate joint the most efficient method for achieving the desired outcome. This involves the incorporation of a centre box in the fuselage with geometry similar to that of the wing. The Airbus A380 centre box is presented in figure 3.7 as an example. The joint between the two components i.e. the outer wing and centre box is then achieved by means of spliced plates.

3.3 Advantages and disadvantages of current wing root joint types

3.3.1 Conventional metallic joints

As discussed earlier, spliced plates are widely used because they are light weight, more reliable and have inherent fail-safe features. They also require no special surface preparation, disassembly is easily achieved without damage and there are no special inspection problems.

Conventional metallic joints tend, however, to have a higher cost and present more difficulties in manufacture. The associated holes cause stress concentrations and the joints can incur a large weight penalty. Furthermore, in-service experience of metallic aircraft structures has revealed ageing aircraft issues including widespread fatigue damage and multiple site damage with conventional metallic joints.

An alternative to mechanical fasteners is adhesively bonded joints. These have lower stress concentrations and incur smaller weight penalties although disassembly is impossible without causing damage. Adhesively bonded joints are susceptible to environmental effects and require surface preparation. Their integrity cannot be confirmed by normal inspection methods.

Tension bolted joints and shear lug joints are easier to manufacture and assemble but with weight penalties. A combination of spliced plates and tension bolts has the advantages of both methods but also the weight penalty associated with tension bolts.

3.3.2 Composite-to-composite or composite-to-metal joints

A potential solution to the problems experienced with metallic aircraft joints is the adoption of non-metallic material solutions. However, the findings of various assessments discussed previously show that great care needs to be taken in the definition of structure and in the assumptions on which the definition is based, since issues such as the spew fillet, residual thermal stresses and the inelastic behaviour of the adhesive material to name a few, can have a significant impact on the integrity of bonded joints.

Other research including a study of the spectrum fatigue life of bolted joints using specimens with a double-lap configuration found that the dominating failure mode in the bolted composite joints assessed, when subjected to the vertical fin spectrum of the Swedish fighter JAS39 Gripen, was bolt failure with the first bolt row transferring the largest amount of load in the specimens. The prediction of the fatigue life of composite joints is still the subject of much research and indications, discussed previously are that a significant amount of further work still needs to be done to improve the accuracy of prediction.

The design of damage tolerant wing root joint structure requires careful consideration of the constituent material, joint configuration and in-service operating environment. Whilst metallic spliced plate, tension bolt or shear lug configurations have been the convention, the availability of non-metallic composite materials provide the opportunity for a step change in the design of wing roots towards achieving the ultimate goal of wing/fuselage interaction structure with a minimum number of joints or splices.

3.4 Design requirements

The design requirements for wing joint design are defined by the various airworthiness regulatory bodies. The requirements as specified by the Federal Aviation Administration are described below.

3.4.1 Loads

Strength requirements are specified in FAR 25 in terms of limit loads (the maximum loads to be expected in service) and ultimate loads (limit loads multiplied by prescribed factors of safety). Unless otherwise provided, prescribed loads are limit loads. The specified air, ground, and water loads are required to be placed in equilibrium with inertia forces, considering each item of mass in the aircraft. These loads must be distributed to conservatively approximate or closely represent actual conditions. Methods used to determine load intensities and distribution must be validated by flight load measurement unless the methods used for determining those loading conditions are shown to be reliable. Where deflections under load would significantly change the distribution of external or internal loads, the redistribution must be taken into account.

3.4.2 Factor of safety

Unless otherwise specified, a factor of safety of 1.5 must be applied to the prescribed limit loads which are considered external loads on the structure. When a loading condition is prescribed in terms of ultimate loads, a factor of safety need not be applied unless otherwise specified.

3.4.3 Strength and deformation.

The structure must be able to support limit loads without detrimental permanent deformation. At any load up to limit loads, the deformation may not interfere with safe operation. The structure must be able to support ultimate loads without failure for at least 3 seconds. However, when proof of strength is shown by dynamic tests simulating actual load conditions, the 3-second limit does not apply. Static tests conducted to ultimate load must include the ultimate deflections and ultimate deformation induced by the loading. When analytical methods are used to show compliance with the ultimate load strength requirements, it must be shown that;

1. The effects of deformation are not significant;
2. The deformations involved are fully accounted for in the analysis; or
3. The methods and assumptions used are sufficient to cover the effects of these deformations.

Where structural flexibility is such that any rate of load application likely to occur in the operating conditions might produce transient stresses appreciably higher than those corresponding to static loads, the effects of this rate of application must be considered.
The aircraft must be designed to withstand any vibration and buffeting that might occur in any likely operating condition up to V_D/M_D, including stall and probable inadvertent excursions beyond the boundaries of the buffet onset envelope. This must be shown by analysis, flight tests, or other tests found necessary by the Administrator. Unless shown to be extremely improbable, the aircraft must be designed to withstand any forced structural vibration resulting from any failure, malfunction or adverse condition in the flight control system. These must be considered limit loads and must be investigated at airspeeds up to V_C.

3.4.4 Proof of structure

Compliance with the strength and deformation requirements must be shown for each critical loading condition. Structural analysis may be used only if the structure conforms to that for which experience has shown this method to be reliable. The Administrator may require ultimate load tests in cases where limit load tests may be inadequate. When static or dynamic tests are used to show compliance for flight structures, appropriate material correction factors must be applied to the test results, unless the structure, or part being tested has features such that a number of elements contribute to the total strength of the structure and the failure of one element results in the redistribution of the load through alternate load paths.

3.4.5 Flight Loads

Flight load factors represent the ratio of the aerodynamic force component (acting normal to the assumed longitudinal axis of the aircraft) to the weight of the aircraft. A positive load factor is one in which the aerodynamic force acts upward with respect to the aircraft. Considering compressibility effects at each speed, compliance with the flight load requirements must be shown;

- At each critical altitude within the range of altitudes selected by the applicant;
- At each weight from the design minimum weight to the design maximum weight appropriate to each particular flight load condition; and
- For each required altitude and weight, for any practicable distribution of disposable load within the operating limitations recorded in the Aircraft Flight Manual.

Enough points on and within the boundaries of the design envelope must be investigated to ensure that the maximum load for each part of the aircraft structure is obtained. The significant forces acting on the aircraft must be placed in equilibrium in a rational or conservative manner. The linear inertia forces must be considered in equilibrium with the thrust and all aerodynamic loads, while the angular (pitching) inertia forces must be considered in equilibrium with thrust and all aerodynamic moments, including moments due to loads on components such as tail surfaces and nacelles. Critical thrust values in the range from zero to maximum continuous thrust must be considered.

3.5 Summary

The challenges faced by manufacturers in joining a circular fuselage section to an aerofoil section wing makes the spliced plate joint the most efficient method for achieving the desired outcome. This involves the incorporation of a centre box in the fuselage with geometry similar to that of the wing. The joint between the two components is then achieved by means of spliced plates.

3.6 Novel root joint for this project

The possibility of uninterrupted wing skin across the wing/fuselage joint has been explored in this research project as one of the benefits of the blended wing body aircraft platform.

An initial assessment of possible root joint configurations yielded two possible solutions. Having reviewed the two initial proposals, the preferred solution was with fuselage frames retained as support structure for internal skins whose main function was aesthetic rather than structural. The internal fuselage pressure was to be reacted by the outer skin which is stiffened by stringers and longerons running fore and aft. The function of the root rib was also changed so that the root rib reacts flight loads. The internal fuselage pressure boundary was moved to the next rib outboard of the wing root. The function of the root rib was therefore simplified.

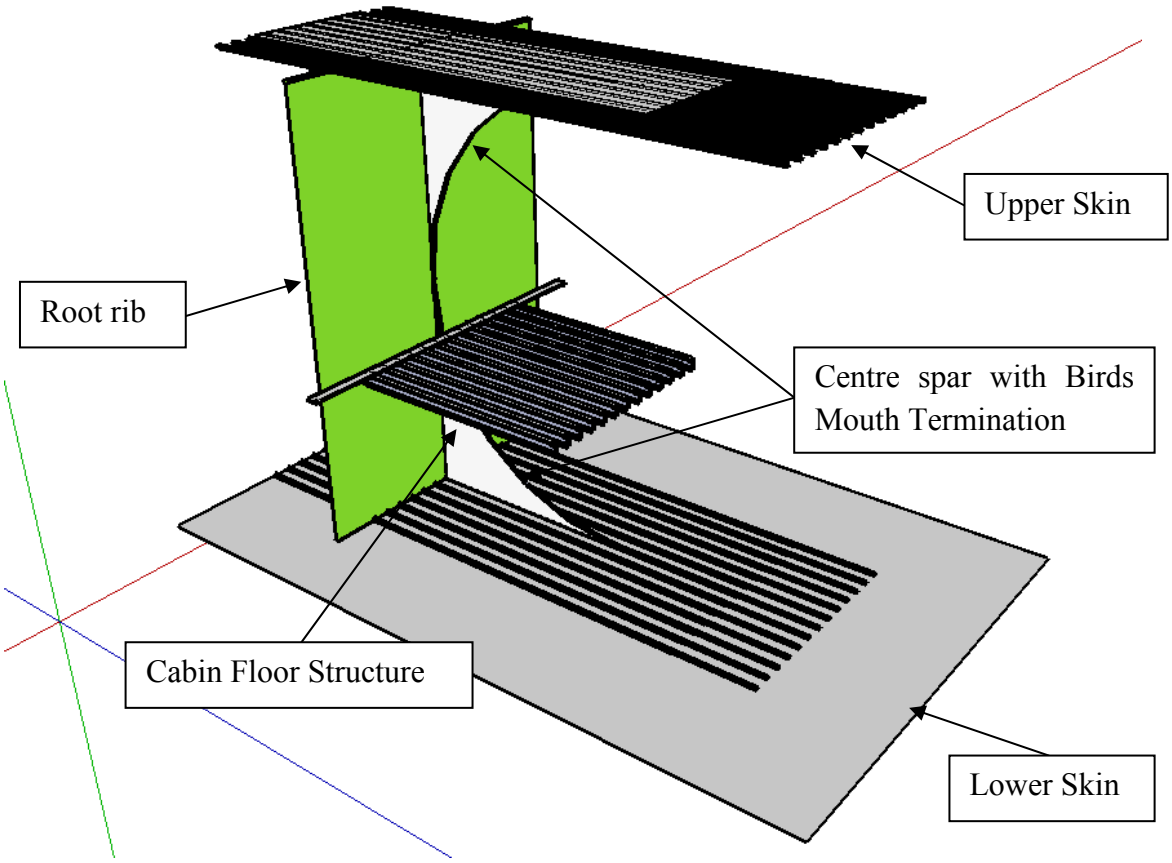

Figure 3.8 Bird's mouth termination of spar within wing

The proposal finally adopted for the project aircraft includes a bird-mouth type runout illustrated in figure 3.8, to ensure a load path into the top and bottom skins of the fuselage thus ensuring that the fuselage volume is largely unobstructed. Stiffening members would still be required to ensure that fuselage crushing loads are adequately reacted.

The airframe skin is continuous across the joint transitioning from wing skin to fuselage skin without a discrete joint. The continuous stringers across the wing root further enhance the integrity of the joint and would result in a relatively smaller number of fasteners and a reduction of parts and other items required to achieve the required joint strength. This proposal is discussed further in chapter 4.

4 Novel design solution for the root joint

4.1 Introduction

The design of the root joint of a large aircraft involves resolution of several complex issues particularly for configurations where there is an interface between a pressurised fuselage cabin and wing structure.

Defining the pressurized passenger cabin for a very large aircraft offers two challenges. First, the square-cube law shows that the cabin surface area per passenger available for emergency egress decreases with increasing passenger count. Second, cabin pressure loads are most efficiently reacted by hoop tension stresses in the skin and frames.

Furthermore, wing joint design is one of the most critical areas in aircraft structures (Niu, 1990). The absence of joints or splices in aircraft structure is preferable where possible. The nature of existing aircraft configurations, however, means that it is almost impossible to avoid joints at the intersection of the wing and the fuselage. One advantage that blended wing body aircraft have over the existing aircraft configurations is the scope for eliminating the wing fuselage joint altogether. In blended wing body aircraft, the wingbox depth at the wing root is equal to fuselage height making it possible for the wing skin to continue uninterrupted across the wing/fuselage boundary. A proposed wing root design that includes a novel bird's mouth type spar termination and that takes advantage of the issues identified in chapter 3 and above is detailed in this chapter.

4.2 BWB structural design activities to date

Previous studies began with an attempt to use the traditional/conventional circular cylinders for the fuselage pressure vessel as shown in figure 4.1. Difficulties experienced in making the concept work, led to abandonment of the requirement for taking pressure loads in hoop tension. The assumption was made that an alternate efficient structural concept could be developed. Removal of this constraint became pivotal for the development of the BWB. Passenger cabin definition became the origin of the design, with the hoop tension structural requirement deleted.

Two structural concepts, sketched in figures 4.2 and 4.3, were considered for the centre body pressure vessel in published NASA studies. Both required that the cabin be composed of longitudinal compartments to provide for wing ribs 150 inches apart to carry the pressure load. The first concept used a thin, arched pressure vessel above and below each cabin, where the pressure vessel skin takes the load in tension and is independent of the wing skin. A thick sandwich structure for both the upper and lower wing surfaces was the basis for the second concept. In this case, both cabin pressure loads and wing bending loads were assumed to be taken by the sandwich structure. A potential safety issue with the separate arched pressure vessel concept was that if a rupture were to occur in the thin arched skin, the cabin pressure would have to be borne by the wing skin, which had therefore in turn to be sized to carry the pressure load.

Thus, once the wing skin was sized by this condition, in principle there was no need for the inner pressure vessel. Consequently, the thick sandwich concept was chosen for the centre body structure.

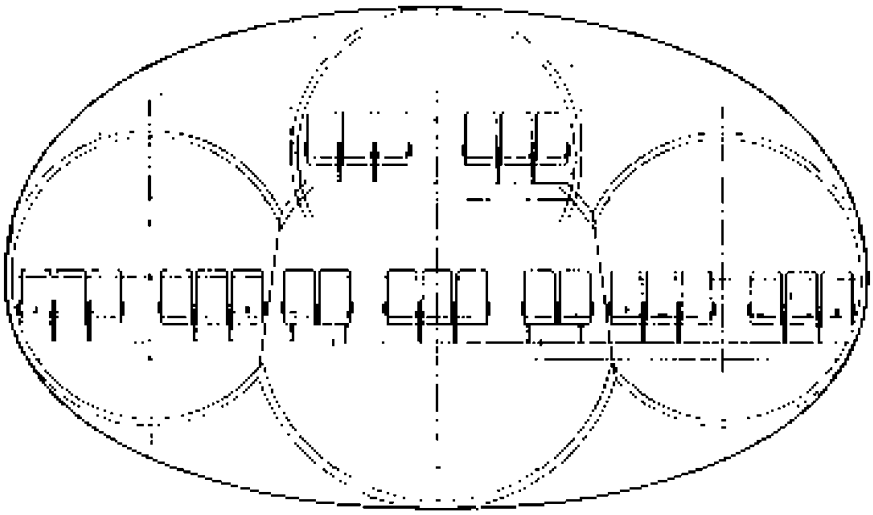

Figure 4.1 Circular cylinder fuselage pressure vessel (Liebeck, 2002)

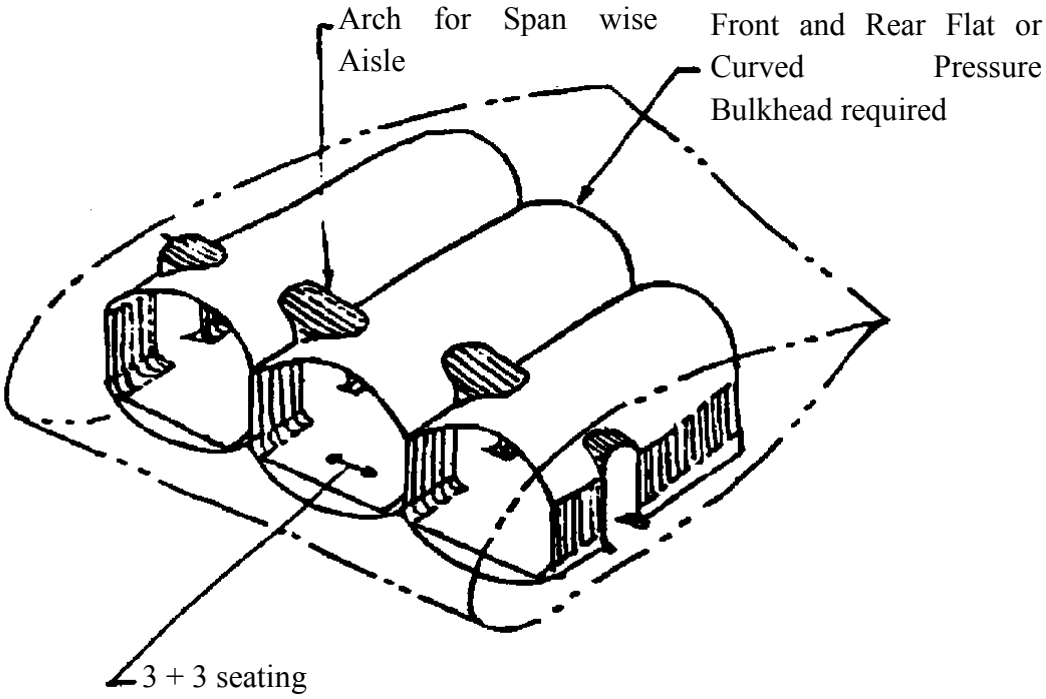

Figure 4.2 BWB separate pressure shell (Liebeck, 2002)

As an integrated aircraft configuration, the BWB had to satisfy a unique set of design requirements. Passengers, cargo and systems had to be packaged within the wing itself, leading to a requirement for the maximum thickness-to-chord ratio in the order of 17%; a value that is much higher than is typically associated with transonic airfoils.

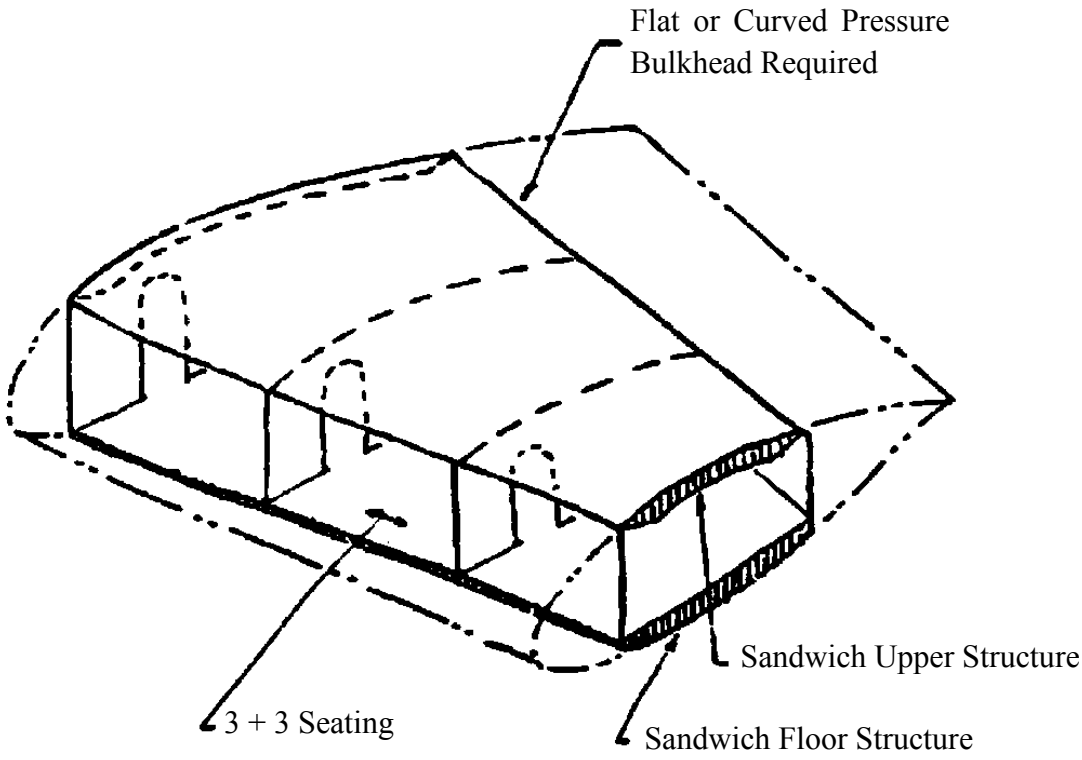

Figure 4.3 BWB integrated skin and shell concept (Liebeck, 2002)

The resulting second-generation BWB developed by NASA, illustrated in figure 4.4, incorporated ten 150-inch wide passenger cabin bays with cargo compartments located outboard. Considerations and constraints included weight and balance, maximum offset of the passengers from the vehicle centre line (ride quality) and the external area of the cabin. Since this is the surface area of the pressure vessel, the extent of this area has a significant effect on the structural weight of the centre body. The cabin partitions are in fact wing ribs that are primary structure. Windows were located in the leading edge on both decks, and the galleys and lavatories were located aft to help provide the passengers with an unobstructed forward view. Egress was via the main cabin doors in the leading edge, and through aft doors in the rear spar.

The unique element of the BWB structure is the centre body: as the passenger cabin it must carry the pressure load in bending, and as a wing it must carry the wing bending load. The primary challenge was to develop a centre body structural concept to absorb

the cabin pressure load. Unlike a wing, which rarely experiences its limit design load (typically via a 2.5g gust), the passenger cabin sees its design pressure load on every flight. Thus, on the basis of fatigue alone, it was recommended that the centre body should be built from composite materials due to their comparative immunity to fatigue and corrosion.

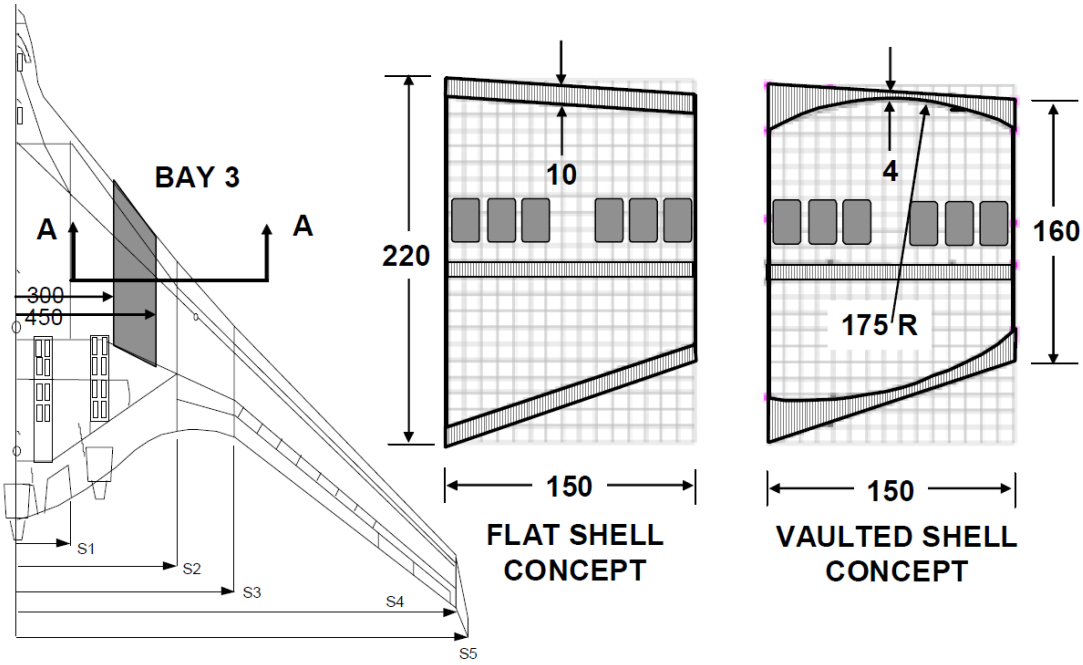

Figure 4.4 BWB fuselage bay-3 section, flat ribbed and vaulted ribbed shell concepts of first generation BWB 800 passenger version (Mukhopadhyay, 2005)

The overall structural concept selected for the NASA sponsored study was composed of outboard wing structure, essentially conventional and assumed to be composite and a centre body structural shell based on two candidate concepts: a 5-inch thick sandwich, or a skin plus 5-inch deep hat-section stringers. The structure of the outer wings was similar to that of a conventional transport. The centre body was subdivided into the forward pressure vessel and the unpressurised after body. Development of the structure for the centre body and its pressure vessel was approached by defining and comparing several concepts. Weight and cost were the primary figures of merit. One of the most viable concepts was based on a skin/stringer outer surface structure where the stringers are on the order of 5 to 6 inches deep. The internal ribs had Y-braces where they met the skin to reduce the bending moment on the skin created by the internal pressure.

The complete centre body pressure vessel was composed of the upper and lower surface panels, the rounded leading edge (which also functioned as the front spar), the rear main spar, the outer ribs (which also carried the cabin pressure load in bending) and the internal ribs (which carried the cabin pressure load in tension). The cabin floor simply supported the payload and did not carry wing bending loads.

The NASA study assumed composite materials for the majority of the BWB primary structure. The outer wings could readily be fabricated from aluminium with the typical 20-percent weight penalty. The weight penalty for using aluminium for the centre body structure would be larger. The design cabin pressure load is experienced on every flight, and thus fatigue becomes the design criterion. Since the cabin pressure loads are taken in bending, the margin required for aluminium was believed to be prohibitive, while composites are essentially immune to fatigue and hence would suffer no penalty.

4.3 Proposed alternative wing root configuration

A cutaway drawing showing the Airbus A300 wing to fuselage joint which is an example of existing wing root joints is previously illustrated in figure 3.6. The proposed alternative wing root configuration for BWB aircraft results in a lower parts count and significant reduction in complexity. This is achieved by taking advantage of the opportunity offered by the BWB configuration for the wing skin to continue uninterrupted across the wing / fuselage boundary. The processes by which the final proposal was arrived at are described in this section.

In blended wing body aircraft, the wingbox depth at the wing root is equal to fuselage height making it possible for the wing skin to continue uninterrupted across the wing/fuselage boundary. An initial assessment of potential root joint configurations yielded two possible solutions illustrated in figures 4.5 and 4.6.

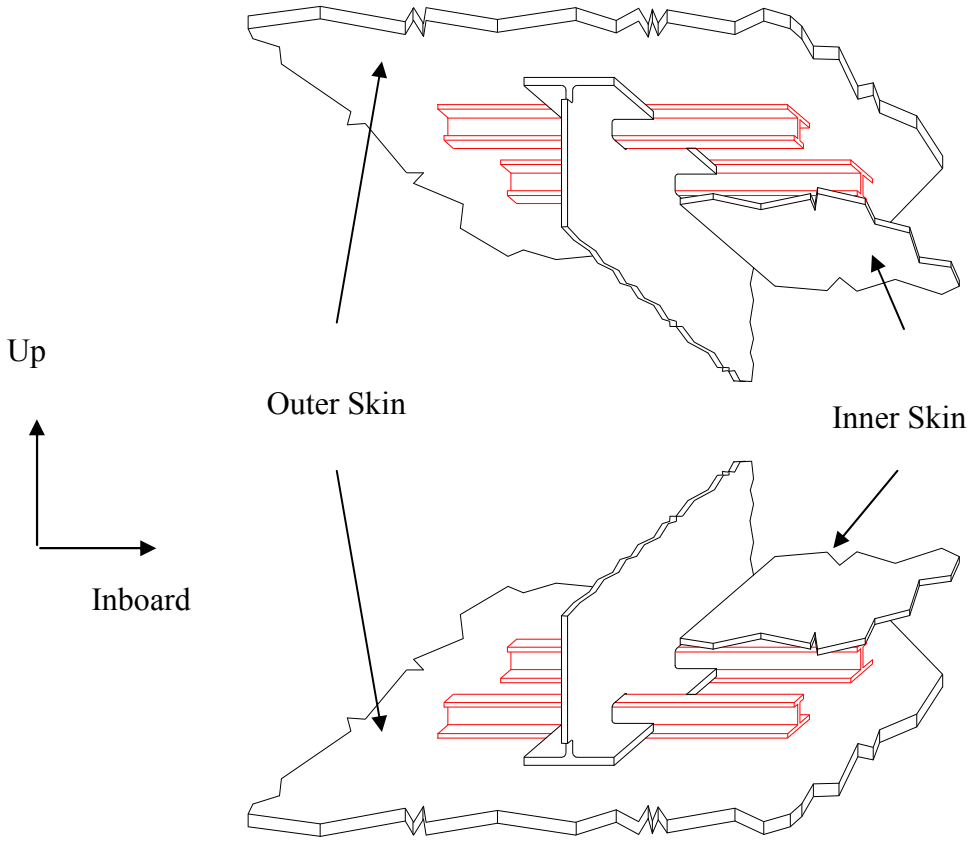

Figure 4.5 Type 1 root joint

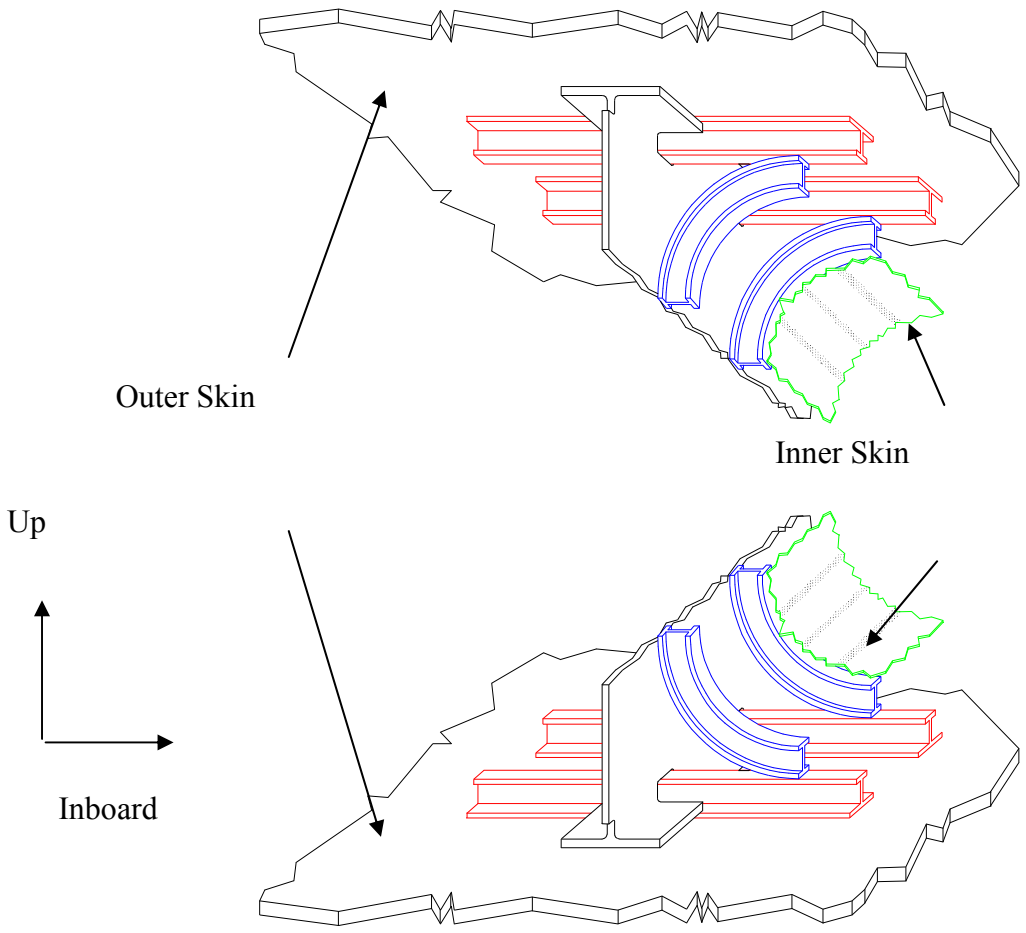

Figure 4.6 Type 2 root joint

The Type 1 root joint was initially proposed as an alternative to existing root joint types. As discussed earlier, the wingbox depth at the wing root is equal to fuselage height making it possible for the wing skin to continue uninterrupted across the wing/fuselage boundary. Figure 4.5 shows the wing skin stringers continuing across the wing root to become fuselage skin stiffeners. In this initial proposal, the stringers also provide structure (flanges) on to which an internal fuselage skin could be mounted providing possible structure for reacting internal fuselage pressurisation loads whilst the external skin reacts the normal flight loads. The root rib was required to react flight and pressurisation loads.

A subsequent proposal outlined in figure 4.6 included the introduction of circular frames that provide supports for circular fuselage skins. The overall internal cross-section of the fuselage becoming oval in shape thus providing a more efficient means of reacting the internal fuselage pressure. The internal fuselage pressure would therefore be reacted by the internal skin and the flight loads reacted by the outer skin and root rib.

Having reviewed the two initial proposals, the preferred solution adopted for this project which is close to the type 2 root joint is illustrated in figures 4.7 and 4.8. In this final proposal, the fuselage frames are deleted. The wing skin stringers being continuous across the wing fuselage joint. Additional stiffeners were introduced in the format of longerons running fore-aft and fuselage stiffeners running parallel to stringers and replacing every third stringer and with considerably greater depth and section properties. The fuselage pressure boundary was moved out from the root rib to the next adjacent outboard rib, thus reducing the role of the root rib to reacting floor structural loads and wing brazier loads only.

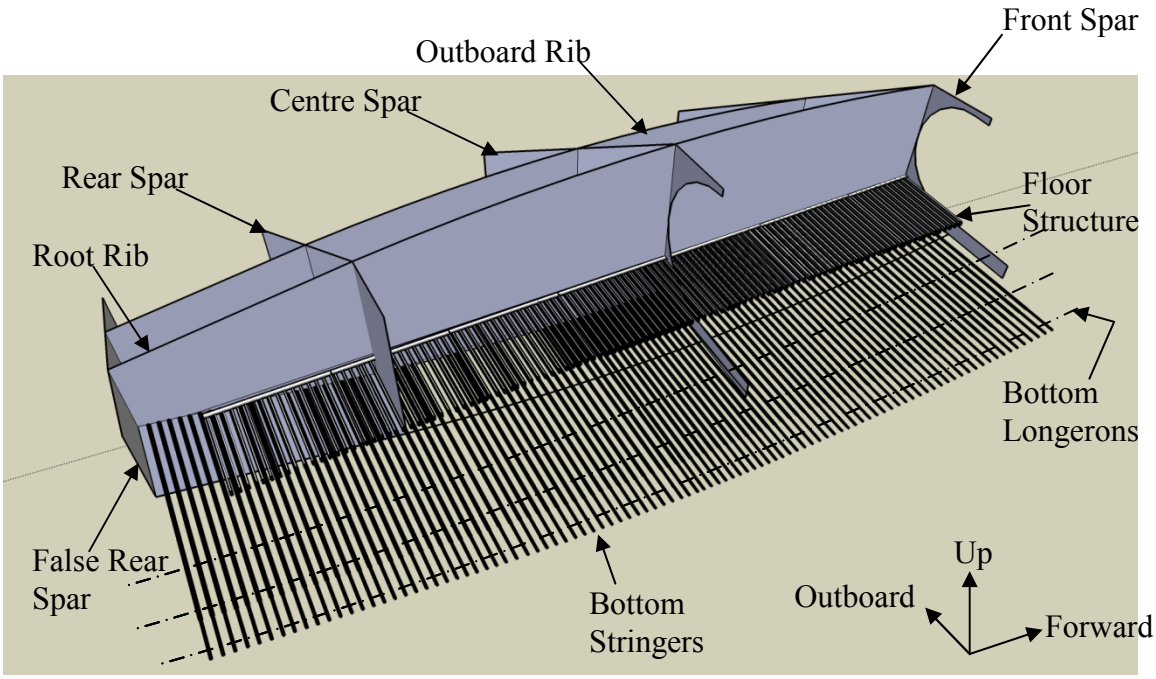

Figure 4.7 Model of proposed wing root design (Ribs, Spars and Bottom Stringers)

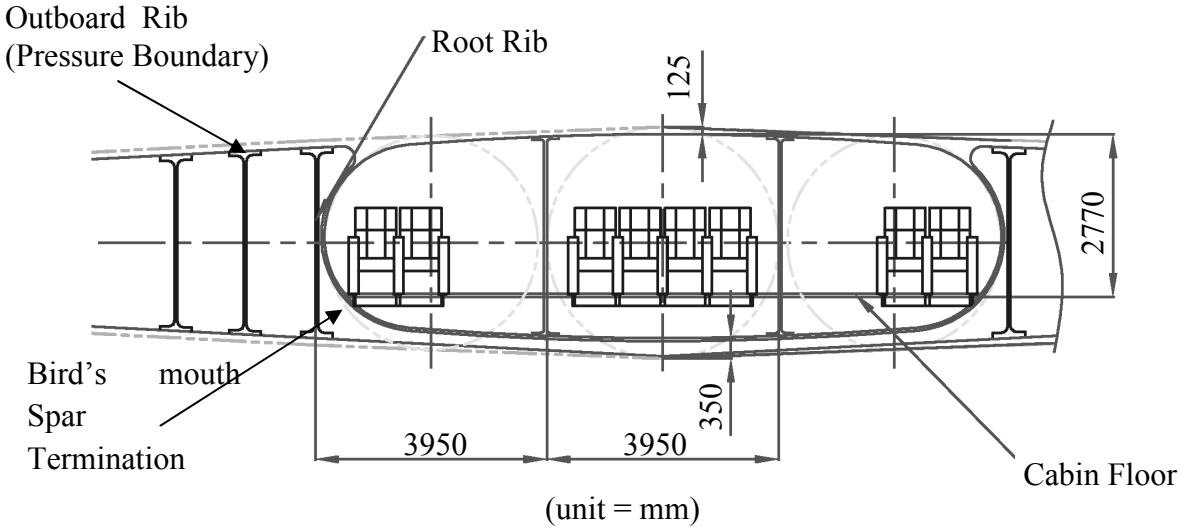

Figure 4.8 Dimensions of proposed wing root design

One key issue impacting the design of the root joint is the nature of the termination of the main wing spars. Current fuselage centre boxes include front and rear spars and in some cases a centre spar thus ensuring continuity of load path. Because the wing of the project aircraft is the depth of the fuselage, continuation of spars through the fuselage introduces other barriers within the fuselage that would require cut-outs.

Most significantly of all therefore, the front and centre spars are designed with a bird's mouth profile. This facilitates a smooth transfer of load from the spar web into the root rib and the top and bottom skins. Continuity of the spars is, however, maintained across the fuselage whilst ensuring that the fuselage volume is largely unobstructed.

The bird's mouth type termination is applicable to the rear spar and false rear spar but is not in this instance, as the habitable portion of the fuselage is forward of the rear spar. The rear spar and false rear spar therefore continue as conventional spars through the fuselage providing additional stiffness to the fuselage. This is consistent with other similar BWB studies (Smith, 2002)(Mukhopadhyay, 2005).

One concern with the above proposal is the damage tolerance capability of the proposed wing joint. A modular root rib is proposed as shown in figure 4.9 which would make it damage tolerant. The spars are single load path structures but with crack arrest features such as stiffeners. The presence of large uninterrupted airframe skin is an advantage but also presents some risk. The damage tolerance capability of the airframe skin is, therefore, enhanced by the presence of fail safe straps and these are therefore proposed for the airframe skin at the wing root. Other fuselage stiffening, including, for example Y-braces where the root rib meets the skin to reduce the bending moment on the skin created by the fuselage pressure discussed by Mukhopadhyay (2005) are options that would facilitate the design. However, these are not the focus of this report and are therefore not discussed further.

4.4 Detailed design of proposed novel structure and its integration into the airframe

The proposed bird's mouth spar termination is designed to facilitate smooth transfer of load from the spar into the root rib and the top and bottom skins. The other benefit of the bird's mouth termination is that it enables the spar to runout and hence not intrude into the passenger cabin. Outboard of the root rib, therefore, the design of the spar is conventional with a web stiffened with vertical and horizontal stiffeners as required to break the spar web into suitable panel sizes to react the shear stresses in the spar web.

The spar is also bounded by upper and lower caps that carry end load and are the means of attachment to the skins. The intent is that the spars are integrally machined with size limited only by the capacity of existing machining facilities. This is discussed further in section 7.

Inboard of the root rib, the spar web in effect includes a cut-out with a diameter that is almost the depth of the fuselage. The upper portion of the web above the cut-out is

reduced to a minimum depth of 125 mm and the portion of the web below the cut-out limited to a minimum depth of 350 mm to facilitate continuity through the fuselage. The edge of the cut-out is capped (flanged) and the upper and lower spar caps are continuous throughout the fuselage so that the cross-section of the spar within the fuselage is effectively comprised of two I-sections.

The attachment of the spar caps to the fuselage skins is to be achieved by conventional high load transfer interference fit bolting. The root rib is modular, which enhances the damage tolerance capability of the joint and is attached to the upper and lower skins by interference fit bolts and spar webs by conventional clearance fit bolted joints to facilitate assembly. The modular root sections are also integrally machined with horizontal and vertical stiffeners.

One of the key benefits of the proposed structure at the wing root including the novel bird's mouth spar termination is its simplicity in contrast to the conventional wing fuselage joint presented in figure 3.6. The design of the proposed bird's mouth spar termination and the wing skin joint as discussed above is as consistent with conventional spar, skin and rib structure as possible. The detailed design of the proposed bird's mouth spar termination has also been kept as simple as possible. The proposed bird's mouth spar termination and associated root rib and skin are integrated into the fuselage with bolted joints. All efforts have been made to keep the number of joints to a minimum and in a manner that greatly simplifies the manufacture and assembly process and hence enhances the inspectability of the joints and associated structure which is a key feature of damage tolerance.

4.5 Novelty of the proposed root joint configuration

A considerable volume of work already exists on the blended wing body aircraft so this research concentrates on the integration of the wing and fuselage and associated structural issues at the wing root. The proposed wing root joint is believed to be novel for reasons explored in detail below.

The airframe skin is continuous across the joint transitioning from wing skin to fuselage skin without the need for a discrete joint. This shows that it is possible to eliminate the wing fuselage joint in its current form in the skin altogether thus ensuring a more structurally efficient skin.

Continuous stringers and other structure across the wing root further enhance the integrity of the joint, result in a relatively smaller number of fasteners and a reduction of parts and other items required to achieve the required joint strength.

In contrast to the conventional wing/fuselage joint shown previously in figure 3.6, the absence of a discrete (concentrated) joint means that the proposed joint structure lends itself more readily to visual inspection of the external surfaces. Visual inspections are, of course, an essential feature of existing aircraft maintenance programmes. This is also true for directed NDT inspections where the ease of inspection is essential for accuracy of inspection.

A key feature of the proposed design is the bird's mouth type spar termination. In contrast also to the existing fuselage structure and some of the existing blended wing body concepts, with the exception of the rear spar, the spar webs terminate just inboard of the root rib hence leaving the passenger cabin relatively unobstructed. The bird's mouth spar termination however, facilitates load path continuity across the fuselage. The need for stiffening members within the fuselage to counteract fuselage crushing loads due to bending are still required and would be the subject of another study. However, the depth of the wingbox and fuselage means that the tensile and compressive skin loads are much lower than for conventional wing skins.

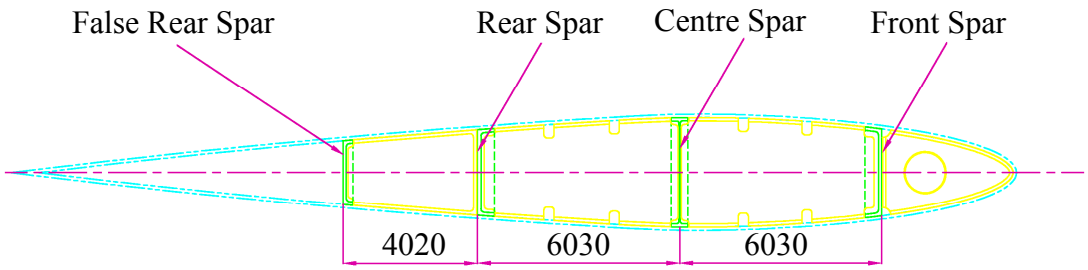

Figure 4.9 Root rib

The bird mouth termination of the spars proposed by this thesis author enables a smooth transfer of loading from the spar web into the root rib and the upper and lower skins and is novel in its application to the blended wing body configuration.

The continuous nature of the spars means that the root rib is required in several sections. The main function of the root rib is to maintain the profile of the wing. The depth of the root rib is such that it is easier to manufacture in short sections rather than as one continuous member. Manufacturing the rib in short sections also makes it possible to reduce the weight of the finished component.

4.6 Conclusions

Wing joint design is one of the most critical areas in aircraft structures, especially for fatigue consideration of long life structure, the best fatigue design being one with no joints or splices. The wing to fuselage joints currently in use in aircraft structures are of three main types; namely spliced plates, tension bolts and shear lugs. The spliced plate joint is clearly the most efficient method of achieving the desired outcome because of the challenges faced by manufacturers in joining a circular fuselage section to an aerofoil section wing. The proposed solution involves the integration of wing structure to fuselage section with similar geometry. This removes the need for a centre box. The availability of uninterrupted skin across the joint in combination with the proposed novel bird's mouth spar termination facilitates the smooth transfer of load across the wing to fuselage joint and ensures continuity of load path across the joint.

5 Design Calculations

5.1 Introduction

This chapter describes the reasoning, methods and processes employed to determine the wing geometry and wing loading data. A global load model created to generate loading data for a local finite element model is also discussed. A finite element analysis of a section of the wing root is presented to confirm the integrity of the proposed design and to generate data for the damage tolerance analysis in chapter 6. The approach adopted to generate the required input data and the results of the finite element analysis are discussed. The local FE model and detailed stress analyses undertaken are discussed together with data from the global load model presented in the Appendices.

5.2 Derivation of Loading

The project BWB aircraft was designed with a payload-range similar to the Boeing 767 and the AIRBUS A330-200 aircraft.

Table 5.1 Comparison of aircraft specifications

Aircraft	BOEING 767-400ER[a]	AIRBUS A330-200[b]
Seating Configurations		
Typical 3-class	245	253
Typical 2-class	304	293
Typical 1-class	up to 375	-
Cargo	129.6m^3	136 m^3
Engines	PW4062 : 281.6kN GE CF6-80C2B8F : 282.5kN	GE CF6-80E : 300kN-334kN PW PW4000 : 287kN-305kN RR Trent 700 : 300kN-316kN
Maximum Fuel Capacity	90770 l	139100 l
MTOW	204120 kg	230000 kg
Maximum Range	10454 km	12500 km
Typical City Pairs	London - Tokyo Newark - Moscow Chicago - Warsaw	
Typical cruise speed at 35000 ft	0.80 Mach 851 km/h	
Basic Dimensions		
Wing Span	51.9 m	60.3 m
Overall Length	61.4 m	59.0 m
Tail height	16.8 m	17.40 m
Interior Cabin Width	4.7 m	5.28 m

a. http://www.boeing.com/commercial/767family/technical.html 30/08/2004
b. http://www.airbus.com/product/a330_a200_specifications.asp 17/09/2004

As stated earlier, this project was originally intended to be a continuation of work undertaken as part of a Cranfield University MSc course in Air Vehicle Design (AVD)

(Smith, 2002). The design study was for a blended wing body aircraft capable of competing with the Boeing 767 aircraft. However, constraints on the availability of data meant that this project had to be completed without access to the results of the MSc study.

The Boeing 767 aircraft was hence maintained as the baseline aircraft for comparison in this project. Since the Airbus A330-200 is considered to be a competitor to the Boeing 767 it is also included for comparison. The specifications of the two aircraft are presented in table 5.1.

Lift and moment data for the various elements of the aircraft are required in order to determine the distributions of the shear forces, bending moments and torques along the wing span and along the fuselage. In the early stages of an aircraft design, empirical estimates are often made concerning the breakdown of mass distribution: these estimates are often based on experience. A fairly typical mass breakdown for a conventional large transport aircraft which may be adapted for particular aircraft of similar configuration is presented in Table 5.2 (ESDU 94009). The fuel and payload mass vary approximately in the range 20-30% and 10-20%, respectively, and are included as part of the wing and fuselage. The particular flight sortie, considered for design, allows determination of the particular fuel and payload requirements for the given flight condition.

Table 5.2 Typical mass breakdown for a large transport aircraft

Aircraft element		Element mass as % of gross mass
Wing	structure	14
	fuel	21
Fuselage	structure	18
	payload	12
Undercarriage		4
Tail + fin		3
Power plant		12
Equipment + systems		16

5.2.1 First estimate of maximum take off weight (MTOW)

"The average weight of the standard man today is nearer 82 kg clothed, with deviations of ±14 per cent" (Stinton, 2001). Stinton's figures are obtained from (AvP970 2, 1955) now superseded by (Defence Standard 00-970, 2007) which presents the 50th percentile body masses of air crew and soldiers as ranging from 71 kg to 78.2 kg unclothed. Other data presented in (NASA-STD-3000, 1995) suggests a 50th percentile male body mass of 82.2 kg.

A clothed body mass of 82 kg was therefore applied for the estimation. A preliminary estimate of the maximum take-off weight of the project aircraft is required and was made to facilitate the derivation of loading and preliminary sizes using data presented in (Stinton, 2001). Copies of above referenced data are presented in Appendix A.

The maximum number of passengers carried by a Boeing 767 in a three class layout is 245 although, as presented in Table 5.1, the Boeing 767-400 is capable of carrying up to 375 passengers in a single class configuration. The AVD study was for a blended wing body aircraft capable of carrying 250 passengers in a single configuration or 210 passengers in a three class layout. A total passenger complement of 245 passengers was therefore assumed for this project, giving a first estimate of Maximum take-off mass (MTOM) of 199920 kg as shown in Table 5.3.

"Aircraft designed for longer ranges and which must carry large quantities of fuel, may have gross weights nearer 6 to 8 times payload." (Stinton, 2002). ESDU 94009 estimates payload as 0.12 of gross weight (i.e. 8.3 x payload). On that basis, an estimate of 8 x payload is used as shown in Table 5.3.

Table 5.3 First estimate of MTOW

Item	Description	Value
1	Total number of passengers	245
2	Mass of each passenger	82 kg
3	Baggage allowance per passenger	20 kg
4	Sum of passenger and baggage mass	102 kg
5	Total passenger and baggage mass	24990 kg
6	Payload factor	8
7	Maximum take-off mass (MTOM)	199920 kg
8	Gravitational acceleration	9.80665 m/s^2
9	First estimate of maximum take-off weight (MTOW)	1960545 N

5.2.2 First estimate of wing area

Definition of wing loading requires a clear definition of the wing geometry, as wing loading is a function of wing geometry. Estimates of the wing area, wing aspect ratio and wing span were made to facilitate the definition of wing geometry and thus loading. A key feature of the BWB configuration is the possibility of wider fuselages compared to the conventional fuselage configuration. A decision was made early in the project to limit the width of the fuselage to three times the width of existing narrow body aircraft fuselages. This was considered adequate for the number of passengers to be transported. The AIRBUS single aisle fuselage width of 3.95m was selected. The BWB fuselage depth at its centre line was therefore 3.95m with a fuselage width three times its depth.

Lift force (L) is the sum of all aerodynamic force components acting on an aircraft when resolved at right angles to the flight path. In steady and level flight, the lift is equal and opposite to the weight of the aircraft. Lift can be defined as $L = C_L$ x q x S, where C_L is the lift coefficient, q dynamic pressure and S wing area.

Replacing the lift with the weight W_0 in level flight,

Wing area $$S_w = \frac{W_0}{(C_L \times q)} \quad (5.1)$$

Dynamic pressure $$q = \frac{V_e^2}{295}\frac{ft^2}{\sec^2} \quad (5.2)$$

The stall speed or minimum flying speed KEAS V_s is set at 135 knots for the project aircraft. V_e in the above equation is the equivalent airspeed in knots which is set to V_s and compares favourably with 137 knots for the Boeing 767 (Jane's, 2001). The dynamic pressure at sea level is determined in Table 5.4.

Table 5.4 First estimate of dynamic pressure and wing area

Item	Description	Value
1	Maximum lift coefficient C_{Lmax}	1.3
2	Stall speed (Minimum flying speed KEAS)	135 knots
3	Aircraft Weight (MTOW)	1960545 N
4	Density of air at sea level[a]	1.2249988 kg/m^3
5	Dynamic pressure at sea level at 135 knots	2953.76 N/m^2
6	Wing area S_w	510.5 m^2
7	Wing loading per unit area	392 kg/m^2
8	Comparative wing loading per unit area for B767[b]	552.3 kg/m^2

a. (Niu, 1990) figure 3.1.5

b. Source Jane's

5.2.3 First drag estimate

Having determined the wing area, an estimate of the drag is required to determine wing loading. The choice of aerofoil section plays a significant role in determining wing drag. However, as the focus of this project is on structural sizing, a detailed assessment of aerofoil sections was not undertaken. A maximum lift coefficient of 1.3, which is consistent with transport aircraft, has been selected for this aircraft as shown in Table 5.4. The approach used to determine the first estimate of drag is presented below. Figure 5.1 describes the total wetted area for delta configuration wings as twice the wing area. The equivalent parasite area was then determined by extrapolation using data from Figure 5.2 and assuming an effective friction drag coefficient for jet aircraft, C_{Dfric} of 0.0035. The speed for maximum range was assumed, as shown in Figure 5.3, to occur at $(L/D)_R$ (gear retracted) at approximately 2.8 times the stall speed of 135 knots i.e.

$2.8V_{so}$ which gives a speed for maximum range of 378 knots. The maximum range occurs at minimum drag at which $C_D = 2$ x C_{Dp}. The parasite drag coefficient C_{Dp} is defined by the equation $C_{Dp} = f / S$ giving a value of 0.008 for C_{Dp} presented in table 5.5. The density of air ρ_{ac} at the cruise altitude of 35000 ft was determined as 0.380456 kg/m^3. The dynamic pressure at cruise is 7192 N/m^2 defined by equation 5.3 and presented in table 5.5.

$$q_{pc} = \frac{1}{2}\rho_{ac}V_{L\_DR}^{\ 2} \tag{5.3}$$

The total drag D was then determined from the equation $D = C_D \; x \; q_{pc} \; x \; S_w$. If the required lift is assumed to be equal to the maximum take off weight (MTOW), the lift to drag ratio L/D can be determined and is presented in table 5.5.

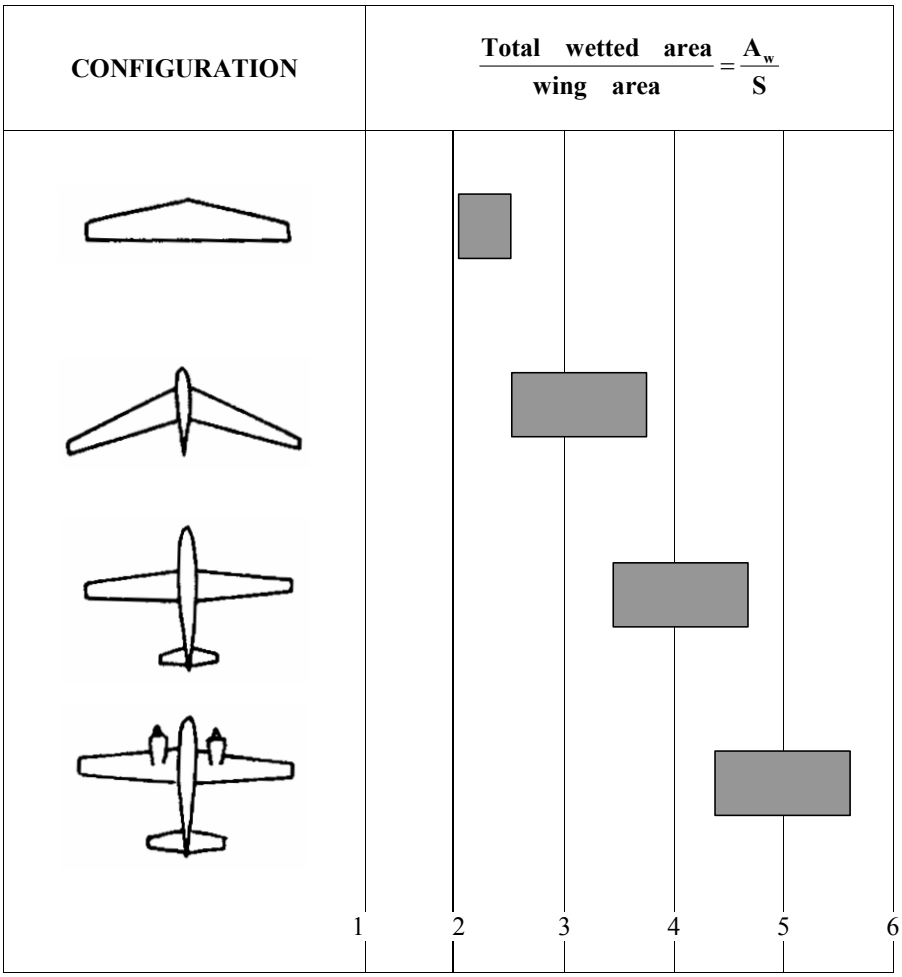

Figure 5.1 Total wetted area of airframe in terms of wing area of different configurations (Stinton, 2001)

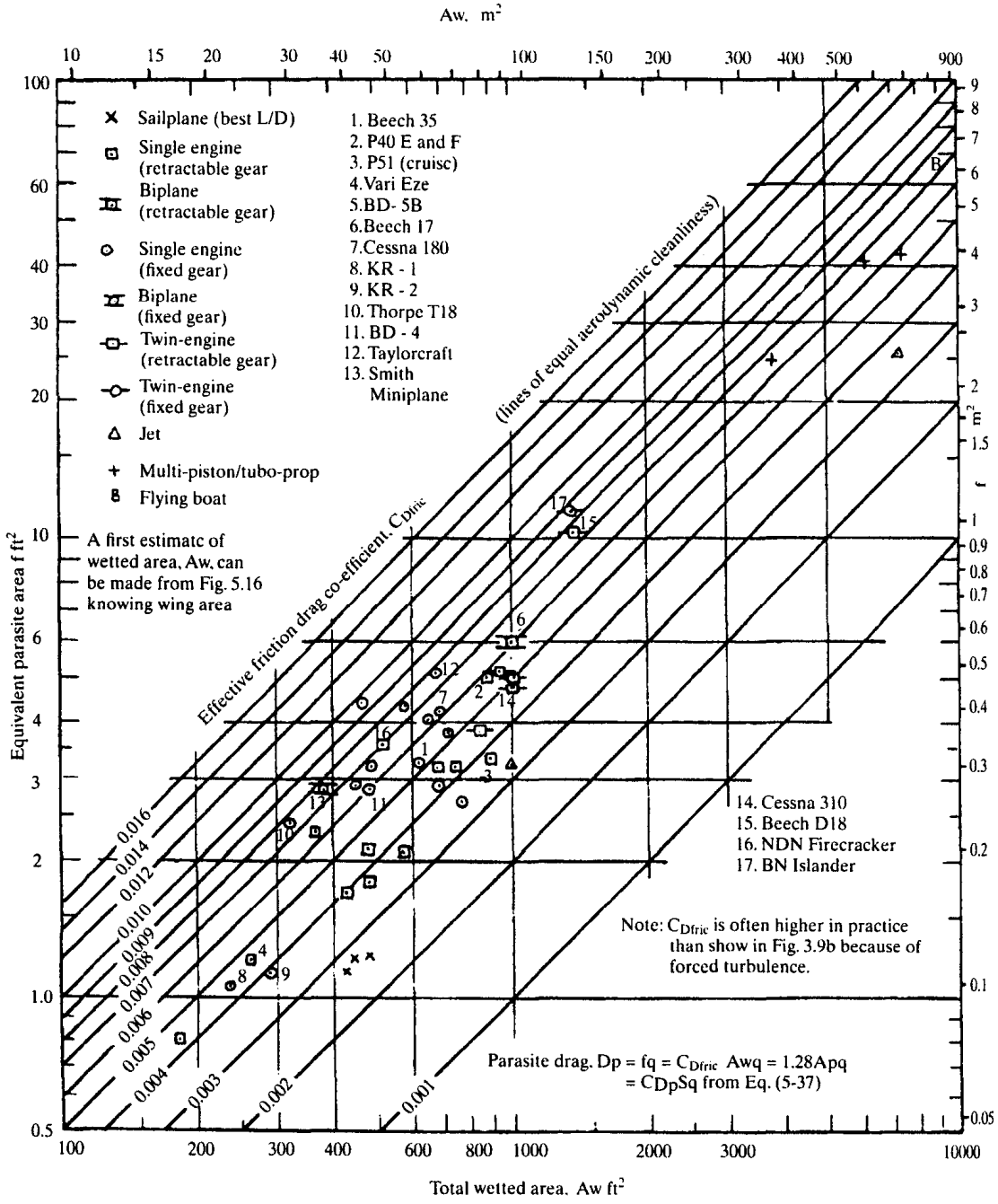

Figure 5.2 Estimates of parasitic drag and equivalent parasitic area, f, as a function of skin friction drag coefficient and wetted area (Stinton, 2001)

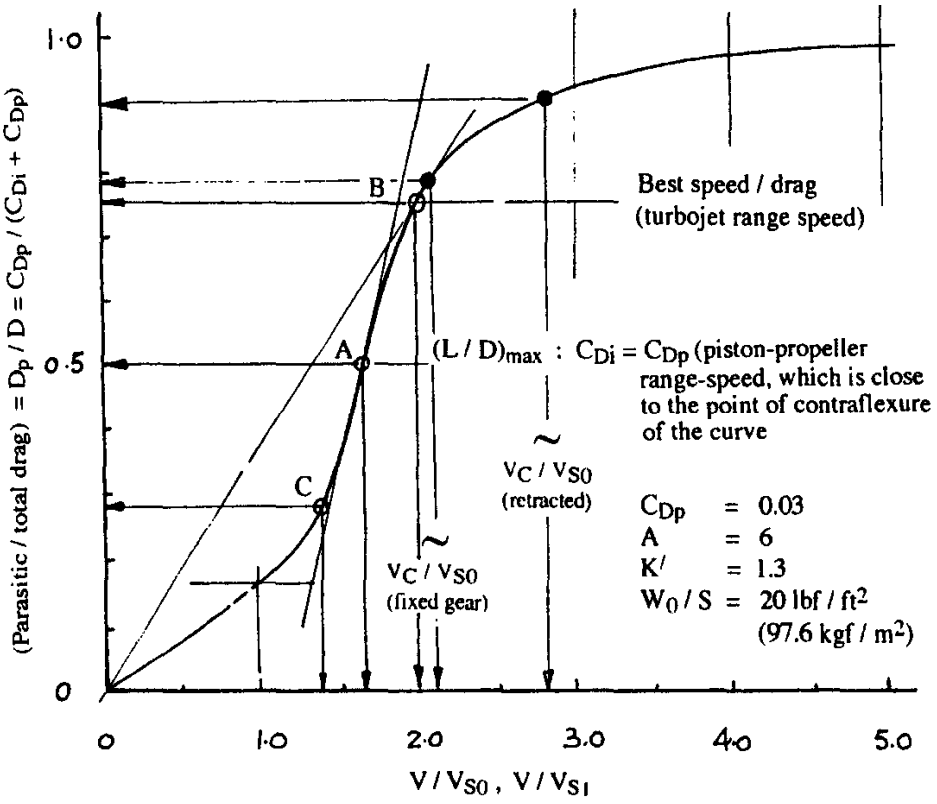

Figure 5.3 Variation of (lift/drag) and power with airspeed at constant lift and weight (Stinton, 2001)

Table 5.5 First drag estimate

Item	Description	Value
1	Wing area, S_w	510.5 m^2
2	Total wetted area, $A_{wt} = 2 \times S_w$	1021 m^2
3	Effective friction drag coefficient for jet aircraft, C_{Dfric}	0.0035
4	Equivalent parasite area, f[a]	4 m^2
5	Stall speed, V_{so}	135 knots
6	Speed for maximum range $V_{L\_DR} = 2.8\ V_{so}$	378 knots
7	Estimated parasite drag coefficient, $C_{Dp} = f / S_w$	0.008
8	Conservative estimated parasite drag coefficient[b]	0.014
9	Total drag coefficient, $C_D = 2\ C_{Dp}$	0.028
10	Density of air at 35000 ft, ρ_{ac}	0.380456 kg/m^3
11	Dynamic pressure at cruise, $q_{pc} = \frac{1}{2}\rho_{ac}V_{L\_DR}^2$	7.192 KPa
12	Total drag, $D = C_D \times q_{pc} \times S_w$	102.82 kN
13	Lift (assumed to be equal to MTOW), L_d	1960.55 kN
14	Lift / Drag in level flight at gross weight, L/D	19

a. (Stinton, 2001 fig 5.17 page 216)

b. (Stinton, 2001 table 5.7 page 218)

5.2.4 First estimate of wing span and aspect ratio

The first estimate of wing span and aspect ratio is determined in table 5.6. With the total wetted area A_{wt}, the equivalent parasite area f, the lift to drag ratio for level flight at gross weight L/D, the effective friction drag coefficient for jet aircraft and the induced drag factor for subsonic jet aircraft known, the aspect ratio and wing span can be determined. The induced drag factor for subsonic jet aircraft K' was taken to be 1.25 (table 5.7 on page 218 of (Stinton, 2001)). The aspect ratio A_R is defined by the equation

$$A_R = \frac{9}{2\pi}\left[K' C_{Dfric} \frac{A_{wt}}{S_w}\left(\frac{L}{D}\right)^2\right] \tag{5.4}$$

and the wing span b by the equation

$$b = \sqrt{A_R S_w} \tag{5.5}$$

Table 5.6 First estimate of wing span and aspect ratio

Item	Description	Value
1	Total wetted area, $A_{wt} = 2 \times S_w$	1021 m^2
2	Equivalent parasite area, f[a]	4 m^2
3	Lift / Drag in level flight at gross weight, L/D	19
4	Effective friction drag coefficient for jet aircraft, C_{Dfric}	0.0035
5	Induced drag factor, K'[a]	1.25
6	Aspect ratio, $A_R = \frac{9}{2\pi}\left[K' C_{Dfric} \frac{A_{wt}}{S_w}\left(\frac{L}{D}\right)^2\right]$	5
8	Wing span, $b = \sqrt{A_R S_w}$	48.24 m

a. (Stinton, 2001 fig 5.17 page 216)

5.2.5 First layout sketch

The fuselage depth of 3.95m which is similar to AIRBUS single aisle aircraft was assumed. The AIRBUS single aisle configuration was deemed a suitable platform on which to base the design of the project aircraft. However the blended wing configuration means it is possible to have a wider and shorter fuselage. The overall fuselage width was, therefore, taken as 3 x single aisle fuselage diameter. Allowing for taper, the fuselage/wingbox depth at wing root joint would be approx. 88.53% of fuselage depth at centre chord resulting in a root joint depth at centre chord of approx. 3.497m as shown in Figure 5.4

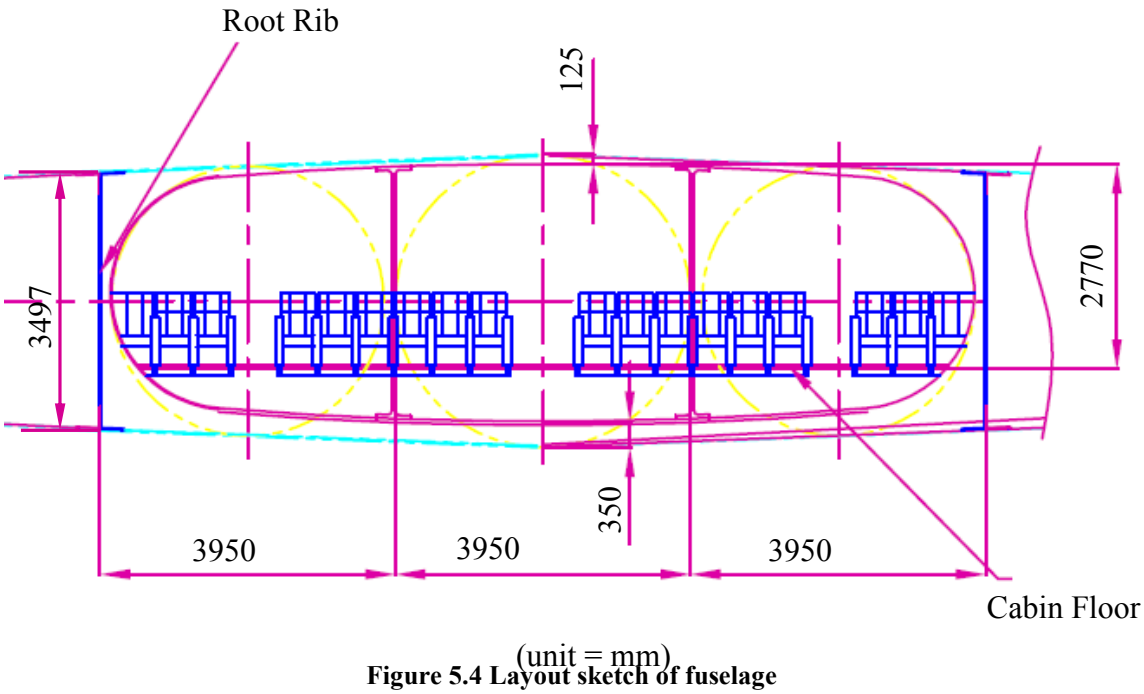

Figure 5.4 Layout sketch of fuselage

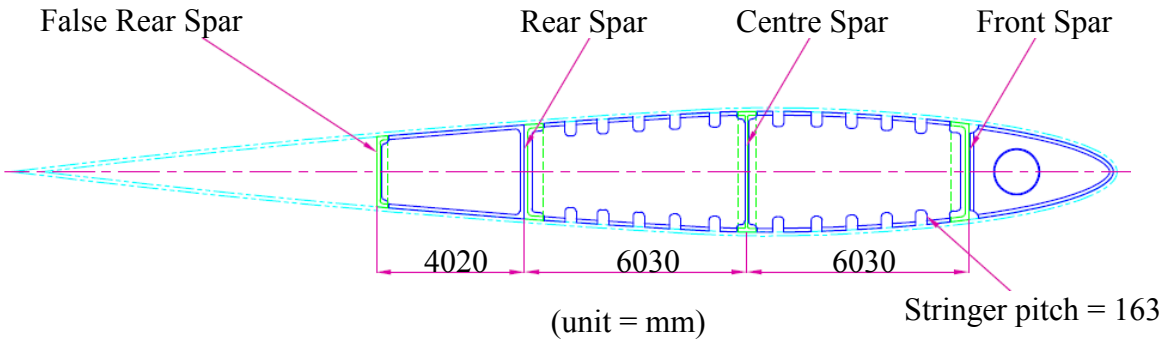

Figure 5.5 Wing profile at fuselage joint

A wing depth to chord ratio of approx. 1:7.6 was assumed resulting in a wing chord of 26.8m. A three spar layout was adopted with the front spar at 15% chord, centre spar at 37.5% chord and the rear spar at 60% chord. A false rear spar was also adopted for trailing edge devices and located at 75% chord as shown in Figure 5.5.

Table 5.7 First layout sketch data

Item	Description	Value
1	AIRBUS single aisle fuselage diameter, d_{sa}[a]	3.95m
2	Project aircraft fuselage width, $W_{fuse} = 3d_{sa}$	11.85 m
3	Wing span, b	48.24 m
4	Distance from wing root to tip, $l_{r\_tip} = (b - W_{fuse})/2$	18.2 m

a. http://www.airbus.com/en/aircraftfamilies/a320/a321/specifications.html 24/02/2008

5.2.6 Wing root shear force, bending moment and torque (SMT loads)

Wing root shear force, bending moment and torque were derived for the project aircraft based on the geometry presented in Table 5.8 and using a method defined in Airframe Structural Design (Niu, 1990). The 2.5g V_D load case which is the most severe load case the aircraft is expected to experience was selected for structural sizing.

A spreadsheet based on the method outlined in (Niu, 1990) formed the basis on which wing Shear Force, Bending Moment and Torque (SMT) loads were derived. The variation of wing SMT loads along the span of the wing obtained from the loads spreadsheet is presented in Figure 5.6. The data was then interpolated to determine wing shear, bending moment and torque at the wing root which corresponds to a normalised wing span η of 0.2456. The SMT data at the wing root are presented in the Table 5.9. A copy of the spreadsheet and associated data is presented in Appendices B, C and D.

Part 25.301 of the US Department of Transport Federal Aviation Regulations (FAR 25.301) requires that "Strength requirements are specified in terms of limit loads (the maximum loads to be expected in service) and ultimate loads (limit loads multiplied by prescribed factors of safety). Unless otherwise provided, prescribed loads are limit loads."

Part 25.365 of the regulations (FAR 25.365) requires the following consideration for aircraft with one or more pressurized compartments:

1. The airplane structure must be strong enough to withstand the flight loads combined with pressure differential loads from zero up to the maximum relief valve setting;
2. The external pressure distribution in flight and stress concentrations and fatigue effects must be accounted for;
3. Landing loads must be combined with pressure differential loads from zero up to the maximum allowed during landing, and;
4. The airplane structure must be designed to be able to withstand the pressure differential loads corresponding to the maximum relief valve setting multiplied by a factor of 1.33 for airplanes to be approved for operation to 45,000 feet or by a factor of 1.67 for airplanes to be approved for operation above 45,000 feet, omitting other loads.

Part 25.303 of the regulations (FAR 25.303) indicates that "unless otherwise specified, a factor of safety of 1.5 must be applied to the prescribed limit load which are considered external loads on the structure.

The proposed design must therefore be capable of sustaining the following loading conditions:

1. Stresses for 2.5g V_D Load case x 1.5 Factor of safety

2. Stresses for (2.5g V_D + 1ΔP) Load case x 1.5 Factor of safety
3. Stresses for 2ΔP Ultimate Load case.

Additional safety factors have therefore been applied to the stresses obtained from the global and local models due to the limit loads calculated below to determine the ultimate design stresses for the proposed structure.

Table 5.8 Project aircraft geometry and lift

Item	Description	Value
1	AIRBUS single aisle fuselage diameter, d_{sa}	3.95 m
2	Wing root depth (85% of fuselage depth)	3.497 m
3	Wing depth to chord ratio	1 : 7.6
4	Wing root chord, C_R	26.8 m
5	Wingbox root chord (60% of C_R)	16.1 m
6	Project aircraft fuselage width, $W_{fuse} = 3d_{sa}$	11.85 m
7	Wing area, S_w	510.5 m^2
8	Wing span, b	48.24 m
9	Assumed tip chord, C_T	2.62 m
10	Aircraft weight (MTOW)	1960545 N
11	Inertia for V_D load case	2.5 g
12	Lift force L_w	4903041.6 N

Table 5.9 Limit shear force, bending moment and torque (SMT) loads at wing root

Description	Value
Shear load (N)	152.143 x 10^4
Bending Moment (Nm)	11.292 x 10^6
Torque (Nm)	0.837 x 10^6

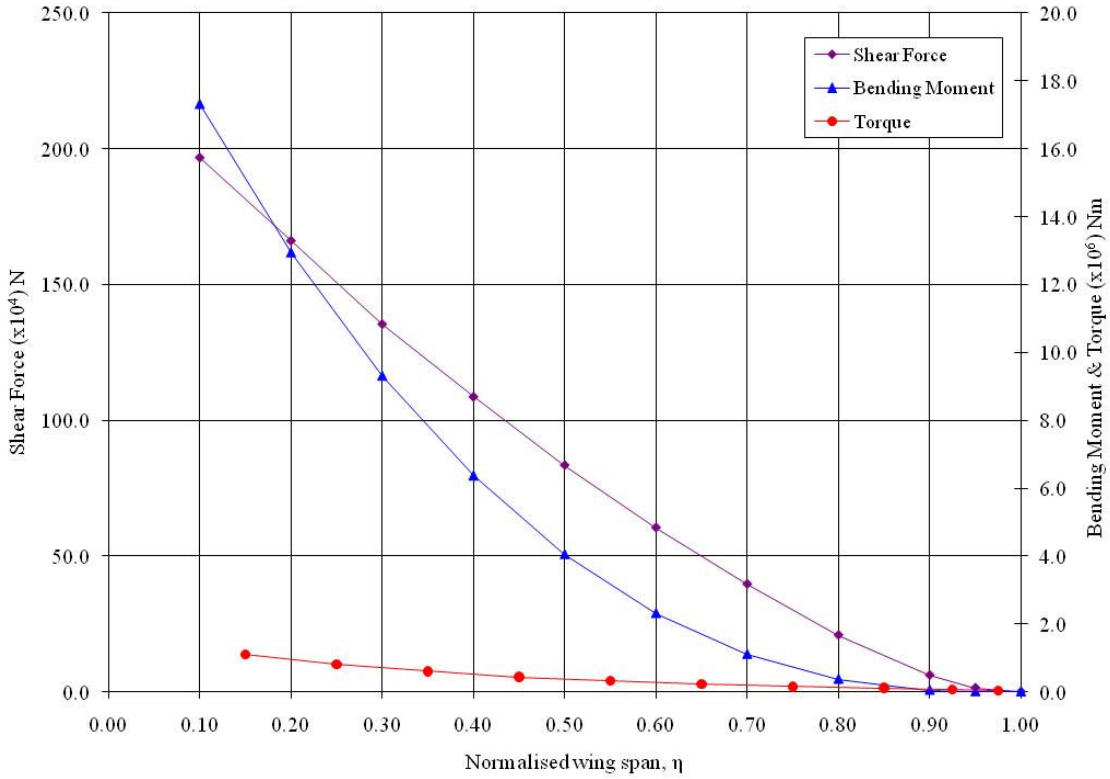

Figure 5.6 Span wise load distribution curves

5.3 Global model analysis using a "beam-cell" model

Finite element analysis is a process that takes an actual structure, subject to its constraints including attachments to other structure, and converts the structure and its environment into a mathematical description in a form that can be assessed using a computer. The output of the assessment is then converted back into parameters that relate to the real world behaviour of the structure (Morris, 2008).

In the case of the blended wing body aircraft being assessed in this project, a real world example does not exist. The purpose of this project is, therefore, to identify the issues associated with wing to fuselage integration in blended wing body aircraft and identify solutions to possible problems that may arise.

A possible approach to finite element analysis is the multi-model approach whereby a low fidelity analysis model with relatively few elements or low order elements is created to provide an initial view of the structure, identifying for example major load paths and inertia characteristics. Once the initial configuration has been established, higher fidelity models can be created for a more detailed assessment of the structure being assessed.

5.3.1 Initial global model

The multi-model approach was the strategy adopted for this assessment initially with a whole wing FE model that comprised two dimensional quadrilateral (QUAD) and triangular (TRI) shell elements numbering in excess of 10,000 elements as illustrated in figures 5.7 and 5.8 to provide an understanding of the structural characteristics of the airframe and its response to structural loads.

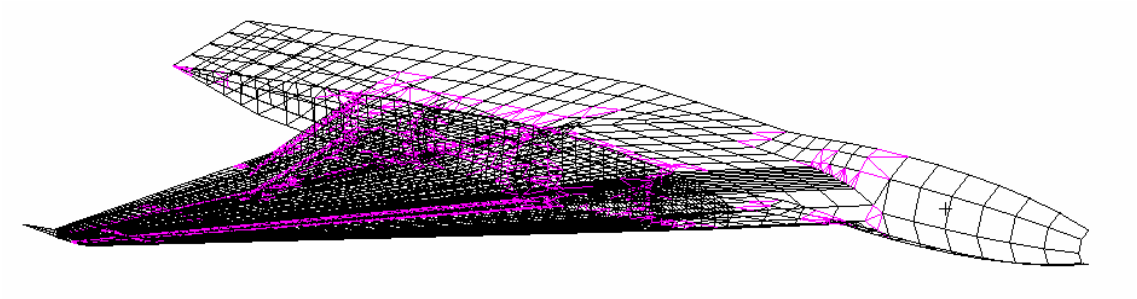

Figure 5.7 Original BWB aircraft finite element mesh

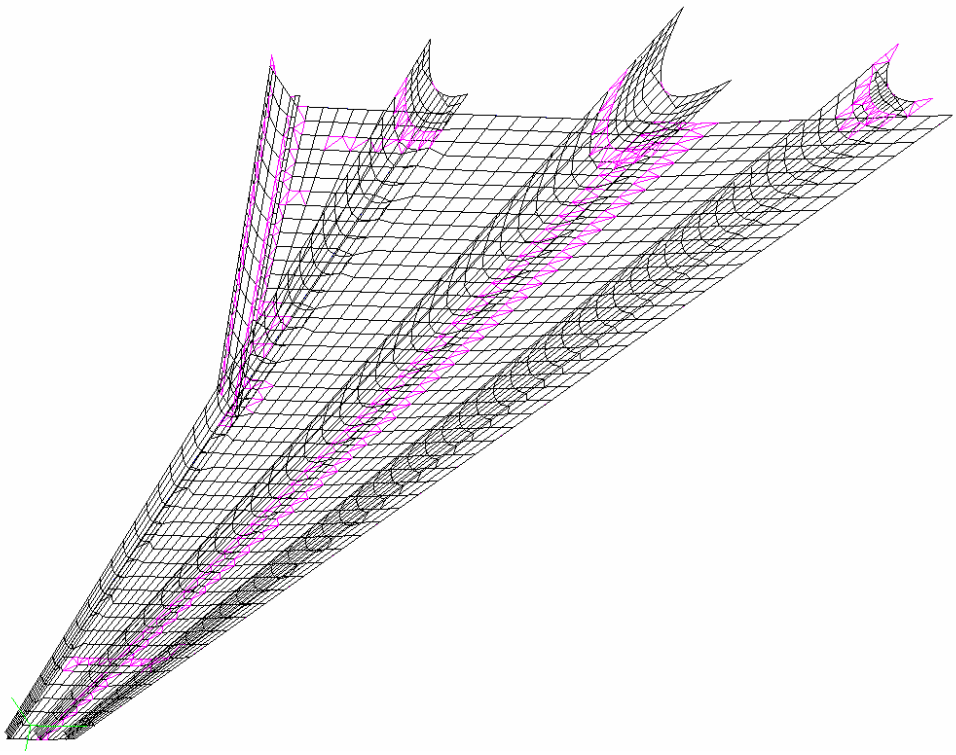

Figure 5.8 View of BWB aircraft bottom skin and spars finite element mesh

The spars were modelled such that they terminated within the fuselage and inboard of, rather than at, the wing root as shown in figures 5.8 and 5.9, thereby facilitating gradual load transfer into the fuselage shell which is a feature of the proposed joint design. The "global" wing FE model presented in figures 5.7 and 5.8 was a coarse mesh with element dimensions typically 1.0 m x 1.0 m and did not include stringers as it was intended to be used to identify potential "hot spots" in the airframe. A detailed model

with a more accurate representation of wing structure was to be created once the "hot spots" on the wing had been determined.

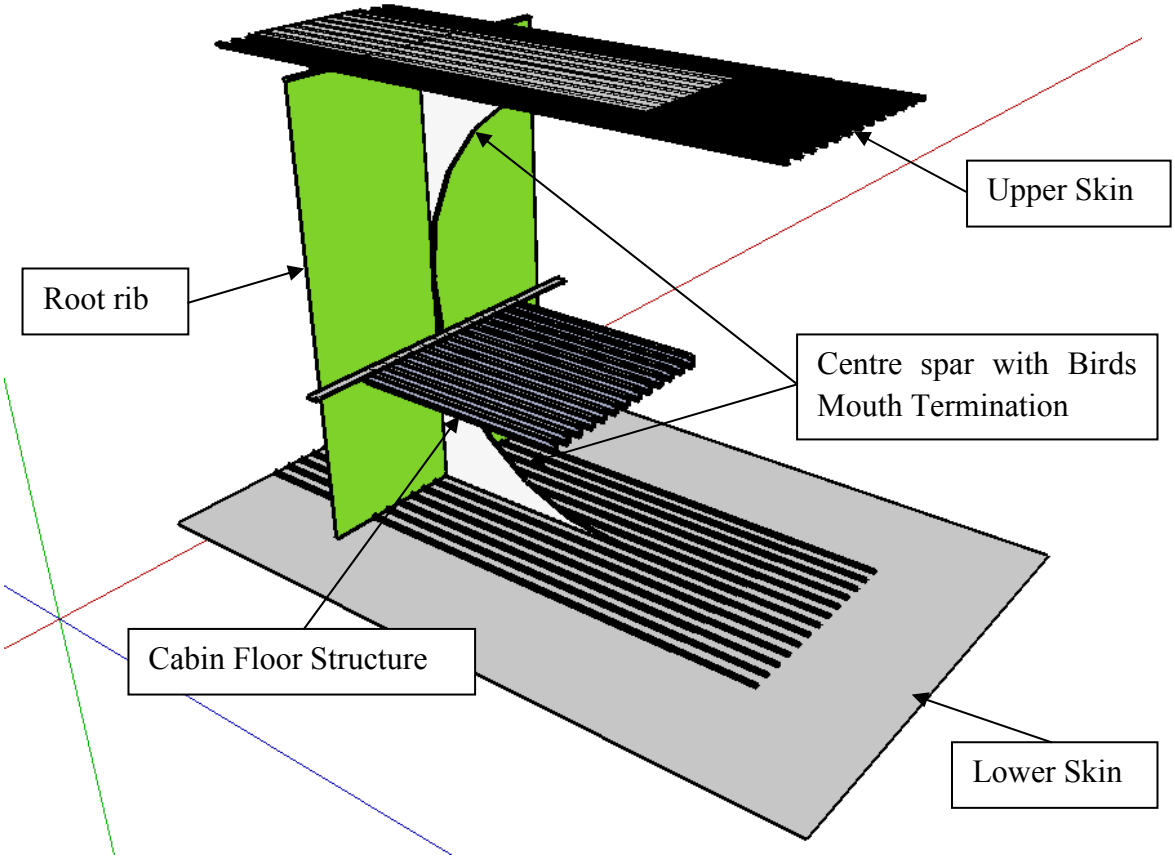

Figure 5.9 Isometric view of wing model illustrating spar termination within wing

After much deliberation, it was decided that although the whole wing model would have helped with an understanding of the hot spots on the wing and because the focus of the assessment was on the wing root, it would be more appropriate to use a low fidelity model to assess loading at the wing root and a higher fidelity finite element model for a more detailed assessment.

5.3.2 Global-local modelling strategy

The multi model global-local strategy and approach was subsequently adopted in this work using a coarse beam-cell model for the global, low fidelity analysis and using the resultant data from the global model to determine the input loads for the local high fidelity FE model. The proposed wing root concepts that demonstrate how continuous wing skin can be maintained at the wing/fuselage interface thus improving the efficiency of the structure have been discussed in chapter 4.

The continuation of wing structure at the fuselage interface and the absence of, in contrast to the presence of, a discrete joint at the wing is one of the claims to novelty of this design which is explored in greater detail in chapter 4.

The use of a global 3-cell box model of the wing root, coupled with a local FE model with 2D quadrilateral (QUAD) and triangular (TRI) shell elements and 1D bar elements instead of a full wing model which is discussed in detail in the section following, facilitates an early focus on wing/fuselage integration and associated structural design and damage tolerance issues. The derived SMT loads at the wing root were, therefore, applied to a thin-walled 3-cell box idealisation of the research aircraft root joint structure illustrated in figure 5.11, using the thin-walled box structure analysis computer program TWboxc3.exe similar to that described by Guo (2002).

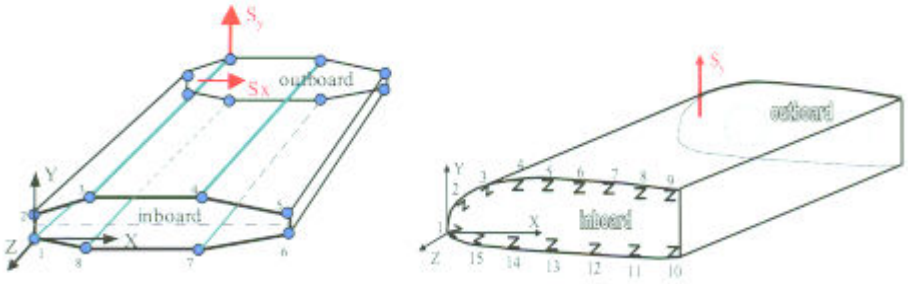

Figure 5.10 Idealised thin walled structures

The thin-walled box structure analysis computer program TWboxc3.exe only takes boom areas into account when determining geometrical properties such as the first and second moments of area of the structural item being analysed as illustrated by Figure 5.10. From engineering bending theory, the shear flow in the skin panels of a symmetrical box section subjected to shear forces as illustrated above can be written as:

$$q_s = -\frac{S_y}{I_x}\sum_{r=1}^{n} A_r \times y_r - \frac{S_x}{I_y}\sum_{r=1}^{n} A_r \times x_r + q_0 \tag{5.6}$$

For an unsymmetrical box section as illustrated above, the shear flow in the skin panels can be expressed as:

$$q_s = -\left(\frac{I_y}{I_x I_y - I_{xy}^2} S_y - \frac{I_{xy}}{I_x I_y - I_{xy}^2} S_x\right)\sum_{r=1}^{n} A_r y_r \ldots$$
$$\ldots - \left(\frac{I_x}{I_x I_y - I_{xy}^2} S_x - \frac{I_{xy}}{I_x I_y - I_{xy}^2} S_y\right)\sum_{r=1}^{n} A_r x_r + q_0 \tag{5.7}$$

where A_r is the rth boom cross-sectional area, y_r and x_r are the distance of the centre of the rth boom from the X and Y axes, S_x and S_y are shear forces applied in the X and Y directions, I_x, I_y and I_{xy} are the second moments of area and product of moments about the X and Y axes respectively (Guo, 2002). The above "beam-cell" analysis program also has the capability for analysis of multi-cell beams. Assumptions made for the thin

walled box idealisation are detailed in Table 5.10 below. A box length of 1000mm was selected as typical of the rib pitch to be applied to the wing. The other geometrical properties for the model were determined as typical of conventional wing root structural components.

Table 5.10 Assumptions for "beam-cell" model

Description	Value
Skin thickness, t_{skin}	10 mm
Spar web thickness, t_{spar}	10 mm
Box length, L	1000 mm
Stringer cross-sectional area, A_{st}	240 mm^2
Spar cap cross-sectional area	480 mm^2

Note: Loads act at (the local wing centre of gravity) 40% chord.
At the outboard rib position, X-coord of Sy = 7806 mm, Y-coord of Sx = 0 mm
Thicknesses set at 10 mm for low fidelity global model.

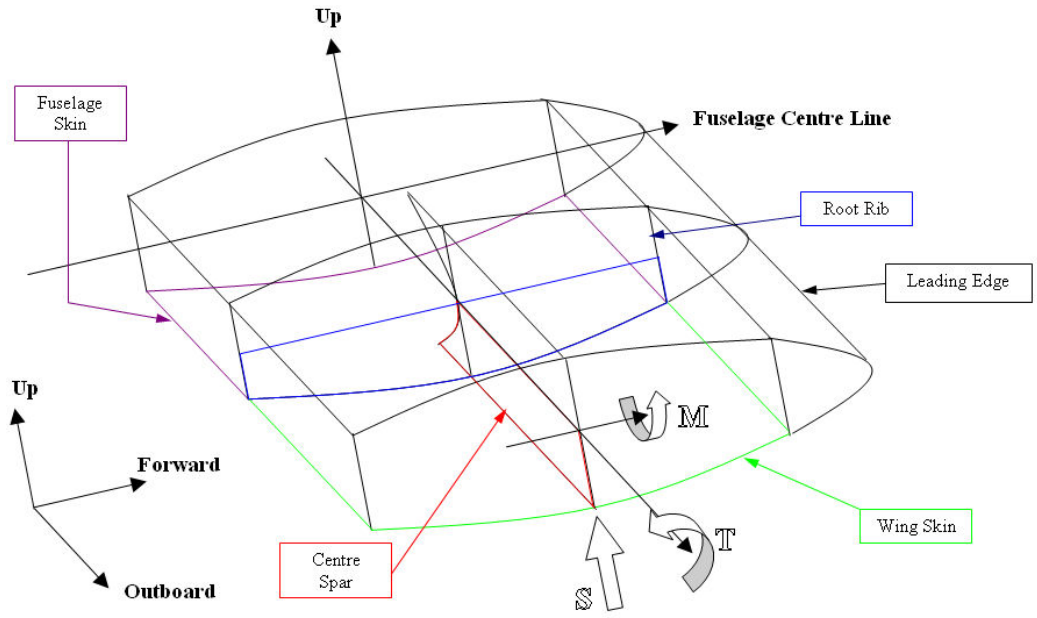

Figure 5.11 3-cell box model

The project aircraft wing comprises of 3 spars (front, centre and rear) and a false rear spar thus defining a 4 cell box. The wing box was however modelled as a 250 boom three cell box, as shown in Figure 5.11, instead of a four cell box, making the results slightly more conservative. The input data comprising of the data in Table 5.10 above and the coordinates of each stiffener (stringer and spar cap) and the results of the analysis are presented in Appendix E. The results of the global model are summarised as follows:

- Maximum limit tensile stress in stiffeners at 2.5g = 164.2 MPa
- Maximum limit shear stress in skin panels at 2.5g = 18.97 MPa

The maximum limit tensile stress of 164.2 MPa was obtained for the stiffener representing the lower centre spar cap. The maximum limit shear stress was obtained for a skin element on the upper surface of the D-nose forward of the front spar. As discussed previously in section 5.2.6, the structure is required to be designed to be capable of withstanding ultimate loads. A safety factor of 1.5 was therefore applied to the limit stresses yielding the following design stresses:

- Maximum ultimate tensile stress in stiffeners at 2.5g = 246.3 MPa
- Maximum ultimate shear stress in skin panels at 2.5g = 28.46 MPa

A rough order of magnitude check of the calculated limit shear stress was performed using Maxwell's theorem of reciprocal rotations for a four cell box with a stringer pitch of 163 mm and 200 stringers. The assessment was performed using a spreadsheet which yielded a limit shear stress of 12.65 MPa (ultimate stress of 18.98 MPa) confirming the conservative nature of the results obtained from the global model. Although the check shows that the calculated ultimate shear stress is below 30 MPa for both models which is in line with expectation due to the depth of the wing root, the differences between the two models are considered significant enough to result in the large differences in percentage terms between the results obtained from both models.

An additional check for shear buckling in the skin was undertaken to verify the results obtained from the global model. The equation for shear buckling is:

$$F_{s,cr} = K_s \eta_s E \left(\frac{t}{b} \right)^2 \tag{5.8}$$

Where, $F_{s,cr}$ is the critical buckling shear stress, K_s the shear buckling factor is 8.3 for a panel with clamped edges, E, young's modulus is 72000 N/mm^2, t skin thickness is 10 mm and b panel width is taken as 166 mm. From equation 5.8 and the data above, $F_{s,cr}/\eta_s$ was determined as 2168.67 MPa which corresponds to a critical shear buckling stress of 172 MPa for 2024 T3 (Clad) material (Niu, 1999) confirming that the applied shear stress was well below the critical buckling stress of the configuration being assessed at the wing root. Inspection of the data also confirmed that the applied shear stress was well below the critical buckling stress for a conservative scenario of a panel with hinged edges with a shear buckling factor of 5.0.

$$F_{c,cr} = K_c \eta_c E \left(\frac{t}{b} \right)^2 \tag{5.9}$$

A similar assessment to determine the critical buckling compressive stress using equation 5.9 gave a critical compressive stress of 282.7 MPa. Again, the applied compressive stress value obtained from the global model, if the compressive stress is assumed to be the same in magnitude to the tensile stress obtained from the global model, is below the critical compressive stress.

5.4 Local model analysis by finite element method

The second phase of the multi-model approach was the creation of a high fidelity local finite element model with more detail and elements to obtain a more accurate understanding of the structure being assessed. From the low fidelity global model, an understanding of the local boom stresses and panel shear flows and stresses had been obtained.

The objective of the high fidelity local model phase was to create a finite element analysis model that predicts the behaviour of the blended wing body root joint to within specified accuracy levels. The design requirements of the blended wing body root include minimum weight, innovation applicable to blended wing, compliance with FAR 25 and capable of withstanding ultimate stresses due to the loading conditions identified in section 5.2.6. An additional requirement for the skin to be capable of withstanding a two bay crack with stable crack growth which is addressed in detail in chapter 6 was also considered during the finite element modelling phase. The stress information required for the crack growth assessment which is described in chapter 6 was also determined from the finite element model.

The design limitations that needed to be considered during the finite element analysis phase included restrictions on skin deflections, maximum allowable panel and stiffener stresses. FAR 25.305 requires that “the structure must be able to support ultimate loads without failure for at least 3 seconds”. The material ultimate strength was the criteria against which the ultimate stresses due to the loading conditions described in section 5.2.6 were assessed. Furthermore, “the structure must be able to support limit loads without detrimental permanent deformation”. For limit load cases, the criterion was the proof stress of the material. It will be seen later in the text that the critical design criteria was not strength. However, both strength requirements were met.

The process of seeking to represent potential real life structure by a mathematical model leaves scope for the introduction of errors that have an impact on the accuracy and veracity of the results obtained from a model. Assessments were therefore made to identify possible sources of error in the finite element modelling process and steps taken to review and quantify these potential error sources to minimise or control their impact on the outcome. Possible sources of error include, the representation of the structure i.e. representation of stringers and stiffeners by boom elements and skin and web by quadrilateral and triangular elements, the mesh density, the regularity of the mesh, the representation of stiffener to skin attachments and the representation of the applied

loading. The steps taken to minimise error are described in the paragraphs and sections following.

The direct and shear stresses derived from the 3-cell box low fidelity global model were applied to the high fidelity local finite element model of the wing root to identify potential structural weaknesses in the proposed design. As noted earlier, the results obtained from the 3-cell low fidelity global model showed that the boom element representing the lower flange of the centre spar returned the maximum limit tensile stress of 164.2 MPa (246.3 MPa Ultimate), identifying that region of the wing root as requiring further assessment. Sections of the main structural components including the wing centre spar, wing bottom skin, wing root rib, stringers, fuselage longitudinal stiffeners and rib 2 outboard of and adjacent to the root rib as shown in figures 5.12, 5.13 and 5.14 below were represented in the local FE model.

The loads were applied to the local FE model in order to replicate the loading conditions at the wing root whilst taking local geometry into account. The constraints were applied such that the stress distribution in the skin reflected the expected stress distribution in the vicinity of the root rib. This is discussed in more detail in the sections following.

5.4.1 Selection of location for local model

The proposed wing root design is described in section 4.3 where the applicability of the bird's mouth type termination to the spars is briefly explored. As one of the objectives of this research project is to demonstrate the feasibility of the novel bird's mouth type termination, the focus of the modelling activity centred on the wing root at the centre spar and associated structure which is consistent with observations from the results of the global model made earlier. Details of how the selected structure was represented in the local model are discussed further in the sections following.

5.4.2 The Mesh

Best results are obtained in finite element analysis when there is equal distribution of strain energy among constituent elements. Furthermore, four noded elements for example, are based on a perfect square. If an element has the same shape as the base shape, the mathematical process of creating the matrix is straightforward (Morris, 2008). Distortion has an impact on accuracy so the mesh was created to be as even as possible. This was more easily achieved on the fuselage skin side of the model. The stringers are at an angle to the fuselage because of the dihedral on the wing so the wing side elements had to be skewed. This source of error was noted. Other attempts at minimising error included keeping the edges of elements as straight as possible, keeping taper to a minimum, matching curvatures and offsets on opposite edges and faces and using optimal sample points where appropriate.

The mesh had to be of a significant density for accuracy. The model is comprised of 114,339 elements. The wing centre spar, wing skin and wing root and outboard ribs

have been modelled using 2D quadrilateral shell (CQUAD) elements. The stringers and stiffeners are modelled by 1D bar (CBAR) elements. Aluminium alloy 2024 material data was assumed for all the components and the stress analysis is linear elastic. Figure 5.15 provides an illustration of the components represented in the FE model. The stringer pitch of the proposed wing had been set at 163 mm approximately and the 2D quadrilateral element area was limited to 20 mm x 20 mm approximately. The selected element density was eight 2D quadrilateral elements per stringer bay. The 2D quadrilateral element geometry is illustrated in figures 5.16 and 5.17.

Some of the other possible sources of error identified include the manner in which the structure is idealised. For this assessment, the skins and spar and rib webs are modelled as quadrilateral or triangular panel elements whilst the stringers and stiffeners are modelled as boom elements. The whole assembly has the form characteristic of shell/plate. The thicknesses of the skin and spar and rib webs are small compared to the other significant dimensions, homogenous isotropic material is employed throughout and through thickness or out-of-plane shear stresses are unlikely to be significant so the quadrilateral and triangular elements are deemed appropriate for this assessment. The use of triangular elements has been kept to a minimum: these were used only when necessary to keep the mesh as even as possible.

The main function of stringers and stiffeners is to carry end load and to react any bending in the panels. As a result, bar elements are employed as adequate for the requirements of this assessment.

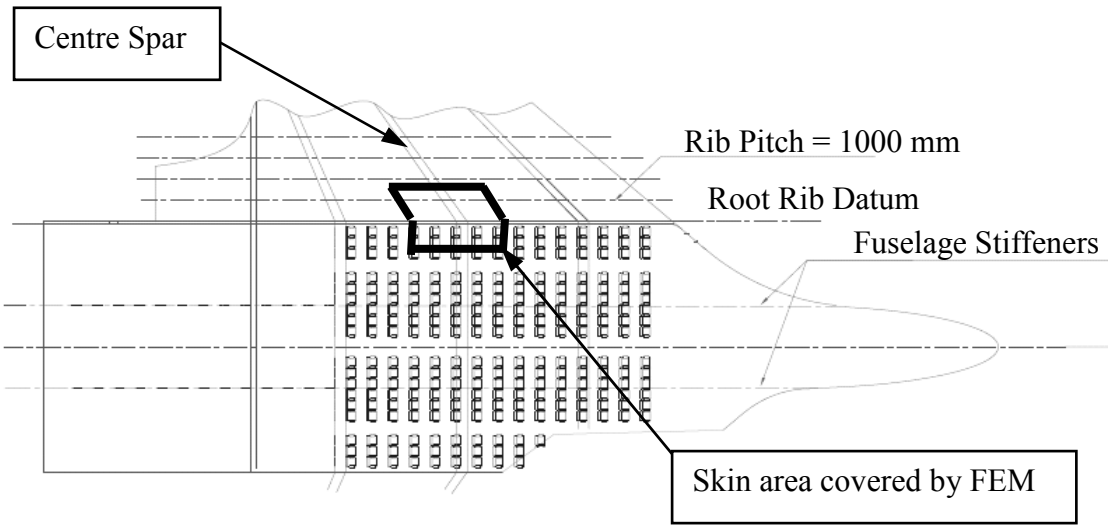

Figure 5.12 FE model of the skin section

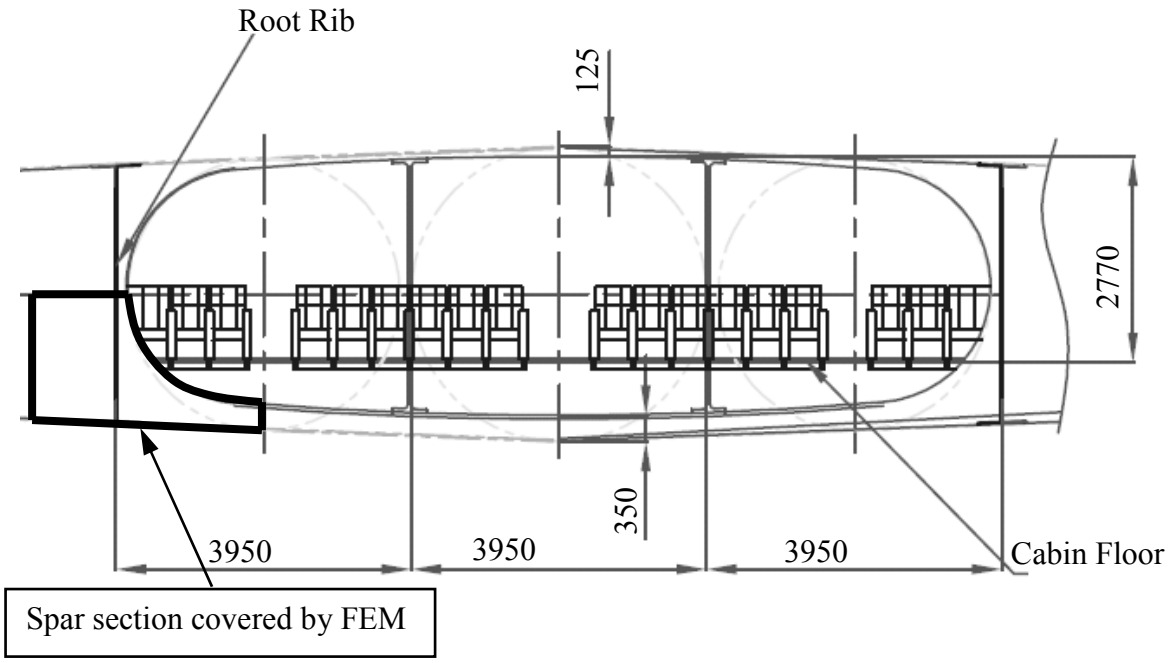

Figure 5.13 Spar section covered by FE local model and its position in the structure

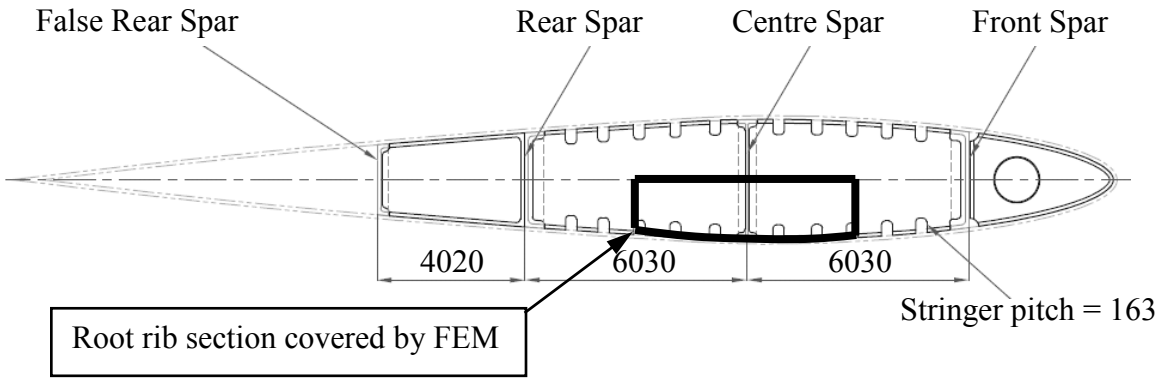

Figure 5.14 Rib section covered by FE local model and its position in the structure

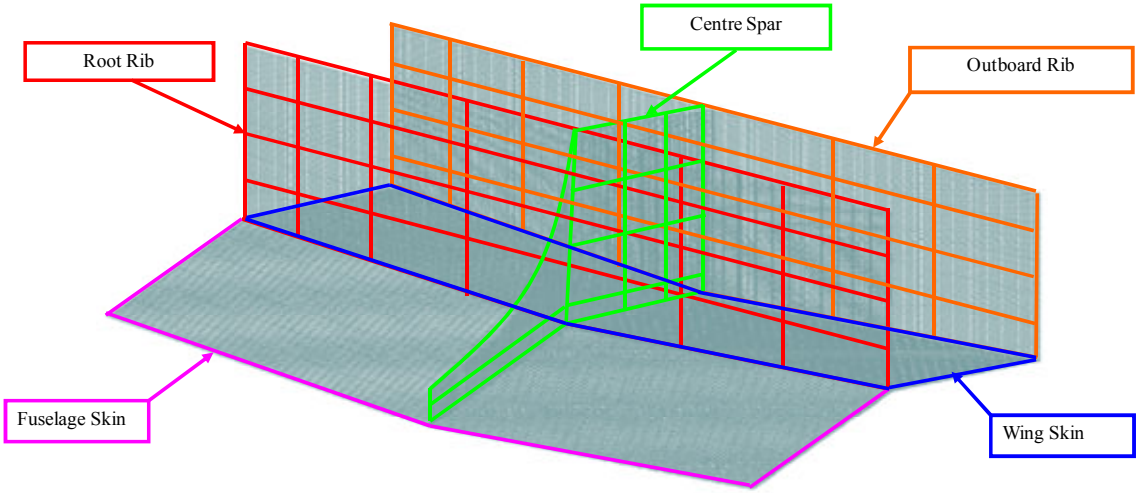

Figure 5.15 Structural items included in FE model

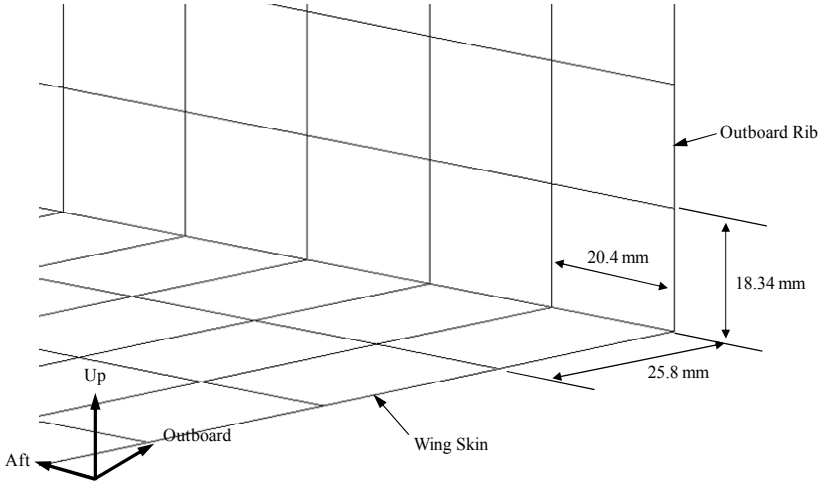

Figure 5.16 FE Model element dimensions

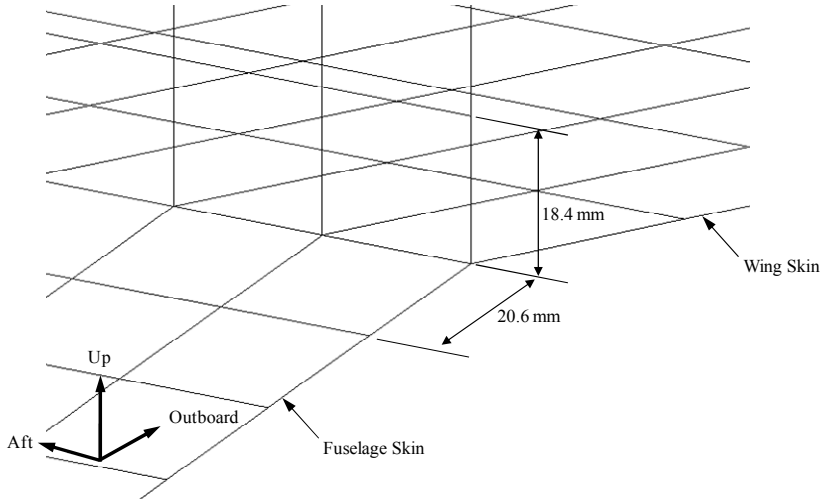

Figure 5.17 FE Model element dimensions

5.4.3 Magnitude, direction, type of loading applied and model restraints

Loading representing the three design cases specified by FAR 25.365 and FAR 25.303 were applied to the FE model. The three load cases considered were:

1. 2.5g V_D x 1.5 Ultimate Load case
2. (2.5g V_D + 1ΔP) x 1.5 Ultimate Load case
3. 2ΔP Ultimate Load case.

As discussed previously, wing bending stresses were derived for the 2.5g V_D limit case and an ultimate factor applied. The most conservative limit stress of 164.2 MPa (246.3 MPa Ultimate) was observed to occur at the lower spar cap and the ultimate equivalent of that stress was applied to the elements representing the spar cap at the outboard rib as a fixed displacement.

The skin and adjacent stringers were assumed to strain with the spar cap and the same fixed displacement was applied to the skin and stringer nodes. The smaller cross-sectional areas of the stringers meant that the resulting stresses in the stringers were consistent with that obtained from the global model. The fixed displacement was applied in an outboard direction to effect a tensile stress in the spar cap, stringers and skin.

The skin and spar stresses obtained from the global model were also applied at nodes as fixed displacements. These were applied to the spar web nodes in an upwards direction and in the skin away from the centre spar in accordance with the results of the global model. The magnitude of the tensile stresses however, was significantly larger than that required to replicate shear in the skin and the tensile fixed displacements are therefore the dominant component of the applied skin/stringer loads.

The fuselage pressures were applied downwards on the skin and outboard on the outboard rib. Further details of the applied loading and model constraints are discussed in the sections following.

5.4.4 Stringer and skin boundary conditions and applied loads

Program TWboxc3.exe has been used to determine local input loads for the high fidelity local FE model. Program TWboxc3.exe assumes that the skins only carry shear load. The contribution of wing skin structure in reacting wing bending loads is accounted for by the stringer cross-sectional area. The output information from Program TWboxc3.exe is presented in boom stresses and skin shear stresses and shear flows. This posed some challenges in applying the derived loads to the local FE model as the skin contribution had to be accounted for.

The bottom skin is modelled with constraints applied at the edges of the skin section as illustrated in figure 5.18. There are no constraints on rotation and the spar and ribs are assumed to act as simple supports perpendicular to the skin.

Vertical constraints are applied at the fuselage cut, to react the applied spar web shear and fuselage pressure loads.

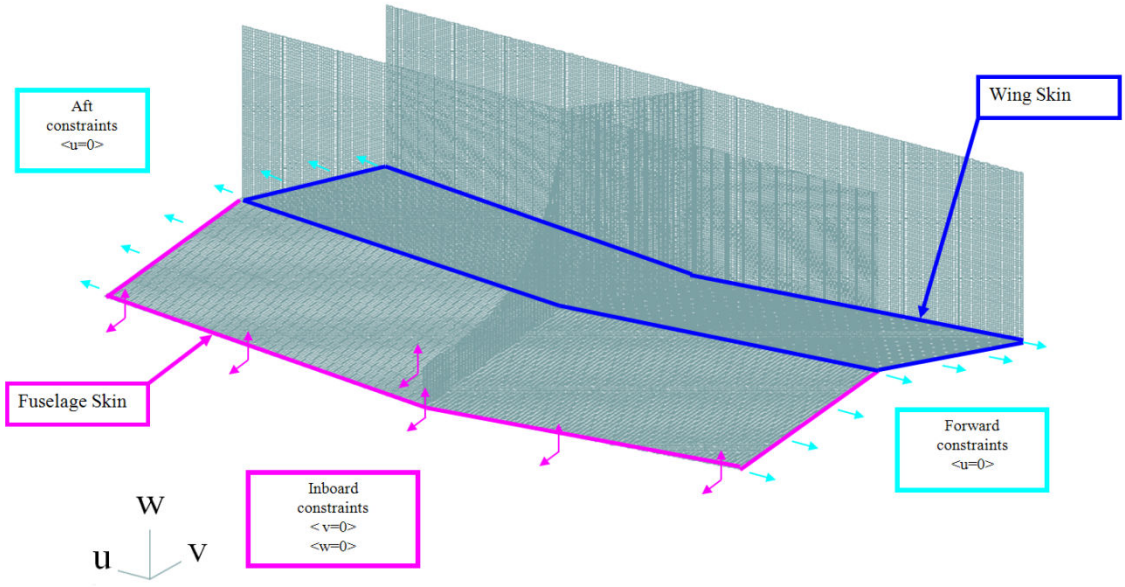

Figure 5.18 Bottom skin with constraints and applied load

Global stresses from the TWboxc3.exe model are replicated as closely as possible. The effective area is assumed to comprise of the stringer and adjacent skin. These loads are then applied as fixed displacements at the relevant FE nodes. There are no constraints on rotation and the spar and ribs were assumed to act as simple supports perpendicular to the skin.

The skin and stringer loads are applied as fixed displacements in the model as illustrated by figure 5.19. The fixed displacement required in each stringer to achieve the required stress is determined as:

$$\delta l = \frac{\sigma \times l}{E} \tag{5.10}$$

where δl is the fixed displacement, σ is the applied stress, l is the length of the stringer section and E is the young's modulus of the stiffener.

Possible sources of error in applying the skin and stringer boundary conditions include the location of the boundary of the skin section being analysed and the representation of stringer stresses. Although the structure is symmetrical about the fuselage centreline, setting the restraints at the fuselage centreline would have been unrepresentative as the low fidelity model is based on the wing root geometry with a box length equivalent to one rib pitch. The restraints are set at the point where the location of minimum spar depth occurs in order to ensure that the bird's mouth termination is accounted for.

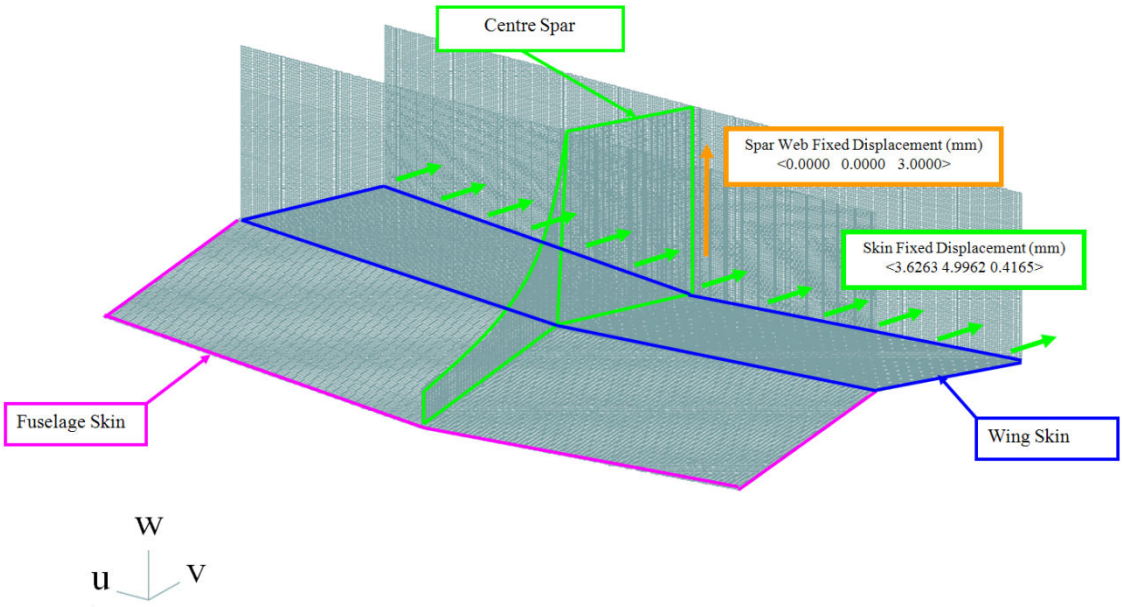

Figure 5.19 Applied fixed displacements

5.4.5 Spar boundary conditions and applied loads

The spar flange loads are derived and applied in a similar manner to the stringers. A fixed displacement, similar to that applied to the stringers to produce the required stress in the stringer flange has been applied.

A previous limit stress assessment of the bird's mouth termination had been undertaken without specific displacements applied to the spar web. This had been done because the low magnitude of the spar web shear stresses and the inclusion of the outboard rib in the model meant that the applied fixed displacement at the skin and rib nodes accounted for the small shear component in the spar web. This ultimate stress assessment has fixed displacements applied to the spar web which is conservative. The difference is however not observed to be significant due to the low magnitude of the spar shear stresses.

The shear stresses in the spar web were therefore replicated as a fixed displacement applied to the shear web at the stiffener ends as illustrated by figure 5.19. The low magnitude of the shear stresses obtained from the global model is reflected in the shear web fixed displacement.

The application of spar flange and web stresses as enforced displacements replicate the stresses obtained from the global model more accurately and minimises the risk of error.

5.4.6 Root rib boundary conditions and applied loads

Vertical constraints were applied to the root rib at the cut section to react the effect of the applied internal pressure on the bottom skin. The internal pressure had previously been applied to the inboard face of the root rib. However the pressure boundary was subsequently moved to the next adjacent outboard rib as other studies have shown it

more appropriate to locate the pressure boundary outboard of the root rib. Restraints were also applied to the vertical edges to replicate the effect of adjacent rib structure.

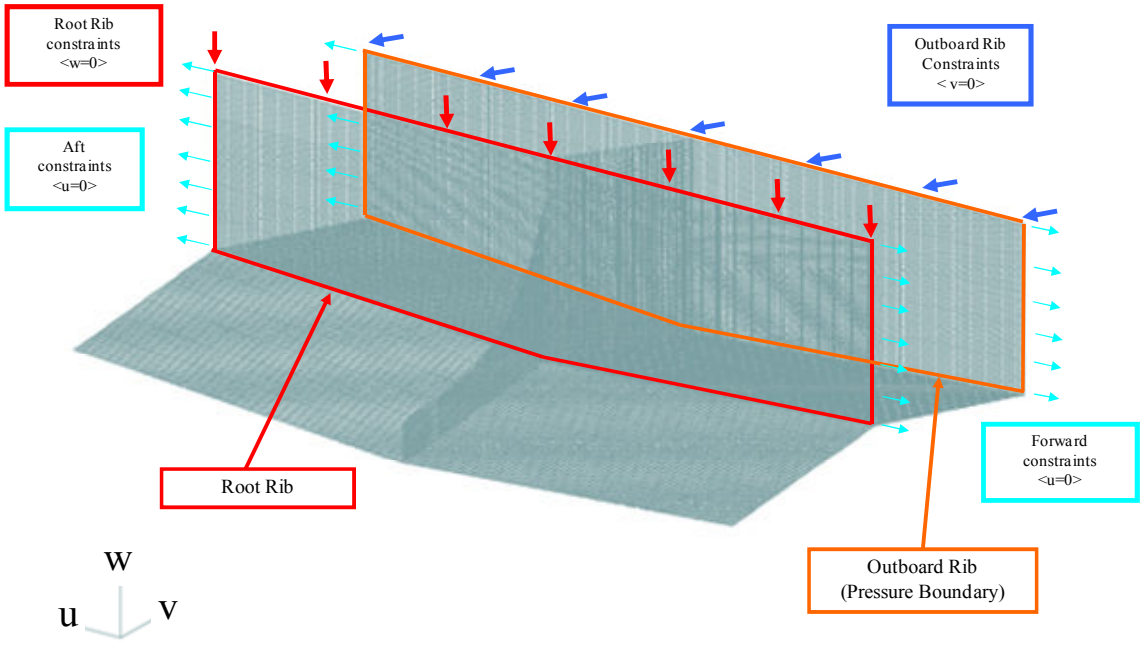

Figure 5.20 Root rib constraints

5.4.7 Outboard rib boundary conditions and applied loads

The outboard rib was included in the model after initial runs had been conducted because previous studies have shown it more appropriate to locate the pressure boundary outboard of the root rib. Horizontal constraints were applied to the outboard rib in the manner illustrated by figure 5.20 at the cut section to react the effect of the applied internal pressure on the outboard rib. The internal pressure was applied to the inboard face of the outboard rib. Additional restraints were applied to the free edges to replicate the effect of adjacent rib structure. The applied constraints meant that the outboard rib was free to move in a vertical direction and also to rotate around the horizontal cut section as the wing deforms due to the applied wing bending loads.

5.4.8 Applied fuselage pressure loads

Fuselage pressurisation loads were applied to the local FEM in addition to the wing bending flight loads obtained from the global model. The maximum positive burst pressure at an altitude of 43,000 ft is defined (Niu, 1990) as 8.85 psi i.e. 0.0610186 N/mm^2. As discussed in section 5.2.6, FAR 25.365 requires the structure to be designed to withstand the pressure differential loads corresponding to the maximum relief valve setting multiplied by a factor of 1.33 for operation to altitudes of 45,000 ft omitting other loads. Furthermore, FAR 25.303 requires a safety factor of 1.5 to be applied to the

prescribed limit load. A design pressure of 2ΔP which is 0.1220372 N/mm^2 was therefore applied. The pressure boundary is shown in Figure 5.21.

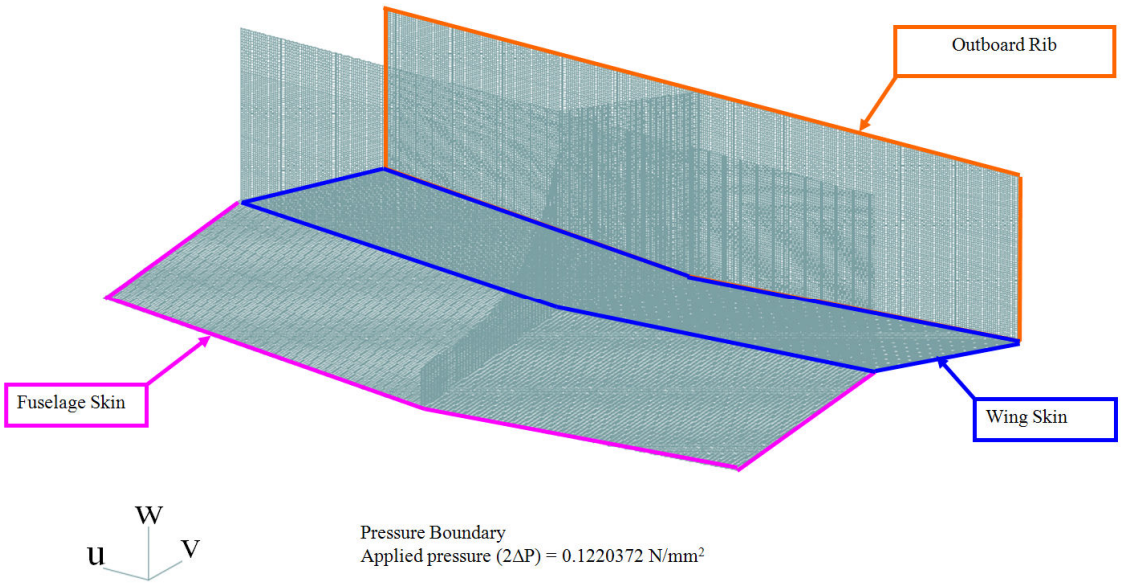

Figure 5.21 Pressure boundary

5.5 Design iterations

In seeking to reduce the differences between the finite element simulation and the actual performance of the blended wing body aircraft, it was necessary to perform the simulation in stages.

Most of the design iteration in the FE model centred on the skin. This was because a significant amount of additional work was required to address skin deflections due to fuselage pressurisation. This is discussed further below. The main changes made to the spar and the bird's mouth cut-out was an increase in spar web thickness. The global model had assumed spar web thicknesses of 10 mm. The low magnitude of the resultant shear stresses meant that lower spar web thicknesses were possible. The spar web thickness was initially set to 1 mm for the earlier iterations of the FE model. The web thickness was subsequently increased to 2 mm to achieve a further reduction in spar web stresses. Scope still exists for achieving significant reduction in spar web stress levels by increasing web thickness. However, as the resultant stresses are within the material allowables and the spar web observed to be the less critical component compared to the skin, more effort was directed towards optimising the skin. The changes made to the spar are included in table 5.11.

Several iterations of the FE analysis were therefore required in order to optimise the proposed wing root design. Quite early in the analysis, skin thicknesses of 1.0 mm were shown to be adequate for reacting wing bending loads. This is because the large depth of the wingbox (3497 mm at the wing root) meant that the resultant direct tensile and

compressive stresses were much lower than would be expected for a comparative wingbox of a thinner wing depth. It meant that it was possible to achieve As/bt ratios of 1.46 in the wing skin which is an important consideration in damage tolerant design.

The application of internal fuselage pressurisation loads resulted in significant skin deflections which required attention. This is because the deflections if not addressed would have a compromising effect on the aerodynamic characteristics of the aircraft. Skin deflections were a concern and skin thicknesses were therefore increased from 1.0 mm to minimise skin deflection. Skin thicknesses of 5.0 mm, 7.0 mm and 10.0 mm were assessed by FE modelling and a skin thickness of 10.0 mm was selected for the final design as it returned the lowest deflections. Stringer and longitudinal stiffener sections were also increased to improve the bending stiffness of the skin panels.

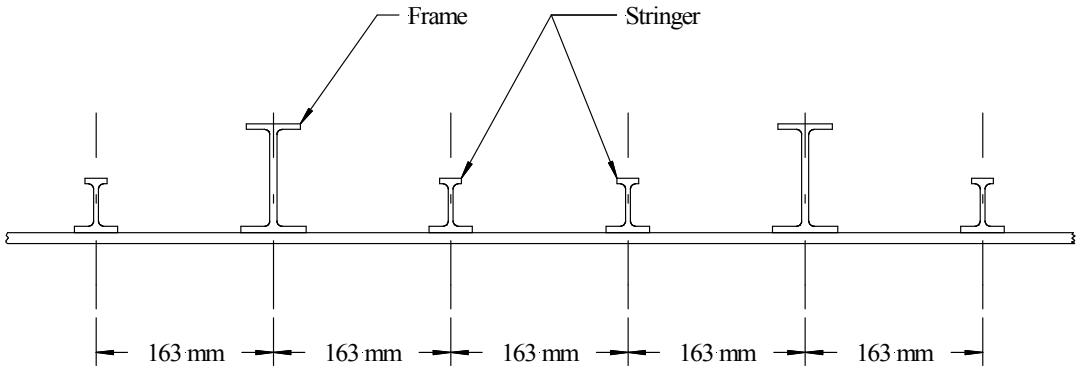

Figure 5.22 Arrangement of stiffeners on skin panel

Table 5.11 Finite element modelling iteration loops

FEM Loop			Loop 1	Loop 2	Loop 3
Skin	Wing	Thickness	3 mm	5 mm	10 mm
	Fuselage	Thickness	2 mm	5mm	10 mm
Stringer		Type	Inverted T	I	I
		Area	240 mm^2	480 mm^2	515 mm^2
Longeron	Wing	Type	Top hat	Top hat	Inverted top hat
		Area	3300 mm^2	3300 mm^2	880 mm^2
	Fuselage	Type			I
		Area			3350 mm^2
Frames		Type			I
		Area			3350 mm^2
Spar	Web	Thickness	1 mm	2 mm	2 mm
	Flange	Area	480 mm^2	1000 mm^2	1000 mm^2

The model was originally created with stringers of 240 mm^2 cross-sectional area and a skin thickness of 1 mm yielding an As/bt ratio of 1.47. The need to increase the bending capability of the panels meant that stringer cross-sectional areas were increased to 515 mm^2 for skin thicknesses ranging from 5 mm to 10 mm yielding As/bt ratios ranging from 0.63 to 0.32. Also included were heavier I-section stiffeners (frames) illustrated in figure 5.22 with cross-sectional areas of 975 mm^2 replacing every third stringer to provide increased stiffness with As/bt ratios ranging from 1.2 to 0.6. These stiffeners run perpendicular to the fuselage centreline in the fuselage and perpendicular to the chord on the wing side. Additional longerons with cross-sectional area of 3350 mm^2 were also included that run parallel to the fuselage centre line to provide additional bending stiffness to react internal fuselage pressurisation loads. The changes in properties are presented in table 5.11.

5.6 Results under internal pressure loads

5.6.1 Introduction

The results of the FE analysis are presented and discussed in the sections following. Three loading conditions were assessed as follows:

1. 2.5g V_D x 1.5 Ultimate Load case
2. (2.5g V_D + 1ΔP) x 1.5 Ultimate Load case
3. 2ΔP Ultimate Load case

With the exception of skin and rib deflection assessments, the (2.5g V_D + 1ΔP) x 1.5 Ultimate load case consistently returned the highest stresses and all stress results presented below are therefore for that case. The skin and rib deflections were assessed using the 2ΔP Ultimate Load case as it gave the most conservative results for deflections.

5.6.2 Skins

MSC NASTRAN 2001 generates extreme fibre stress data for both faces of CQUAD4 shell elements which have a bending capability with a specified thickness. Fringe plots of the von-Mises and max shear stress distribution on the skins are presented in figures 5.23 and 5.24.

The results illustrated by the fringe plot in figure 5.23 show peak von Mises stresses in the region of 405 MPa to 435 MPa in the skin at the vertices of the model. The fringe plot has been limited to 435 MPa which is just below the ultimate tensile strength of 2024 Al Alloy of 438 MPa quoted in ESDU (2002) as any values greater than that are due to the applied constraints and therefore not taken into account. Most of the skin area show stresses in the range of 75 MPa to 315 MPa for the (2.5g + 1ΔP) x 1.5 Ultimate loadcase. Maximum stringer stresses in the region of 270 MPa which are consistent with the stresses obtained from the global model were also obtained. The peaks are located at the stringer restraints with much lower stresses being experienced away from

the restraints. This is due in part to the increased skin thickness required to reduce the deflection in the wing skin as a result of internal fuselage pressure.

The stress pattern obtained for von Mises stresses is repeated in the maximum shear stress fringe plot presented in figure 5.24. The peak maximum shear stresses are located at the vertices with a significant drop in magnitude at locations away from the attachments.

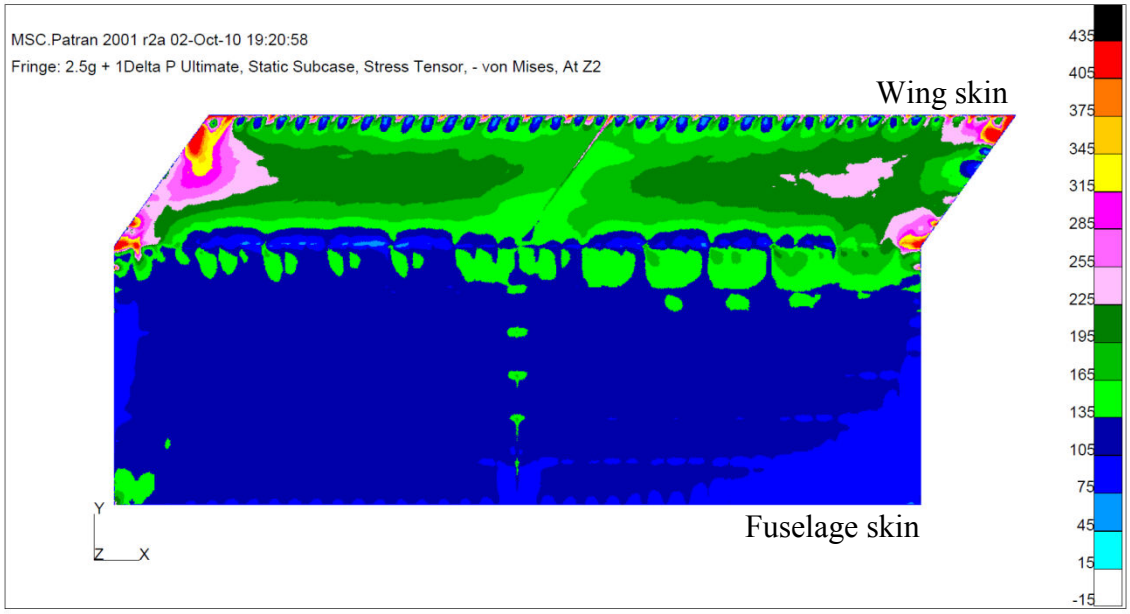

Figure 5.23 Von Mises stresses in wing and fuselage skins

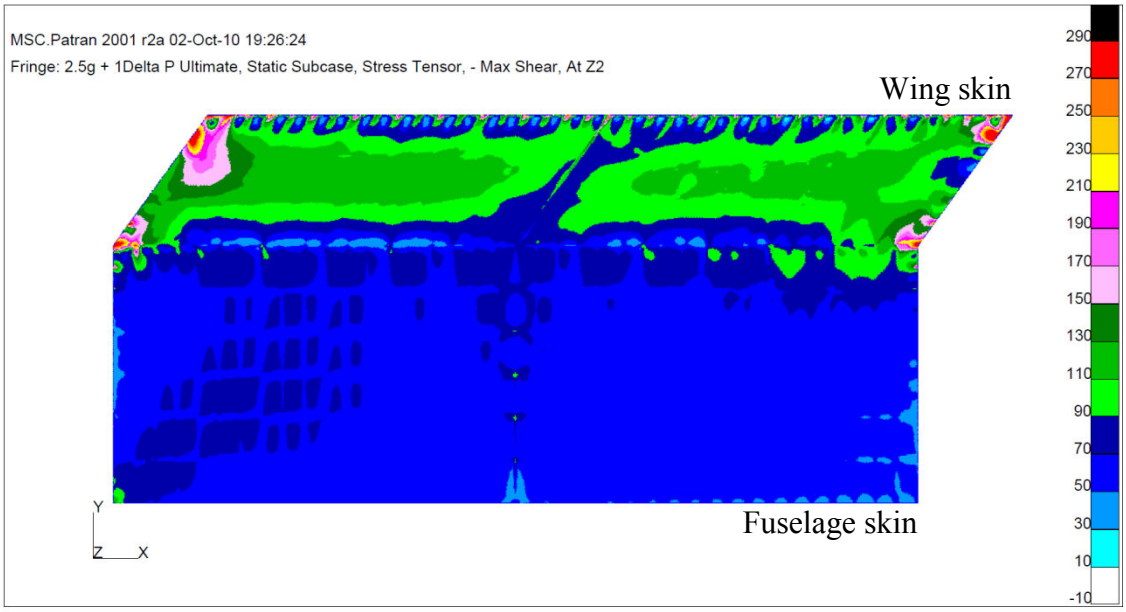

Figure 5.24 Max shear stresses in wing and fuselage skins

As discussed in the preceding section, the main criterion in determining final skin thicknesses was the need to reduce skin deflections. The lower magnitude of the stresses observed in the skin away from the vertices is a reflection of the final skin thickness selected. It should be noted that the peak stresses presented in these figures are extreme fibre stresses and are conservative. Average skin stresses would be applied in any subsequent analysis and would be of a lower magnitude.

5.6.3 Spars

Fringe plots for the (2.5g V_D + 1ΔP) x 1.5 Ultimate load case are presented in figures 5.25 to 5.27 for the centre spar. The plots show peak von Mises stresses in the 405 MPa to 435 MPa range with the web stresses much lower away from the peak stress. The spar web thickness is 2 mm.

The peak stress range of 405 MPa to 435 MPa shown in figure 5.25 occurs in the lower part of the spar web and the spar flange where fixed displacements have been applied to simulate the loading in the spar flange and web. The peak stresses are not independent of the applied boundary conditions and have therefore been limited to ultimate tensile strength of the spar material which is 2024 Al Alloy. Any stresses above the material allowable are localised and a function of the manner in which the loading has been applied and are therefore discounted. Away from the peak stress, the von Mises stresses range from 15 MPa to 345 MPa increasing from the cut section of the spar which is mid spar to the lower flange.

The fringe plots show an increase in web stress inboard of the root rib from the full depth web to the spar runout. The increase in stress at the most inboard end of the spar runout is also attributed to the applied restraint at the inboard end.

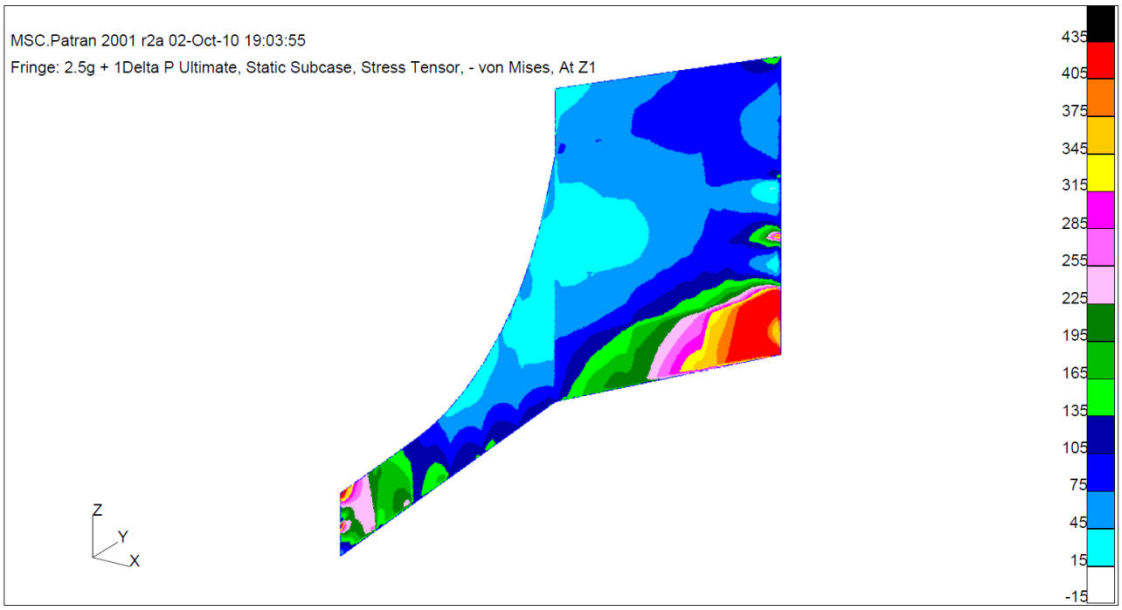

Figure 5.25 Spar von Mises stresses

Figures 5.26 and 5.27 illustrate the variation in local shear and maximum shear in the spar web. The magnitudes of the observed shear and maximum shear stresses fall below the shear strength of 2024 Al. alloy of 283 MPa. However, the trend of the shear patterns is of most interest. A definite change can be observed in the fringe plots at the spar joint with the root rib.

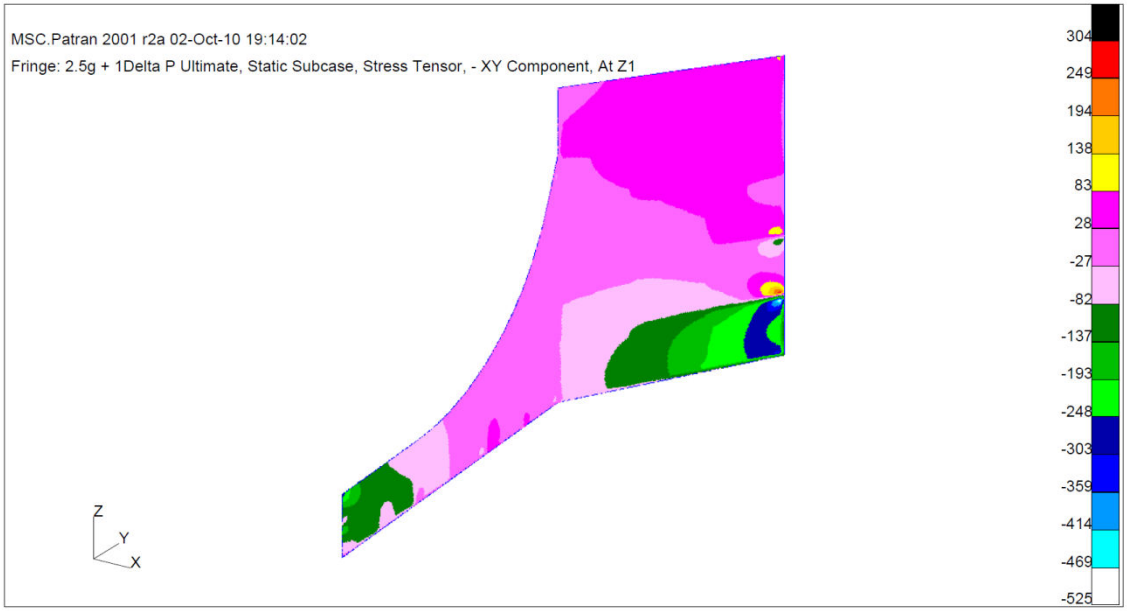

Figure 5.26 Shear stresses in spar

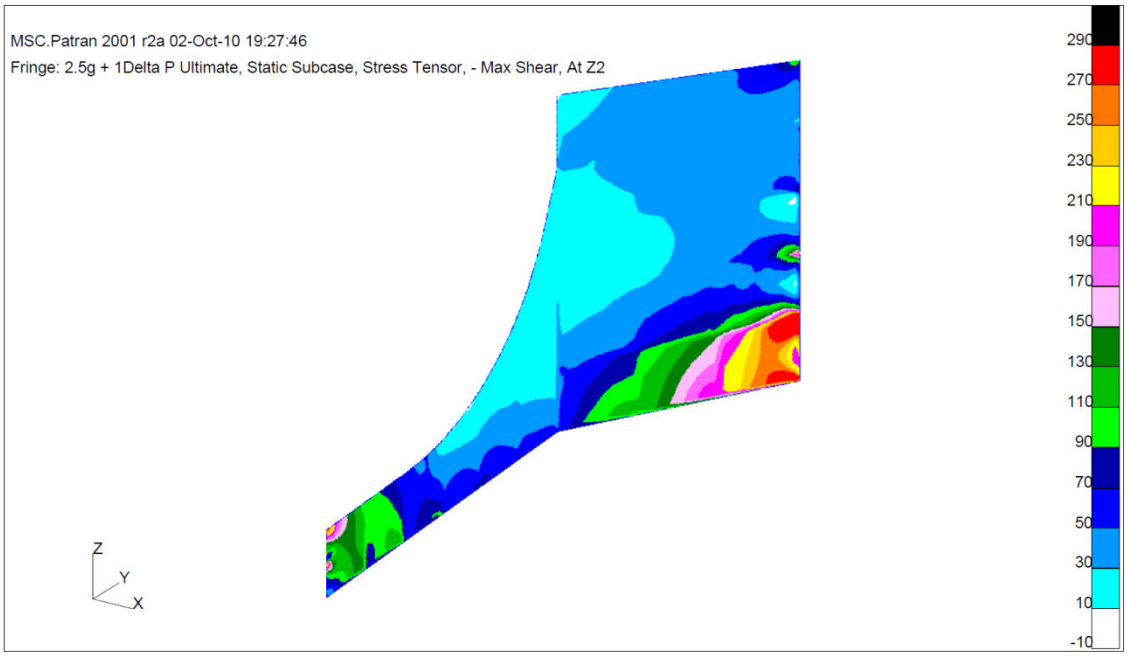

Figure 5.27 Maximum shear stresses in spar

The “bird’s mouth” type spar termination was designed purposely to effect gradual load transfer from the spar into the root rib and skin. This is demonstrated in figures 5.26 and

5.27 with a definite change in stress profile at the root rib location. A significant portion of the shear in the spar web is transferred to the root rib. Inboard of the root rib, a gradual increase in the spar web stresses as the spar depth decreases can be observed. With increasing load transfer into the skin, a further decrease in spar web stresses can be observed. The increase in spar web stresses at the spar web cut section is attributed to the application of boundary conditions as discussed previously and is therefore discounted.

5.6.4 Root rib and Outboard rib

The fringe plots for the (2.5g V_D + 1ΔP) x 1.5 Ultimate load case von Mises and maximum shear stresses in the root rib are presented in figures 5.28 and 5.29. The plots show maximum von Mises stresses in the rib web ranging from 135 MPa to 315 MPa. The peak values occur at the vertices of the model and are ignored for reasons discussed previously.

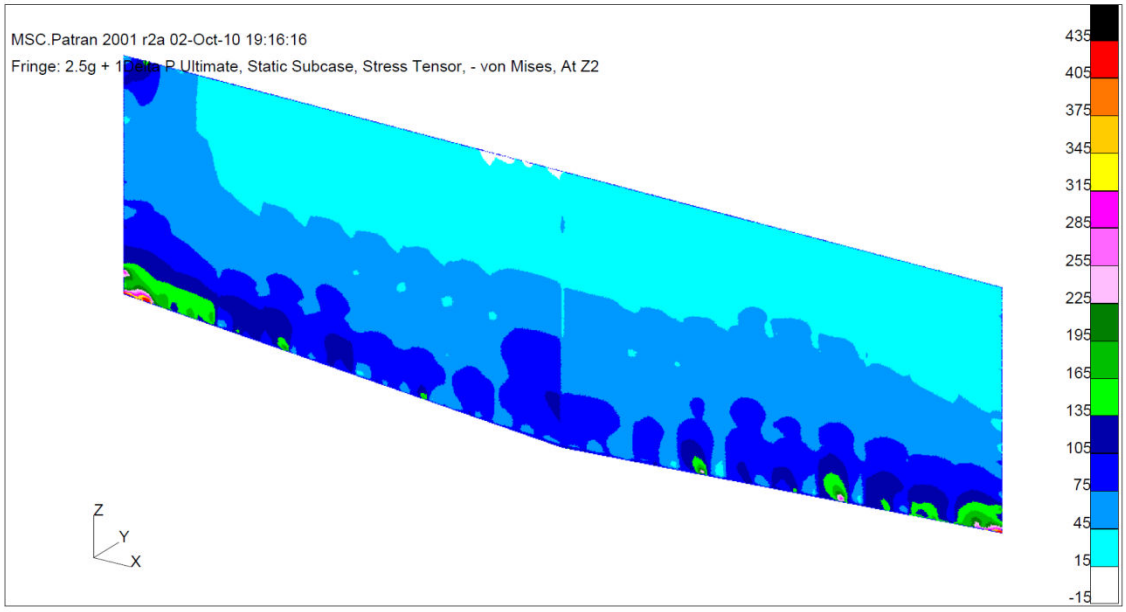

Figure 5.28 Root rib von Mises stresses

Away from the vertices, the von Mises stresses in the root rib web range from 15 MPa to 195 MPa and the maximum shear stresses from 15 MPa to 135 MPa reflecting the fact that the loading on the root rib web is much lower than the outboard rib which is the pressure boundary. An increase in stress is evident at the joint between the root rib and the spar demonstrating load transfer from the spar web into the root rib web.

The von Mises and maximum shear stress fringe plots for the outboard rib are presented in figures 5.30 and 5.31. The plots show peak von Mises stresses ranging between 315 and 435 MPa and peak maximum shear stresses ranging from 230 MPa to 270 MPa. The outboard rib is the pressure boundary and as a result, the stresses are greater than at the root rib. As discussed previously, the stresses at the vertices of the model are

ignored due to the distortion in the data at those points from the application of the model boundary conditions.

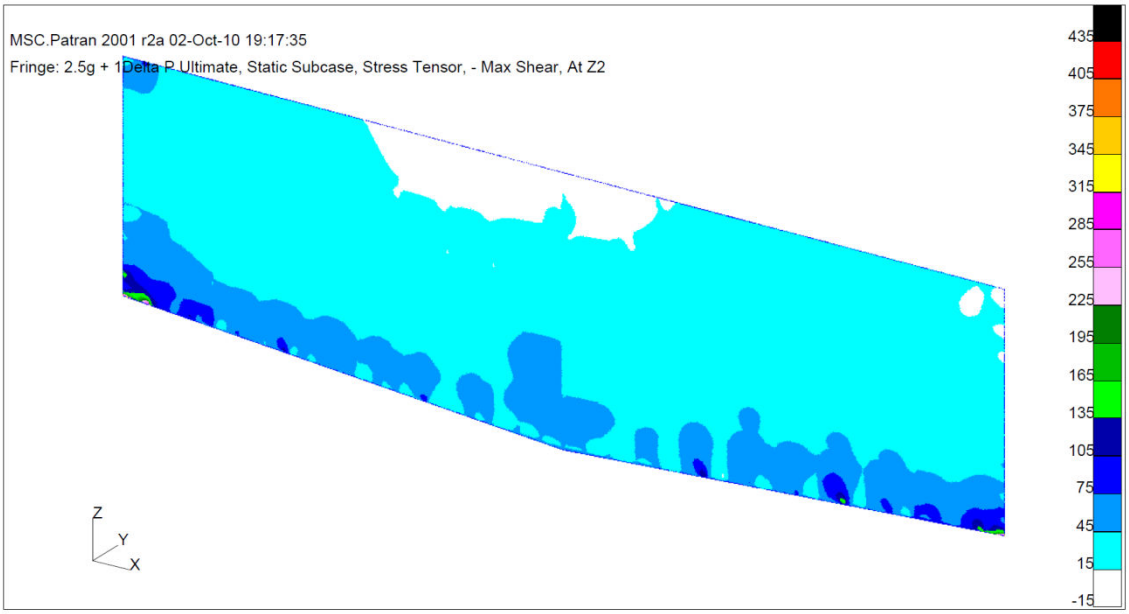

Figure 5.29 Root rib maximum shear stresses

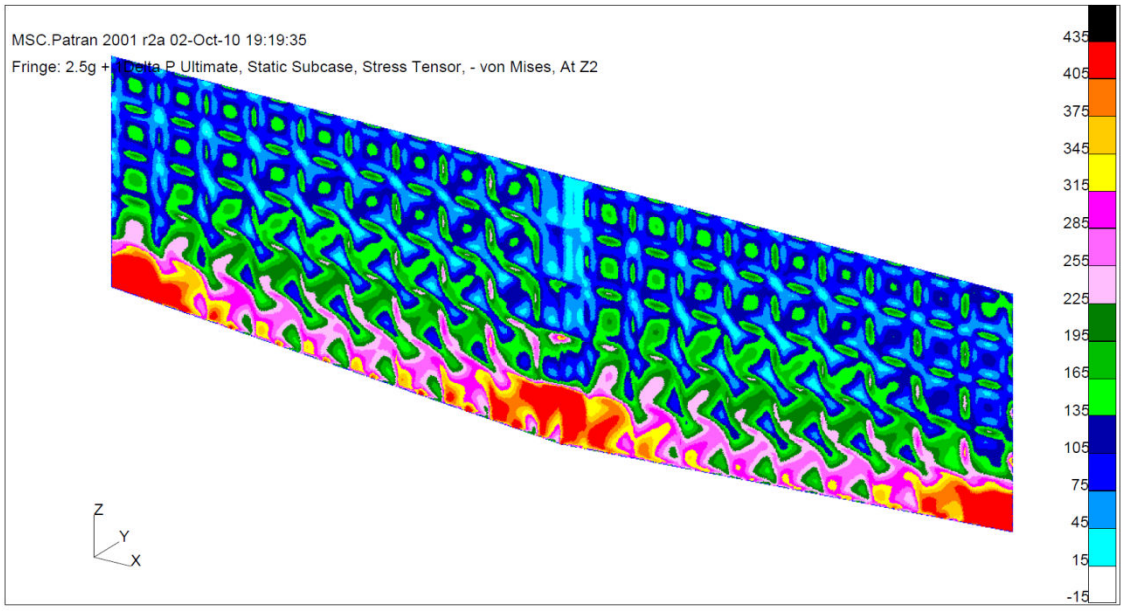

Figure 5.30 Outboard rib von Mises stresses

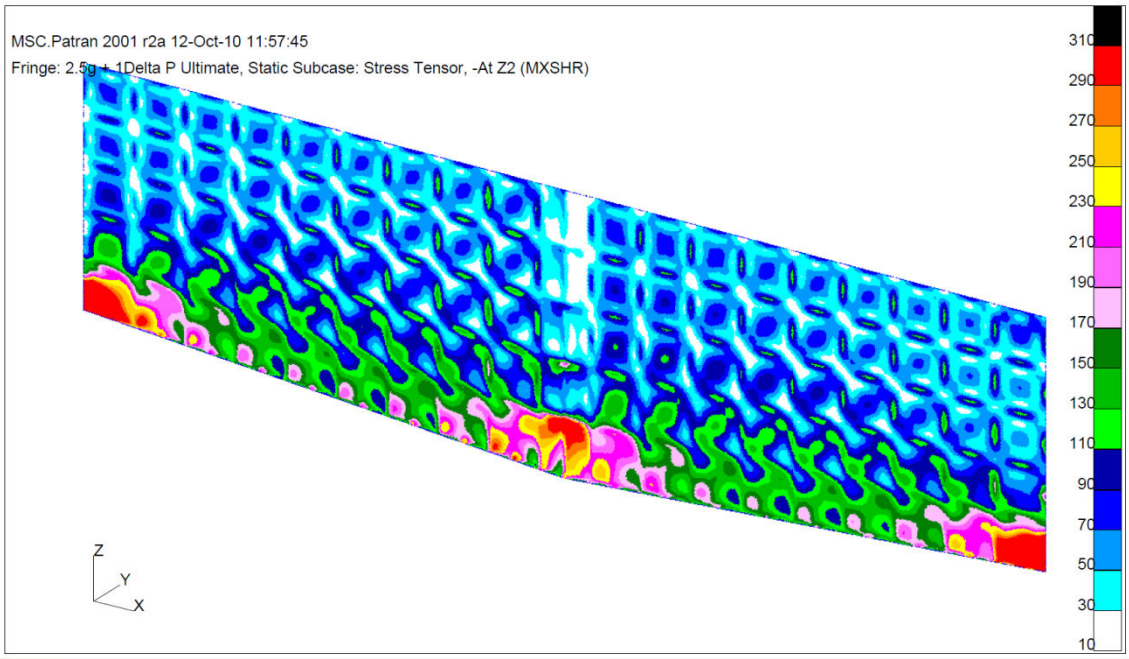

Figure 5.31 Outboard rib shear stresses

5.6.5 Deflections

The deflections due to the applied loads are presented in figures 5.32 and 5.33. These show a maximum vertical deflection of 11 mm occurring in the wing skin and 13 mm in the fuselage skin. The applied load case for deflection is the 2ΔP Ultimate Load case. The deflections for normal operating conditions are significantly lower.

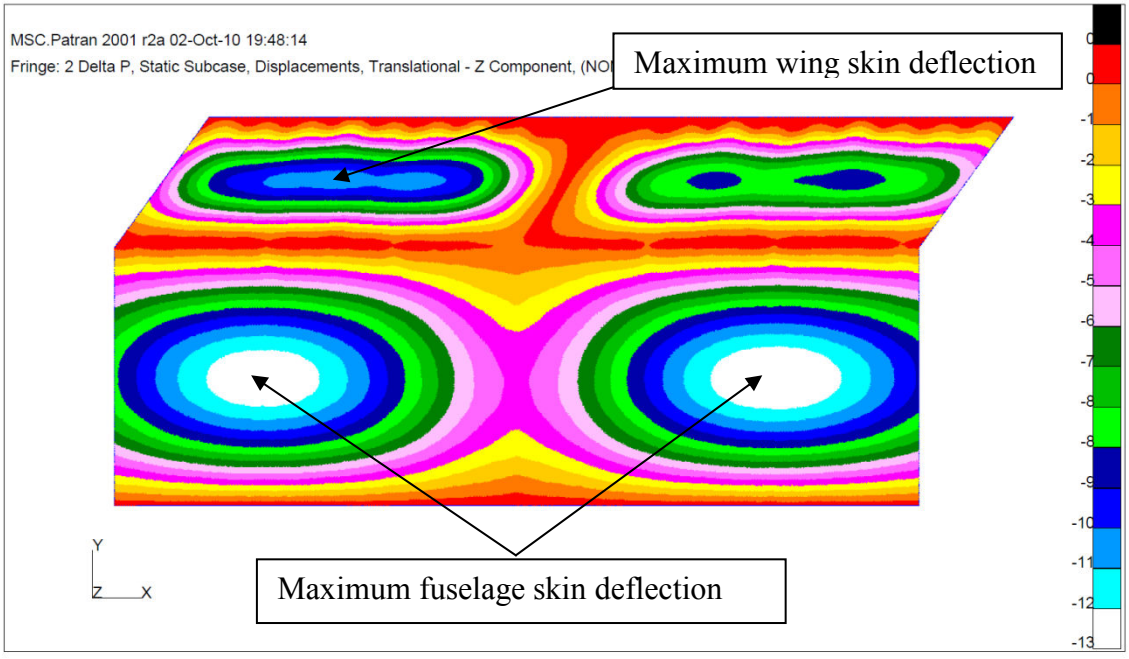

Figure 5.32 Skin deflections

A maximum deflection of 26 mm was observed on the outboard rib. This is over a panel depth of 1.6m (i.e. less than 2% of panel depth) approximately and is for an ultimate load case of V_D with $2\Delta P$ pressure applied. The rib is not an aerodynamic surface and therefore not subject to the deflection constraints of aerodynamic surfaces.

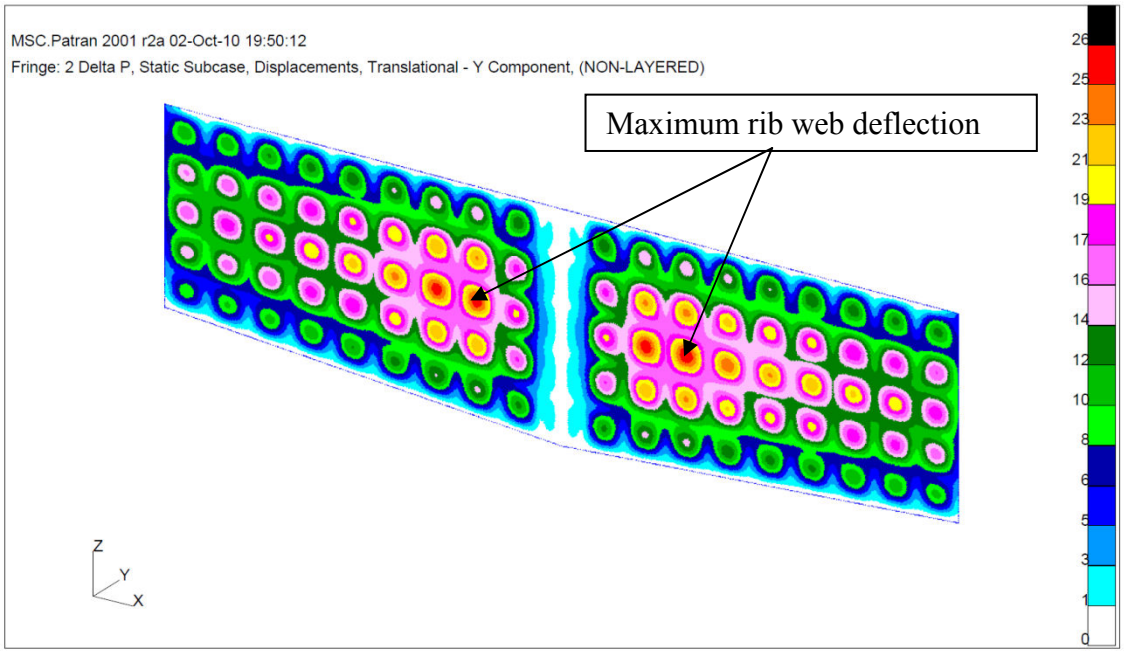

Figure 5.33 Outboard Rib deflections

Table 5.12 Summary of beam column and plate analysis and optimisation results (Mukhopadyay, 2005)

Concept	Initial				Optimised					
	Depth (m)	Skin t (m)	P/Pcr	Wt/area Kg/m^2	Depth (m)	Skin t (m)	P/Pcr	Wt/area Kg/m^2	Max. Disp. (m)	Material
2D HC Beam	0.15	0.006	0.4	42.4	0.264	0.0045	0.18	37.9	0.03	AL
2D HC Beam	0.1524	0.0064	0.42	25.55	0.1778	0.0051	0.37	21.3	0.048	SRFI
Flat HC	0.137	0.003	0.5	15.3	0.201	0.0046	0.66	24.1	0.0086	SRFI
Flat Ribbed	0.152	0.003	0.5	13.5	0.184	0.0058	0.66	25.6	0.0064	SRFI
Flat HC + cat	0.167	0.003	0.5	15.4	0.201	0.0046	0.71	24.2	0.009	SRFI
Vaulted HC	0.2	0.003	0.5	17	0.17	0.0033	0.66	25.4	0.0112	SRFI

Table 5.12 presents the results of an assessment by NASA of different fuselage skin configurations (Mukhopadyay, 2005). The skin displacements show that the results obtained from this assessment do not differ significantly from those presented by

Mukhopadyay (2005). The deflection is, therefore, considered acceptable. As discussed earlier, deflection is a key criterion in this configuration and presents much scope for further analysis / investigation.

5.7 Identification of critical areas with respect to fatigue and damage tolerance issues

The results of the FE assessment confirm that the structure at the wing root has the capacity to sustain the design loadcases specified by the airworthiness authorities. Of further interest is the damage tolerance capability of the wing root structure including the proposed novel bird's mouth spar termination. In order to demonstrate damage tolerance capability, the structure needs to be assessed for crack growth and residual strength. The two components identified as requiring assessment are the novel bird's mouth spar termination and the skin.

An examination of the results of the FE assessment show that the region of the spar just inboard of the root rib and which constitutes the bird's mouth termination yielded the highest stresses free of distortion from the application of boundary conditions. That location was selected for crack growth assessment.

A survey of the skin showed that it was the one component that consistently returned the highest stresses. The region outboard of the root rib returned significantly larger stresses and a location aft of the centre spar and outboard of the root rib was selected. Distance was maintained away from the vertices to minimise the impact of boundary constraints as the growth assessment required the application of representative field stresses.

Of the two components, the skin returned higher stresses overall and although the novel bird's mouth termination required validation, a further reduction in stresses could have been obtained in the spar web by an increase in thickness.

5.8 Conclusions

Calculations undertaken to demonstrate the feasibility of the proposed wing root design have been detailed in this chapter. A three step process was applied to demonstrate the feasibility of the proposed design. Firstly, loads were derived for the 2.5g V_D limit load case. These loads were then applied to a global model of the joint, created for assessment of wing root loads. The resulting loads obtained from the global model were limit loads. The appropriate factors were therefore applied to these local limit loads to determine the required ultimate loads for FE analysis using a local model of the wing root. Three loading conditions were assessed as follows:

1. 2.5g V_D x 1.5 Ultimate Load case
2. (2.5g V_D + 1ΔP) x 1.5 Ultimate Load case
3. 2ΔP Ultimate Load case.

With the exception of skin and rib deflection assessments, the (2.5g V_D + 1ΔP) x 1.5 Ultimate load case consistently returned the highest stresses and all stress results

discussed in the preceding sections were therefore for that case. The skin and rib deflections were assessed using the 2ΔP Ultimate Load case as it gave the most conservative results for deflections.

Several iterations of the local FE model were undertaken to address issues including boundary conditions, high skin stresses and large skin deflections. The FEM has been modified with changes including additional stiffening members to the fuselage skin, and additional restraints to the spar web to improve joint stiffness.

It was considered more appropriate to move the pressure boundary outboard of the wing root. This has the benefit of separating the loads on the wing root structure thus resulting in a more efficient wing root design. The pressure boundary has therefore been moved outboard to reflect current practice. A sketch of the final design proposal is presented in figures 4.7 and 4.8 of chapter 4.

Previous iterations of the FE model showed significant deflection of the spar web and the outboard edge of the skin under the applied loading. An additional restraint was therefore applied to the spar web and to the skin free edge to stop bending and to effect a more accurate representation of the structure being modelled.

The results show wing root joint stresses and deflections in line with expectation. The magnitudes of the stresses obtained indicate that scope remains for optimisation of the structure with the reduction of skin and web thicknesses albeit with a requirement for additional stiffening members.

The results also show that a significant proportion of the shear in the spar web is transferred into the root rib web resulting in significantly lower stresses in the spar termination inboard of the root rib. As a result, the novel feature of this proposed design which is the spar termination is not the most highly loaded location. The skins still remain the location with the highest stresses at the wing root.

As a result of the FE assessment, two locations, the first on the spar at the bird's mouth termination and the second in the skin, outboard of the root rib and aft of the centre spar were selected for damage tolerance assessment. The skin was judged to be the more critical of the two components,

The FE model has yielded the stresses to be applied in the crack growth assessment presented in Chapter 6. The stresses obtained are for the (2.5g V_D + 1ΔP) x 1.5 Ultimate load case. These were factored to obtain the corresponding 1g stresses, which have been used as the mean stresses in the fatigue load spectrum presented in chapter 6.

An assessment of the above issues should facilitate a better understanding of the BWB concept and contribute to the body of knowledge relating to next generation aircraft.

6 Damage tolerance substantiation

6.1 Introduction

This chapter describes the analysis undertaken to evaluate the damage tolerance capability of the proposed wing root design with the novel bird's mouth spar termination. The FE analysis of the wing root presented in Chapter 5 shows a significant difference in magnitude between the stresses obtained in the skin at the wing root and those in the spar web. A significant proportion of the shear stresses in the spar web are transferred into the web of the root rib. The resultant stresses in the spar web at the bird's mouth termination are hence lower than those in the skin. The conclusion drawn is that the skin is the more critical component at the wing root. The life of a crack occurring in the spar web would therefore be expected to be significantly greater than in the skin at the wing root meaning that any inspections set at the required frequency for a skin location would be adequate for the spar location. A crack growth assessment of both the spar web and the skin at the wing root has been undertaken in the sections following.

There are three aspects to damage tolerance, namely; fatigue crack growth, residual strength at limit load and design for inspection. The damage tolerance capability of the proposed wing design was assessed by a crack growth assessment and residual strength assessment using the two-bay crack criterion at the critical skin location. The construction of the spar and the bird's mouth termination meant that the two-bay crack criterion which is discussed in detail below, was not applicable to the spar. The damage tolerance capability of the spar web was determined by crack growth assessment and residual strength using net section yield criteria. The fatigue loading required for crack growth prediction was determined from the aircraft service stresses and other performance data (ESDU 97018). The crack growth life of the spar web was determined for one scenario whilst the crack growth life of the more critical two-bay skin crack was determined for three different scenarios. A separate residual strength assessment was also undertaken for a skin crack demonstrating that the proposed wing design will sustain a two-bay skin crack thus satisfying the criteria for damage tolerance.

6.2 The two-bay crack criterion

Prior to the development of the FAA/JAA requirements for damage tolerance, the two-bay crack criterion had evolved as a means by which aircraft designers could satisfy themselves that, in the event of a crack initiating on aircraft structure, the risk of fast fracture occurring before a predetermined critical crack length was achieved was avoided. The experiences of aircraft designers in the late 1960s confirmed that the pressure cabins of aircraft needed to be designed to sustain a two-bay skin crack with a broken central crack stopper at limit load (Swift, 1994). A broken central crack stopper was considered, as flat panel cyclic testing had indicated that in the event of a skin crack over a crack stopper a considerable amount of hoop loading was transferred to the crack stopper, creating a high cyclic load and eventual fatigue failure even for small crack

sizes. Assessments came to be made for longitudinal and circumferential fuselage skin cracks with broken central stiffeners and chord wise wing skin cracks (Swift, 1990).

6.2.1 Current application

For conventional aircraft structure, the two-bay crack criterion has been applied to the design of fuselage and wing structure since it was first conceived in the late 1960s. Its application has found more use in fuselage design as a stated criterion. Its use in the design of wing structure also continues but not as a named criterion for wing structure design.

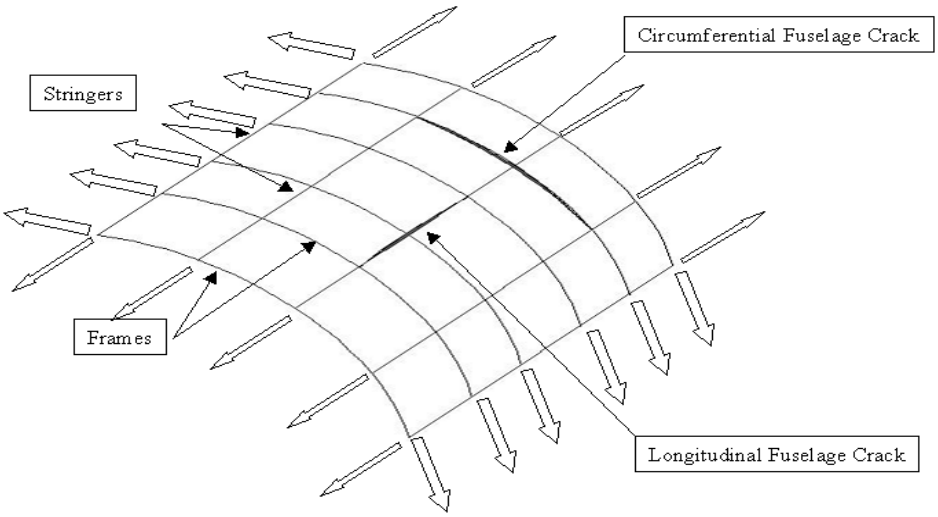

Figure 6.1 Two-bay cracks in fuselage skin (Swift, 1994)

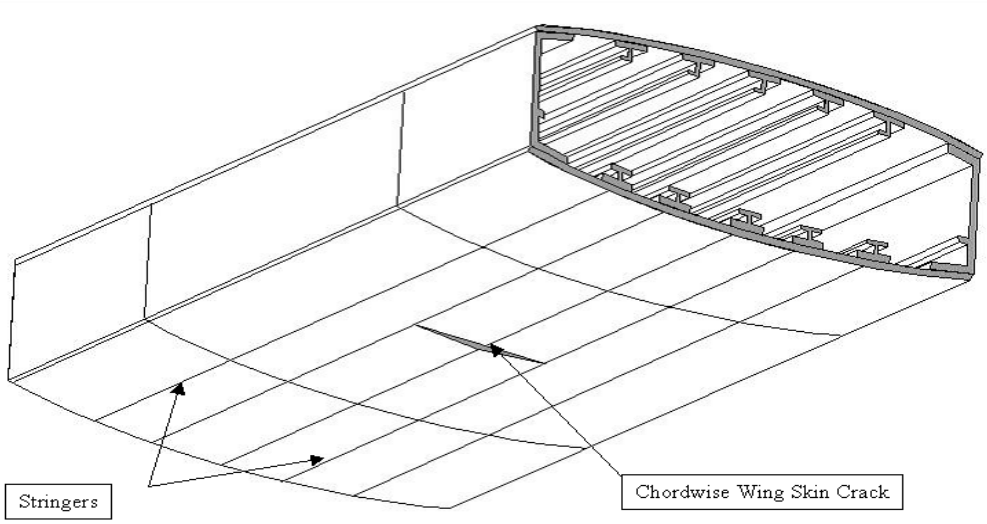

Figure 6.2 Two-bay wing skin crack

Large damage sizes are chosen to allow the opportunity to establish an external visual inspection at reasonable intervals so that the crack can be detected on a walk around

inspection as illustrated by figures 6.1 and 6.2. The choice of large damage sizes means that the criterion is best suited to large stiffened panels.

6.2.2 Key factors governing the two-bay criterion

The key aspects of the two-bay criterion can be described as follows;

- A requirement for a limit stress level about the same or a little lower than the residual strength capability of the structure for sustaining a two-bay crack in order to keep structural weight to a minimum.
- Visual inspection based on crack growth from detectable crack to crack arresting stiffeners (maximum spectrum load for normal usage is about 60% of limit load and occurs only once in one tenth of lifetime).
- Resulting inspection burden on operator is not excessive.

6.3 Identification of detail design areas

FAR/JAR part 56.561 states clearly that each evaluation required must include the evaluation of principal structural elements and detail design points, the failure of which could cause catastrophic failure of the airplane.

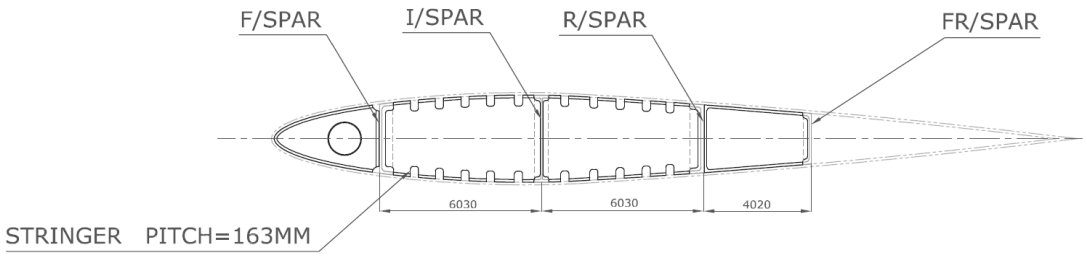

Section AA of figure 6.4

Figure 6.3 Profile of root and outboard ribs

The wing root has been identified as a principal structural element with detail design points requiring investigation. For the purposes of this thesis, the spar web at the bird's mouth termination and the skin/stringer interface at the root joint were deemed to require further assessment. The results of the FE analysis also identified the critical locations requiring further assessment as the web of the spar at the bird's mouth termination and the skin outboard of the root rib and aft of the centre spar. The root rib shown in figure 6.3 was not considered because in chapter 5 it was shown to be relatively lower loaded. Similarly, the outboard rib was not assessed as the magnitudes of normal flight loading are not considered to be of great concern. The location of the spar at the bird's mouth termination selected for analysis is presented in figure 6.4. The aspect of the skin/stringer interface at the root joint selected for further assessment is illustrated in figures 6.5 and 6.6.

The inspectability requirement of damage tolerance meant that it was preferable if the spar web required little or no inspection as any inspection of the spar web would be an

internal inspection. The FE analysis showed that there was significant scope for achieving further reduction in spar web stresses. As a result and due to its relatively lower loading, only one crack growth scenario was assessed for the bird's mouth spar termination. A through thickness crack in the spar flange which is by definition an edge crack in the spar web growing up towards the upper flange of the spar was assumed at a location inboard of the root rib in a region with stresses considered to be representative and free of distortions due to modelling constraints.

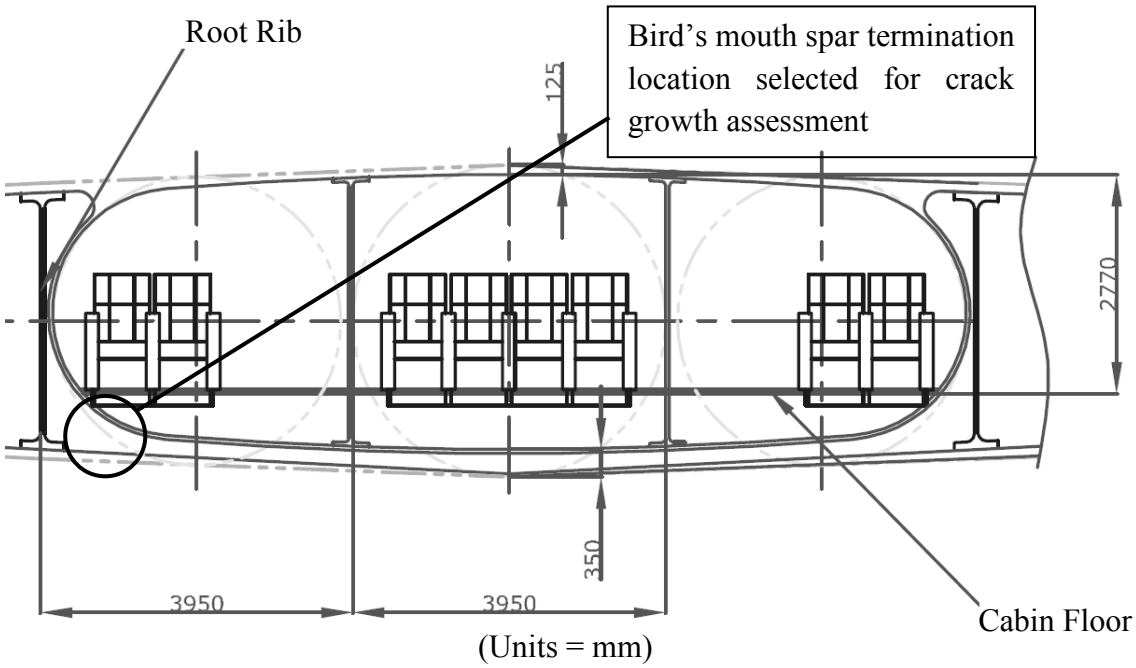

Figure 6.4 Bird's mouth spar termination location selected for crack growth assessment

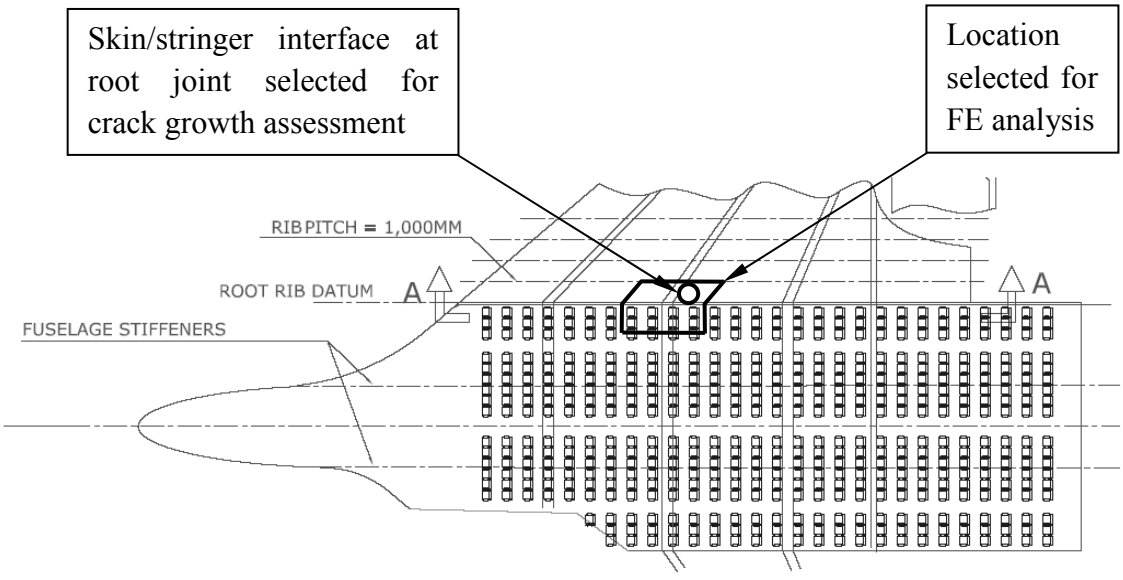

Note: Section AA presented in figure 6.3

Figure 6.5 Skin/stringer interface selected for crack growth assessment

Three crack growth scenarios were assessed for the skin at the wing root in this report as follows;

a. Scenario 1, mid-bay crack in the skin panel (figure 6.8);
b. Scenario 2, crack in skin panel at stringer (figure 6.11)
c. Scenario 3, crack in skin under fully broken stringer (figure 6.14).

The spar web and three skin scenarios were selected and assessed to identify which was most critical for the airframe configuration and to demonstrate the damage tolerance capability of the airframe. The analysis of the spar web and three skin scenarios is presented in the subsections following.

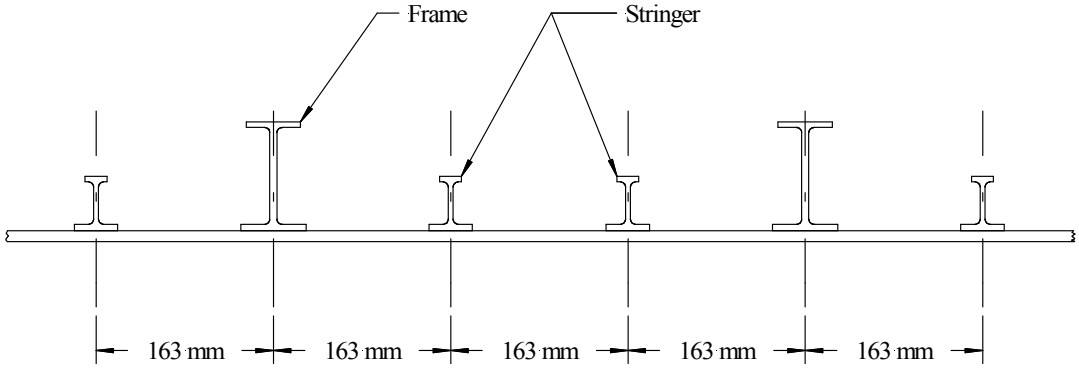

Figure 6.6 Arrangement of stiffeners on skin panel at selected location

6.4 Fatigue loading spectra

The FE analysis described in chapter 5 was the source of stress data required to compile the fatigue loading spectra for the spar and skin locations presented in the sections below.

6.4.1 Spar web fatigue loading spectrum

The FE analysis described in chapter 5 had been undertaken for the (2.5g V_D + 1ΔP) x 1.5 Ultimate load case, the (2.5g V_D) x 1.5 Ultimate load case and the (2ΔP) Ultimate load case. An additional analysis of the (1g V_D + 1ΔP) Fatigue load case was also undertaken. The 1ΔP stress was determined from the above FE analysis making it possible to isolate the effects of fuselage pressure from those of wing bending on the resultant stresses.

Table 6.1 Spar web fatigue stresses

Description	Stress (MPa)
Wing bending only (1g)	9.4
Effect of pressure only (ΔP)	32.7

The fatigue stresses for the spar were compiled by combining the effects of pressure with the 1g stresses. The fatigue stresses for the spar web are presented in table 6.1. It can be seen that the spar web fuselage pressurisation loads are significantly greater than the spar web wing bending loads at the bird's mouth termination.

Table 6.2 Acceleration spectrum for 4000 flight block

Inertia Factors			
Load Level	Min Acceleration (g)	Max Acceleration (g)	Frequency
1	-0.8	2.8	1
2	-0.7	2.7	1
3	-0.4	2.4	3
4	-0.2	2.2	13
5	0.0	2.0	34
6	0.1	1.9	100
7	0.3	1.7	648
8	0.4	1.6	3370
9	0.6	1.4	30630
10	0.7	1.3	323865

Table 6.3 Spar web fatigue stress spectrum

Factored Stresses				Spar Web Fatigue Spectrum			
Wing Bending Only		Wing Bending + Press.					
Min Stress (MPa)	Max Stress (MPa)	Min Stress (MPa)	Max Stress (MPa)	Load Level	Min Stress (MPa)	Max Stress (MPa)	Frequency
-7.2	26.0	25.6	58.8	1	25.6	58.8	1
-6.3	25.1	26.5	57.9	2	26.5	57.9	1
-3.6	22.4	29.2	55.2	3	29.2	55.2	3
-1.8	20.7	30.9	53.4	4	30.9	53.4	13
0.0	18.9	32.7	51.6	5	32.7	51.6	34
1.1	17.7	33.9	50.5	6	33.9	50.5	100
3.1	15.7	35.9	48.5	7	35.9	48.5	648
4.0	14.8	36.8	47.6	8	36.8	47.6	3370
5.8	13.0	38.6	45.8	9	38.6	45.8	30630
6.7	12.1	39.5	44.9	10	39.5	44.9	323865

The TWIST fatigue loading spectrum from ESDU 97018 was applied. The TWIST standard loading sequence was developed to be representative of the loading in the lower wing skin at the wing root of a transport aircraft, since this was found to be typically the most fatigue critical location (ESDU 97018). The standard loading sequence was considered applicable to the spar at the bird's mouth termination as it is in the region of the wing root and adjacent to the bottom skin.

The TWIST load sequence, which represents 40,000 flights, is made up of 10 identical repeated blocks of 4,000 flights each comprising up to 10 load levels. The inertia spectrum for a block of 4,000 flights is presented in table 6.2. This block was applied in the crack growth calculation of the skin/stringer interface. The spar web fatigue stress spectrum is derived from the data in tables 6.1 and 6.2 and is presented in table 6.3.

The sum of the stresses presented in table 6.1 defines the mean stress of the spar web at the location of interest. The inertias presented in table 6.2 only apply to the wing bending component of the stresses. The minimum and maximum stresses at each load level are therefore determined after the inertias have been applied as presented in table 6.3. Conventional wing structure returns R ratios (of minimum stress to maximum stress) of 0.1. This is not the case in the spar web. This is due to the distorting effects of fuselage pressurisation on the total stress which is significantly greater than the wing bending component.

6.4.2 Skin fatigue loading spectrum

The skin fatigue stresses and loading spectrum were derived in a similar manner to the spar web and are presented in tables 6.4 and 6.5 respectively.

Table 6.4 Skin fatigue stresses

Description	Stress (MPa)
Wing bending only (1g)	22.8
Effect of pressure only (ΔP)	26.2

It can be observed that the difference in the observed magnitudes of the fuselage pressurisation and wing bending stresses presented in table 6.4 is not as significant as it is on the spar web. Furthermore, the R ratio (of minimum stress to maximum stress) obtained for the wing skin is observed to be 0.1 at load level 1 and consistent with expectation.

Table 6.5 Fatigue stress spectrum

Factored Stresses				Skin Fatigue Spectrum			
Wing Bending Only		Wing Bending + Press.					
Min Stress (MPa)	Max Stress (MPa)	Min Stress (MPa)	Max Stress (MPa)	Load Level	Min Stress (MPa)	Max Stress (MPa)	Frequency
-17.4	63.0	8.8	89.2	1	8.8	89.2	1
-15.2	60.9	11.0	87.0	2	11.0	87.0	1
-8.7	54.3	17.5	80.5	3	17.5	80.5	3
-4.3	50.0	21.8	76.2	4	21.8	76.2	13
0.0	45.6	26.2	71.8	5	26.2	71.8	34
2.7	42.9	28.9	69.1	6	28.9	69.1	100
7.6	38.0	33.8	64.2	7	33.8	64.2	648
9.8	35.9	36.0	62.0	8	36.0	62.0	3370
14.1	31.5	40.3	57.7	9	40.3	57.7	30630
16.3	29.3	42.5	55.5	10	42.5	55.5	323865

6.5 Material Properties

2024-T3 aluminium alloy was selected for the spar, the bottom skin and stringers. This alloy has been used extensively in high strength tension aircraft applications where its properties including fracture toughness, slow crack growth rate and good fatigue life are required. A summary of its properties are presented in table 6.6.

Table 6.6 Property summary for 2024-T3 Al. Alloy

Item	Value
Density[a]	2.78 g/cc
Ultimate Tensile Strength[a]	483 MPa
Tensile Yield Strength[a]	345 MPa
Elongation at Break[a]	18 %
Modulus of Elasticity[a]	73.1 GPa
Poisson's Ratio[a]	0.33
Shear Modulus[a]	28 GPa
Shear Strength[a]	283 MPa
Plane Strain Fracture Toughness (L-T)[b]	30.4 MPa$\sqrt{m}$
Plane Strain Fracture Toughness (T-L)[b]	29.2 MPa$\sqrt{m}$
Plane Strain Fracture Toughness (S-L)[b]	21 MPa$\sqrt{m}$

a. http://asm.matweb.com/search/SpecificMaterial.asp?bassnum=MA2024T3 25 July 2009

b. ESDU Metallic Materials Data Handbook, Specification L97, Data Sheet Issue 2, January 2002

The computer program AFGROW was used in the crack growth analysis detailed in this report. AFGROW includes material data for standard aerospace materials such as 2024-T3 aluminium alloy. The crack growth rate data for 2024-T3 aluminium alloy, obtained from AFGROW is for the Harter T-method with shift parameter “m” and is presented in table 6.7.

Table 6.7 2024-T3 Bare sheet long crack data (L-T)

Plane strain fracture toughness			34.064 MPa√m
Yield stress			324.054 MPa
Young's modulus			72394.9 N/mm^2
Item	da/dN	Delta K @ R=0.0	m
1	2.54E-11	3.3	0.25
2	5.08E-11	3.4	0.25
3	2.54E-10	3.4	0.25
4	5.08E-10	3.4	0.25
5	1.02E-09	3.5	0.25
6	1.52E-09	3.8	0.275
7	2.54E-09	4.9	0.275
8	5.08E-09	7.2	0.28
9	7.62E-09	8.0	0.34
10	1.02E-08	8.5	0.38
11	1.52E-08	9.0	0.4
12	2.54E-08	9.3	0.45
13	5.08E-08	10.1	0.5
14	1.02E-07	11.8	0.5
15	2.54E-07	16.0	0.5
16	5.08E-07	19.6	0.5
17	1.02E-06	23.7	0.47
18	2.54E-06	29.7	0.42
19	5.08E-06	33.0	0.38
20	1.02E-05	35.7	0.36
21	1.52E-05	37.0	0.35
22	2.03E-05	37.9	0.34
23	2.54E-05	38.5	0.33
24	1.02E-04	40.7	0.3
25	2.54E-04	41.8	0.28

(Harter, 2006)

6.6 Crack growth assessment

The crack growth lives of cracks in the spar web and the skin were determined using the AFGROW computer code with the fatigue spectra presented in tables 6.3 and 6.5. AFGROW is a program developed by the US Air Force for crack growth life prediction. The required inputs include material data, stress intensity factors (if known) and a fatigue stress spectrum, component geometry, initial and final crack sizes. AFGROW has the capability for calculating stress intensity factors for simple geometries in its database of geometry models. AFGROW also provides options for various crack growth material laws including the Harter T-method, Walker, Forman and Nasgro, and various crack retardation models including Closure, FASTRAN, Hsu, Wheeler, and Willenborg models. The inputs selected for this assessment are described in detail in the sections following and cover a crack growing in the spar web and three skin crack scenarios.

The bird's mouth spar termination is assessed for an edge crack (figure 6.7). The crack would be expected to grow at a 45 degree angle since the dominant loading in the spar web is shear. Since, the section presented in figure 6.7 shows the minimum distance the crack could possibly travel towards the nearest free edge this has been adopted for the spar analysis.

The three skin crack growth scenarios assessed are:

1. Mid-bay crack in the skin panel (figure 6.8)
2. Crack in the skin panel at stringer (figure 6.11)
3. Crack in skin panel under a broken stringer (figure 6.14)

6.6.1 Spar web crack growth assessment

The geometry of the spar web at the location of interest is presented in figure 6.7. As discussed previously, the crack in the spar is assessed as a through thickness crack in the spar flange which is by definition an edge crack in the spar web growing up towards the upper flange of the spar at a location inboard of the root rib in a region with stresses considered to be representative and free of distortions due to modelling constraints.

The severity of the stresses at the crack tip can be described in terms of the stress intensity factor K, which is a function of the loading on the cracked configuration and of the size and shape of the crack and other geometrical boundaries (Rooke, Cartwright 1974).

Table 6.8 Spar web geometrical data

Description	Value
Spar Web Thickness, t	2 mm
Spar Web Depth, h	350 mm

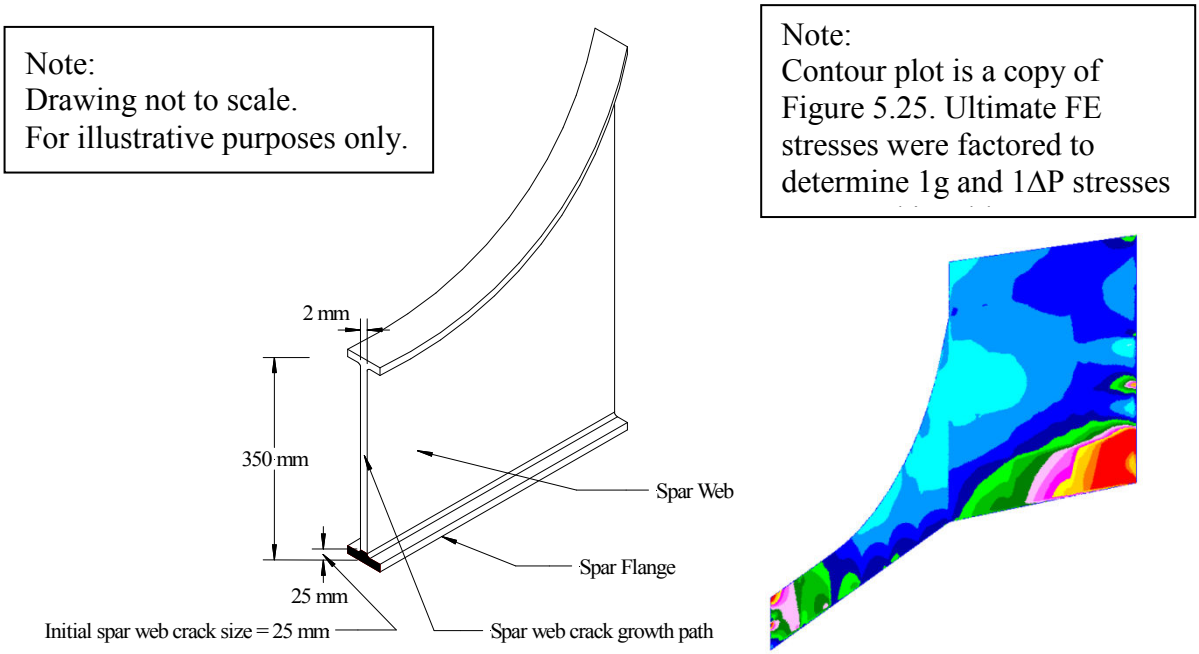

(a) Geometry at Spar web crack datum

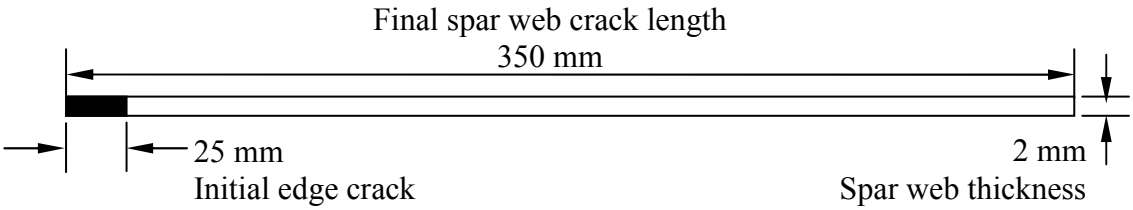

(b) Idealisation of spar web single edge crack geometry

Figure 6.7 Crack growth in spar web at bird's mouth termination

Table 6.9 Normalised SIFs β from AFGROW for a single edge crack in a finite width plate

a (mm)	β	a (mm)	β	a (mm)	β	a (mm)	β
25.0	1.1652	40.2	1.2148	55.5	1.2831	70.7	1.3713
26.3	1.1686	41.5	1.2198	56.8	1.2896	72.0	1.3796
27.5	1.1722	42.8	1.2249	58.0	1.2963	73.3	1.3881
28.8	1.1759	44.1	1.2301	59.3	1.3032	74.5	1.3967
30.1	1.1797	45.3	1.2354	60.6	1.3102	75.8	1.4055
31.4	1.1837	46.6	1.2409	61.8	1.3173	77.1	1.4144
32.6	1.1877	47.9	1.2466	63.1	1.3246	78.3	1.4235
33.9	1.1919	49.1	1.2523	64.4	1.3320	79.6	1.4328
35.2	1.1963	50.4	1.2582	65.6	1.3396	79.8	1.4345
36.4	1.2007	51.7	1.2642	66.9	1.3473		
37.7	1.2053	52.9	1.2704	68.2	1.3551		
39.0	1.2100	54.2	1.2766	69.5	1.3631		

Due to the relatively simple nature of the assembly at the bird's mouth termination, the crack in the spar was assessed as a single edge crack in a finite width plate. The geometrical and material data of interest in order to obtain the required stress intensities are presented in table 6.8. AFGROW has the capability for calculating stress intensity factors for simple geometries in its database of geometry models. The normalised stress intensities (β) obtained from AFGROW for a single edge crack in a finite width plate are presented in table 6.9.

The program AFGROW was run for a single edge crack in a finite width plate with the above geometry and βs from its database of geometry models presented in table 6.9 and other input data to determine the crack growth life of an edge crack in the spar web growing up towards the upper flange of the spar with and without retardation. The results are discussed in section 6.6.5.

6.6.2 Mid-bay crack in the skin panel (Scenario 1)

The first scenario assessed was for a mid-bay crack in the wing skin at the wing root joint of the project aircraft. The geometry of the structure assessed is presented in figure 6.8. It can be seen from figure 6.8 that every third stringer is replaced by a frame. The frames were required to improve the bending capability of the skin stringer assembly due to the magnitude of the applied fuselage pressurisation loads. For analysis purposes and to reduce complexity, the stringer cross-sectional areas have been applied in determining the stress intensity factors. This will give a conservative prediction as the "frame" would provide more constraint to crack growth rate.

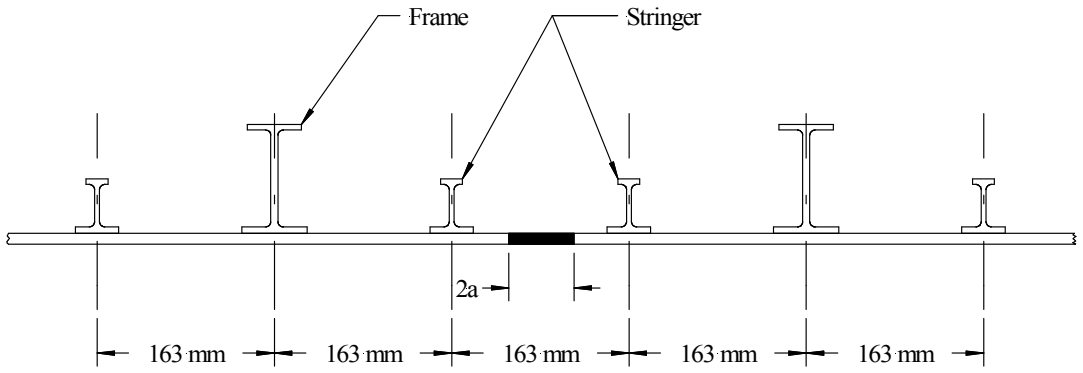

Figure 6.8 Crack growth scenario 1 - Mid-bay crack in the skin panel

The severity of the stresses at the crack tip can be described in terms of the stress intensity factor K which is a function of the loading on the cracked configuration and of the size and shape of the crack and other geometrical boundaries (Rooke, Cartwright 1974).

Normalised stress intensities (β) were obtained from (Rooke, Cartwright 1974) for a mid-bay crack in the skin panel. The geometrical data is of interest in order to obtain the

required stress intensities: these are presented in table 6.10. The extracts from (Rooke, Cartwright 1974) are presented in figures 6.9 and 6.10.

Table 6.10 Geometrical data

Description	Value
Stringer pitch, b	163 mm
Fastener pitch, h	25.4 mm
Ratio of h/b	0.1558
Sheet thickness, t	10 mm
Stringer cross-sectional area, A	515.5 mm^2
Sheet Young's modulus, E_1	73.1 GPa
Stiffener Young's modulus, E_2	73.1 GPa
Ratio of stiffener and sheet stiffnesses, $s = E_2A / E_1bt$	0.316

The data from figures 6.9 and 6.10 were digitised and interpolated to obtain β values for a mid-bay crack. β values are determined for a mid-bay crack growing across three bays in order to ensure adequate crack length as the two-bay crack criterion assumed a crack initiating at a stringer datum. A copy of the spreadsheets used to generate the stress intensity factors from figures 6.9 and 6.10 are presented in Appendix F. The final results are presented in table 6.11.

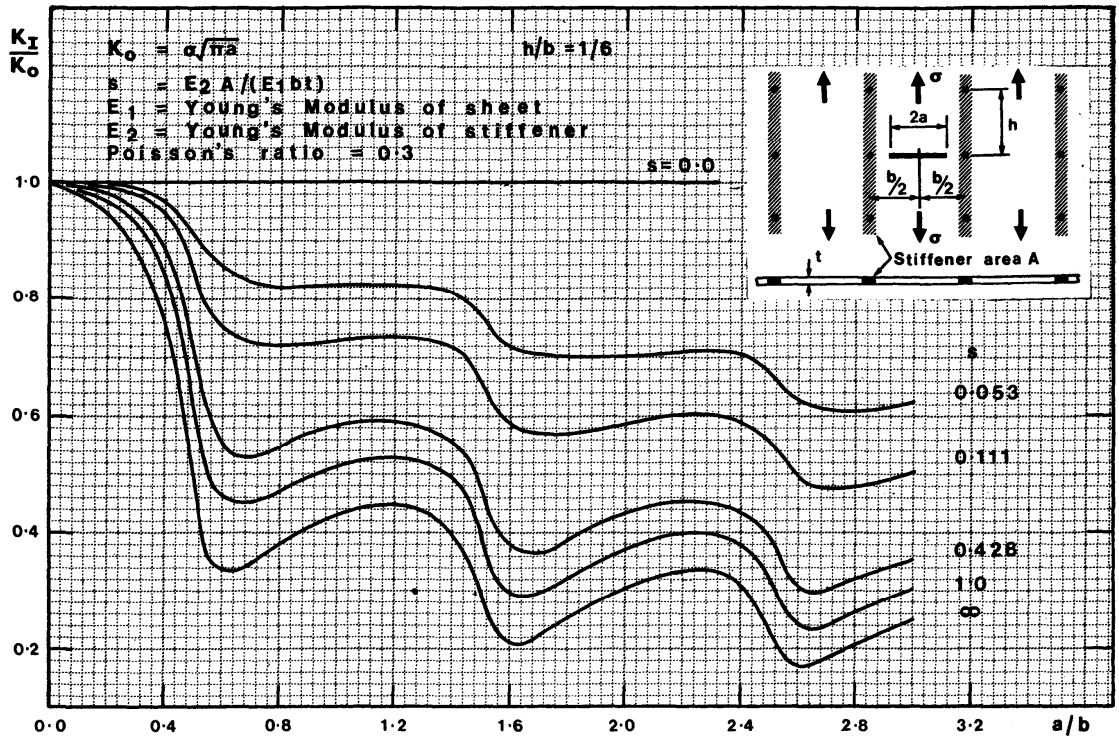

Figure 6.9 β for a crack between two stiffeners in a periodically stiffened sheet subjected to a uniaxial tensile stress (Case h/b=1/6 figure 141, Rooke, Cartwright 1974)

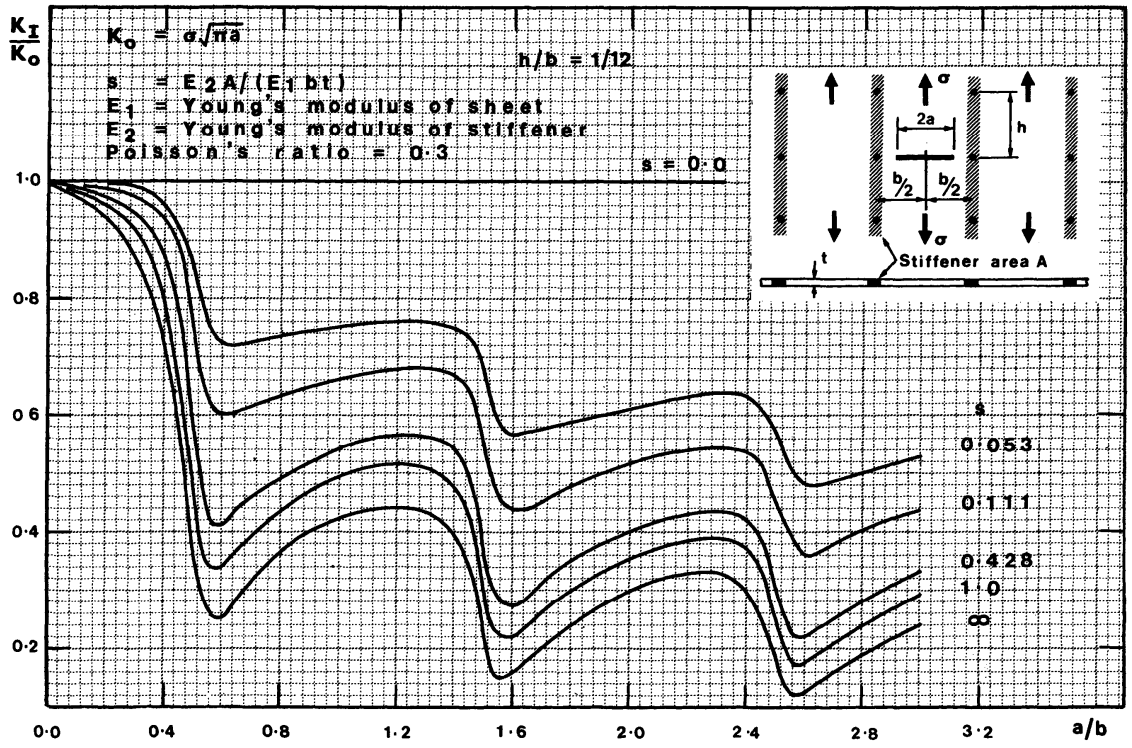

Figure 6.10 β for a crack between two stiffeners in a periodically stiffened sheet subjected to a uniaxial tensile stress (Case h/b=1/12 figure 142, Rooke, Cartwright 1974)

Table 6.11 Normalised SIFs β (h/b=0.1558, s=0.316) for a crack between two stiffeners in a periodically stiffened sheet subjected to a uniaxial tensile stress

a (mm)	a/b	β	a (mm)	a/b	β	a (mm)	a/b	β
4.0	0.024	0.998	78.7	0.483	0.779	151.2	0.928	0.577
10.0	0.061	0.997	79.8	0.489	0.761	156.6	0.961	0.583
17.6	0.108	0.995	81.4	0.499	0.737	162.6	0.998	0.587
24.7	0.151	0.989	83.0	0.509	0.716	170.3	1.045	0.590
30.1	0.185	0.984	85.2	0.523	0.672	177.3	1.088	0.595
34.5	0.212	0.980	87.4	0.536	0.649	184.5	1.132	0.597
40.0	0.245	0.973	89.0	0.546	0.622	189.4	1.162	0.596
44.9	0.275	0.964	92.3	0.566	0.600	196.9	1.208	0.597
49.8	0.305	0.957	94.5	0.580	0.582	202.9	1.245	0.593
53.6	0.329	0.943	96.7	0.593	0.567	209.5	1.285	0.590
57.4	0.352	0.934	101.6	0.623	0.553	215.5	1.322	0.584
61.2	0.376	0.919	104.8	0.643	0.544	222.0	1.362	0.576
65.0	0.399	0.902	111.4	0.683	0.541	228.0	1.399	0.566
67.2	0.412	0.889	117.9	0.723	0.542	232.9	1.429	0.551
71.0	0.436	0.864	123.9	0.760	0.547	237.3	1.456	0.533
71.6	0.439	0.851	131.0	0.804	0.554	241.1	1.479	0.512
74.8	0.459	0.830	137.0	0.841	0.563	244.3	1.499	0.483
75.9	0.466	0.809	145.2	0.891	0.572	245.0	1.503	0.467

The program AFGROW was run with the βs presented in table 6.11 and other input data to determine the crack growth life of a through thickness mid-bay crack in the skin with and without crack retardation. AFGROW only allows provision for 25 β entries at a time. Three runs of AFGROW were therefore undertaken with varying initial and final crack sizes of 10mm to 89mm, 89mm to 228mm and 228mm to 245mm to cover the full extent required.

6.6.3 Crack in the skin panel under an intact stringer (Scenario 2)

The second scenario assessed was for a crack in the wing skin at the wing root joint of the project aircraft, in the skin, propagating under an intact stringer and initiating from a fastener hole. The geometry of the structure assessed is presented in figure 6.11.

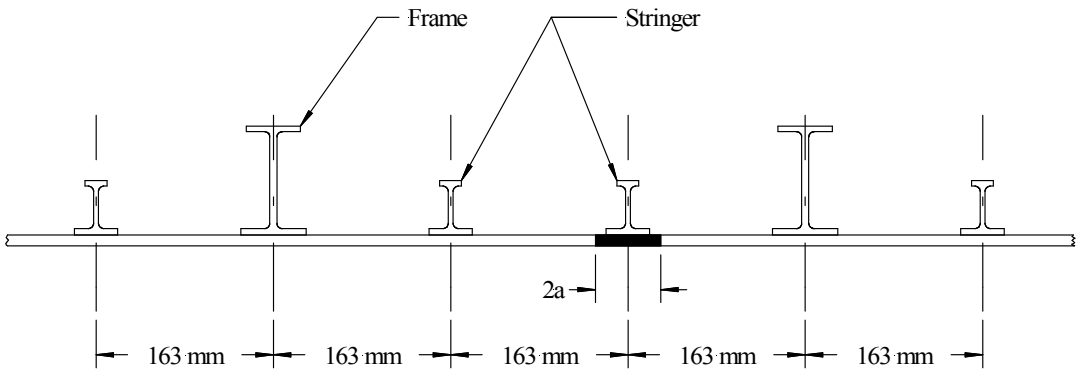

Figure 6.11 Crack growth scenario 2 - Crack in the skin panel at stringer datum with intact stringer

Similar to the previous section, normalised stress intensities were obtained from (Rooke, Cartwright 1974) for a crack in the skin panel under an intact stringer. The geometrical data and the ratios of interest in order to obtain the required stress intensities remain unchanged from those presented in table 6.10. For simplicity and due to limited β data, the geometry of the "frame" is replaced by that of a "stringer"

β values are determined for a crack originating at a fastener hole under a stringer and growing towards the adjacent stringers. A copy of the spreadsheets used to generate the stress intensity factors from figures 6.12 and 6.13 are presented in Appendix F. The final results are presented in table 6.12.

As was previously the case, AFGROW was run with the βs presented in table 6.12, to determine the crack growth life of a through crack in the skin originating at the stringer for an initial half crack length of 25 mm and a final half crack length of 163 mm which is the 2-bay half crack length with and without crack retardation.

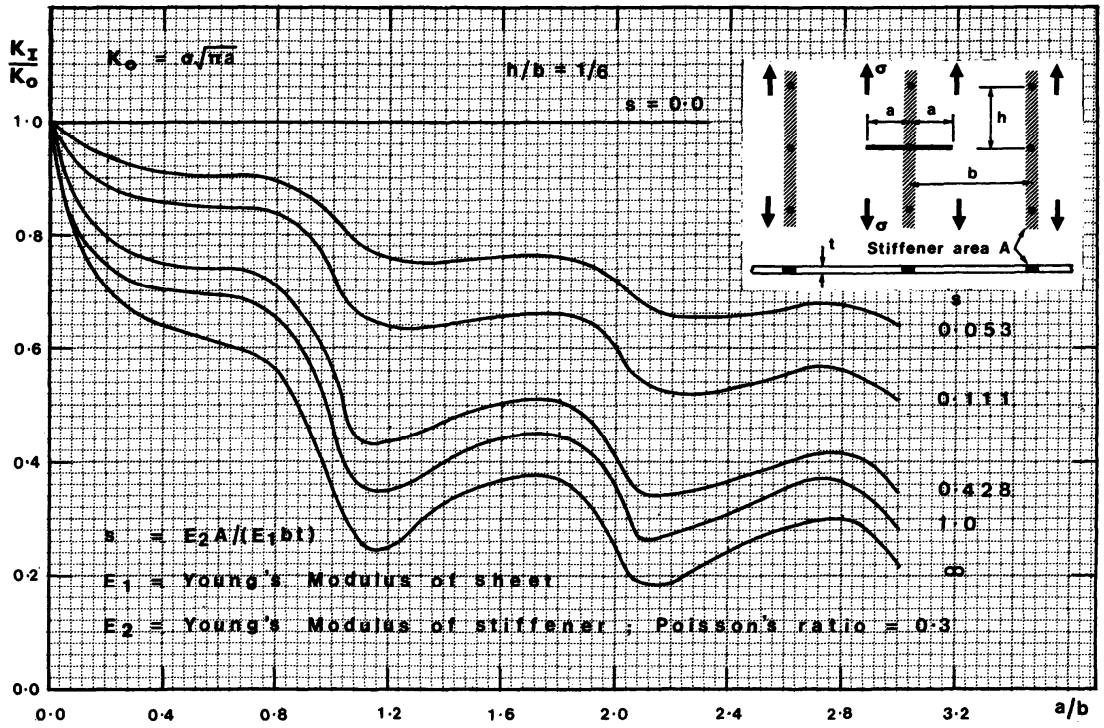

Figure 6.12 β for a crack across a stiffener in a periodically stiffened sheet subjected to a uniaxial tensile stress (Case h/b=1/6 figure 136, Rooke, Cartwright 1974)

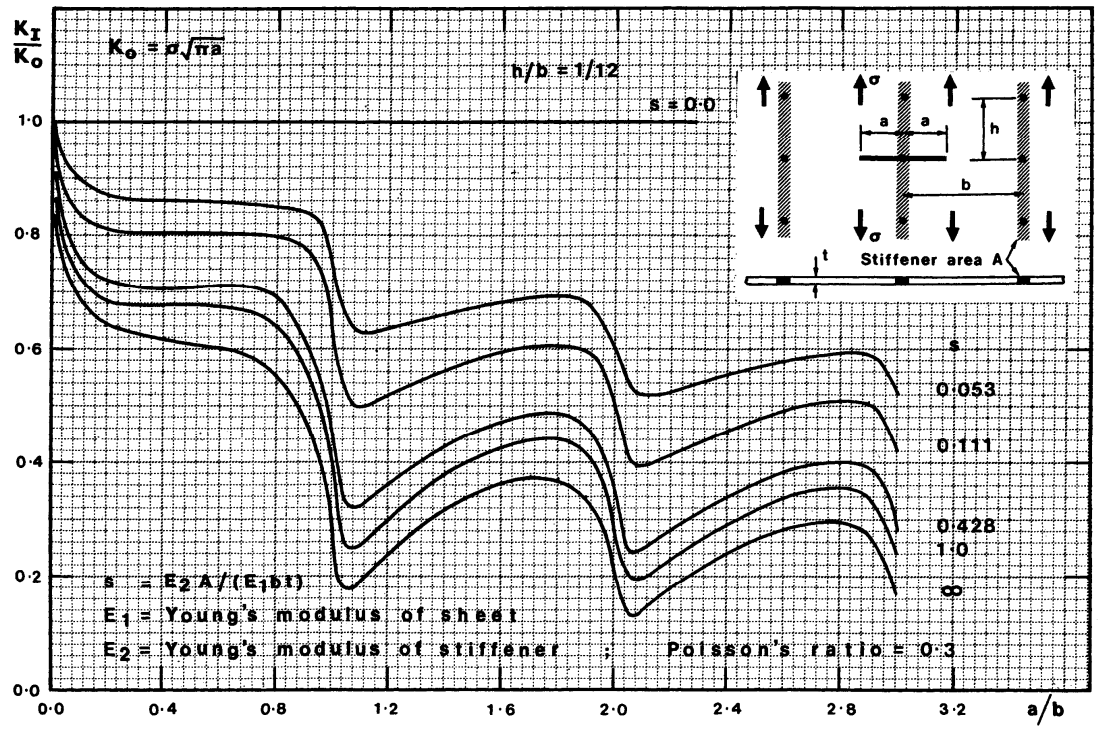

Figure 6.13 β for a crack across a stiffener in a periodically stiffened sheet subjected to a uniaxial tensile stress (Case h/b=1/12 figure 137, Rooke, Cartwright 1974)

Table 6.12 Normalised SIFs β (h/b=0. 0.1558, s=0.316) for a crack across a stiffener in a periodically stiffened sheet subjected to a uniaxial tensile stress

a (mm)	a/b	β	a (mm)	a/b	β	a (mm)	a/b	β
4.9	0.030	0.953	117.4	0.720	0.769	229.8	1.410	0.524
9.8	0.060	0.913	122.3	0.750	0.764	234.7	1.440	0.529
14.7	0.090	0.879	127.1	0.780	0.757	239.6	1.470	0.535
19.6	0.120	0.857	132.0	0.810	0.746	244.5	1.500	0.540
24.5	0.150	0.840	136.9	0.840	0.735	249.4	1.530	0.543
29.3	0.180	0.826	141.8	0.870	0.721	254.3	1.560	0.547
34.2	0.210	0.815	146.7	0.900	0.705	259.2	1.590	0.551
39.1	0.240	0.806	151.6	0.930	0.685	264.1	1.620	0.555
44.0	0.270	0.798	156.5	0.960	0.659	269.0	1.650	0.555
48.9	0.300	0.792	161.4	0.990	0.627	273.8	1.680	0.556
53.8	0.330	0.790	166.3	1.020	0.585	278.7	1.710	0.556
58.7	0.360	0.786	171.2	1.050	0.530	283.6	1.740	0.558
63.6	0.390	0.782	176.0	1.080	0.506	288.5	1.770	0.558
68.5	0.420	0.778	180.9	1.110	0.496	293.4	1.800	0.556
73.4	0.450	0.776	185.8	1.140	0.493	298.3	1.830	0.551
78.2	0.480	0.774	190.7	1.170	0.493	303.2	1.860	0.544
83.1	0.510	0.773	195.6	1.200	0.495	308.1	1.890	0.537
88.0	0.540	0.773	200.5	1.230	0.497	313.0	1.920	0.524
92.9	0.570	0.773	205.4	1.260	0.500	317.9	1.950	0.506
97.8	0.600	0.773	210.3	1.290	0.504	322.7	1.980	0.485
102.7	0.630	0.773	215.2	1.320	0.509	327.6	2.010	0.458
107.6	0.660	0.773	220.1	1.350	0.513	332.5	2.040	0.425
112.5	0.690	0.772	224.9	1.380	0.518	337.4	2.070	0.406

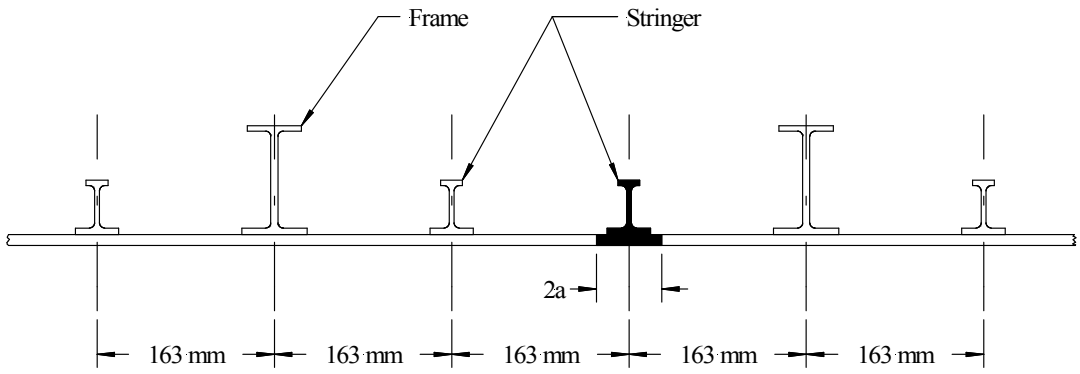

Figure 6.14 Crack growth scenario 3 - Crack in the skin panel at stringer datum with broken stringer

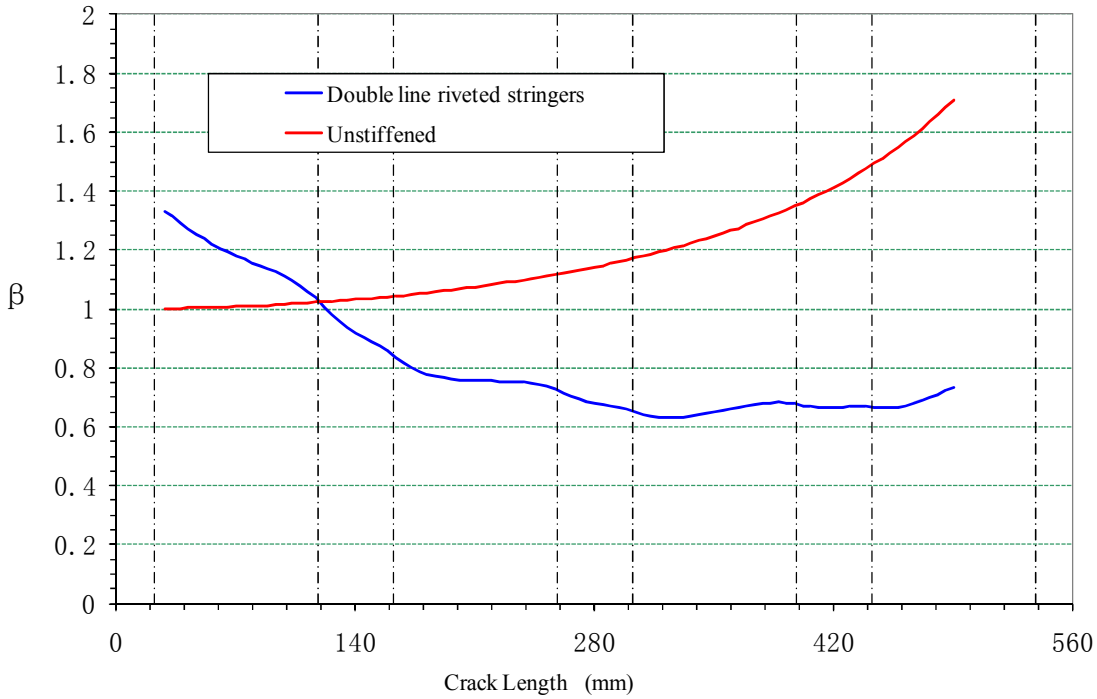

Figure 6.15 Dimensionless stress intensity factor β of rivetted and unstiffened panel with broken stringer (Zhang and Li, 2005) (s=0.62)

Table 6.13 Normalised SIFs β for crack in the skin panel at stringer datum with broken stringer (s=0.62)

a (mm)	K_1/K_0	a (mm)	K_1/K_0	a (mm)	K_1/K_0	a (mm)	K_1/K_0
28.0	1.332	107.3	1.08	186.7	0.77	266.0	0.702
32.7	1.314	112.0	1.06	191.3	0.765	270.7	0.693
37.3	1.293	116.7	1.037	196.0	0.762	275.3	0.686
42.0	1.272	121.3	1.006	200.7	0.759	280.0	0.68
46.7	1.253	126.0	0.98	205.3	0.757	284.7	0.676
51.3	1.236	130.7	0.956	210.0	0.756	289.3	0.672
56.0	1.22	135.3	0.936	214.7	0.755	294.0	0.667
60.7	1.205	140.0	0.919	219.3	0.755	298.7	0.661
65.3	1.192	144.7	0.904	224.0	0.754	303.3	0.651
70.0	1.18	149.3	0.889	228.7	0.753	308.0	0.643
74.7	1.169	154.0	0.874	233.3	0.752	312.7	0.637
79.3	1.157	158.7	0.857	238.0	0.751	317.3	0.633
84.0	1.146	163.3	0.834	242.7	0.748	322.0	0.631
88.7	1.135	168.0	0.816	247.3	0.744	326.7	0.632
93.3	1.124	172.7	0.8	252.0	0.737	331.3	0.633
98.0	1.111	177.3	0.787	256.7	0.728	336.0	0.636
102.7	1.097	182.0	0.777	261.3	0.713	340.7	0.64

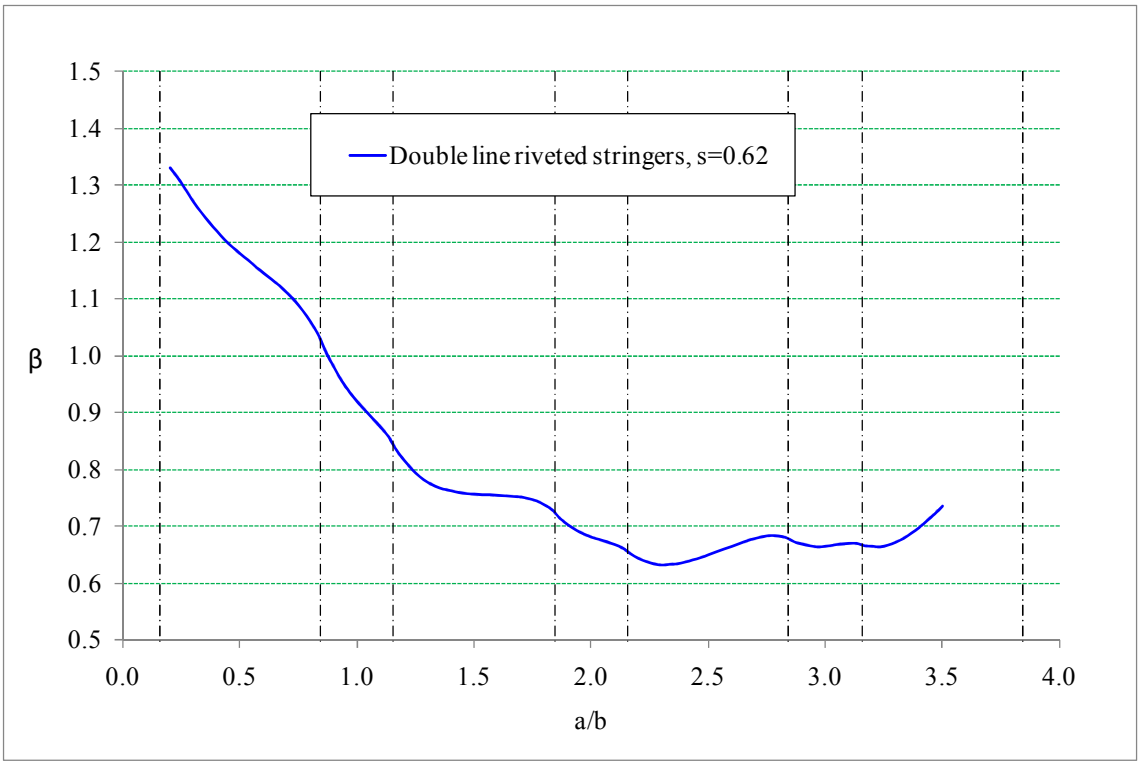

Figure 6.16 Dimensionless stress intensity factor β of rivetted and unstiffened panel with broken stringer (Zhang and Li, 2005)

6.6.4 Crack in the skin panel under a broken stringer (Scenario 3)

The third scenario assessed was for a crack in the wing skin at the wing root joint of the project aircraft in the skin panel under a broken stringer. The geometry of the structure assessed is presented in figure 6.14.

The normalised stress intensities for this scenario were obtained from the results of an investigation by (Zhang and Li, 2005) into the "Damage tolerance and fail safety of welded aircraft wing panels". The investigation included a comparison of the damage tolerance and fail safety characteristics of riveted, integrally machined and welded integral stiffened panels. The stress intensity factors obtained from (Zhang and Li, 2005) for a crack in a riveted skin-stringer panel under a broken stringer are presented in figure 6.15 and table 6.13.

The effective panel width b, for the configuration assessed in figure 6.14 was 140 mm whereas the effective panel width for this study is 163 mm. The dimensionless stress intensity factors presented in figure 6.14 and table 6.12 are therefore plotted in terms of a/b in figure 6.16.

The β solution was adjusted to account for differences in the effective panel width b to determine the crack growth life of a through crack in the skin under a broken central stringer. The β solution with adjusted crack lengths is presented in table 6.14.

AFGROW was run for scenario 3 with the β solution presented in figures 6.15 and 6.16 and table 6.14 for a crack in a stiffened panel with a broken stringer with and without crack retardation. The crack growth analysis is unconservative at stringer locations because of the use of the β solution for a stiffened panel with an As/bt ratio of 0.62 compared to the design panel As/bt ratio which ranges between 0.6 at frame locations and 0.316 at stringer locations. The results of the crack growth assessment, discussed in the section following suggest that As/bt ratios of 0.62 or greater are required.

Table 6.14 Normalised SIFs (β) for crack in integral skin-stringer panel under a broken stringer (Scenario 3)

a (mm)	a/b	β	a (mm)	a/b	β	a (mm)	a/b	β
32.6	0.200	1.332	157.6	0.967	0.936	282.5	1.733	0.748
38.0	0.233	1.314	163.0	1.000	0.919	288.0	1.767	0.744
43.5	0.267	1.293	168.4	1.033	0.904	293.4	1.800	0.737
48.9	0.300	1.272	173.9	1.067	0.889	298.8	1.833	0.728
54.3	0.333	1.253	179.3	1.100	0.874	304.3	1.867	0.713
59.8	0.367	1.236	184.7	1.133	0.857	309.7	1.900	0.702
65.2	0.400	1.22	190.2	1.167	0.834	315.1	1.933	0.693
70.6	0.433	1.205	195.6	1.200	0.816	320.6	1.967	0.686
76.1	0.467	1.192	201.0	1.233	0.8	326.0	2.000	0.68
81.5	0.500	1.18	206.5	1.267	0.787	331.4	2.033	0.676
86.9	0.533	1.169	211.9	1.300	0.777	336.9	2.067	0.672
92.4	0.567	1.157	217.3	1.333	0.77	342.3	2.100	0.667
97.8	0.600	1.146	222.8	1.367	0.765	347.7	2.133	0.661
103.2	0.633	1.135	228.2	1.400	0.762	353.2	2.167	0.651
108.7	0.667	1.124	233.6	1.433	0.759	358.6	2.200	0.643
114.1	0.700	1.111	239.1	1.467	0.757	364.0	2.233	0.637
119.5	0.733	1.097	244.5	1.500	0.756	369.5	2.267	0.633
125.0	0.767	1.08	249.9	1.533	0.755	374.9	2.300	0.631
130.4	0.800	1.06	255.4	1.567	0.755	380.3	2.333	0.632
135.8	0.833	1.037	260.8	1.600	0.754	385.8	2.367	0.633
141.3	0.867	1.006	266.2	1.633	0.753	391.2	2.400	0.636
146.7	0.900	0.98	271.7	1.667	0.752	396.6	2.433	0.64
152.1	0.933	0.956	277.1	1.700	0.751			

6.6.5 Results of crack growth predictions

The results of the crack growth prediction are presented in table 6.15, figure 6.17 for the spar web, figure 6.18 for the mid-bay crack and figure 6.19 for the crack under either an intact or broken stringer.

Table 6.15 Results of crack growth analysis

Item	Scenario	Description	FCG life Without Retardation (Flights)	FCG life With Retardation (Flights)
1	Spar	Edge crack in spar web at bird's mouth termination	72000	76000
2	Skin Scenario 1	Mid-bay crack in the skin panel	44101	44047
3	Skin Scenario 2	Crack in skin panel at stringer	46680	46920
4	Skin Scenario 3	Crack in skin under fully broken stringer	9279	9297

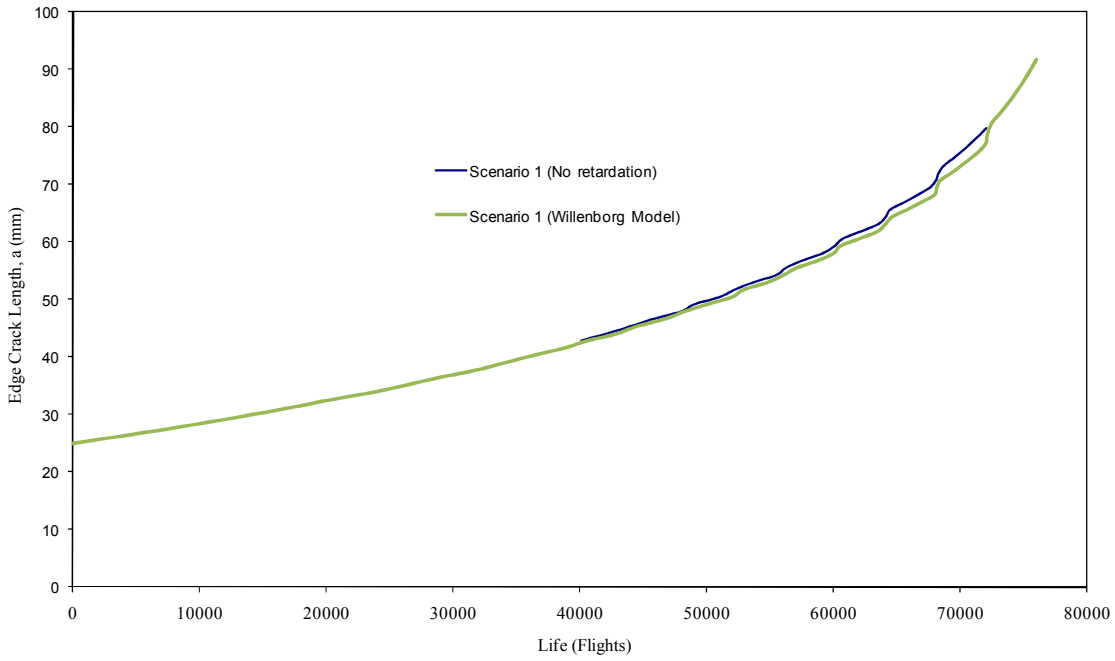

Figure 6.17 Predicted crack growth life of edge crack in spar web at bird's mouth termination

The crack growth analyses were undertaken with and without retardation. In fatigue crack growth propagation, there is an interaction effect of cycles of different amplitudes if the applied fatigue loading spectrum consists of cycles of varying amplitude. The application of an overload introduces a large plastic zone resulting in a slowing down of the crack growth rate when smaller amplitude load cycles are subsequently applied (Broek, 1991). The effect of crack retardation was accounted for using the Willenborg model. The Generalized Willenborg model is one of the most common load interaction models used in crack growth life prediction programs. The model is based on early fracture mechanics work performed at Wright-Patterson Air Force Base, Ohio, USA.

The model uses an "effective" stress intensity factor based on the size of the yield zone in front of the crack tip (Harter, 2006).

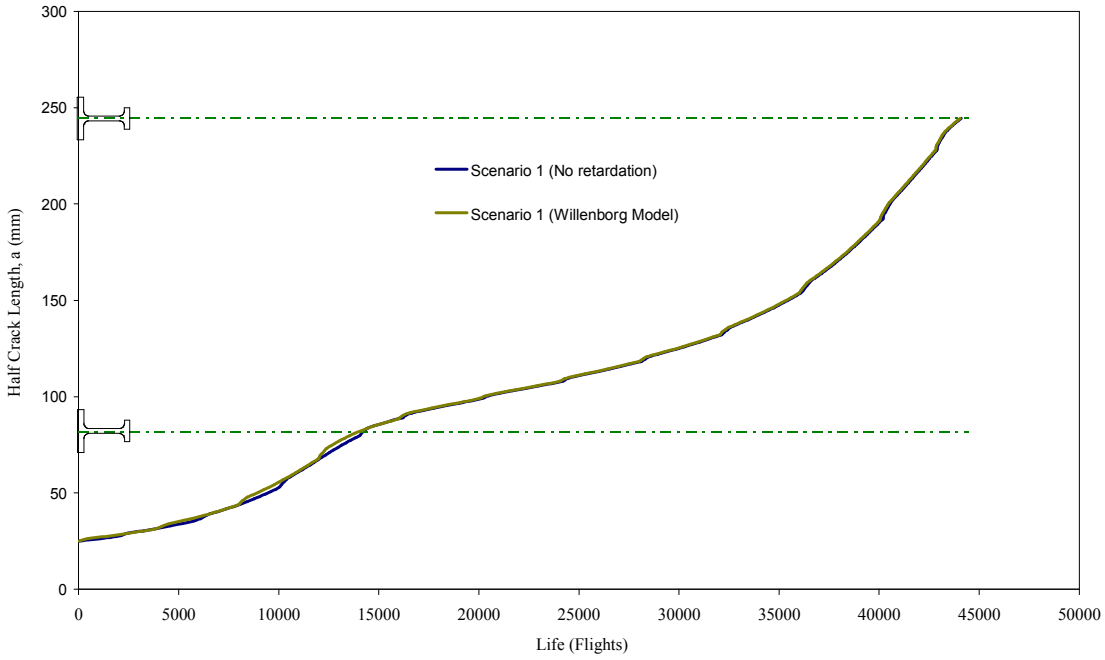

Figure 6.18 Predicted crack growth life of mid-bay crack in skin

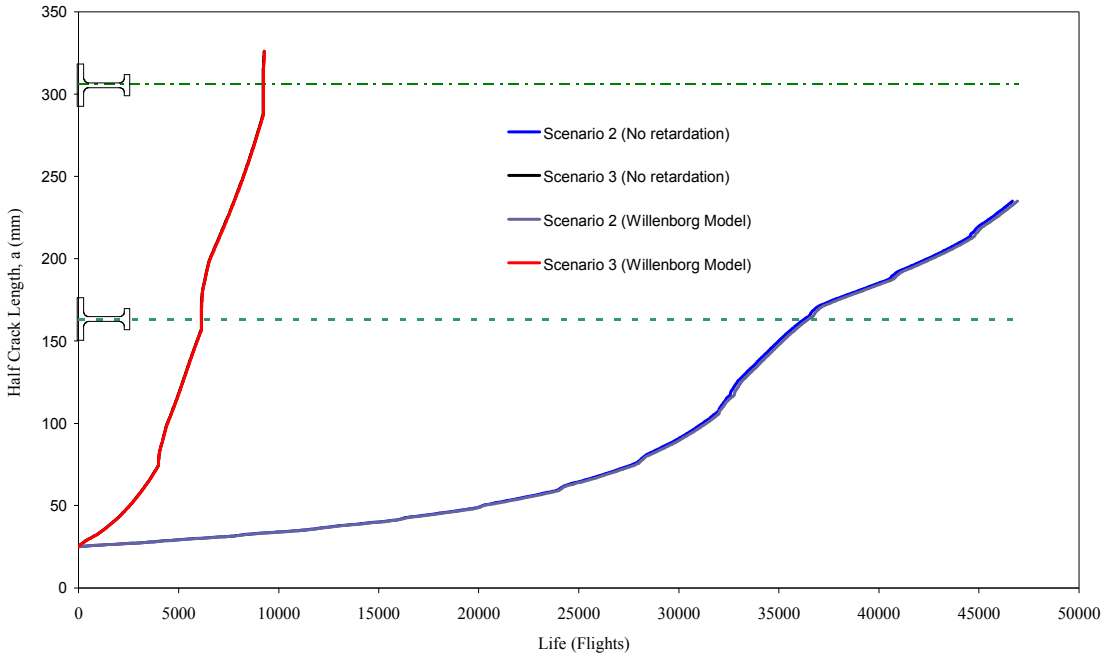

Figure 6.19 Predicted crack growth lives for skin crack growth scenarios 2 and 3

The crack growth lives of 72000 and 76000 flights without and with retardation respectively are presented in Table 6.15 and Figure 6.17 for an edge crack in the spar

web at the bird's mouth termination. The plot shows an increase in crack growth rate as the crack approaches the upper flange of the spar. In reality, the skin is an alternative load path that would attract more load as the spar's load transmitting capability is reduced due to the presence of the crack which would result in further deceleration.

Furthermore, the upper spar cap would provide additional resistance to crack growth as the crack progresses towards the upper cap. Crack growth was set to terminate when either the fracture toughness of the material was exceeded or net section yield occurred. For both crack growth assessments without and with retardation, the crack growth was terminated due to the fracture toughness of the material being exceeded and prior to the onset of net section yielding due to the application of fatigue stresses. A greater final crack length was achieved with crack retardation.

Figures 6.18 and 6.19 show similar crack growth lives for scenario 1, the mid-bay crack and scenario 2, the crack from an intact stringer of 44101 and 44047 flights for scenario 1 without and with retardation respectively and 46680 and 46920 flights for scenario 2, without and with retardation respectively. The plots show a reduction in crack growth rate as the crack approaches the outer stringer at 81.5 mm for scenario 1, the mid-bay crack and 163 mm for scenario 2, the intact stringer crack Scenario.

Figures 6.18 and 6.19 also show an acceleration in crack growth as the crack approaches the stiffener and a subsequent reduction in crack growth rate once past the outer stiffeners. Figure 6.19 shows a rather shorter crack growth life for scenario 3, a crack under a broken central stringer. Crack growth lives of 9279 and 9297 flights without and with retardation respectively were obtained which is 20% of the crack growth life for scenario 2, with an intact central stringer.

In contrast to crack growth in the spar web at the bird's mouth termination, the impact of crack retardation on overall crack growth life for the skin has been shown to be minimal. The reasons for the lack of crack retardation at the skin locations can be explained by the low magnitude of the peak applied stress of 89 MPa in the fatigue stress spectrum presented in table 6.5. Overload retardation is caused by very extensive crack tip plastic deformation at the overload. Elementary tests carried out to confirm this are described by Schijve (2001). In that test, a baseline peak stress of 112 MPa with interim overloads of 188 MPa (peak stress) was applied. The minimum stress was 48 MPa for all the stress cycles. The applied peak stress of 188 MPa in the test described by Schijve is twice as high as the peak value of 89 MPa applied in this assessment.

Furthermore, the ratio of (overload stress range) / (subsequent stress range) is significant; it needs to be greater than 1.5 to cause retardation. In the above case it is (188 - 48)/(112-48) = 2.19. In the case of this assessment, e.g. level 1 vs. level 9, it is (89 - 40)/(57 - 40) = 2.88, which is significant if the level 1 minimum stress was 40. However, the level 1 minimum is 8.8, which leads to the third reason.

The minimum stress in level 1 is not at the same level as the level 9 minimum stress; level one is 8.8 MPa (this is the so-called "underload followed by an overload" scenario, which will cancel the overload retardation effect. Hence the lack of overload retardation in the prediction.

6.7 Residual Strength Calculation

Two residual strength assessments were conducted. The first was a net section yield assessment of the crack in the spar web at the bird's mouth termination to confirm whether the spar web was capable of sustaining an edge crack at the final crack size under limit stress. The second was an assessment of the crack in the skin to establish whether the requirements of the two bay crack criterion had been met.

6.7.1 Residual strength calculation in spar web at bird's mouth termination

Broek (1991) explains that linear elastic fracture mechanics (LEFM) can only be usefully applied as long as the plastic zone is small compared to the crack size. This is usually the case in materials where fracture occurs at stresses appreciably below the yield stress and under conditions of plane strain. In such circumstances the fracture can be characterised by K_{IC}.

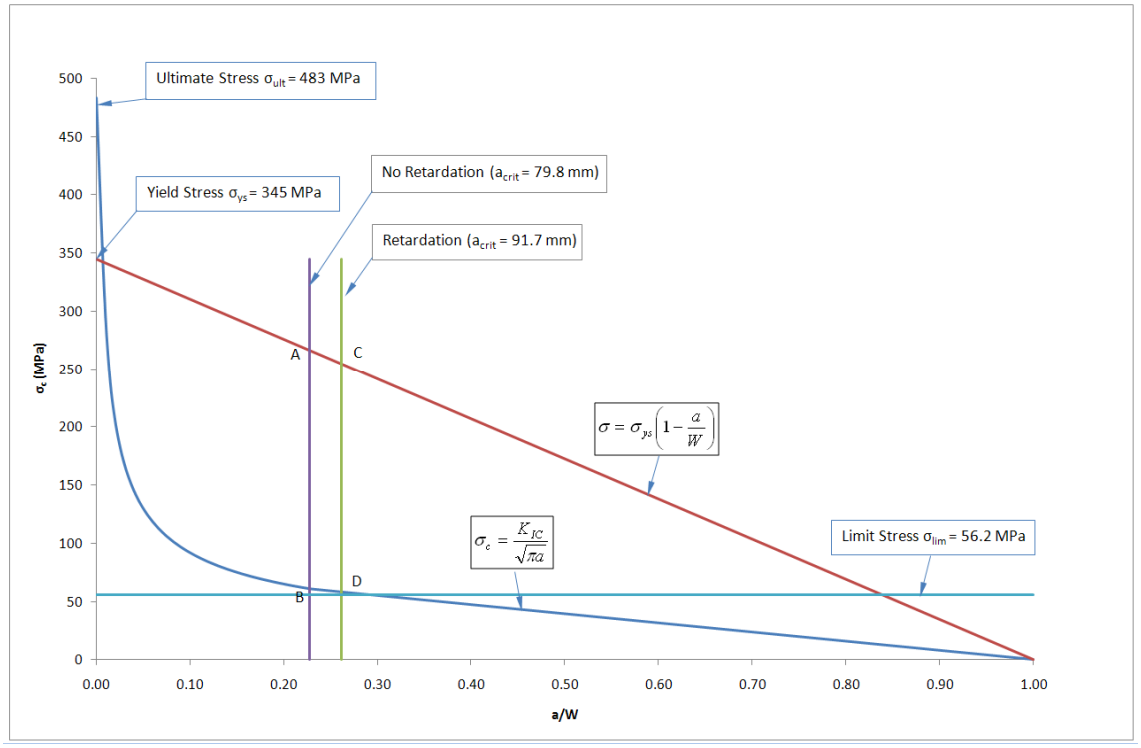

Figure 6.20 Predicted residual strength diagram for crack in spar web at bird's mouth termination

When plane stress prevails the crack tip plastic zone is larger than in the case of plane strain. Figure 6.20 shows that the fracture stress in the spar web when K_{IC} is applied occurs at B with no retardation and at D with retardation which is lower than A and C

respectively showing that under plane stress conditions, scope exists for additional crack growth until the net section stress in the web equals the yield stress of the material.

Generally, the plastic zone will become large and spread through the whole cracked section if the net section stress is equal to the yield stress. This is described by the following equation:

$$\sigma_{net} = \sigma \frac{W}{W-a} \geq \sigma_{ys} \quad (6.1)$$

Where;

σ_{net} = net section stress
W = component width
a = crack size
σ_{ys} = the yield stress of the material

The above equation is used to determine the net section stress of the spar web at the final crack size from AFGROW due to K_{IC} being exceeded and to determine whether the crack could have sustained limit stress. Crack growth was terminated at crack sizes of 79.8 mm and 91.7 mm for no retardation and with retardation respectively.

The limit stress is applied to the larger crack size to establish the net section stress in table 6.16. The results show that net section yield does not occur under limit stress at the crack sizes at which crack growth was terminated.

Table 6.16 Bird's mouth spar termination residual strength assessment

Item	Description	Value
1	Spar web height, W	350 mm
2	Final crack size from AFGROW, a	91.7 mm
3	Spar web limit stress, σ	56.2 MPa
4	Net section stress, $\sigma_{net} = \sigma \frac{W}{W-a}$	76.2 MPa
5	Yield stress of 2024 material, σ_{ys}	345 MPa
6	Reserve Factor, $RF = \frac{\sigma_{ys}}{\sigma_{net}}$	4.5

The usual expectation is that K_{IC} can be used until the failure stress σ_c approaches in the yield stress. Broek explains that in practice it turns out that σ_c should be lower than 66 percent of yield criterion.

For the purpose of this assessment failure has conservatively been set at the point where K_{IC} is exceeded. The crack growth life attained at this point is significantly larger than that obtained in the skin and no further crack growth is therefore required.

6.7.2 Residual strength calculation in skin

A residual strength assessment was made to establish the ability of the structure to sustain a two-bay crack at limit load. Indications are that a much higher frequency of inspection is however required for a two-bay crack with a broken central stringer and a visual detectable inspection. Alternatively, a longer repeat inspection interval would be possible with a smaller detectable crack size.

The residual strength of the wing skin with a two-bay crack is assessed using the approach described by Swift (1994). The residual strength is assessed as a function of half crack length and is presented in figure 6.21 and table 6.17. Point A in figure 6.21 identifies the onset of fast fracture in the skin with a subsequent reduction in crack growth rate as the crack approaches B. The allowable stress for the two-bay crack configuration is given by point B. Any fast fracture below this point will be arrested.

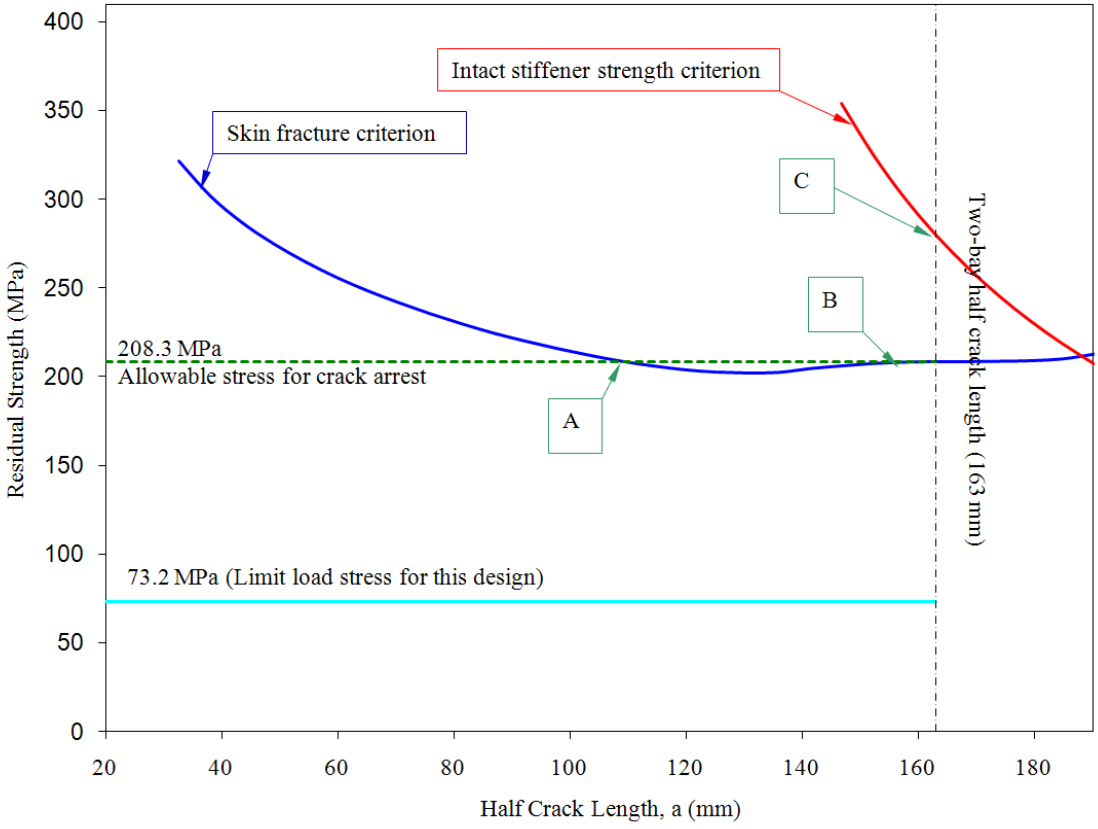

Figure 6.21 Predicted residual strength diagram for two-bay skin crack under broken central stiffener (scenario 3)

Figure 6.21 demonstrates that the two-bay skin crack is stable due to the relatively low levels of loading. The lower applied stress is a function of the need to increase skin thickness in order to reduce skin deflections at the design load case resulting in a consequent reduction in bending stresses.

Table 6.17 Residual strength as function of half crack length

Limit Load Stress (σ_{lim})			73.2	MPa			
K_c			137.0	MPa√m (Plane Stress)[a]			
F_{tu}			469.0	MPa			
a (mm)	a/b	K (MPa√m)	K/σ (√m)	β	σ_{os} (MPa)	σ_r (MPa)	σ_{st} (MPa)
32.6	0.200	31.2	0.426273	1.332	0.830	321.4	
38.0	0.233	33.3	0.454208	1.314	0.836	301.6	
43.5	0.267	35.0	0.477804	1.293	0.843	286.7	
48.9	0.300	36.5	0.498559	1.272	0.851	274.8	
54.3	0.333	37.9	0.517679	1.253	0.860	264.6	
59.8	0.367	39.2	0.535577	1.236	0.868	255.8	
65.2	0.400	40.4	0.552152	1.22	0.879	248.1	
70.6	0.433	41.6	0.567634	1.205	0.891	241.4	
76.1	0.467	42.7	0.582703	1.192	0.903	235.1	
81.5	0.500	43.7	0.597084	1.18	0.915	229.4	
86.9	0.533	44.7	0.610919	1.169	0.932	224.3	
92.4	0.567	45.6	0.623254	1.157	0.950	219.8	
97.8	0.600	46.5	0.635227	1.146	0.967	215.7	
103.2	0.633	47.3	0.646371	1.135	0.986	212.0	
108.7	0.667	48.1	0.656733	1.124	1.012	208.6	
114.1	0.700	48.7	0.665169	1.111	1.038	206.0	
119.5	0.733	49.2	0.672244	1.097	1.064	203.8	
125.0	0.767	49.5	0.676698	1.08	1.098	202.5	
130.4	0.800	49.7	0.678453	1.06	1.141	201.9	
135.8	0.833	49.6	0.677419	1.037	1.184	202.2	
141.3	0.867	49.1	0.670181	1.006	1.226	204.4	
146.7	0.900	48.7	0.665298	0.98	1.325	205.9	354.0
152.1	0.933	48.4	0.660915	0.956	1.442	207.3	325.2
157.6	0.967	48.2	0.65854	0.936	1.559	208.0	300.8
163.0	1.000	48.1	0.657634	0.919	1.676	208.3	279.8
168.4	1.033	48.1	0.657594	0.904	1.793	208.3	261.5
173.9	1.067	48.1	0.657029	0.889	1.911	208.5	245.5
179.3	1.100	48.0	0.655959	0.874	2.028	208.9	231.3
184.7	1.133	47.8	0.652873	0.857	2.145	209.8	218.7
190.2	1.167	47.2	0.644626	0.834	2.262	212.5	207.3

a. (Swift, 1994)

The allowable stress for crack arrest for the two-bay crack criterion is given by point B at the two-bay crack length as 208.3 MPa and is obtained from the range of values for the "residual strength based on skin fracture (σ_r)" presented in table 6.16 for a range of crack lengths. The "residual strength based on skin fracture (σ_r)" is defined as:

$$\sigma_r = \frac{K_c}{\sqrt{\pi a \beta}} \tag{6.2}$$

Any fast fracture higher than this value will not be arrested. At any stress lower than this value but greater than 201 MPa, fast fracture taking place at point A for example would be arrested at point B.

Furthermore, the intact stiffener is not critical for this material at crack sizes up to the two-bay crack as illustrated by point C in figure 6.20 and the "stress in outer intact stiffener for unit applied gross stress" σ_s and "residual strength based on stiffener strength" σ_{st} presented in table 6.16, making it possible for an inspection programme to be based on visually detectable cracking. The "stress in outer intact stiffener for unit applied gross stress" σ_s is the stringer stress obtained from FE modelling for the specified crack length, divided by the applied limit load stress. The "residual strength based on stiffener strength" σ_{st} is defined as:

$$\sigma_{st} = \frac{F_{tu}}{\sigma_{os}} \tag{6.3}$$

A decrease in stiffener strength can be seen with increasing crack size. Neither the skin nor intact stiffener are critical for a two-bay crack with an applied stress up to the allowable stress for crack arrest of 208.3 MPa. It can be seen from figure 6.21 that the applied stress of 73.2 MPa is much lower than the maximum allowable stress for crack arrest of 208.3 MPa.

6.8 Conclusions

The processes required in order to establish the damage tolerance capability of the blended wing body airframe at the wing root joint and the novel bird's mouth spar termination have been explored in the preceding sections.

The FE assessment of the wing root assembly indicated that the skin is the more critical component at the wing root when compared to the bird's mouth spar termination. The lower magnitude of the stresses in the spar at the bird's mouth termination are due to the transfer of load from the spar web into the root rib.

The crack growth assessment of the spar at the bird's mouth termination has confirmed the above indication with spar crack growth lives of 72000 and 76000 flights without and with retardation respectively for a visual detectable crack of 25 mm and a broken spar flange, that are almost double that of the skin at the root when all stringers are intact and significantly more with a broken central stiffener.

The results show that it would be possible to undertake 3 repeat inspections at intervals of a minimum of 24,000 flights for the spar web. For an aircraft with a 40,000 flight design service goal and assuming a crack free life of 20,000 flights, the results show

that only one inspection may be necessary at the inspection threshold of 20,000 flights. Any inspection of the bird's mouth spar termination would have to be an internal inspection in contrast to the external inspection that is possible for the wing skin. Keeping the number of required internal inspections to a minimum will be welcomed by operators of the aircraft.

Also explored is the two-bay crack criterion, established as a means of confirming the damage tolerance capability of transport aircraft structure. Skin thicknesses at the wing root are driven primarily by a need to minimise wing skin deflection due to internal fuselage pressurisation.

The use of the β solution for a stiffened panel with an As/bt ratio of 0.62 compared to the design panel As/bt ratio which ranges between 0.6 at frame locations and 0.316 at stringer locations means that the crack growth analysis is unconservative at stringer locations. The results of the crack growth assessment, discussed in the sections above suggest that As/bt ratios of 0.62 or greater are required.

The combination of relatively large skin thicknesses combined with low wing bending loads which are a function of the depth of the wing box result in low magnitude wing bending stresses at the wing root. The crack growth analysis results show similar crack growth lives for scenario 1, the mid-bay crack and scenario 2, the crack from an intact stringer of 44101 and 44047 flights for scenario 1, without and with retardation respectively and 46680 and 46920 flights for scenario 2 without and with retardation respectively and a reduction in crack growth rate as the crack approaches the outer stringer at 81.5 mm for the mid-bay crack, scenario 1 and 163 mm for the intact stringer crack, scenario 2.

The results show a shorter crack growth life for scenario 3 - the crack under a broken central stringer. Crack growth lives of 9279 and 9297 flights without and with retardation respectively were obtained which are 20% of the crack growth life for scenario 2, with an intact central stringer.

The low magnitude of the peak stress in the applied spectrum, caused by the lower bending stress due to the BWB structure, results in an "underload" effect which cancels the overload retardation. As a result, the difference in crack growth life due to retardation effects is not significant in the skin.

Scenarios 1 and 2 present preferred conditions with stable crack growth. For a visual detectable crack size of 50 mm, the results show that it would be possible to undertake three repeat inspections at intervals in excess of 14,500 flights for scenarios 1 and 2. For an aircraft with a 40,000 flight design service goal and assuming a crack free life of 20,000 flights, that represents intervals that are more than twice the 7000 flight repeat inspection interval that would be required.

The situation for scenario 3 is rather different and represents the most conservative case. The results of the assessment show that it would only be possible to achieve one inspection of 7000 flights. Consequently, stable crack growth occurs with all stringers intact. A significant increase in crack growth rate is observed with failure of the central stiffener in a two-bay crack.

The low magnitude skin stresses mean that the structure will sustain a two-bay crack at limit load. However, the inspection frequency required for a two-bay crack with a broken stiffener is significantly greater than for a two-bay crack with an intact central stringer.

7 Manufacturing Issues

7.1 Introduction

The essential features of the processes applied in the manufacture of aircraft components and their assembly into transport aircraft are explored in this chapter with a specific focus on wing fuselage integration. The manufacturing and assembly issues associated with the bird's mouth spar termination are discussed. The impact of design on operations management and cost control is also explored and the relevance of the proposed wing fuselage integration structure in taking advantage of the developments in aircraft manufacture and assembly is discussed.

7.2 Manufacturing and assembly processes

Aircraft assembly is a labour intensive and time consuming process which accounts for around one third of total manufacturing cost (Jin, et al., 2008). Most assembly operations in aircraft manufacturing are currently done manually. Although aircraft are small in lot size, numerous repetitive assembly operations have to be performed on a single aircraft. (Asada, H., Binayak, R)

Typical processes adopted in aircraft manufacture and assembly depend on the type of material selected and its properties. The material type is selected during the scoping and design phases of the aircraft programme in order to take advantage of specific material properties which are seen as beneficial.

For metallic components, the processes applied include casting, forming, shaping and precision machining of individual structural component parts and the application of specific heat treatments required to enhance the properties of the component. Processes such as cold expansion and shot peening are also employed to enhance the properties of the components as required. The individual components are then treated and painted to provide the required protection from environmental and other in-service damage.

For non metallic components and depending on the nature of the material considered, the processes involved include, layup of the material which may involve the use of tools, bagging involving processes such as vacuum debulking and removal of any air pockets that may exist in the layup and curing which may involve the application of heat.

For both metallic and non metallic components, the inspection of individual components is an essential part of the manufacturing process to ensure that the integrity of components is maintained throughout the manufacturing process.

The processes described above apply at the component level. Through a process of increasing integration, the components are assembled into sub assemblies such as stringers attached to skin panels to create wing skins. The joining methods applied in creating sub assemblies include fastening, bonding, brazing and new technologies such as friction stir welding.

There are six major subassemblies which make currently up conventional aircraft, namely; the fuselage, the empennage, the wings, the landing gear assemblies, the power plant and the flight control systems and instruments.

The production of aircraft relies on the precise and accurate alignment and mating of these subassemblies. For subassembly production and assembly mating, a series of assembly jigs are used. These jigs hold, support, and locate the individual work pieces or subassemblies until they can be riveted, bonded, or bolted in place. Rigidity of the assembly jigs is critical to prevent misalignment, so most of these tools are large and heavy. Some of the jigs are permanently installed, while others are on rollers so they can be moved to the assembly line when needed.

Tooling and jigs, although not components, are an essential part of the assembly process if the required tolerances are to be achieved. During the development phase, tooling costs account for more than a third in the civil sector and nearly a quarter for the military. Consequently, savings in this aspect of aircraft manufacture are significant and they also impact on the time from concept to market. Jigless assembly does not mean tool-less assembly, rather, it implies the eradication or at least the reduction in jigs. Simple fixtures may still be needed to hold the parts during particular operations but other methods are being found to correctly locate parts relative to one another.

Assembly techniques can be simplified by using precision positioned holes in panels and other parts of the structure to "self locate" the panels. This process, known as determinant assembly uses part-to part indexing, rather than the conventional part-to tool systems used in the past. Within the airframe manufacturing industry, it is generally accepted that approximately 10% of the overall manufacturing costs of each airframe can be attributed to the manufacture and maintenance of assembly jigs and fixtures. Traditional "hard tooling" philosophy requires that the desired quality of the finished structure be built into the tooling. The tooling must, therefore, be regularly calibrated to ensure build quality.

An alternative philosophy, "Flyaway tooling", has been conceived with the purpose of reducing tooling costs and improving build quality. This approach envisages that future airframe components will be designed with integral location features and that they will incorporate positional datum's that will transfer into the assembly. This will enable in-process measurement, and aid in-service repairs. It may also be possible to design an aerospace structure having sufficient inherent stiffness so that the assembly tooling can be reduced to simple, reusable and re-configurable, supporting structure. (Curran, et al., 2002)

Fabrication and assembly of a commercial aircraft involve a variety of detail part fabrication and assembly operations. Fuselage assembly involves riveting/fastening operations at five major assembly levels. The wing has three major levels of assembly.

The propulsion systems, landing gear, interiors, and several other electrical, hydraulic, and pneumatic systems are installed to complete the aircraft structurally.

Aircraft manufacturing techniques are well developed. Fabrication and assembly processes follow a defined sequence, and process parameters for manual and mechanized/automated manufacturing are precisely controlled. Process steps are inspected and documented to meet the established regulatory body quality requirements, ensuring reliable functions of components, structures, and systems, which result in dependable aircraft performance. (Sarh, et al, 2009)

Conventional wing assembly typically consists of the centre wing section, outboard wing sections, and aileron and flap assemblies. The building of the outboard wing section involves the use of many different jigs for drilling, riveting, and build-up and to integrate the forward outboard wing assembly, rear spar assembly, trailing edge assemblies and supporting structure.

The construction of the centre wing section also requires the use of many different build-up jigs to integrate the centre section subassembly, wheel well structure, rib and skin assemblies and supporting structure.

In some aircraft assembly processes, the wing assembly mate jig is used to assemble both the left and right outboard wings with the centre wing. The wing sections and centre section are located in the jig by locators and contour boards. The centre section is loaded first, followed by the left and right outboard wings. The completed wing assembly is then mated to the fuselage section.

In other aircraft assembly processes, the centre section is mated to the fuselage section first and the outer wings then subsequently mated to the fuselage and centre section assembly.

7.3 Operations management and cost control

The accurate estimation and analysis of aircraft assembly times are important for process planning, cost control and reducing product development lead times. One way of achieving the desired cost reductions is by increased automation of the manufacturing and assembly processes.

The assembly of an airplane entails a synchronized series of manufacturing processes that are organized as a network of concurrent and merging flows. These manufacturing processes are organized into a network of work centres or departments. These work centres, staffed with varying numbers of line employees, have responsibility to perform preassigned tasks within the manufacturing process. The operations performed by these work centres vary from tasks as simple as finishing the surface of an airplane wing to tasks as complex as integrating the major body sections of the entire airplane. For example, a work centre might be responsible for joining the completed left and right wings to the wing-stub section of the airplane fuselage.

The manufacturing flow time for a work centre is the elapsed time planned for a work centre to perform and complete its required tasks. The flow time is the length of time that an airplane (or subassembly) will remain at a work centre before moving to the next work centre. Different work centres within the manufacturing sequence can have (and will have) different flow times.

The production cycle time is the elapsed time (in work days) between consecutive job completions for a work centre or between airplane deliveries for the entire manufacturing system. Unlike manufacturing flow time, all work centres within the manufacturing system operate with the same production cycle time (i.e., at the same rate). An airplane manufacturer operating on a 3-day production cycle completes and ships an airplane from the production line every 3 days. Consequently, every work centre also must complete work on an airplane every 3 days, no matter what the individual flow time of the work centre is. Correspondingly, every 3 days, one new job enters each work centre in the manufacturing process.

The assembly times for different sub-assembly modules may not be in the same scale, making line balancing difficult. The gap between methods engineers, process planners and even designers, imposes negative effects on the success of a company in the competitive aerospace industry today. In addition, time consumed on the shop floor may not be traceable, making it difficult to identify the time driver once a big project fails to complete in the pre-assigned schedule. Elimination of the gap and the establishment of a rapid, effective and traceable mechanism is essential for an aircraft company to build and maintain a competitive advantage. (Jin, et al., 2008).

7.4 Conformance and standards

The quality of aircraft depends on good design, documentation, and electronic record keeping to meet regulatory body requirements and certification requirements. The windshields, wing leading edges, engines and other critical components must meet bird strike requirements before the aircraft is certified for commercial use. Many different forms and checklists are used throughout the manufacturing process to detail the history of each part made. Various laboratory tests and standardized aerospace material specifications have been developed specially for aircraft. To check how well bonded panels have adhered, they are placed in a water tank for ultrasonic testing. Stress testing is used extensively. A section of the aircraft is assembled and then placed in a test fixture which simulates actual use under varying conditions. Some of the tests are run until the parts fail, to see if the design safety factor is acceptable.

7.5 Design applications

Designing for ease of assembly is not restricted exclusively to the task of concept design engineers. Tooling engineers make a contribution to reducing non-recurring costs through a jig-less assembly approach to manufacturing. During the development phase, tooling costs account for more than a third in the civil sector and nearly a quarter

for the military. Consequently, savings in this aspect of aircraft manufacture are significant and they also impact on the time from concept to market.

The manufacturing and assembly processes discussed earlier all require careful consideration during the design phase of an aircraft project if cost savings are to be achieved. Crosby, et al. (2003) argue for example, that airframe components designed with integral location features incorporating positional datum's that will transfer into the assembly facilitate in-process measurement which is beneficial to the manufacturing/assembly process, and aid in-service repairs which is a further benefit over the total life cycle of the aircraft.

All the above issues are as relevant to the bird's mouth spar termination and associated wing fuselage integration structure discussed in this report. Wing fuselage integration structure incorporating bird's mouth spar terminations can be designed with sufficient inherent stiffness so that the assembly tooling can be reduced to simple, reusable and re-configurable, supporting structure.

Technological change is a major driving force in the evolution of aircraft manufacturing. Many developments underway involve computerized controls and automation designed to improve economy and quality and lower energy consumption and pollution. More assembly operations, such as riveting, may become completely automated. "Smart" sensors—sensors with predictive abilities involving fuzzy logic and artificial intelligence—are becoming more prevalent. Artificial intelligence or "fuzzy controls" enable the sensors to predict changes needed in the settings due to changes in load or production volume. In addition to these developments, increasing economic and environmental needs will bring further technical refinements to aircraft manufacturing.

7.6 Investigation of manufacturing and assembly issues with respect to integration of novel bird's mouth spar termination.

(Liebeck, 2002) describes the BWB as simply a big wing with an integrated fuselage and no empennage, save the winglets/verticals. There are no complex wing-fuselage and fuselage-empennage joints of highly loaded structures at 90 degrees to one another, and there are no fillets. All trailing-edge control surfaces are simple-hinged with no track motion, and there are no spoilers. This manifests a substantial reduction (on the order of 30-percent) in the number of parts when compared to a conventional configuration. A similar reduction in manufacturing recurring cost is implied.

There is agreement in the industry as evidenced by Liebeck's comment above that the BWB platform results in reduced complexity and the number of components at the wing root is also reduced. Other issues requiring additional clarification include the limitations on manufacturing and assembly of BWB components, particularly in relation to the novel proposed bird's mouth spar termination.

Discussions with Mr. Frank Bamford, Vice President - GKN Aerospace and other senior personnel within the aerospace industry suggest that for primarily metallic solutions, there are no doubts that there is a deficiency in the ability, facilities and plant to produce “one piece” solutions in the sizes proposed in this research project, considering today's conventional concepts. To machine and form the proposed structure may be outside some of the aerospace industry’s current capability. GKN Aerospace for example, have a gantry machine that is 143 metres long with a 3 metre bed width highlighting the limitations of today’s conventional capabilities.

Mr. Bamford explained that “If I were to answer your question in terms of what we have today it would fall into the all too difficult box but given the pace of change we are now seeing in manufacturing technology and techniques I would not be so prescriptive in terms of the future goal.”

He explained further that there are other solutions available to get around these limitations. Creep and stretch forming techniques exist that could help in the forming of large scale shapes although perhaps not in a single piece. Furthermore, current advanced welding techniques mean that the possibility of achieving the desired objective of manufacturing large components is significantly improved. For example GKN Aerospace produce welded primary structure for the F22 that are considered virtually seamless structures. This further demonstrates the possibility of large “one piece” structural items using thermal jointing to achieve the results in the scale proposed and with a single surface requiring no joints or fasteners.

Alternatively a “one piece” solution could be achieved through advanced coatings that produce a seamless surface with the same surface performance as a single piece structure. This is also an option under investigation by GKN.

Another approach could be the use of composite materials. This also presents similar challenges through the limitations of current plant and equipment. However with the advent of microwave curing the conventional constraint of autoclaves may be removed and this may further extend the size of fasternerless single piece structure that can be manufactured by using melding techniques for composites. In essence this constitutes a part cured set of structural components effectively joined using this technique and alleviating the constraints of conventional plant. This brings into play a directed energy solution that removes the constraints of pressure vessels and opens the door to unitary structures in large complex forms.

Discussions with other senior manufacturing personnel, including Mr. Paul Ashton-Rickardt, A350 Manufacturing Engineering, GKN Aerospace indicate agreement about the manufacturability of the proposed structure. In reality, the wingbox ribs and spars for the proposed aircraft would be bigger than A380, and A380 stretched the machining envelope. Three piece ribs, top and bottom feet with a rib body, making up an assembly are recommended for manufacturability. A similar approach is recommended for the novel bird’s mouth spar termination and the spars, comprising of a spar body with bolt

on spar caps. As a rule of thumb, anything machined out of plate over two metres wide is into high cost and restricted machining capability. In the current machining environment therefore, the components would have to be limited to two metre widths. However discussions with Mr. Bamford anticipated that this limitation will be exceeded in the near future.

It can be seen from the discussions above that the main difficulty with the manufacture of the individual components that together constitute the wing root structure with the novel bird's mouth spar termination is the capability of existing manufacturing processes. These limitations notwithstanding however, it is possible to manufacture the components in a modular manner and still return a reduced parts count.

The assembly of the wing structure at the wing root should be possible with current assembly practices and the reduced part count would be of benefit in minimising the risk of error in assembly. A drawback that will require detailed attention is the impact of assembly errors involving large components as the cost of scrapping these would be significant when compared to the cost of replacing smaller components.

7.7 Conclusion

The proposed birds mouth spar termination and associated wing fuselage integration structure simplify the structure at the wing fuselage joint thus making it possible to take advantage of the substantial savings available as a result of improved manufacturing and assembly processes.

The proposed bird's mouth spar termination design simplifies the wing fuselage integration structure and process, reduces parts count, makes possible a more rigid assembly thus reducing the need for complicated jig and tooling. The simplicity of the design means that the assembly lends itself to automation thus improving work flow times with the associated improvements in quality and savings in manufacturing and assembly costs.

Aircraft assembly is a labour intensive and time consuming process which accounts for around one third of total manufacturing cost. The proposed birds mouth spar termination and associated wing fuselage integration structure of the BWB aircraft makes it possible to achieve significant reductions in part count and associated manufacturing and assembly costs in the order of 30 percent.

The manufacturing and assembly issues associated with the proposed wing root structure and bird's mouth termination could be perceived to fall into the "all too difficult" box but given the pace of change in manufacturing technology and techniques scope exists for the manufacture of large "one piece" structural items. The current proposal will require the manufacture of sub components then assembled to complete the structure albeit with larger sub components than currently exist for conventional airframes.

8 Final Discussions

8.1 Introduction

The Blended Wing Body airplane concept represents a potential revolution in subsonic transport efficiency for large airplanes. Studies have shown the BWB to be superior to the conventional configuration in all key measures (Liebeck et al., 1998). Previous blended wing body aircraft research projects have identified several structural integrity issues with wing/fuselage joints, non-circular fuselage structure (with associated problems of pressurisation) and temperature differentials between inner and outer skins on the fuselage and the resulting stress issues. All of the above issues were identified as suitable starting points for this research project. Wing to fuselage integration was selected as the focus for this project.

8.2 Damage tolerance capability

The damage tolerance capability of the proposed solution to BWB wing to fuselage integration was considered to be an essential part of this project. At the core of the damage tolerance philosophy is the requirement that any damage sustained by aircraft structure is identified and addressed prior to the damage becoming unstable. While the damage may take several forms, the traditional approach has been to assess damage in the form of cracks (Swift et al, 1969) (Goranson, 1997). Large crack capability, adequate residual strength, sufficient crack growth life and the inspectability of the proposed design are core requirements. These were addressed by applying net section yield criteria to the spar web at the bird's mouth termination and the two bay crack criterion to the skin at the wing root. The two bay crack criterion has evolved as a means by which aircraft designers can satisfy themselves that, in the event of a crack initiating on aircraft structure, the risk of fast fracture occurring before a predetermined critical crack length is achieved is avoided (Swift, 1990).

8.3 Design requirements

In addition to the requirements of the regulatory bodies, the design requirements applied to the proposed bird's mouth termination and the skin at the wing fuselage joint included the key success criteria for the two-bay criterion, as described by Swift (1994). Swift's criteria includes; limit stress level about the same or a little lower than residual strength capability thus keeping structural weight to a minimum; visual inspection based on crack growth from detectable crack to crack arresting stiffeners (maximum spectrum load for normal usage is about 60% of limit load and occurs only once in one tenth of lifetime); resulting inspection burden on operator is not excessive.

8.4 Advantages and disadvantages of current wing root joint types

Spliced plates are widely used in current conventional transport aircraft wing to fuselage joints because they are light weight, more reliable and have inherent fail-safe features. They, however, tend to have a higher cost and present more difficulties in manufacture. Tension bolted joints and shear lug joints are easier to manufacture and assemble but

with weight penalties. A combination of spliced plates and tension bolts has the advantages of both methods but also the weight penalty associated with tension bolts.

Matthews (1990) takes the view that mechanically fastened joints have the advantage that they require no special surface preparation, disassembly is easily achieved without damage and there are no special inspection problems. However, the associated holes cause stress concentrations and the joints can incur a large weight penalty. An alternative to mechanical fasteners is adhesively bonded joints which have lower stress concentrations and incur smaller weight penalties (though disassembly is impossible without causing damage), are susceptible to environmental effects, require surface preparation and their integrity cannot be confirmed by normal inspection methods.

In-service experience of metallic aircraft structure has revealed ageing aircraft issues including widespread fatigue damage and multiple site damage that have received a significant amount of attention. Means of assessing the above issues in ageing aircraft structure have been discussed by Swift (1999), Bellinger et al. (2001) and Wanhill and Koolloos (2001).

A potential solution to the problems experienced with metallic aircraft joints is the adoption of non-metallic material solutions. Great care needs to be taken in the definition of design with non-metallic material since issues such as the spew fillet, residual thermal stresses and the inelastic behaviour of the adhesive material to name a few, can have a significant impact on the integrity of bonded joints. Schön and Nyman (2002) found that bolt failure was the dominant failure mode in the bolted composite joints they assessed.

The design of damage tolerant wing root joint structure requires careful consideration of the constituent material, joint configuration and in-service operating environment. Whilst the metallic spliced plates/tension bolts/shear lugs configuration has been the convention, the availability of non-metallic composite materials provide the opportunity for a step change in the design of wing roots towards achieving the ultimate goal of minimum weight and fatigue resistant wing/fuselage integration structure without joints or with a significantly reduced or minimum number of joints or splices.

8.5 Proposed bird's mouth spar termination wing to fuselage joint

The absence of joints or splices in aircraft structure is preferable where possible (Niu, 1990). The nature of existing aircraft configurations, however, means that it is almost impossible to avoid joints at the intersection of the wing and the fuselage. One advantage that blended wing body aircraft appear to have over existing aircraft configurations is the scope for eliminating the wing fuselage joint altogether. In blended wing body aircraft, the wingbox depth at the wing root is equal to fuselage height making it possible for the wing skin to continue uninterrupted across the wing/fuselage boundary.

The possibility of uninterrupted wing skin across the skin/fuselage joint was explored in this research project. An initial assessment of potential root joint configurations yielded two possible solutions. The Type 1 root joint was initially proposed as an alternative to existing root joint types. In this initial proposal, the stringers also provide structure (flanges) on to which an internal fuselage skin could be mounted providing structure for reacting internal fuselage pressurisation loads whilst the external skin reacts normal flight loads. The root rib was required to react flight and pressurisation loads.

A subsequent Type 2 proposal included the introduction of circular frames that provide supports for circular fuselage skins. The overall internal cross-section of the fuselage becoming oval in shape thus providing a more efficient means of reacting the internal fuselage pressurisation. The internal fuselage pressure would, therefore, be reacted by the internal skin and the flight loads reacted by the outer skin and root rib.

In the final proposal, the fuselage frames were deleted. The wing skin stringers are continuous across the wing fuselage joint. Additional stiffeners were introduced in the format of longerons running fore-aft and fuselage stiffeners running parallel to stringers and replacing every third stringer and with considerably greater depth and section properties. The fuselage pressure boundary was moved out from the root rib to the next adjacent outboard rib, thus reducing the role of the root rib to reacting floor structural loads and wing brazier loads and the wing skin reacting flight and fuselage pressurisation loads.

A key issue impacting the design of the root joint was the nature of the termination of the main wing spars. Current fuselage centre boxes include front and rear spars and in some cases a centre spar thus ensuring continuity of load path. Because the wing of the project aircraft is the depth of the fuselage, continuation of spars through the fuselage introduces barriers within the fuselage that require additional cut-outs.

Most significantly, the spars were designed with a bird's mouth profile. This facilitated a smooth transfer of loads from the spar web into the root rib and the top and bottom skins. Continuity of the spars was maintained across the fuselage whilst ensuring that the passenger cabin is largely unobstructed.

A modular root rib was proposed making it damage tolerant. The spars are single load path structures but with crack arrest features such as stiffeners. The presence of large uninterrupted airframe skin is an advantage but also presents some risk. The damage tolerance capability of the airframe skin would be enhanced by the presence of fail safe straps and these are proposed for the airframe skin at the wing root.

8.6 Design Calculations

The project BWB aircraft was designed with a payload-range similar to the Boeing 767 and the AIRBUS A330-200 aircraft. This project was originally intended to be a continuation of work undertaken as part of a Cranfield University MSc course in Air

Vehicle Design (AVD) (Smith, 2002) for a blended wing body aircraft capable of competing with the Boeing 767 aircraft. Constraints on access to the AVD data meant that the project had to be completed without access to the results of the MSc study. The Boeing 767 aircraft was, however, maintained as the baseline aircraft for comparison in this project.

A total passenger complement of 245 passengers was assumed, giving a first estimate of Maximum take-off mass (MTOM) of 199920 kg. The AIRBUS single aisle fuselage width of 3.95m was selected as a typical narrow body section. The BWB fuselage depth at its centre line was, therefore, 3.95m with a fuselage width three times its depth.

The stall speed or minimum flying speed KEAS V_s was set at 135 knots for the project aircraft. This compares favourably with 137 knots for the Boeing 767 (Jane's, 2001). The choice of aerofoil section plays a significant role in determining wing drag. As the focus of this project was on structural sizing, a detailed assessment of aerofoil sections was not undertaken.

A maximum lift coefficient of 1.3, which is consistent with transport aircraft, was selected for this aircraft and an effective friction drag coefficient for jet aircraft, C_{Dfric} of 0.0035 assumed. The speed for maximum range was assumed to occur at $(L/D)_R$ (gear retracted) at approximately 2.8 times the stall speed of 135 knots i.e. $2.8V_{so}$ giving a speed for maximum range of 378 knots.

8.7 Wing root shear force, bending moment and torque (SMT loads)

Wing root shear force, bending moment and torque were derived for the project aircraft using a method defined in Airframe Structural Design (Niu, 1990) and in spreadsheet format. The 2.5g V_D limit load case which is the most severe load case the aircraft is expected to experience was selected for structural sizing.

The data was then interpolated to determine limit wing shear, bending moment and torque at the wing root corresponding to a normalised wing span η of 0.2456 as follows:

- Limit shear load 152.143×10^4 N
- Limit bending moment 11.292×10^6 Nm
- Limit torque 0.837×10^6 Nm

8.8 Global model analysis using a "beam-cell" model

The multi model global-local strategy and approach was adopted in this work using a coarse beam-cell model for the global low fidelity analysis and using the resultant data from the global model to determine the input loads for the local high fidelity FE model.

The project aircraft wing comprises of 3 spars (front, centre and rear) and a false rear spar thus defining a 4 cell box. The wing box was modelled as a 250 boom three cell box, instead of a four cell box, making the results slightly more conservative. The results of the global model are summarised as follows:

- Maximum limit tensile stress in stringers at 2.5g = 164.2 MPa
- Maximum limit shear stress in skin panels at 2.5g = 18.97 MPa

The structure is required to be designed to be capable of withstanding ultimate loads. A safety factor of 1.5 was therefore applied to the limit stresses yielding the following design stresses:

- Maximum ultimate tensile stress in stiffeners at 2.5g = 246.3 MPa
- Maximum ultimate shear stress in skin panels at 2.5g = 28.46 MPa

The above stress values demonstrate the low magnitude of the resultant wing bending stresses at the ultimate design load case. This effect has been attributed to the depth of the wing box which, being the same as the height of the fuselage section results in relatively low wing bending stresses at the root.

8.9 Local model analysis by finite element method

The second phase of the multi-model approach was the creation of a high fidelity local finite element model with more detail and elements aimed at obtaining a more accurate understanding of the structure being assessed. From the low fidelity global model, an understanding of the local boom stresses and panel shear flows and stresses was obtained.

The stresses derived from the 3-cell box low fidelity global model were applied to the high fidelity local finite element model of the wing root to identify potential structural weaknesses in the proposed design. Sections of the main structural components, including the wing centre spar, wing bottom skin, wing root rib, stringers, fuselage longitudinal stiffeners and rib 2 outboard of and adjacent to the root rib were represented in the local FE model. The three load cases considered were:

1. 2.5g V_D x 1.5 Ultimate Load case
2. (2.5g V_D + 1ΔP) x 1.5 Ultimate Load case
3. 2ΔP Ultimate Load case.

The loads were applied to the local FE model in order to replicate the loading conditions at the wing root whilst taking local geometry into account. The constraints were applied such that the stress distribution in the skin reflected the expected stress distribution in the vicinity of the root rib.

8.10 Observations and design iteration

In seeking to eliminate the differences between the prediction from the finite element simulation and the actual future performance of the blended wing body aircraft, it was necessary to perform the simulation in stages.

Several iterations of the FE analysis were required in order to optimise the proposed wing root design. Quite early in the analysis, skin thicknesses of 1.0 mm were shown to

be adequate for reacting wing bending loads. This is because the depth of the wingbox meant that the resultant direct tensile and compressive stresses were much lower than would be expected for a comparative wingbox with a thinner wing depth. It also meant that it was possible to achieve As/bt ratios of 1.46 in the wing skin which is an important consideration in damage tolerant design.

The application of internal fuselage pressurisation loads resulted in significant skin deflections which required attention. The deflections if not addressed would have a compromising effect on the aerodynamic characteristics of the aircraft. Skin deflections were a concern and skin thicknesses were, therefore, increased from 1.0 mm to minimise skin deflection. Skin thicknesses of 5.0 mm, 7.0 mm and 10.0 mm were assessed and skin thicknesses of 10.0 mm retained as they returned the lowest deflections. Stringer and longitudinal stiffener sections were also increased to improve the bending stiffness of the skin panels.

The model was originally created with stringers of 240 mm^2 cross-sectional area. The need to increase the bending capability of the panels meant that stringer cross-sectional areas were increased to 515 mm^2. Also included were heavier I section stiffeners with cross-sectional areas of 975 mm^2 replacing every third stringer to provide increased stiffness. These stiffeners run perpendicular to the fuselage centreline in the fuselage and perpendicular to the chord on the wing side. Additional longerons with cross-sectional area of 3350 mm^2 were also included: these run parallel to the fuselage centre line to provide additional bending stiffness.

8.11 Results with internal pressure

Peak von Mises stresses in the region of 405 MPa to 435 MPa were obtained in the skin at the vertices of the model for the (2.5g + 1ΔP) x 1.5 Ultimate loadcase which was the worst load case. Most of the skin area show stresses in the range of 75 MPa to 315 MPa for the (2.5g + 1ΔP) x 1.5 Ultimate loadcase. Maximum stringer stresses in the region of 270 MPa which are consistent with the stresses obtained from the global model were also obtained. The peaks are located at the stringer restraints with much lower stresses being experienced away from the restraints. This is due in part to the increased skin thickness required to reduce the deflection in the wing skin as a result of internal fuselage pressure. The peak stresses discussed in chapter 5 are extreme fibre stresses that are conservative. Average skin stresses should be applied in any subsequent analysis and will be of a lower magnitude.

Peak von Mises stresses ranging from 405 MPa to 435 MPa occur in the lower part of the spar web and the spar flange where fixed displacements have been applied to simulate the loading in the spar flange and web. Away from the peak stresses, the von Mises stresses range from 15 MPa to 345 MPa increasing from the cut section of the spar which is mid spar to the lower flange. The fringe plots show an increase in web stress inboard of the root rib from the full depth web to the spar runout. The increase in

stress at the most inboard end of the spar runout is also attributed to the applied restraint at the inboard end. The trend of the shear patterns is of interest. A definite change can be observed in the fringe plots at the spar joint with the root rib. The "bird's mouth" type spar termination was designed purposely to effect gradual load transfer from the spar into the root rib and skin. This is clearly demonstrated with a definite change in stress profile reflecting a decrease in spar web stress at the root rib location. Inboard of the root rib, a gradual increase in the spar web stresses as the spar depth decreases can be observed. With increasing load transfer into the skin, a further decrease in spar web stresses can be observed.

The plots show maximum von Mises stresses in the root rib web ranging from 135 MPa to 315 MPa. Away from the vertices, the von Mises stresses in the root rib web range from 15 MPa to 195 MPa and the maximum shear stresses from 15 MPa to 135 MPa reflecting the fact that the loading on the root rib web is much lower than the outboard rib which is the pressure boundary. An increase in stress is evident at the joint between the root rib and the spar demonstrating load transfer from the spar web into the root rib web.

The outboard rib is the pressure boundary and as a result, the stresses are greater than at the root rib. The plots show peak von Mises stresses ranging between 315 and 435 MPa and peak maximum shear stresses ranging from 230 MPa to 270 MPa.

A maximum vertical deflection of 11 mm occurring in the wing skin and 13 mm in the fuselage skin was observed. The applied load case for deflection is the 2ΔP Ultimate Load case. The deflections for normal operating conditions are significantly lower. A maximum deflection of 26 mm was observed on the outboard rib. This is over a panel depth of 1.6m (i.e. less than 2% of panel depth) approximately and is for an ultimate load case of V_D with $2\Delta P$ pressure applied. The rib is not an aerodynamic surface and therefore not subject to the deflection constraints of aerodynamic surfaces.

A comparison of the results of an assessment by NASA of different fuselage skin configurations (Mukhopadyay, 2005) showed that the results obtained from this assessment are similar. The deflection is, therefore, considered acceptable. Deflection is a key criterion in this configuration and presents much scope for further analysis / investigation.

8.12 Identification of detail design points

FAR/JAR part 56.561 states clearly that each evaluation required must include the evaluation of principal structural elements and detail design points, the failure of which could cause catastrophic failure of the airplane. To some extent, that identification has been made in the sense that the wing root and its components have been identified as principal structural elements requiring investigation. For the purposes of this project, the skin/stringer interface at the root joint is deemed to require further assessment.

The root rib was not considered as it was relatively lower loaded. Similarly, the outboard rib was not assessed as the magnitudes of normal flight loading are not considered to be of great concern. The relatively lower loading in the spar meant that only one crack growth assessment was undertaken. Three crack growth scenarios were assessed at the more critical skin/stringer interface as follows:

a. Mid bay crack in the skin panel;
b. Crack in skin panel at stringer datum, and;
c. Crack in skin panel at stringer datum with fully broken stringer.

8.13 Loading spectrum

The FE analysis was the source of stress data required to compile a fatigue loading spectrum. The fatigue stresses were compiled by combining the stresses for 1g loading and the stress component due to 1ΔP fuselage pressurisation.

The TWIST fatigue loading spectrum from ESDU 97018 was applied. The TWIST load sequence, which represents 40,000 flights, is made up of 10 identical repeated blocks of 4,000 flights each comprising up to 10 load levels. The inertia spectrum for a block of 4,000 flights was applied in the crack growth calculation of the skin/stringer interface.

8.14 Crack growth assessment

Crack growth lives of 72000 and 76000 flights without and with retardation respectively were obtained for an edge crack in the spar web at the bird's mouth termination using AFGROW. The results show an increase in crack growth rate as the crack approaches the upper flange of the spar. In reality, the skin is an alternative load path that would attract more load as the spar's load transmitting capability is reduced due to the presence of the crack which would result in further deceleration. Furthermore, the upper spar cap will provide additional resistance to crack growth as the crack progresses towards the upper cap. Crack growth was set to terminate when either the fracture toughness of the material was exceeded or net section yield occurred. For both crack growth assessments without and with retardation, the crack growth was terminated due to the fracture toughness of the material being exceeded and prior to the onset of net section yielding due to the application of fatigue stresses. A greater final crack length was achieved with crack retardation.

The crack growth life of the two-bay crack in the skin was also determined using AFGROW. The crack growth analysis results show similar crack growth lives for scenario 1, the mid-bay crack and scenario 2, the crack from an intact stringer of 44101 and 44047 flights for scenario 1, without and with retardation respectively and 46680 and 46920 flights for scenario 2 without and with retardation respectively and a reduction in crack growth rate as the crack approaches the outer stringer at 81.5 mm for the mid-bay crack, scenario 1 and 163 mm for the intact stringer crack, scenario 2.

The results show a shorter crack growth life for scenario 3 - the crack under a broken central stringer. Crack growth lives of 9279 and 9297 flights without and with retardation respectively were obtained which are 20% of the crack growth life for scenario 2, with an intact central stringer.

The low magnitude of the peak stress in the applied spectrum, caused by the lower bending stress due to the BWB structure, results in an "underload" effect which cancels the overload retardation. As a result, the difference in crack growth life due to retardation effects is not significant.

Scenarios 1 and 2 present preferred conditions with stable crack growth. For a visual detectable crack size of 50 mm, the results show that it would be possible to undertake three repeat inspections at intervals in excess of 14,500 flights for scenarios 1 and 2. For an aircraft with a 40,000 flight design service goal and assuming a crack free life of 20,000 flights, this represents intervals that are more than twice the 7000 flight repeat inspection interval that would be required.

The situation for scenario 3 is rather different and represents the most conservative case. The results of the assessment show that it would only be possible to achieve one inspection of 7000 flights. Whilst scenario 3 would not form the basis of a maintenance programme due to the conservatism of the assessment, what it does demonstrate is adequate crack growth life amounting to 23% of the design life of the aircraft within which it would be possible to observe a two bay crack during a visual inspection of the aircraft.

8.15 Residual Strength Calculation

The residual strength of the spar web was determined using a method described by Broek (1991). The net section stress of the spar web was determined at the crack size from AFGROW at which the spar web was assumed to have failed due to K_{IC} being exceeded to determine whether the crack could have sustained limit stress. Crack growth was terminated at crack sizes of 79.8 mm and 91.7 mm for no retardation and retardation respectively. The larger crack size was conservatively applied to determine the residual strength in table 6.16. The results show that net section yield does not occur: a stress of a much higher magnitude would have been required for net section yield to occur.

The residual strength of the wing skin with a two bay crack was assessed using the approach detailed in (Swift, 1994). Neither the skin nor intact stiffener are critical for a two bay crack with an applied stress up to 224.5 MPa. The applied stress of 73.2 MPa is much lower than the maximum allowable stress of 224.5 MPa. The lower applied stress is a function of the increased skin thickness required to reduce skin deflections at the design load case resulting in a consequent reduction in bending stresses.

8.16 Manufacturability of proposed BWB wing fuselage integration structure

Aircraft assembly is a labour intensive and time consuming process which accounts for around one third of total manufacturing cost (Jin, et al., 2008). Most assembly operations in aircraft manufacturing are currently done manually. Although aircraft are small in lot size, numerous repetitive assembly operations have to be performed on a single aircraft. (Asada, H., Binayak, R)

Typical processes adopted in aircraft manufacture and assembly depend on the selected material type and its properties. The material type is selected during the scoping and design phases of the aircraft programme in order to take advantage of specific material properties which are seen as beneficial.

Lieber (2002) describes the BWB as simply a big wing with an integrated fuselage and no empennage, save the winglets/verticals. There are no complex wing-fuselage and fuselage-empennage joints of highly loaded structures at 90 degrees to one another, and there are no fillets. All trailing-edge control surfaces are simple-hinged with no track motion, and there are no spoilers. This manifests a substantial reduction (on the order of 30-percent) in the number of parts when compared to a conventional configuration. A similar reduction in manufacturing recurring cost is implied.

The proposed wing fuselage integration structure suggested in this project simplifies the structure at the wing fuselage joint thus making it possible to take advantage of the substantial savings available as a result of the improved manufacturing and assembly processes.

The manufacturing and assembly issues associated with the proposed wing root structure and bird's mouth termination could be perceived to fall into the "all too difficult" box but given the pace of change in manufacturing technology and techniques scope exists for the successful manufacture of large "one piece" structural items. The current proposal will require the manufacture of sub components then assembled to complete the structure albeit with larger sub components than currently exist for conventional airframes.

9 Conclusions and Recommendations

9.1 Literature Review

The review of available literature has shown that the design of damage tolerant wing root joint structure requires careful consideration of the constituent material, joint configuration and in-service operating environment. Whilst the metallic spliced plates/tension bolts/shear lugs configuration has been the convention, the availability of composite materials provides the opportunity for a step change in the design of wing roots towards achieving the ultimate goal of wing/fuselage interaction structure with a minimum number of joints or splices.

The literature review shows that there is a market for effective and efficient 21st century airplanes such as the BWB concept. Wing joint design is a critical area requiring particular attention. This thesis addresses damage tolerance issues associated with the BWB wing to fuselage joint.

The wing to fuselage joints currently in use in aircraft structures are of three main types. The challenges faced by manufacturers in mating a circular fuselage section to an aerofoil section wing makes the spliced plate joint the most efficient method for achieving the desired outcome. This involves the incorporation of a centre box in the fuselage with geometry similar to that of the wing. The joint between the two components is then achieved by means of spliced plates.

9.2 Novel design solution for root joint

This thesis addresses the possibility and assesses one of the benefits of uninterrupted wing skin across the skin/fuselage joint in metallic structures. An initial assessment of possible root joint configurations yielded two possible solutions. Having examined the two initial proposals, the preferred solution is one with internal fuselage pressure reacted by an outer skin which is stiffened by stringers and longerons running fore and aft. The function of the root rib is also changed so that the root rib reacts flight loads but the internal fuselage pressure boundary is moved to the next rib outboard of the wing root. The function of the root rib is, therefore, simplified. The proposal for the project aircraft is a bird-mouth type runout to ensure a load path into the root rib and the top and bottom skins of the fuselage thus ensuring that the fuselage volume is largely unobstructed. Stiffening members will still be required to ensure that fuselage crushing loads are adequately reacted.

The airframe skin is continuous across the joint transitioning from wing skin to fuselage skin without a discrete joint. The continuous stringers across the wing root further enhance the integrity of the joint and will result in a relatively smaller number of fasteners and a reduction of parts and other items required to achieve the required joint strength.

The absence of a discrete joint means that the proposed joint structure lends itself more readily to visual inspection of the external surfaces. This is also true for directed NDT inspections where the ease of inspection is essential for accuracy of inspection. In contrast to the existing fuselage structure and some of the existing blended wing body concepts, the spars are not continuous through the fuselage but terminate just inboard of the root rib hence leaving the fuselage relatively unobstructed. The need for stiffening members within the fuselage to counteract fuselage crushing loads due to bending are still required and could be the subject of another study. However, the depth of the wingbox and fuselage means that the tensile and compressive skin loads are much lower than for conventional wing skins.

The bird's mouth termination of the spars enables a smooth transfer of loading from the spar web into the root rib and the upper and lower skins and is believed to be novel in its application to the blended wing body configuration.

The continuous nature of the spars means that the root rib is required in several sections. The main function of the root rib is to maintain the profile of the wing. Keeping the root rib in short sections rather than as one continuous member will aid manufacture and make it more possible to reduce the weight of the finished components.

9.3 Design Calculations

Calculations have been undertaken to demonstrate the feasibility of the proposed wing root design. Wing loads were derived for three load cases including; 2.5g V_D x 1.5 Ultimate Load case, (2.5g V_D + 1ΔP) x 1.5 Ultimate Load case, and 2ΔP Ultimate Load case. A global model of the joint was created for assessment of wing root loads and the derived loads applied to a local model of the wing root.

Several iterations of the local FE model were undertaken to address issues including boundary conditions, high skin stresses and large skin deflections. The FEM has been modified with changes including additional stiffening members to the fuselage skin to improve joint stiffness and additional restraints to the spar web.

It was considered appropriate to move the pressure boundary outboard of the wing root. This has the benefit of separating the loads on the wing root structure thus resulting in a more efficient wing root design. The pressure boundary was moved outboard to reflect current practice.

The results show wing root joints stresses and deflections in line with expectation. The magnitudes of the stresses obtained indicate that scope remains for optimisation of the structure with the reduction of skin and web thicknesses albeit with a requirement for additional stiffening members.

9.4 Damage tolerance substantiation

The processes applied to demonstrate the damage tolerance capability of the blended wing body airframe at the wing root joint included crack growth analyses and residual

strength assessments based on net section yield for the bird's mouth spar termination and the two-bay crack criterion for the skin.

The spar web at the bird's mouth termination was seen to be the less critical of the two components and returned crack growth lives well in excess of those required for inspection of the structure of 72000 and 76000 flights without and with retardation respectively for a visual detectable crack of 25 mm and a broken spar flange.

The results show that it would be possible to undertake 3 repeat inspections at intervals of a minimum of 24,000 flights for the spar web. For an aircraft with a 40,000 flight design service goal and assuming a crack free life of 20,000 flights, the results show that only one inspection may be necessary at the inspection threshold of 20,000 flights. Any inspection of the bird's mouth spar termination would need to be an internal inspection in contrast to the external inspection that is possible for the wing skin. Any attempt to keep the number of required internal inspections to a minimum would be welcomed by operators of the aircraft.

The skin thicknesses at the wing root were driven primarily by a need to minimise wing skin deflection due to internal fuselage pressurisation resulting in relatively large skin thicknesses.

The combination of relatively large skin thicknesses and low wing bending loads, which are a function of the depth of the wing box, result in low magnitude wing bending stresses at the wing root.

Consequently, stable crack growth occurs with all stringers intact. A significant increase in crack growth rate is observed with failure of the central stiffener in a two bay crack. The low magnitude skin stresses mean that the structure will sustain a two bay crack at limit load. However, the inspection frequency required for a two bay crack with a broken stiffener is significantly greater than that for a two bay crack with an intact central stringer.

The assessments demonstrate that for a visual detectable crack size of 50 mm, it would be possible to undertake three repeat inspections at intervals in excess of 14,500 flights with all stringers intact. For an aircraft with a 40,000 flight design service goal and assuming a crack free life of 20,000 flights. This represents intervals that are more than twice the 7000 flight repeat inspection interval that would be required.

The situation for a broken central stiffener is rather different and represents the most conservative case. The assessments show that it would only be possible to achieve one inspection of 7000 flights. Whilst the broken central stiffener scenario would not form the basis of a maintenance programme due to the conservatism of the assessment, what it does demonstrate is adequate crack growth life amounting to 23% of the design life of the aircraft within which it would be possible to observe a two bay crack during a visual inspection of the aircraft.

9.5 Manufacturing Issues

Aircraft assembly is a labour intensive and time consuming process which accounts for around one third of total manufacturing cost. The proposed birds mouth spar termination and associated wing fuselage integration structure makes it possible to achieve significant reductions in part count and associated manufacturing and assembly costs in the order of 30 percent.

The manufacturing and assembly issues associated with the proposed wing root structure and bird's mouth termination could be perceived to fall into the "all too difficult" box but given the pace of change in manufacturing technology and techniques scope exists for the manufacture of large "one piece" structural items. The current proposal will require the manufacture of sub components then assembled to complete the structure albeit with larger sub components than currently exist for conventional airframes.

9.6 Recommendations for further work

Wing fuselage integration structure has been reviewed in this research project and a novel bird's mouth concept for spar termination has been proposed. The relevant loading has been derived and a fatigue and damage tolerance assessment has been undertaken that has identified the skins as the critical component at the wing fuselage joint.

The results show that only one inspection of the novel bird's mouth spar termination may be necessary at the inspection threshold of 20,000 flights. Any inspection of the bird's mouth spar termination would have to be an internal inspection in contrast to the external inspection that is possible for the wing skin. Keeping the number of required internal inspections to a minimum would be welcomed by operators of the aircraft.

The skin has been assessed and shown to be capable of sustaining a two bay crack under limit loading hence demonstrating the damage tolerant capability of the proposed wing fuselage integration structure.

The assessment has also confirmed that skin deflections that are outside the scope of this project remain a critical factor and require further assessment.

Other items which require further investigation include the following:

- The effect of adhesively bonded joints rather than mechanically fasteners on the integrity of the proposed and other BWB wing fuselage integration structures;
- Ageing BWB aircraft and end of life issues;
- Non-metallic wing fuselage integration issues;
- The need for stiffening members within the fuselage to counteract fuselage crushing loads;
- Impact of aerofoil sections on BWB wing fuselage integration.

An assessment of the above and other issues will facilitate a better understanding of the BWB concept and contribute towards the body of knowledge of next generation aircraft concepts.

9.7 Conclusion

Wing fuselage integration structure has been reviewed in this research project and a novel bird's mouth concept for spar termination has been proposed. The relevant loading has been derived and a fatigue and damage tolerance assessment has been undertaken that has identified the skins as the critical component at the wing fuselage joint.

The bird's mouth spar termination has been assessed and shown to be damage tolerant and requiring a minimum amount of inspection which would be welcomed by operators of the aircraft.

The skin has been assessed and shown to be capable of sustaining a two bay crack under limit loading hence demonstrating the damage tolerant capability of the proposed wing fuselage integration structure.

The assessment has confirmed that skin deflections, which are outside the scope of this project, remain a critical factor and require further assessment.

10 References

Abrate, S. (1998) *Impact on Composite Structures*, Cambridge University Press.

AvP970 (1955). Design requirements for Aircraft for the Royal Air Force and Royal Navy. *Ministry of Aviation.* AvP970 2, Book 2, App. 8.

Bellinger, N., Komorowski, T., Benak, T. (2001). Residual life predictions of corroded fuselage lap joints. *International Journal of Fatigue* 23 (2001) S349-S356.

Blaha, F., Grenier, L. (1994). A Fibre-Optics Loads Monitoring System for the CL-600 Challenger Aircraft. In: *Proceedings of the 1994 USAF Structural Integrity Program Conference*.

Bogdanovich, A.E., Kizhakkethara, I. (1999). Three-dimensional finite element analysis of double-lap composite adhesive bonded joint using submodeling approach. *Composites Part B,* 30 (1999), No.6, 537-51.

Boyd-Lee, A., Harrison, G., Henderson, M. (2001). Evaluation of standard life assessment procedures and life extension methodologies for fracture-critical components. *International Journal of Fatigue* 23 (2001) S11-S19.

Broek, D. (1991). *Elementary Engineering Fracture Mechanics*. Kluwer Academic Publishers, The Netherlands.

Broek, D. (1991). *The practical use of Fracture Mechanics*. Kluwer Academic Publishers, The Netherlands.

Bruzzi, M. S., McHugh, P. E. (2002). Methodology for modelling the small crack fatigue behaviour of aluminium alloys. ” *International Journal of Fatigue* 24 (2002) 1071-1078.

Chao, J., Graves, S. (1998). Reducing flow time in aircraft manufacturing Production and Operations Management. *Production and Operations Management.* Spring 1998, Vol. 7, No. 1, pp. 38-52.

Collins, R., Dean, M., Williams, A., Bishop, M., van Griensven, B., Alexander, A., (1997). Fatigue and Damage Tolerance Tests in Support of the Certification of Airbus A330/A340 Metallic Wing Structure. In: *Proc. Of the 19th Symposium of the International Committee on Aeronautical Fatigue,* 18-20 June, 1997.

Crosby, S., Kundu, A, Curran, R., Raghunathan, S. (2003). Fabrication And Assembly Cost Drivers For Aircraft Manufacturing. In: *AIAA's 3rd Annual Aviation Technology, Integration, and Operations (ATIO) Tech*, 17 - 19 November 2003, Denver, Colorado.

Curran, R., Raghunathan, S. Kundu, A., Crosby, S. Shields, P., Eakin, D. (2002) Competitive Aircraft Design And Manufacture. *Integration, and Operations (ATIO) 2002 Technical*, 1-3 October 2002, Los Angeles, California.

Dawicke, D., Newman, J. (1992) Analysis and Prediction of Multiple-Site Damage (MSD) Fatigue Crack Growth. *NASA TP-3231*.

Defence Standard 00-970 (2007). Design and Airworthiness Requirements for Service Aircraft Part 1 - Combat Aircraft. Defence Standard 00-970 Part 1 Issue 5. Section 4 - Design and Construction. *Ministry of Defence*, 31 January 2007.

Dobyns, A.L. (1980). Analysis of simply supported plates subjected to static and dynamic loads. In: *AIAA J.* 19(5):642-650.

Dobyns, A.L., and Porter. (1981). A study of the structural integrity of graphite composite structure subjected to a low velocity impact. *Polym. Eng. Science* 21(8):493-498.

Döker, H. (1997). Fatigue crack growth threshold: implications, determination and data evaluation. *International Journal of Fatigue*, Volume 19 Supplement Number 1.

Dorey, G. (1984). Impact and crashworthiness of composite structures. In: *Structural Impact and Crashworthiness*, Vol. 1, Edited by. GAO Davies, Chapter 6: p155-192.

ESDU 70018. General Principles Of Design In Relation To Fatigue.

ESDU 97018. Standard fatigue loading sequences.

ESDU (2002), IHS ESDU: MMDH Section 6. Aluminium alloys, L97 (accessed 20th April 2009)

FAR 25.301. Loads. *FAA Regulations Part 25.301*.

FAR 25.303. Factor of safety. *FAA Regulations Part 25.303*.

FAR 25.305. Strength and deformation. *FAA Regulations Part 25.305*.

FAR 25.365. Pressurized compartment loads. *FAA Regulations Part 25.365*.

FAR 25.571 Damage-tolerance and Fatigue Evaluation of Structure. *FAA Regulations Part 25.571*.

Fatemi, A., Yang, L. (1998). Cumulative fatigue damage and life prediction theories: a survey of the state of the art for homogeneous materials. *International Journal of Fatigue,* Vol. 20, No. 1, pp. 9-34.

Fielding, J. P. (1999) *Introduction to Aircraft Design*. Cambridge University Press.

Flight International (2003). Citing internet resources (WWW document). http://www.flightglobal.com/articles/2003/05/27/165974/first-subassembly-for-a380.html (accessed 8th December 2009)

Flight International (2007). Citing internet resources (WWW document). http://www.flightglobal.com/airspace/media/civilaviation1949-2006cutaways/images/6666/airbus-a300-mid-section-cutaway.jpg (accessed 8th December 2009)

Forman, R.G., Kearney, V.E. and Engle, R.M. (1967). Transactions of the American Society of Mechanical Engineers. Series D; Journal of Basic Engineering, 89(3): 459–465, Sept. 1967

Friedrich, K. (1989). *Application of Fracture Mechanics to Composite Materials*, Composite Materials Series, Vol. 6, Elsevier.

Gaedke, M. (1995). From damage mechanics of composite materials to damage tolerant structures. *ICAF'95,* Australia, 1995.

Goranson, U. (1997). Fatigue issues in aircraft maintenance and repairs. *International Journal of Fatigue*, Volume 19 Supplement Number 1.

Guo, S. (2002). Stress Analysis for a Thin-Walled Composite Box Using Program TWboxsc2.exe. Cranfield University. 2002.

Hagemaier, D., Wilson, D. (1997). Improved non-destructive inspection techniques for aircraft inspection. *Proceedings of FAA-NASA Symposium on the Continued Airworthiness of Aircraft Structures,* DOT/FAA/AR-97/2, pp 403-416, August 28-30.

Harter, J. A. (2006), *AFGROW Users Guide And Technical Manual*, Air Vehicles Directorate, Air Force Research Laboratory, Wright-Patterson Air Force Base Oh 45433-7542

Hepperle, M. (2002). The Sonic Cruiser – A Concept analysis. International Symposium "Aviation Technologies of the XXI Century: New Aircraft Concepts and Flight Simulation", Aviation Salon ILA-2002, Berlin, 7-8 May 2002.

Himmel, N. (2002). Fatigue life prediction of laminated polymer matrix composites. *International Journal of Fatigue*, Volume 24, Pages 349-360.

Hoffman, M., Hoffman, P. (2001). Corrosion and fatigue research – structural issues and relevance to naval aviation. *International Journal of Fatigue,* 23 (2001) S1-S10.

Howard, A. Q. (1997). The role of new-technology non-destructive techniques. *Proceedings of FAA-NASA Symposium on the Continued Airworthiness of Aircraft Structures,* DOT/FAA/AR-97/2, pp 597-604, August 28-30, 1997.

Hunt, E., Williams, A., Jones, M. (1999). Fatigue and Damage Tolerance Design of Large Airbus Wing Structures. *Proceedings of the 20th Symposium of the International Committee on Aeronautical Fatigue*.

JAA. (2000). Damage-tolerance and fatigue evaluation of structure. *JAA Regulations Part 25.571,* Change 15, 1 October 2000.

Jane's (2001). Jane's All the world's aircraft. Jane's Information Group; 81st Ed.

Jin, Y., Curran, R., Butterfield, J., Burke, R., Welch, B. (2008). Automated Assembly Time Analysis Using a Digital Knowledge Based Approach. *The 26th Congress of International Council of the Aeronautical Sciences (ICAS)*, 14 - 19 September 2008.

Jones, R. (1999) *Mechanics of Composite Materials*. 2nd ed. Taylor and Francis.

Jones, R., Sawyer, J.P.G., Chiu, W.K. (1999). Studies in the matrix dominated failures of composite joints. *Composite Structures,* Vol. 44, 1999, 1-16.

Jonge, J. (1976). The requirements of damage tolerance an analysis of damage tolerance requirements with specific reference to MIL-A-83444. *National Aerospace Laboratory, The Netherlands* NLR TR 77005 U, 1976.

Ko, M., Leifsson, L.T., Schetz, J.A., Mason, W.H., Grossman, B., Haftka, R.T. (2003). MDO of a Blended-Wing-Body Transport aircraft with Distributed Propulsion. *AIAA's 3rd Annual Aviation Technology, Integration and Operations (ATIO) Technical forum*, Denver, Colorado, 17-19 November 2003.

Kong, C., Park, J., Cho, J., Hong, C., Kim, C. (2002). Testing and Analysis of Downscaled Composite Wing Box. *Journal of Aircraft* Vol. 39, No. 3, May-June 2002.

Kwofie, S. (2001). An exponential stress function for predicting fatigue strength and life due to mean stresses. *International Journal of Fatigue,* 23 (2001), pages 829-836, 2001.

Lauder, A. J., Amateau, M. F., and Queeney, R. A. (1993). Fatigue resistance of impact damaged specimens vs. machined hole specimens. *Composites,* 24 (1993), 443-445, 1993.

Leon, A. (1998). Benefits of split mandrel cold working. *International Journal of Fatigue,* Vol. 20, No. 1, pp. 1-8, 1998.

Liebeck, R.H. (2002). Design of the Blended-Wing-Body Subsonic Transport. *AIAA 2002 Wright Brothers Lecture*, 2002.

Liebeck, R.H., Page, M.A., Rawdon, B.K. (1998). Blended-Wing-Body Subsonic Commercial Transport. *AIAA 36th Aerospace sciences Meeting and Exhibit*, Reno, Nevada, January 12-15, 1998, AIAA 98-0438.

Lundin, S. (2001). Engine Debris Fuselage Penetration Testing, Phase 1. *FAA Report DOT/FAA/AR-01/27*, August 2001.

Mars, W., Fatemi, A. (2002). A literature survey on fatigue analysis approaches for rubber. *International Journal of Fatigue* 24 (2002) 949-961, 2002.

Matthews, F.L. (1990). Load-carrying joints. *Composite materials in aircraft structures,* Longman.

McMasters, J., Cummings, R. (2002). Airplane Design – Past, Present, and Future. *Journal of Aircraft* Volume 39 Number 1, 2002.

MIL-HDBK-5H (1998). *Metallic Materials and Elements for Aerospace Vehicle Structures*, Military Handbook, US Department of Defence, 1 December 1998.

Miner, M. A. (1945). Cumulative Damage in Fatigue. *Journal of Applied Mechanics*, Vol. 67, No. 12, 1945, pp. A159-A182.

Morris, A. (2008). *A Practical Guide to Reliable Finite Element Modelling*. John Wiley and Sons Ltd., 2008.

Mukhopadhyay, V. (1996). Structural Concepts Study of Non-circular Fuselage Configurations" *SEA/AIAA World Aviation Congress*, Los Angeles, California, October 22-24, 1996, WAC-67.

Mukhopadyay, V. (2005). Blended-Wing-Body (BWB) Fuselage Structural Design for Weight Reduction. *46th AIAA/ASME/ASCE/AHS/ASC Structures, Structural Dynamics and Materials Conference*, 18-21 April 2005, Austin, TX.

Nagar, A. (1994). Damage Tolerance Concept for Aerospace Structures. *AD-Vol. 43, Durability and Damage Tolerance ASME*, 1994.

NASA-STD-3000. (1995). Anthropometry and Biomechanics, Man-Systems Integration Standards, Volume I, Section 3, Revision B. *National Aeronautics and Space Administration*, July 1995.

Nelson, W.D., Bunin, B.L., Hart-Smith, L.J. (1983). Critical Joints in Large Composite Aircraft Structures. *NASA CR-. 3710*. August 1983.

Nesterenko, G. (1997). Fatigue and Damage Tolerance of Aging Aircraft Structures. *Proc. Of the 19th Symposium of the International Committee on Aeronautical Fatigue,* 18-20 June, 1997.

Newman, J. C., Phillips, E. P. (1997). Fatigue-life prediction methodology using small-crack theory and crack-closure model. *Proceedings of FAA-NASA Symposium on the Continued Airworthiness of Aircraft Structures.* DOT/FAA/AR-97/2, pp 331-356, August 28-30, 1997.

Niu, M. (1990). *Airframe Structural Design*. Conmilit Press Ltd.

Niu, M. (1992). *Composite Airframe Structures*. Conmilit Press Ltd.

Niu, M. (1999). *Airframe Stress Analysis and Sizing*. 2nd ed. Michael C. Y. Niu's Aiframe Book Series, Conmilit Press Ltd., 1997.

NMAB-476. (1996) New Materials for Next-Generation Commercial Transports, NASA no. 19980016306; PB96-181680.

Oberti, A. (1984). Structural Analysis of the CL-600 Rear Pressure Bulkhead, using Nastran Non-Linear Analysis Capabilities (Solution 64). *Canadian Aeronautics and Space Journal.* Vol. 30, No. 4, December 1984.

Ong, C., Shen, M. (1991). Study of the fatigue characteristics of the composite after impact. *Int SAMPE Symp and Exhibition,* 36 (1991), Part 1, 912-923.

Osgood, C. (1982). *Fatigue Design*. International Series on the Strength and Fracture of Materials and Structures. Pergamon Press.

Pandey, P.C., Shankaragouda, H, Singh, A.K. (1998). Nonlinear analysis of adhesively bonded lap joints considering viscoplasticity in adhesives. *Computers and Structures.* 70, No. 4, 387-413, 1998.

Paris, P., Erdogan, F (1963), A critical analysis of crack propagation laws, *Journal of Basic Engineering, Transactions of the American Society of Mechanical Engineers,* December 1963, pp.528-534

Paris, P., Tada, H., Donald, J. (1999). Service load fatigue damage – a historical perspective. *International Journal of Fatigue.* 21 (1999) S35-S46.

Paul, D., Kelly, L., Venkayya, V., Hess, T. (2002). Evolution of U.S. Military Aircraft Structures Technology. *Journal of Aircraft.* Volume 39 Number 1.

Petit, R., Wang, J., Toh, C. (2000). Validated Feasibility Study of Integrally Stiffened Metallic Fuselage Panels for Reducing Manufacturing Costs. *NASA/CR-2000-209342*, May 2000.

Pidaparti, R., Jayanti, S., Sowers, C., Palakal, M. (2002). Classification, Distribution, and Fatigue Life of Pitting Corrosion for Aircraft Materials. *Journal of Aircraft Vol. 39*, No. 3, May-June 2002.

Quenet, G. (2002). BWB-01 Blended Wing Body Airliner Advanced Technology Integration. *Cranfield University College of Aeronautics.* AVD MSc Thesis.

Rooke, D., Cartwright, D. (1974). *Compendium of Stress Intensity Factors*. Her Majesty's Stationary Office.

Roudet, F., Desplanques, Y., Degallaix, S. (2002). Fatigue of glass/epoxy composite in three-point-bending with predominant shearing. *International Journal of Fatigue 24 (2002) 327-337*.

Sarh, B., Buttrick, J., Munk, C., Bossi, R. (2009). Aircraft Manufacturing and Assembly. In: *Springer Handbook of Automation.* 893-910, 2009.

Schijve, J. (2001), *Fatigue of Structures and Materials*, Kluwer Academic Publishers, The Netherlands.

Schon, J. Nyman, T. (2002). Spectrum fatigue of composite bolted joints. *International Journal of Fatigue.* 24 (2002) 273-279, 2002.

Schon, J., Blom, A., (2002). Fatigue life prediction and load cycle elimination during spectrum loading of composites. *International Journal of Fatigue*. 24 (2002) 361-367, 2002.

Schutz, D; Gerharz, J. (1977). Fatigue Strength of a Fibre-Reinforced Material. *Composites.* Vol. 8, no. 4, pp. 245-250. Oct. 1977.

Simpson, D., Brooks, C. (1999). Tailoring the structural integrity process to meet the challenges of aging aircraft. *International Journal of Fatigue.* 21 (1999) S1-S14, 1999.

Smith, C. W. (1992). Optical Methods of Stress Analysis Applied to Cracked Components. *Proceedings of International Workshop on Structural Integrity of Aging Airplanes.* Atlanta Technology Publ., 1992.

Smith, H. (2002). Aerospace Vehicle Design Group Project: BW-01 Blended Wing-Body advanced technology integration study, *Cranfield University Aerogram.* Vol. 10 No. 4, 2002.

Spottswood, S., Wolfe, H. (2002). Comparing Fatigue Life Estimates Using Experimental and Spectral Density Based Probability Distributions. *Journal of Aircraft.* Vol. 39, No. 3, May-June 2002.

Stinton, Darrol. (2001). *The design of the aeroplane*, 2nd ed. Blackwell, Oxford.

Swift, T. (1971). Development of the Fail-safe Design Features of the DC-10. *ASTM Special Technical Publication* 486.

Swift, T. (1978). Fracture Analysis of Adhesively Bonded Cracked Panels. *ASME.* Paper No. 77-WA/Mat-2.

Swift, T. (1981). Application of Damage Tolerance Technology to Type Certification. *SAE Technical Paper Series* No. 811062.

Swift, T. (1981). Fracture Analysis of Stiffened Structure. *Damage Tolerance of Metallic Structures: Analysis Methods and Applications.* ASTM STP 842, pp 69-107.

Swift, T. (1985). Damage Tolerance Assessment of Commercial Airframes. *Fracture Problems in the Transportation Industry.* ASCE, pp 97-138, 1985.

Swift, T. (1986). Important Considerations in Commercial Aircraft Damage Tolerance. *International Journal of Vehicle Design.* Vol. 7, Nos 3 / 4.

Swift, T. (1990). Repair to Damage Tolerant Aircraft. Proceedings of International Symposium on Structural Integrity of Aging Airplanes. March 20-22, 1990.

Swift, T. (1994). Damage Tolerance Capability. *International Journal of Fatigue*. Volume 16 Number 1.

Swift, T. (1999). Effect of Multiple-Site-Damage on Certified Lead Crack Residual Strength. *Proceedings Royal Aeronautical Society.* (A99-29951 07-05).

Swift, T., Wang, D. (1969). Damage Tolerant Design – Analysis Methods and Test Verification of Fuselage Structure. *Proc Air Force Conf Fatigue and Fracture of Aircraft Structures and Materials.* Dec 15-18, 1969.

Tenney, D., Pipes, R. B. (2001). Advanced Composites Development for Aerospace Applications. *7th Japan International SAMPE Symposium and Exhibition.* Tokyo, Japan, November 13-16, 2001.

Terada, H. (1997). Statistics of Aircraft Accidents and Case Studies on Structure or Material Related Accidents. P*roc. Of the 19th Symposium of the International Committee on Aeronautical Fatigue.* 18-20 June, 1997.

Terada, H. (2001). Structural fatigue and joint degradation. *International Journal of Fatigue.* 23 (2001) S321-S30, 2001.

To, P. (1986). A Study of the Structural Integrity of the Canadair Challenger at Ditching. *Proceedings of the International Congress on Aeronautical Sciences.* ICAS-86-4.5.2, 1986.

Turner, D., Banister, R., To, P. (1985). Continued Airworthiness of Damage Tolerant Aircraft. *Durability and Damage Tolerance in Aircraft Design: Proceedings of the 13th Symposium*, May 22-24 1985.

Turner, D., Manders, C. (1983). The Damage Tolerance Approach to the Canadair CL-600. *Canadian Aeronautics and Space Journal.* Vol. 29, No. 3, September 1983.

Wang, J., Banbury, A., Kelly, D.W. (1998). Evaluation of approaches for determining design allowables for bolted joints in laminated composites. *Composite Structures.* 41 (1998), No. 2, 167-176.

Wanhill, R., Kooloos, M. (2001). Fatigue and corrosion in aircraft pressure cabin lap splices. *International Journal of Fatigue.* 23 (2001) S337-347, 2001.

Zhang, X., Li, Y. (2005). Damage Tolerance and Fail Safety of Welded Aircraft Wing Panels. *AIAA Journal.* Vol. 43, No. 7, July 2005.

Zilberstein, V., Schlicker, D., Walrath, K., Weiss, V., Goldfine, N. (2001). MWM eddy current sensors for monitoring of crack initiation and growth during fatigue tests and in service. *International Journal of Fatigue.* 23 (2001) S477-S485, 2001.

APPENDIX A

Table A.1 Whole body mass of year 2000 crewmember population (age 40)

Male (American)			Female (Japanese)		
5th percentile	50th percentile	95th percentile	5th percentile	50th percentile	95th percentile
65.8 kg (145.1 lb)	82.2 kg (181.3 lb)	98.5 kg (217.2 lb)	41.0 kg (90.4 lb)	51.5 kg (113.5 lb)	61.7 kg (136.0 lb)

http://msis.jsc.nasa.gov/sections/section03.htm 27/12/2008

Table A.2 Characteristics of a standard person (Stinton, 2001)

Part of (clothed) body	Per cent Weight	kg
Head and neck	8.3	7
Upper trunk	27.2	22
Lower trunk	15.5	13
Thighs	22.2	18
Legs and feet	16.7	13.5
Upper arms	5.6	4.5
Forearms and hands	4.5	4
Total	100	82

Notes: For a small man multiply by 0.86
For a large man multiply by 1.14
For a woman or young person multiply by 0.55

Table A.3 Typical baggage allowances (Stinton, 2001)

Airline class	Baggage allowance
	kg
First	30
Economy	20

Notes: Both of the above include 5 kg hand luggage.
The 5 kg hand luggage is limited in size to the sum of length + breadth + width = 1.15 m

APPENDIX B

Table B.1 Project aircraft geometrical data

Fuselage dia	3.95	m	
Fuselage width	11.85	m	
Wing area	510.5	m^2	See Appendix C
Wing span	48.24	m	See Appendix C
	1899.2	in	
Tip chord	2.62	m	Assumed value
	103.1	in	
Root chord	16.1	m	Sweep back not taken into account for preliminary estimates
	633.1	in	
Taper (Tip/Chord) ratio λ	0.16		
Note:			
Wing root chord	26.8	m	To accommodate false rear spar
Wing box effective over	45	%	Chord at wing root (i.e. front spar = 15%, rear spar = 60%)
Wing box effective over	12.06	m	Compared to required root chord above

Aspect ratio parameter obtained from Niu page 46. Values given for taper ratios of 0 and 0.5 are the same. 45 degree compressible sweep parameter selected. This gives aspect ratio parameter of 3.5

Table B.2 Tabulation of span wise loading coefficient values

A	B	C	D		
	$C_{la}C$	$C_{la}C$	$C_{la}C$		
$\frac{y}{(b/2)}$	C_LC_{av}	C_LC_{av}	C_LC_{av}	Input to Appendix D	
	(λ=0.0)	(λ=0.25)	(λ=0.16)*		
0.000	1.320	1.210	1.248	0.000	1.248
0.383	1.220	1.170	1.187	0.383	1.187
0.707	0.860	0.940	0.912	0.707	0.912
0.921	0.390	0.540	0.488	0.921	0.488
1.000	0.000	0.000	0.000	1.000	0.000

Note:

1. Data obtained from Niu Fig. 3.4.13 on Niu Page 47
2. Wing aspect ratio parameter and taper ratios defined in Niu on pages 77 and 74 respectively
3. *Values in Column D obtained by interpolation.

Table B.3 Tabulation of span wise loading coefficient and additional lift

n	η ①	$\frac{\Delta\eta}{2}$ ②	$\frac{C_{la}C}{C_L C_{av}}$ ③	$\frac{S_z}{C_L q(S/2)}$ ④	$\frac{M_x}{C_L q(S/2)(b/2)}$ ⑤
				$\uparrow\int$ ③ dη	$\uparrow\int$ ④ dη
1	0		1.248	0.998	0.4240
		0.05			
2	0.1		1.255	0.873	0.3305
		0.05			
3	0.2		1.251	0.748	0.2495
		0.05			
4	0.3		1.228	0.624	0.1809
		0.05			
5	0.4		1.176	0.503	0.1246
		0.05			
6	0.5		1.093	0.390	0.0799
		0.05			
7	0.6		0.9991	0.285	0.0461
		0.05			
8	0.7		0.9169	0.190	0.0224
		0.05			
9	0.8		0.8361	0.101885	0.0078
		0.05			
10	0.9		0.5836	0.0309	0.0012
		0.025			
11	0.95		0.3262	0.008155	0.0002
		0.025			
12	1		0	0	0

η	$\frac{C_{la}C}{C_L C_{av}}$
0	1.248
0.1	1.255
0.2	1.251
0.3	1.228
0.4	1.176
0.5	1.093
0.6	0.9991
0.7	0.9169
0.8	0.8361
0.9	0.5836
0.95	0.3262
1	0

Note: Column 4 reverse integration. See Figure 3.11.11 on Niu page 80

Table B.4 Wing load computation

①	②	③	④	⑤	⑥	⑦
n	η	$d\eta = \Delta\eta/2$	y (in)	$\frac{\Delta y}{2}$	c (in)	c Mid. Strip (in)
		$\frac{②_{n+1}-②_n}{2}$	[b/2][η] b/2 x ②	$\frac{④_{n+1}-④_n}{2}$	$C_R-(C_R-C_T)\eta$ $C_R-(C_R-C_T)$ x ②	$\frac{C_n+C_{n-1}}{2}$ $\frac{⑥_n+⑥_{n+1}}{2}$
2	0.1		94.96034		580.1	
		0.05		47.48017		553.6
3	0.2		189.9207		527.1	
		0.05		47.48017		500.6
4	0.3		284.881		474.1	
		0.05		47.48017		447.6
5	0.4		379.8414		421.1	
		0.05		47.48017		394.6
6	0.5		474.8017		368.1	
		0.05		47.48017		341.6
7	0.6		569.7621		315.1	
		0.05		47.48017		288.6
8	0.7		664.7224		262.1	
		0.05		47.48017		235.6
9	0.8		759.6827		209.1	
		0.05		47.48017		182.6
10	0.9		854.6431		156.1	
		0.025		23.74009		142.9
11	0.95		902.1233		129.6	
		0.025		23.74009		116.4
12	1		949.6034		103.1	

Note:

Wing span b	1899.2	in
Root Chord C_R	633.1	in
Tip Chord C_T	103.1	in
Lift distribution on wing (fuselage blanketed by wing) assumed to be	1.00	
Aircraft weight	440899	lbf
Loads derived for steady manoeuvre @	2.5	g
Lift L_w	1102247.5	lbf
Lift L_w	4903041.6	N

Table B.4 Wing load computation continued

①	Additional Air load		
	⑧	⑨	⑩
n	$\frac{C_{la}C}{C_L C_{av}}$	$\frac{S_z}{C_L qS/2}$	S_z Additional air load
	(Niu, 1990, Fig. 3.11.11)	↑∫ ⑧ dη	$(L_w/2)$⑨
2	1.255	0.873	481043
3	1.251	0.748	411987
4	1.228	0.624	343675
5	1.176	0.503	277430
6	1.093	0.390	214905
7	0.9991	0.285	157255
8	0.9169	0.190	104457
9	0.8361	0.102	56151
10	0.5836	0.031	17030
11	0.3262	0.008	4494
12	0	0	0

Table B.4 Wing load computation continued

①	②	③	Basic Air load		
			⑪	①	①
n	η	$d\eta = \Delta\eta /2$	$C_{lb}C$ C_{av}	S_z $q(S/2)$	S_z Basic air load
		$\frac{②_{n+1}-②_n}{2}$	Basic Lift (Niu 1990, Fig. 3.11.14)	$\uparrow \int ⑪ d\eta$	$q(S/2)$ ⑫
2	0.1	0.05	0.025	-0.00285	-4011
3	0.2	0.05	0.0205	-0.00513	-7213
4	0.3	0.05	0.014	-0.00685	-9641
5	0.4	0.05	0.006	-0.00785	-11049
6	0.5	0.05	-0.002	-0.00805	-11330
7	0.6	0.05	-0.01	-0.00745	-10486
8	0.7	0.05	-0.0175	-0.00608	-8550
9	0.8	0.05	-0.0235	-0.00403	-5665
10	0.9	0.025	-0.024	-0.00165	-2322
11	0.95	0.025	-0.021	-0.00053	-739
12	1		0	0	0

Note:			
Aircraft speed	360	knots	See Appendix C
Dynamic pressure, q	512	lbf/ft^2	
Wing surface area, S	5498	ft^2	See Appendix C
q x (S/2)	1407488	lbf	
Wing CG position	0.4	Chord	
Maximum Inertia Case	2.5	g	

Table B.4 Wing load computation continued

①	②	③	⑭	Additional Torsion due to Additional and Basic Loads			
				⑮	⑯	⑰	⑱
n	η	$d\eta = \Delta\eta / 2$ $\frac{②_{n+1} - ②_n}{2}$	S_z additional + basic load ⑩+⑬	S_z ⑭$_n$ - ⑭$_{n+1}$	$\frac{X_{AC}}{C}$ Aerodynamic centre (Niu 1990, Fig 3.11.13)	ΔX (CG-⑯)⑦	M_y Additional + basic load ↑Σ⑮x⑰
2	0.1	0.05	477032	72258	0.261	76.9	28287466
3	0.2	0.05	404774	70740	0.26	70.1	22727387
4	0.3	0.05	334034	67653	0.257	64.0	17769774
5	0.4	0.05	266381	62806	0.248	60.0	13439579
6	0.5	0.05	203575	56806	0.24	54.7	9672447
7	0.6	0.05	146769	50862	0.225	50.5	6567549
8	0.7	0.05	95907	45421	0.205	45.9	3998557
9	0.8	0.05	50486	35779	0.182	39.8	1911583
10	0.9	0.025	14707	10952	0.16	34.3	487056
11	0.95	0.025	3755	3755	0.145	29.7	111468
12	1		0				

Table B.4 Wing load computation continued

①	②	③	Inertia Loads			
			⑲	⑳	㉑	㉒
n	η	$d\eta = \Delta\eta / 2$	$\frac{S_z}{n_z}$	$\frac{M_y}{n_z}$	S_z Inertia 2.5⑲	M_y Inertia -2.5⑳
		$\frac{②_{n+1}-②_n}{2}$	Wing inertia data (Niu 1990, fig. 3.11.16)			
2	0.1	0.05	13849	0	-34621.6	0
3	0.2	0.05	12481	0	-31201.4	0
4	0.3	0.05	11824	0	-29559.5	0
5	0.4	0.05	8858	0	-22144.5	0
6	0.5	0.05	6364	0	-15908.9	0
7	0.6	0.05	4317	0	-10793.5	0
8	0.7	0.05	2667	0	-6667.06	0
9	0.8	0.05	1433	0	-3581.62	0
10	0.9	0.025	386	0	-963.859	0
11	0.95	0.025	217	0	-543.617	0
12	1		0	0	0	0

Table B.4 Wing load computation continued

①	②	③	⑥	Propeller air loads		Torsion load due to C_{mo}		
				㉓	㉔	㉕	㉖	㉗
n	η	$d\eta = \Delta\eta / 2$ $\frac{②_{n+1}-②_n}{2}$	c (in) $C_R-(C_R-C_T)\,\eta$ $C_R-(C_R-C_T)$ x ②	S_z Propeller air load	M_y Propeller air load	$C_{mo}CC_{av}$ Pitching Moment (Niu, 1990)	dM_y $q(S/2)\uparrow\int$㉕ ⑥$d\eta$	$M_y(10^6)$ due to C_{mo} $q(S/2)$㉖ (in-lb)
2	0.1		580.1	0	0	-0.105		
		0.05					-27.015	-38.023
3	0.2		527.1	0	0	-0.1		
		0.05					-21.334	-30.027
4	0.3		474.1	0	0	-0.095		
		0.05					-16.447	-23.149
5	0.4		421.1	0	0	-0.089		
		0.05					-12.321	-17.341
6	0.5		368.1	0	0	-0.084		
		0.05					-8.901	-12.528
7	0.6		315.1	0	0	-0.08		
		0.05					-6.094	-8.578
8	0.7		262.1	0	0	-0.076		
		0.05					-3.838	-5.402
9	0.8		209.1	0	0	-0.072		
		0.05					-2.089	-2.940
10	0.9		156.1	0	0	-0.066		
		0.025					-0.821	-1.155
11	0.95		129.6	0	0	-0.063		
		0.025					-0.359	-0.505
12	1		103.1	0	0	-0.06		

Table B.4 Wing load computation continued

①	②	Net wing loads plotted vs. wing span (□)			
		㉘	㉙		㉚
n	η	Sz (net) ⑭+㉑+㉓ (lb)	M_x (net) ↑∫㉘dy (in-lb)	$M_x(10^6)$ (net) ↑∫㉘dy (in-lb)	$M_y(10^6)$ (net) ⑱+㉒+㉔+㉗ (in-lb)
2	0.1	442410	1.53E+08	153.379	
					-9.736
3	0.2	373572	1.15E+08	114.636	
					-7.300
4	0.3	304474	82442051	82.442	
					-5.379
5	0.4	244237	56389143	56.389	
					-3.902
6	0.5	187666	35882321	35.882	
					-2.855
7	0.6	135976	20515761	20.516	
					-2.010
8	0.7	89240	9822499	9.822	
					-1.403
9	0.8	46904	3358349	3.358	
					-1.028
10	0.9	13744	478772	0.479	
					-0.668
11	0.95	3212	76249.97	0.076	
					-0.394
12	1	0	0	0	

Table B.4 Wing load computation continued

②	Net wing loads plotted vs. wing span (η)					
	㉘		㉙		㉚	
η	Sz (net) ⑭+㉑ +㉓ (lb)	$Sz(10^4)$ (net) ⑭+㉑ +㉓ (lb)	M_x (net) ↑∫㉘dy (in-lb)	$M_x(10^7)$ (net) ↑∫㉘dy (in-lb)	η	$M_y(10^6)$ (net) ⑱+㉒ +㉔+㉗ (in-lb)
η Normalised wing span	Shear Force		Bending Moment		η Normalised wing span	Torque
0.1	442410	44.241	1.53E+08	15.338	0.15	9.736
0.2	373572	37.357	1.15E+08	11.464	0.25	7.300
0.3	304474	30.447	82442051	8.244	0.35	5.379
0.4	244237	24.424	56389143	5.639	0.450	3.902
0.5	187666	18.767	35882321	3.588	0.550	2.855
0.6	135976	13.598	20515761	2.052	0.650	2.010
0.7	89240	8.924	9822499	0.982	0.75	1.403
0.8	46904	4.690	3358349	0.336	0.850	1.028
0.9	13744	1.374	478772	0.048	0.925	0.668
0.95	3212	0.321	76249.97	0.008	0.975	0.394
1	0	0	0	0		

Table B.4 Wing load computation continued

η	$S_z(10^4)$ N	$M_x(10^9)$ Nmm	η	$-M_y(10^9)$ Nmm
0.100	196.794	17.330	0.15	1.100
0.200	166.173	12.952	0.25	0.825
0.300	135.437	9.315	0.35	0.608
0.400	108.642	6.371	0.450	0.441
0.500	83.478	4.054	0.550	0.323
0.600	60.485	2.318	0.650	0.227
0.700	39.696	1.110	0.75	0.159
0.800	20.864	0.379	0.850	0.116
0.900	6.113	0.054	0.925	0.075
0.950	1.429	0.009	0.975	0.044
1.000	0	0	0	0

Distance from fuselage centreline to wing tip	24120 mm
Distance from fuselage centreline to wing root	5925 mm
η at wing root	0.246

η	$S_z(10^4)$ N	$M_x(10^9)$ Nmm	η	$-M_y(10^9)$ Nmm
0.246	152.143	11.292	0.246	0.837

η	$S_z(10^4)$ N	$M_x(10^6)$ Nm	η	$-M_y(10^6)$ Nm
0.246	152.143	11.292	0.246	0.837

APPENDIX C

PRELIMINARY SIZING USING MATHCAD

FIRST ESTIMATE OF MAXIMUM TAKE OFF WEIGHT (MTOW)

Using the data presented in table C.1 obtained from table 9.1 of Stinton (2001) an assessment of the MTOW of the aircraft is made.

Table C.1 Characteristics of a standard man

Part of (clothed) body	Per cent Weight	lb	kg
Head and neck	8.3	15	7
Upper trunk	27.2	49	22
Lower trunk	15.5	28	13
Thighs	22.2	40	18
Legs and feet	16.7	30	13.5
Upper arms	5.6	10	4.5
Forearms and hands	4.5	8	4
Total	100	180	82

Note:
For a small man multiply by 0.86;
For a large man multiply by 1.14;
For a woman or young person multiply by, say, 0.55

Table C.2 Typical baggage allowances

Airline class	Baggage allowance	
	lbs	kg
First	66	30
Economy	44	20

Note:
Both of the above include 5 kg (11 lb) hand luggage.
The 5 kg hand luggage is limited in size to the sum of length + breadth + width = 45 in (1.15 m)

The maximum number of passengers carried by a Boeing 767 in a three class layout is 245 passengers. The maximum number of passengers for the BWB is 250 passengers.

Assuming a total number of passengers similar to the B767 three class layout,

Total number of passengers $No_{passengers} := 245$

Mass of each passenger $Mass_{passenger} := 82 \cdot kg$

Baggage allowance per passenger $Mass_{baggage} := 20 \cdot kg$

Sum of passenger and baggage mass $Mass_{sum} := Mass_{passenger} + Mass_{baggage}$

$Mass_{sum} = 102\,kg$

Total passenger and baggage mass $Mass_{total} := No_{passengers} \cdot Mass_{sum}$

$Mass_{total} = 24990\,kg$

"Aircraft designed for longer ranges, which must therefore carry large quantities of fuel may have gross weights nearer 6 to 8 times payload." [(Stinton, 2001) page 528]. ESDU 94009 estimates payload as 0.12 of gross weight (i.e. 8.3 x payload). On that basis, an estimate of 8 x payload is used as follows;

Payload factor $F_{payload} := 8$

Maximum take-off mass $MTOM := F_{payload} \cdot Mass_{total}$

$MTOM = 199920\,kg$

$MTOM = 440748\,lb$

Gravitational acceleration $a_{grav} := 9.81 \cdot \frac{m}{s^2}$

First estimate of maximum take-off weight $MTOW := F_{payload} \cdot Mass_{total} \cdot a_{grav}$

$MTOW = 1961215\,N$

$MTOW = 440899\,lbf$

FIRST ESTIMATE OF WING AREA USING

From Stinton (2001) eqn 2.3a, Lift L = C_L x q x S

where

C_L = Lift coefficient

q = dynamic pressure

S = wing area

Replacing lift with weight W_0 in level flight,

Wing area $S_w = W_0 / (C_L \times q)$

Dynamic pressure $q = V_e^2/295\ ft^2/sec^2$

where

V_e is the equivalent airspeed in knots.

Maximum lift coefficient $C_{Lmax} := 1.3$ (Niu, 1990) page 76

Stall speed or minimum flying speed KEAS $V_s := 135 \cdot knots$ Compare with 137 kt for B767 (Jane's, 2001)

Aircraft weight $W_0 := MTOW$ $W_0 = 1961215N$

Density of air at sea level $\rho_{a0} := 0.237689 \cdot 10^{-2} \cdot \frac{slug}{ft^3}$ (Niu, 1990) fig 3.1.5)

Dynamic pressure at sea level $q_{p0} := \frac{1}{2} \cdot \rho_{a0} \cdot V_s^2$ (at 135 knots)

$q_{p0} = 62 \frac{lbf}{ft^2}$

Wing area $S_w := \frac{W_0}{C_{Lmax} \cdot q_{p0}}$

$S_w = 511\,m^2$ Compare with 290.70 m2 (3,129.0 sqft) for B767 (Jane's, 2001)

$S_w = 5498\,ft^2$

Wing loading $Load_w := \frac{MTOM}{S_w}$

$Load_w = 80\,\frac{lb}{ft^2}$ $Load_w = 391\,\frac{kg}{m^2}$

Comparative figures for B767

B767 Wing loading $Load_{767} := 552.3 \cdot \frac{kg}{m^2}$ $Load_{767} = 113\,\frac{lb}{ft^2}$

(Jane's, 2001)

FIRST DRAG ESTIMATE

From Stinton (2001) fig. 5.16 page 215, total wetted area for delta configuration = 2 x wing area

Total wetted area $A_{wt} := 2 \cdot S_w$

$A_{wt} = 1021\,m^2$ $A_{wt} = 10995\,ft^2$

Extrapolating from Stinton (2001) fig 5.17 page 216 and assuming effective friction dra coefficient for jet aircraft,

$C_{Dfric} := 0.0035$

Equivalent parasite area $f := 45 \cdot ft^2$ $f = 4\,m^2$

From Stinton (2001) fig. 5.15c, the speed for maximum range occurs at (L/D)R (gear retracted) i.e at approx. 2.8Vso so that:

Speed for (L/D)max $V_{L\_DR} := 2.8 \cdot V_s$

$V_{L\_DR} = 378\,\text{knots}$

Compare with V_C and V_D for BWB

$V_c := 185 \cdot \frac{m}{s}$ $V_c = 360\,\text{knots}$

$V_D := 200 \cdot \frac{m}{s}$ $V_D = 389\,\text{knots}$

Maximum range occurs at minimum drag at which $C_D = 2 \times C_{Dp}$ Ref Stinton page 208.

From Stinton page 529, $C_{Dp} = f / S$, hence

Estimated parasite drag coefficient $C'_{Dp} := \frac{f}{S_w}$

$C'_{Dp} = 0$

Assume parasite drag coefficient $C_{Dp} := 0.014$ (Ref. Stinton Table 5.7 page 218)

Total Drag coefficient $C_D := 2 \cdot C_{Dp}$

$C_D = 0$

Density of air at 35000 ft $\rho_{ac} := 0.738206 \cdot 10^{-3} \cdot \frac{slug}{ft^3}$ (Ref Niu fig 3.1.5)

Dynamic pressure at cruise $q_{pc} := \frac{1}{2} \cdot \rho_{ac} \cdot V_{L\_DR}^2$ (at 378 knots)

$q_{pc} = 150 \frac{lbf}{ft^2}$ $q_{pc} = 7192\,\text{Pa}$

Total Drag $D := C_D \cdot q_{pc} \cdot S_w$

$D = 102855\,\text{N}$ $D = 23123\,\text{lbf}$

Lift is assumed to be equal to MTOW, Hence $L_d := \text{MTOW}$ $L_d = 440899\,\text{lbf}$

Lift / Drag in level flight at gross weight $L\_D_R := \frac{L_d}{D}$

$L\_D_R = 19$

FIRST ESTIMATE OF WING SPAN AND ASPECT RATIO

Total wetted area $A_{wt} = 10995\,ft^2$

Equivalent parasitic area $f = 45\,ft^2$

Lift / Drag in level flight at gross weight $L\_D_R = 19$

From Stinton table 5.7, page 218

Induced drag factor $K' := 1.25$ for subsonic jet aircraft

From Stinton fig 5.17 page 216, $C_{Dfric} = 0$

Also, from Stinton pages 218 and 536

Aspect ratio $A_R := \frac{9}{2\cdot\pi}\cdot\left[K'\cdot C_{Dfric}\cdot\left(\frac{A_{wt}}{S_w}\right)\cdot L\_D_R^{\,2}\right]$

$A_R = 5$

Note:
The lower the aspect ratio, the more weight efficient the wing will be.

Wing span $b := \sqrt{A_R\cdot S_w}$

$b = 48\,m$ $b = 158\,ft$

FIRST LAYOUT SKETCH

Fuselage depth assumed to be similar to AIRBUS single aisle aircraft. However blende wing configuration means it is possible to have wider and shorter fuselage. Overall fuse width taken as 3 x single aisle diameter.

Single aisle fuselage diameter $d_{sa} := 3.95\cdot m$

Project aircraft fuselage width $W_{fuse} := 3\cdot d_{sa}$

$W_{fuse} = 12\,m$

Wing span $b = 48.24\,m$

Approximate distance from wing root to tip

$$l_{r\_tip} := \frac{b - W_{fuse}}{2}$$

$$l_{r\_tip} = 18\,m$$

Initial estimate of max wing root depth allowing for taper of fuselage (scaled off initial sketches)

$$d_{root\_max} := 3.4974 \cdot m$$

Wing root chord estimated at 26.8 m (by inspection) to facilitate estimation of prelimin sizes.

DYNAMIC PRESSURE AT DIVE VELOCITY

The wing shear load due to flight inertia is determined below.

Aircraft dive velocity $V_D = 389\,knots$

Air density at sea level $\rho_0 := 0.237689 \cdot 10^{-2} \cdot \frac{slug}{ft^3}$

Dynamic pressure at sea level q_0 $q_0 := \frac{1}{2} \cdot \rho_0 \cdot V_D^{\,2}$

$$q_0 = 512 \frac{lbf}{ft^2}$$

11 APPENDIX D

CURVE FITTING TO DETERMINE SPANWISE LOADING COEFFICIENT USING MATHCAD

The data points obtained from table B.2 of Appendix B are presented below.

data := ..\BWB wing SMT.xl

data =

	0	1
0	0	1.248
1	0.383	1.187
2	0.707	0.912
3	0.921	0.488
4	1	0

vx := data$^{\langle 0 \rangle}$ vy := data$^{\langle 1 \rangle}$

A cubic spline was fitted to the data points obtained from Appendix B to obtain the cur figure D.1 plotted below.

vs := lspline(vx, vy)

x := ..\BWB wing SMT.xl

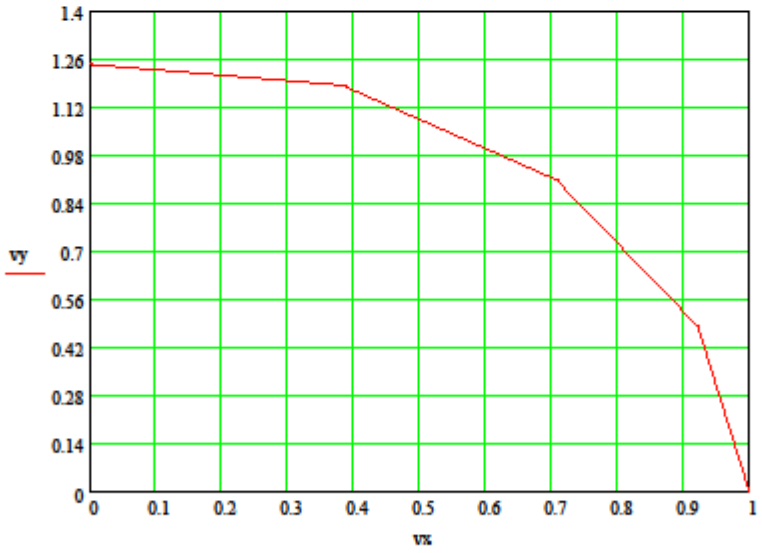

Figure D.1 Variation of spanwise loading coefficient with compressible sweep paramet

The curve presented in figure D.1 was interpolated to determine the compressible sweep parameters at the locations of interest below.

results := interp(vs, vx, vy, x)

results =

	0
0	1.248
1	1.255
2	1.251
3	1.228
4	1.176
5	1.093
6	0.999
7	0.917
8	0.836
9	0.584
10	0.326
11	0

APPENDIX E

--- INPUT DATA FOR THE THIN-WALLED BOX STRUCTURE ANALYSIS---
Project aircraft at root rib modelled as four box beam
Total Number of Cells NCELL= 3
Total Number of Booms NB= 250

Boom No.	X-Y coord.		Boom Area	x-y coord.		Ei
1.00	.00	.00	240.00	.00	.00	7.200E+04
2.00	63.00	154.00	240.00	63.00	154.00	7.200E+04
3.00	126.00	309.00	240.00	126.00	309.00	7.200E+04
4.00	188.00	463.00	240.00	188.00	463.00	7.200E+04
5.00	251.00	617.00	240.00	251.00	617.00	7.200E+04
6.00	314.00	772.00	240.00	314.00	772.00	7.200E+04
7.00	377.00	926.00	240.00	377.00	926.00	7.200E+04
8.00	439.00	1080.00	240.00	439.00	1080.00	7.200E+04
9.00	502.00	1235.00	240.00	502.00	1235.00	7.200E+04
10.00	565.00	1389.00	240.00	565.00	1389.00	7.200E+04
11.00	727.00	1425.00	240.00	727.00	1425.00	7.200E+04
12.00	889.00	1461.00	240.00	889.00	1461.00	7.200E+04
13.00	1051.00	1497.00	240.00	1051.00	1497.00	7.200E+04
14.00	1212.00	1532.00	240.00	1212.00	1532.00	7.200E+04
15.00	1374.00	1568.00	240.00	1374.00	1568.00	7.200E+04
16.00	1536.00	1604.00	240.00	1536.00	1604.00	7.200E+04
17.00	1698.00	1640.00	240.00	1698.00	1640.00	7.200E+04
18.00	1860.00	1676.00	240.00	1860.00	1676.00	7.200E+04
19.00	2021.00	1712.00	240.00	2021.00	1712.00	7.200E+04
20.00	2183.00	1747.00	240.00	2183.00	1747.00	7.200E+04
21.00	2345.00	1783.00	240.00	2345.00	1783.00	7.200E+04
22.00	2507.00	1819.00	240.00	2507.00	1819.00	7.200E+04
23.00	2669.00	1855.00	240.00	2669.00	1855.00	7.200E+04
24.00	2830.00	1891.00	240.00	2830.00	1891.00	7.200E+04
25.00	2984.00	1900.00	240.00	2984.00	1900.00	7.200E+04
26.00	3137.00	1910.00	240.00	3137.00	1910.00	7.200E+04
27.00	3291.00	1920.00	240.00	3291.00	1920.00	7.200E+04
28.00	3444.00	1929.00	480.00	3444.00	1929.00	7.200E+04
29.00	3607.00	1940.00	240.00	3607.00	1940.00	7.200E+04
30.00	3770.00	1950.00	240.00	3770.00	1950.00	7.200E+04
31.00	3933.00	1960.00	240.00	3933.00	1960.00	7.200E+04
32.00	4096.00	1970.00	240.00	4096.00	1970.00	7.200E+04
33.00	4258.00	1980.00	240.00	4258.00	1980.00	7.200E+04
34.00	4421.00	1990.00	240.00	4421.00	1990.00	7.200E+04

35.00	4584.00	2001.00	240.00	4584.00	2001.00	7.200E+04
36.00	4747.00	2011.00	240.00	4747.00	2011.00	7.200E+04
37.00	4909.00	2021.00	240.00	4909.00	2021.00	7.200E+04
38.00	5072.00	2031.00	240.00	5072.00	2031.00	7.200E+04
39.00	5235.00	2041.00	240.00	5235.00	2041.00	7.200E+04
40.00	5398.00	2051.00	240.00	5398.00	2051.00	7.200E+04
41.00	5560.00	2062.00	240.00	5560.00	2062.00	7.200E+04
42.00	5723.00	2072.00	240.00	5723.00	2072.00	7.200E+04
43.00	5886.00	2082.00	240.00	5886.00	2082.00	7.200E+04
44.00	6049.00	2092.00	240.00	6049.00	2092.00	7.200E+04
45.00	6212.00	2102.00	240.00	6212.00	2102.00	7.200E+04
46.00	6374.00	2113.00	240.00	6374.00	2113.00	7.200E+04
47.00	6537.00	2123.00	240.00	6537.00	2123.00	7.200E+04
48.00	6700.00	2133.00	240.00	6700.00	2133.00	7.200E+04
49.00	6863.00	2143.00	240.00	6863.00	2143.00	7.200E+04
50.00	7025.00	2153.00	240.00	7025.00	2153.00	7.200E+04
51.00	7188.00	2163.00	240.00	7188.00	2163.00	7.200E+04
52.00	7351.00	2174.00	240.00	7351.00	2174.00	7.200E+04
53.00	7514.00	2184.00	240.00	7514.00	2184.00	7.200E+04
54.00	7676.00	2194.00	240.00	7676.00	2194.00	7.200E+04
55.00	7839.00	2204.00	240.00	7839.00	2204.00	7.200E+04
56.00	8002.00	2214.00	240.00	8002.00	2214.00	7.200E+04
57.00	8165.00	2225.00	240.00	8165.00	2225.00	7.200E+04
58.00	8328.00	2235.00	240.00	8328.00	2235.00	7.200E+04
59.00	8490.00	2245.00	240.00	8490.00	2245.00	7.200E+04
60.00	8653.00	2255.00	240.00	8653.00	2255.00	7.200E+04
61.00	8816.00	2265.00	240.00	8816.00	2265.00	7.200E+04
62.00	8979.00	2275.00	240.00	8979.00	2275.00	7.200E+04
63.00	9141.00	2286.00	240.00	9141.00	2286.00	7.200E+04
64.00	9304.00	2296.00	240.00	9304.00	2296.00	7.200E+04
65.00	9467.00	2306.00	240.00	9467.00	2306.00	7.200E+04
66.00	9630.00	2316.00	240.00	9630.00	2316.00	7.200E+04
67.00	9467.00	2306.00	480.00	9467.00	2306.00	7.200E+04
68.00	9630.00	2296.00	240.00	9630.00	2296.00	7.200E+04
69.00	9793.00	2287.00	240.00	9793.00	2287.00	7.200E+04
70.00	9956.00	2277.00	240.00	9956.00	2277.00	7.200E+04
71.00	10120.00	2268.00	240.00	10120.00	2268.00	7.200E+04
72.00	10283.00	2258.00	240.00	10283.00	2258.00	7.200E+04
73.00	10446.00	2249.00	240.00	10446.00	2249.00	7.200E+04
74.00	10609.00	2239.00	240.00	10609.00	2239.00	7.200E+04
75.00	10772.00	2229.00	240.00	10772.00	2229.00	7.200E+04
76.00	10935.00	2220.00	240.00	10935.00	2220.00	7.200E+04

77.00	11099.00	2210.00	240.00	11099.00	2210.00	7.200E+04
78.00	11262.00	2201.00	240.00	11262.00	2201.00	7.200E+04
79.00	11425.00	2191.00	240.00	11425.00	2191.00	7.200E+04
80.00	11588.00	2182.00	240.00	11588.00	2182.00	7.200E+04
81.00	11751.00	2172.00	240.00	11751.00	2172.00	7.200E+04
82.00	11915.00	2163.00	240.00	11915.00	2163.00	7.200E+04
83.00	12078.00	2153.00	240.00	12078.00	2153.00	7.200E+04
84.00	12241.00	2143.00	240.00	12241.00	2143.00	7.200E+04
85.00	12404.00	2134.00	240.00	12404.00	2134.00	7.200E+04
86.00	12567.00	2124.00	240.00	12567.00	2124.00	7.200E+04
87.00	12730.00	2115.00	240.00	12730.00	2115.00	7.200E+04
88.00	12894.00	2105.00	240.00	12894.00	2105.00	7.200E+04
89.00	13057.00	2096.00	240.00	13057.00	2096.00	7.200E+04
90.00	13220.00	2086.00	240.00	13220.00	2086.00	7.200E+04
91.00	13383.00	2076.00	240.00	13383.00	2076.00	7.200E+04
92.00	13546.00	2067.00	240.00	13546.00	2067.00	7.200E+04
93.00	13710.00	2057.00	240.00	13710.00	2057.00	7.200E+04
94.00	13873.00	2048.00	240.00	13873.00	2048.00	7.200E+04
95.00	14036.00	2038.00	240.00	14036.00	2038.00	7.200E+04
96.00	14199.00	2029.00	240.00	14199.00	2029.00	7.200E+04
97.00	14362.00	2019.00	240.00	14362.00	2019.00	7.200E+04
98.00	14525.00	2009.00	240.00	14525.00	2009.00	7.200E+04
99.00	14689.00	2000.00	240.00	14689.00	2000.00	7.200E+04
100.00	14852.00	1990.00	240.00	14852.00	1990.00	7.200E+04
101.00	15015.00	1981.00	240.00	15015.00	1981.00	7.200E+04
102.00	15178.00	1971.00	240.00	15178.00	1971.00	7.200E+04
103.00	15341.00	1962.00	240.00	15341.00	1962.00	7.200E+04
104.00	15504.00	1952.00	480.00	15504.00	1952.00	7.200E+04
105.00	15665.00	1937.00	240.00	15665.00	1937.00	7.200E+04
106.00	15825.00	1923.00	240.00	15825.00	1923.00	7.200E+04
107.00	15986.00	1908.00	240.00	15986.00	1908.00	7.200E+04
108.00	16146.00	1893.00	240.00	16146.00	1893.00	7.200E+04
109.00	16307.00	1879.00	240.00	16307.00	1879.00	7.200E+04
110.00	16467.00	1864.00	240.00	16467.00	1864.00	7.200E+04
111.00	16628.00	1849.00	240.00	16628.00	1849.00	7.200E+04
112.00	16788.00	1834.00	240.00	16788.00	1834.00	7.200E+04
113.00	16949.00	1820.00	240.00	16949.00	1820.00	7.200E+04
114.00	17109.00	1805.00	240.00	17109.00	1805.00	7.200E+04
115.00	17270.00	1790.00	240.00	17270.00	1790.00	7.200E+04
116.00	17430.00	1776.00	240.00	17430.00	1776.00	7.200E+04
117.00	17590.00	1761.00	240.00	17590.00	1761.00	7.200E+04
118.00	17751.00	1746.00	240.00	17751.00	1746.00	7.200E+04

119.00	17911.00	1731.00	240.00	17911.00	1731.00	7.200E+04
120.00	18072.00	1717.00	240.00	18072.00	1717.00	7.200E+04
121.00	18232.00	1702.00	240.00	18232.00	1702.00	7.200E+04
122.00	18393.00	1687.00	240.00	18393.00	1687.00	7.200E+04
123.00	18553.00	1673.00	240.00	18553.00	1673.00	7.200E+04
124.00	18714.00	1658.00	240.00	18714.00	1658.00	7.200E+04
125.00	18874.00	1643.00	240.00	18874.00	1643.00	7.200E+04
126.00	19035.00	1628.00	240.00	19035.00	1628.00	7.200E+04
127.00	19195.00	1614.00	240.00	19195.00	1614.00	7.200E+04
128.00	19356.00	1599.00	240.00	19356.00	1599.00	7.200E+04
129.00	19516.00	1584.00	480.00	19516.00	1584.00	7.200E+04
130.00	19516.00	-421.00	480.00	19516.00	-421.00	7.200E+04
131.00	19356.00	-435.00	240.00	19356.00	-435.00	7.200E+04
132.00	19195.00	-450.00	240.00	19195.00	-450.00	7.200E+04
133.00	19035.00	-465.00	240.00	19035.00	-465.00	7.200E+04
134.00	18874.00	-479.00	240.00	18874.00	-479.00	7.200E+04
135.00	18714.00	-494.00	240.00	18714.00	-494.00	7.200E+04
136.00	18553.00	-509.00	240.00	18553.00	-509.00	7.200E+04
137.00	18393.00	-524.00	240.00	18393.00	-524.00	7.200E+04
138.00	18232.00	-538.00	240.00	18232.00	-538.00	7.200E+04
139.00	18072.00	-553.00	240.00	18072.00	-553.00	7.200E+04
140.00	17911.00	-568.00	240.00	17911.00	-568.00	7.200E+04
141.00	17751.00	-582.00	240.00	17751.00	-582.00	7.200E+04
142.00	17590.00	-597.00	240.00	17590.00	-597.00	7.200E+04
143.00	17430.00	-612.00	240.00	17430.00	-612.00	7.200E+04
144.00	17270.00	-627.00	240.00	17270.00	-627.00	7.200E+04
145.00	17109.00	-641.00	240.00	17109.00	-641.00	7.200E+04
146.00	16949.00	-656.00	240.00	16949.00	-656.00	7.200E+04
147.00	16788.00	-671.00	240.00	16788.00	-671.00	7.200E+04
148.00	16628.00	-685.00	240.00	16628.00	-685.00	7.200E+04
149.00	16467.00	-700.00	240.00	16467.00	-700.00	7.200E+04
150.00	16307.00	-715.00	240.00	16307.00	-715.00	7.200E+04
151.00	16146.00	-730.00	240.00	16146.00	-730.00	7.200E+04
152.00	15986.00	-744.00	240.00	15986.00	-744.00	7.200E+04
153.00	15825.00	-759.00	240.00	15825.00	-759.00	7.200E+04
154.00	15665.00	-774.00	240.00	15665.00	-774.00	7.200E+04
155.00	15504.00	-788.00	480.00	15504.00	-788.00	7.200E+04
156.00	15341.00	-798.00	240.00	15341.00	-798.00	7.200E+04
157.00	15178.00	-808.00	240.00	15178.00	-808.00	7.200E+04
158.00	15015.00	-817.00	240.00	15015.00	-817.00	7.200E+04
159.00	14852.00	-827.00	240.00	14852.00	-827.00	7.200E+04
160.00	14689.00	-836.00	240.00	14689.00	-836.00	7.200E+04

161.00	14525.00	-846.00	240.00	14525.00	-846.00	7.200E+04
162.00	14362.00	-855.00	240.00	14362.00	-855.00	7.200E+04
163.00	14199.00	-865.00	240.00	14199.00	-865.00	7.200E+04
164.00	14036.00	-874.00	240.00	14036.00	-874.00	7.200E+04
165.00	13873.00	-884.00	240.00	13873.00	-884.00	7.200E+04
166.00	13710.00	-894.00	240.00	13710.00	-894.00	7.200E+04
167.00	13546.00	-903.00	240.00	13546.00	-903.00	7.200E+04
168.00	13383.00	-913.00	240.00	13383.00	-913.00	7.200E+04
169.00	13220.00	-922.00	240.00	13220.00	-922.00	7.200E+04
170.00	13057.00	-932.00	240.00	13057.00	-932.00	7.200E+04
171.00	12894.00	-941.00	240.00	12894.00	-941.00	7.200E+04
172.00	12730.00	-951.00	240.00	12730.00	-951.00	7.200E+04
173.00	12567.00	-961.00	240.00	12567.00	-961.00	7.200E+04
174.00	12404.00	-970.00	240.00	12404.00	-970.00	7.200E+04
175.00	12241.00	-980.00	240.00	12241.00	-980.00	7.200E+04
176.00	12078.00	-989.00	240.00	12078.00	-989.00	7.200E+04
177.00	11915.00	-999.00	240.00	11915.00	-999.00	7.200E+04
178.00	11751.00	-1008.00	240.00	11751.00	-1008.00	7.200E+04
179.00	11588.00	-1018.00	240.00	11588.00	-1018.00	7.200E+04
180.00	11425.00	-1028.00	240.00	11425.00	-1028.00	7.200E+04
181.00	11262.00	-1037.00	240.00	11262.00	-1037.00	7.200E+04
182.00	11099.00	-1047.00	240.00	11099.00	-1047.00	7.200E+04
183.00	10935.00	-1056.00	240.00	10935.00	-1056.00	7.200E+04
184.00	10772.00	-1066.00	240.00	10772.00	-1066.00	7.200E+04
185.00	10609.00	-1075.00	240.00	10609.00	-1075.00	7.200E+04
186.00	10446.00	-1085.00	240.00	10446.00	-1085.00	7.200E+04
187.00	10283.00	-1094.00	240.00	10283.00	-1094.00	7.200E+04
188.00	10120.00	-1104.00	240.00	10120.00	-1104.00	7.200E+04
189.00	9956.00	-1114.00	240.00	9956.00	-1114.00	7.200E+04
190.00	9793.00	-1123.00	240.00	9793.00	-1123.00	7.200E+04
191.00	9630.00	-1133.00	240.00	9630.00	-1133.00	7.200E+04
192.00	9467.00	-1142.00	480.00	9467.00	-1142.00	7.200E+04
193.00	9304.00	-1132.00	240.00	9304.00	-1132.00	7.200E+04
194.00	9141.00	-1122.00	240.00	9141.00	-1122.00	7.200E+04
195.00	8979.00	-1112.00	240.00	8979.00	-1112.00	7.200E+04
196.00	8816.00	-1102.00	240.00	8816.00	-1102.00	7.200E+04
197.00	8653.00	-1091.00	240.00	8653.00	-1091.00	7.200E+04
198.00	8490.00	-1081.00	240.00	8490.00	-1081.00	7.200E+04
199.00	8328.00	-1071.00	240.00	8328.00	-1071.00	7.200E+04
200.00	8165.00	-1061.00	240.00	8165.00	-1061.00	7.200E+04
201.00	8002.00	-1051.00	240.00	8002.00	-1051.00	7.200E+04
202.00	7839.00	-1040.00	240.00	7839.00	-1040.00	7.200E+04

203.00	7676.00	-1030.00	240.00	7676.00	-1030.00	7.200E+04
204.00	7514.00	-1020.00	240.00	7514.00	-1020.00	7.200E+04
205.00	7351.00	-1010.00	240.00	7351.00	-1010.00	7.200E+04
206.00	7188.00	-1000.00	240.00	7188.00	-1000.00	7.200E+04
207.00	7025.00	-990.00	240.00	7025.00	-990.00	7.200E+04
208.00	6863.00	-979.00	240.00	6863.00	-979.00	7.200E+04
209.00	6700.00	-969.00	240.00	6700.00	-969.00	7.200E+04
210.00	6537.00	-959.00	240.00	6537.00	-959.00	7.200E+04
211.00	6374.00	-949.00	240.00	6374.00	-949.00	7.200E+04
212.00	6212.00	-939.00	240.00	6212.00	-939.00	7.200E+04
213.00	6049.00	-929.00	240.00	6049.00	-929.00	7.200E+04
214.00	5886.00	-918.00	240.00	5886.00	-918.00	7.200E+04
215.00	5723.00	-908.00	240.00	5723.00	-908.00	7.200E+04
216.00	5560.00	-898.00	240.00	5560.00	-898.00	7.200E+04
217.00	5398.00	-888.00	240.00	5398.00	-888.00	7.200E+04
218.00	5235.00	-878.00	240.00	5235.00	-878.00	7.200E+04
219.00	5072.00	-867.00	240.00	5072.00	-867.00	7.200E+04
220.00	4909.00	-857.00	240.00	4909.00	-857.00	7.200E+04
221.00	4747.00	-847.00	240.00	4747.00	-847.00	7.200E+04
222.00	4584.00	-837.00	240.00	4584.00	-837.00	7.200E+04
223.00	4421.00	-827.00	240.00	4421.00	-827.00	7.200E+04
224.00	4258.00	-817.00	240.00	4258.00	-817.00	7.200E+04
225.00	4096.00	-806.00	240.00	4096.00	-806.00	7.200E+04
226.00	3933.00	-796.00	240.00	3933.00	-796.00	7.200E+04
227.00	3770.00	-786.00	240.00	3770.00	-786.00	7.200E+04
228.00	3607.00	-776.00	240.00	3607.00	-776.00	7.200E+04
229.00	3444.00	-766.00	480.00	3444.00	-766.00	7.200E+04
230.00	3293.00	-748.00	240.00	3293.00	-748.00	7.200E+04
231.00	3141.00	-731.00	240.00	3141.00	-731.00	7.200E+04
232.00	2989.00	-714.00	240.00	2989.00	-714.00	7.200E+04
233.00	2837.00	-696.00	240.00	2837.00	-696.00	7.200E+04
234.00	2685.00	-679.00	240.00	2685.00	-679.00	7.200E+04
235.00	2534.00	-662.00	240.00	2534.00	-662.00	7.200E+04
236.00	2382.00	-645.00	240.00	2382.00	-645.00	7.200E+04
237.00	2230.00	-627.00	240.00	2230.00	-627.00	7.200E+04
238.00	2071.00	-582.00	240.00	2071.00	-582.00	7.200E+04
239.00	1911.00	-538.00	240.00	1911.00	-538.00	7.200E+04
240.00	1752.00	-493.00	240.00	1752.00	-493.00	7.200E+04
241.00	1593.00	-448.00	240.00	1593.00	-448.00	7.200E+04
242.00	1434.00	-403.00	240.00	1434.00	-403.00	7.200E+04
243.00	1274.00	-358.00	240.00	1274.00	-358.00	7.200E+04
244.00	1115.00	-314.00	240.00	1115.00	-314.00	7.200E+04

```
 245.00    956.00    -269.00    240.00    956.00    -269.00    7.200E+04
 246.00    796.00    -224.00    240.00    796.00    -224.00    7.200E+04
 247.00    637.00    -179.00    240.00    637.00    -179.00    7.200E+04
 248.00    478.00    -134.00    240.00    478.00    -134.00    7.200E+04
 249.00    319.00    -90.00    240.00    319.00    -90.00    7.200E+04
 250.00    159.00    -45.00    240.00    159.00    -45.00    7.200E+04
Mid-Wall Boom No.  Ei  Thickness
 67.00  192.00  7.200E+04  1.000E+01
 104.00  155.00  7.200E+04  1.000E+01

Applied Sy  at Xsy   and   Sx  at Ysx      Mx         My          T
   1.521E+06  7806.00    0.000E+00    .00  1.129E+10  0.000E+00  8.370E+08

--- ANALYSIS RESULTS OF THE THIN-WALLED BOX STRUCTURE ---

Number of Cells and Booms: 3    250

Centroid Coordinates Xc= 9646.57    Yc= 588.95 mm

Boom-based 2nd Moment of Area Ixx          Iyy             Ixy (mm^4)
                1.190E+11           2.074E+12           3.507E+09

Bending Stiffness  EIxx           EIyy           EIxy (N.mm^2)
            8.571E+15         1.493E+17         2.525E+14

Total Mean Area at Root =   5.381E+07  mm^2
Total Mean Area at Tip =    5.381E+07  mm^2

 --- Direct Stress in Booms ---

   Boom No.   Stress(MPa)
      1        54.32472
      2        39.72534
      3        25.03109
      4        10.43155
      5       -4.167837
      6       -18.86209
      7       -33.46147
      8       -48.06101
      9       -62.75526
      10       -77.35464
      11       -80.74387
```

12	-84.13308
13	-87.5223
14	-90.81681
15	-94.20603
16	-97.59525
17	-100.9845
18	-104.3737
19	-107.7631
20	-111.0574
21	-114.4466
22	-117.8359
23	-121.2251
24	-124.6145
25	-125.4436
26	-126.3677
27	-127.2916
28	-128.1209
29	-129.1383
30	-130.0608
31	-130.9833
32	-131.9059
33	-132.8285
34	-133.7511
35	-134.7684
36	-135.691
37	-136.6136
38	-137.5362
39	-138.4587
40	-139.3812
41	-140.3988
42	-141.3213
43	-142.2438
44	-143.1663
45	-144.0888
46	-145.1064
47	-146.0289
48	-146.9514
49	-147.874
50	-148.7966
51	-149.7192
52	-150.7365
53	-151.6591

54	-152.5817
55	-153.5043
56	-154.4268
57	-155.4442
58	-156.3667
59	-157.2894
60	-158.2119
61	-159.1344
62	-160.0569
63	-161.0745
64	-161.997
65	-162.9195
66	-163.8421
67	-162.9195
68	-161.9447
69	-161.0648
70	-160.09
71	-159.2099
72	-158.235
73	-157.3551
74	-156.3803
75	-155.4055
76	-154.5255
77	-153.5505
78	-152.6706
79	-151.6958
80	-150.8158
81	-149.841
82	-148.9609
83	-147.9861
84	-147.0113
85	-146.1313
86	-145.1565
87	-144.2766
88	-143.3016
89	-142.4216
90	-141.4468
91	-140.472
92	-139.592
93	-138.6171
94	-137.7371
95	-136.7623

96	-135.8824
97	-134.9075
98	-133.9327
99	-133.0526
100	-132.0778
101	-131.1979
102	-130.223
103	-129.3431
104	-128.3683
105	-126.9194
106	-125.5657
107	-124.1168
108	-122.6682
109	-121.3142
110	-119.8655
111	-118.4167
112	-116.968
113	-115.6141
114	-114.1654
115	-112.7166
116	-111.3628
117	-109.9141
118	-108.4653
119	-107.0166
120	-105.6626
121	-104.214
122	-102.7651
123	-101.4113
124	-99.96252
125	-98.51385
126	-97.06503
127	-95.71122
128	-94.2624
129	-92.81372
130	97.39423
131	98.6967
132	100.0939
133	101.4912
134	102.7935
135	104.1909
136	105.588
137	106.9854

138	108.2877
139	109.685
140	111.0822
141	112.3847
142	113.7818
143	115.1792
144	116.5765
145	117.8788
146	119.2762
147	120.6733
148	121.9758
149	123.373
150	124.7703
151	126.1675
152	127.47
153	128.8671
154	130.2645
155	131.5668
156	132.4893
157	133.4118
158	134.2395
159	135.162
160	135.9897
161	136.912
162	137.7397
163	138.6622
164	139.4898
165	140.4124
166	141.3349
167	142.1624
168	143.0849
169	143.9126
170	144.8351
171	145.6627
172	146.5851
173	147.5076
174	148.3353
175	149.2578
176	150.0854
177	151.008
178	151.8354
179	152.758

180	153.6805
181	154.5081
182	155.4307
183	156.2582
184	157.1807
185	158.0083
186	158.9309
187	159.7585
188	160.681
189	161.6034
190	162.4311
191	163.3536
192	164.1812
193	163.2064
194	162.2316
195	161.2569
196	160.2821
197	159.2124
198	158.2376
199	157.263
200	156.2882
201	155.3133
202	154.2437
203	153.2688
204	152.2942
205	151.3194
206	150.3446
207	149.3698
208	148.3002
209	147.3254
210	146.3506
211	145.3758
212	144.4011
213	143.4263
214	142.3566
215	141.3818
216	140.407
217	139.4324
218	138.4575
219	137.3879
220	136.413
221	135.4384

222	134.4636
223	133.4888
224	132.5139
225	131.4444
226	130.4696
227	129.4948
228	128.52
229	127.5452
230	125.8133
231	124.1762
232	122.5391
233	120.8071
234	119.17
235	117.533
236	115.8959
237	114.1639
238	109.8694
239	105.6696
240	101.3751
241	97.08059
242	92.78608
243	88.49141
244	84.29176
245	79.99725
246	75.70257
247	71.40807
248	67.11355
249	62.91391
250	58.61924

Mean Area of Cell-1 & Cell-2 & Cell-3:
2.561E+07 1.871E+07 9.529E+06 mm^2

--- Basic Shear Flows ---

SKB=EIXX * EIYY - EIXY ^ 2 SK1 = EIXY / SKB SK2 = EIYY / SKB SK3 = EIXX / SKB
1.28E+33 1.97E-19 1.17E-16 6.70E-18

Cell- 1 Skin Panel No.	Basic Shear Flow QB (N/mm)
1 - 2	0
2 - 3	1.28457151464408

3 - 4	2.09398325817133
4 - 5	2.43129769844956
5 - 6	2.29652002299624
6 - 7	1.68658257642608
7 - 8	0.604553014124372
8 - 9	-0.949573851426362
9 - 10	-2.97886048809392
10 - 11	-5.48023924049304
11 - 12	-8.09121320893153
12 - 13	-10.8117823934094
13 - 14	-13.6419467939266
14 - 15	-16.5786439426154
15 - 16	-19.6249363073436
16 - 17	-22.7808238881111
17 - 18	-26.0463068721529
18 - 19	-29.421385072234
19 - 20	-32.906063675872
20 - 21	-36.497269840164
21 - 22	-40.1980712204955
22 - 23	-44.0084678168663
23 - 24	-47.9284596292764
24 - 25	-51.9580518452435
25 - 26	-56.0144540819872
26 - 27	-60.1007391824105
27 - 28	-64.2169019589957
28 - 29	-72.5028579287546
29 - 30	-76.6787345575241
30 - 31	-80.8844421747983
31 - 32	-85.1199807805773
32 - 33	-89.385350374861
33 - 34	-93.680556145167
34 - 35	-98.0055929039777
35 - 36	-102.363528306679
36 - 37	-106.751294697884
37 - 38	-111.168897265112
38 - 39	-115.616330820844
39 - 40	-120.093595365082
40 - 41	-124.600690897824
41 - 42	-129.140690261973
42 - 43	-133.710520614627
43 - 44	-138.310181955786
44 - 45	-142.93967428545

45 - 46	-147.598997603619
46 - 47	-152.291224753195
47 - 48	-157.013282891276
48 - 49	-161.765172017861
49 - 50	-166.546892132951
50 - 51	-171.358448424064
51 - 52	-176.199835703681
52 - 53	-181.074121627189
53 - 54	-185.978238539201
54 - 55	-190.912191627235
55 - 56	-195.875975703774
56 - 57	-200.869590768818
57 - 58	-205.896104477752
58 - 59	-210.95244917519
59 - 60	-216.038630048651
60 - 61	-221.154641910617
61 - 62	-226.300484761087
62 - 63	-231.476158600062
63 - 64	-236.684736270445
64 - 65	-241.923144929332
65 - 66	-247.191384576725
66 - 67	-252.489455212621
67 - 68	-263.025934507406
68 - 69	-252.407862265335
69 - 70	-247.130348263501
70 - 71	-241.884356380867
71 - 72	-236.669881429917
72 - 73	-231.486928598167
73 - 74	-226.338565541003
74 - 75	-221.22172460304
75 - 76	-216.136400596761
76 - 77	-211.082598709682
77 - 78	-206.060318941804
78 - 79	-201.072628948511
79 - 80	-196.11646107442
80 - 81	-191.191810132012
81 - 82	-186.298681308804
82 - 83	-181.437074604798
83 - 84	-176.606990019992
84 - 85	-171.811490022254
85 - 86	-167.047512143717
86 - 87	-162.315056384382

87 - 88	-157.614122744246
88 - 89	-152.944706035794
89 - 90	-148.306811446543
90 - 91	-143.703506631878
91 - 92	-139.131723936413
92 - 93	-134.59146336015
93 - 94	-130.082719715569
94 - 95	-125.60549819019
95 - 96	-121.162866439396
96 - 97	-116.751756807803
97 - 98	-112.372164107893
98 - 99	-108.024093527184
99 - 100	-103.707545065676
100 - 101	-99.4225187233685
101 - 102	-95.1720769681296
102 - 103	-90.9531573320914
103 - 104	-86.7657598152539
104 - 105	-82.6098844176172
105 - 106	-74.3611778607452
106 - 107	-70.2928256943825
107 - 108	-66.2774121722252
108 - 109	-62.3149372942734
109 - 110	-58.4084687159124
110 - 111	-54.5549387817568
111 - 112	-50.7543423042892
112 - 113	-47.0066844710271
113 - 114	-43.3150329373557
114 - 115	-39.7622507112998
115 - 116	-36.3452753249915
116 - 117	-33.0671692462987
117 - 118	-29.9279324752214
118 - 119	-26.9275648245247
119 - 120	-24.066071668961
120 - 121	-21.3403801656274
121 - 122	-18.7535579699093
122 - 123	-16.3056102693242
123 - 124	-13.9965318763545
124 - 125	-11.8263227910002
125 - 126	-9.79191535787621
126 - 1	-7.89638241988511

Cell- 2 Skin Panel No.	Basic Shear Flow QB (N/mm)
1 - 2	0

2 - 3	-5.2367175281914
3 - 4	-10.4449805925673
4 - 5	-15.6217215377425
5 - 6	-20.7700028315848
6 - 7	-25.8867620062263
7 - 8	-30.9750667170524
8 - 9	-36.0318493086777
9 - 10	-41.0571097811023
10 - 11	-46.0539157897114
11 - 12	-51.0191944916023
12 - 13	-55.9560187296778
13 - 14	-60.8613208485525
14 - 15	-65.7381685036117
15 - 16	-70.5834940394702
16 - 17	-75.4003599239958
17 - 18	-80.1857036893206
18 - 19	-84.9395253354447
19 - 20	-89.6648925177534
20 - 21	-94.3587375808612
21 - 22	-99.0241281801537
22 - 23	-103.657991472728
23 - 24	-108.263400301487
24 - 25	-112.837287011045
25 - 26	-117.379651601402
26 - 27	-121.893561727944
27 - 28	-126.375944547767
28 - 29	-130.829872903775
29 - 30	-135.252279140583
30 - 31	-139.646230913575
31 - 32	-144.008660567366
32 - 33	-148.339568101956
33 - 34	-152.642015985214
34 - 35	-156.912941749271
35 - 36	-161.155413049512
36 - 37	-165.366362230553
37 - 38	-169.548856947778
38 - 39	-177.850802143827
39 - 40	-169.34199582857
40 - 41	-165.057761682436
41 - 42	-160.743696547799
42 - 43	-156.402868080041
43 - 44	-152.032208623779

44 - 45	-147.634785834397
45 - 46	-143.207537244028
46 - 47	-138.75352532054
47 - 48	-134.269682408547
48 - 49	-129.759076163434
49 - 50	-125.218638929817
50 - 51	-120.648370707695
51 - 52	-116.05134433997
52 - 53	-111.424486983741
53 - 54	-106.770866294393
54 - 55	-102.08741461654
55 - 56	-97.3771996055672
56 - 57	-92.6371587936072
57 - 58	-87.8672869931425
58 - 59	-83.0706518595583
59 - 60	-78.2441857374694
60 - 61	-73.390956282261
61 - 62	-68.5078958385478
62 - 63	-63.5980772492326
63 - 64	-58.6584276714127
64 - 65	-53.688947105088
65 - 66	-48.6927032056438
66 - 67	-43.6666283176949
67 - 68	-38.6137952841439
68 - 69	-33.5311312620882
69 - 70	-28.421703906913
70 - 71	-23.2824455632331
71 - 72	-18.1164238864337
72 - 73	-12.9205712211295
73 - 74	-7.69489275483802
74 - 75	-2.44245095542708
75 - 76	2.83982183248862
76 - 1	0

Cell- 3 Skin Panel No.	Basic Shear Flow QB (N/mm)
1 - 2	0
2 - 3	-4.10412257693221
3 - 4	-8.16446797567501
4 - 5	-12.1779633533256
5 - 6	-16.1446138974016
6 - 7	-20.0674820757706
7 - 8	-23.9435054205649
8 - 9	-27.7726787442671

9 - 10	-31.5550072343946
10 - 11	-35.2935533588152
11 - 12	-38.9852546496611
12 - 13	-42.6301059194148
13 - 14	-46.2311800109791
14 - 15	-49.7854092689687
15 - 16	-53.2927885058662
16 - 17	-56.7533229091889
17 - 18	-60.1700749468048
18 - 19	-63.5399821508459
19 - 20	-66.8630393337949
20 - 21	-70.1423193385545
21 - 22	-73.3747493222219
22 - 23	-76.5603344723146
23 - 24	-79.6990696013151
24 - 25	-82.7940275521263
25 - 26	-85.8421352946104
26 - 27	-91.8446611124293
27 - 28	-85.5458888352964
28 - 29	-82.3543855241317
29 - 30	-79.1177027597357
30 - 31	-75.8358351673562
31 - 32	-72.5118555898959
32 - 33	-69.1426911844521
33 - 34	-65.7283471385422
34 - 35	-62.2688182646487
35 - 36	-58.7671774056744
36 - 37	-55.2203517187166
37 - 38	-51.6283463912927
38 - 39	-47.9942238912705
39 - 40	-44.3149217507823
40 - 41	-40.5904347823105
41 - 42	-36.8207629858552
42 - 43	-33.008979204319
43 - 44	-29.1520105947994
44 - 45	-25.2498623448136
45 - 46	-21.3055969222296
46 - 47	-17.3161518591795
47 - 48	-13.2815219681458
48 - 49	-9.20171243664611
49 - 50	-5.07978573254811
50 - 51	-0.912679387984035

```
    51 - 52            3.29961178456359
    52 - 1             0

Cell No. K = 1
 SUM OF CELL MQB=          -1.09E+10

Cell No. K = 2
 SUM OF CELL MQB=          -2.08E+10

Cell No. K = 3
 SUM OF CELL MQB=          -2.54E+10

 Moment due to Sx, Sy: MSL=   1.19E+10

 MSL - Torq =              1.10E+10

            (AA)=              {BB}

1.000E+00  7.305E-01  3.721E-01   2.809E+02
1.000E+00  -9.978E-01  1.314E-01   7.931E+01
1.000E+00  -6.863E+00  8.085E+00   -3.312E+02

 INVERSE OF 3X3 (AA)=(GIK)=

4.727E-01  5.581E-01  -3.083E-02
5.247E-01  -5.088E-01  -1.588E-02
3.869E-01  -5.010E-01  1.140E-01

 constant Q0i in cell-1    cell-2    cell-3

         1.872E+02    1.123E+02    3.118E+01
 ------------------------------------------------------------

 Final shear flows Qs in cell-1
  1 - 2        1.872E+02
  2 - 3        1.885E+02
  3 - 4        1.893E+02
  4 - 5        1.897E+02
  5 - 6        1.895E+02
  6 - 7        1.889E+02
  7 - 8        1.878E+02
  8 - 9        1.863E+02
```

9 - 10	1.843E+02
10 - 11	1.818E+02
11 - 12	1.792E+02
12 - 13	1.764E+02
13 - 14	1.736E+02
14 - 15	1.707E+02
15 - 16	1.676E+02
16 - 17	1.645E+02
17 - 18	1.612E+02
18 - 19	1.578E+02
19 - 20	1.543E+02
20 - 21	1.507E+02
21 - 22	1.470E+02
22 - 23	1.432E+02
23 - 24	1.393E+02
24 - 25	1.353E+02
25 - 26	1.312E+02
26 - 27	1.271E+02
27 - 28	1.230E+02
28 - 29	1.147E+02
29 - 30	1.106E+02
30 - 31	1.064E+02
31 - 32	1.021E+02
32 - 33	9.786E+01
33 - 34	9.356E+01
34 - 35	8.924E+01
35 - 36	8.488E+01
36 - 37	8.049E+01
37 - 38	7.607E+01
38 - 39	7.163E+01
39 - 40	6.715E+01
40 - 41	6.264E+01
41 - 42	5.810E+01
42 - 43	5.353E+01
43 - 44	4.893E+01
44 - 45	4.430E+01
45 - 46	3.964E+01
46 - 47	3.495E+01
47 - 48	3.023E+01
48 - 49	2.548E+01
49 - 50	2.070E+01
50 - 51	1.588E+01

51 - 52	1.104E+01
52 - 53	6.169E+00
53 - 54	1.265E+00
54 - 55	-3.669E+00
55 - 56	-8.633E+00
56 - 57	-1.363E+01
57 - 58	-1.865E+01
58 - 59	-2.371E+01
59 - 60	-2.880E+01
60 - 61	-3.391E+01
61 - 62	-3.906E+01
62 - 63	-4.423E+01
63 - 64	-4.944E+01
64 - 65	-5.468E+01
65 - 66	-5.995E+01
66 - 67	-6.525E+01
67 - 68	-7.578E+01
68 - 69	-6.516E+01
69 - 70	-5.989E+01
70 - 71	-5.464E+01
71 - 72	-4.943E+01
72 - 73	-4.424E+01
73 - 74	-3.910E+01
74 - 75	-3.398E+01
75 - 76	-2.889E+01
76 - 77	-2.384E+01
77 - 78	-1.882E+01
78 - 79	-1.383E+01
79 - 80	-8.874E+00
80 - 81	-3.949E+00
81 - 82	9.442E-01
82 - 83	5.806E+00
83 - 84	1.064E+01
84 - 85	1.543E+01
85 - 86	2.020E+01
86 - 87	2.493E+01
87 - 88	2.963E+01
88 - 89	3.430E+01
89 - 90	3.894E+01
90 - 91	4.354E+01
91 - 92	4.811E+01
92 - 93	5.265E+01

93 - 94	5.716E+01
94 - 95	6.164E+01
95 - 96	6.608E+01
96 - 97	7.049E+01
97 - 98	7.487E+01
98 - 99	7.922E+01
99 - 100	8.354E+01
100 - 101	8.782E+01
101 - 102	9.207E+01
102 - 103	9.629E+01
103 - 104	1.005E+02
104 - 105	1.046E+02
105 - 106	1.129E+02
106 - 107	1.170E+02
107 - 108	1.210E+02
108 - 109	1.249E+02
109 - 110	1.288E+02
110 - 111	1.327E+02
111 - 112	1.365E+02
112 - 113	1.402E+02
113 - 114	1.439E+02
114 - 115	1.475E+02
115 - 116	1.509E+02
116 - 117	1.542E+02
117 - 118	1.573E+02
118 - 119	1.603E+02
119 - 120	1.632E+02
120 - 121	1.659E+02
121 - 122	1.685E+02
122 - 123	1.709E+02
123 - 124	1.732E+02
124 - 125	1.754E+02
125 - 126	1.775E+02
126 - 127	1.793E+02

Final shear flows Qs in cell-2

1 - 2	1.123E+02
2 - 3	1.070E+02
3 - 4	1.018E+02
4 - 5	9.665E+01
5 - 6	9.150E+01
6 - 7	8.639E+01

7 - 8	8.130E+01
8 - 9	7.624E+01
9 - 10	7.121E+01
10 - 11	6.622E+01
11 - 12	6.125E+01
12 - 13	5.632E+01
13 - 14	5.141E+01
14 - 15	4.653E+01
15 - 16	4.169E+01
16 - 17	3.687E+01
17 - 18	3.209E+01
18 - 19	2.733E+01
19 - 20	2.261E+01
20 - 21	1.791E+01
21 - 22	1.325E+01
22 - 23	8.614E+00
23 - 24	4.008E+00
24 - 25	-5.655E-01
25 - 26	-5.108E+00
26 - 27	-9.622E+00
27 - 28	-1.410E+01
28 - 29	-1.856E+01
29 - 30	-2.298E+01
30 - 31	-2.737E+01
31 - 32	-3.174E+01
32 - 33	-3.607E+01
33 - 34	-4.037E+01
34 - 35	-4.464E+01
35 - 36	-4.888E+01
36 - 37	-5.309E+01
37 - 38	-5.728E+01
38 - 39	-6.558E+01
39 - 40	-5.707E+01
40 - 41	-5.279E+01
41 - 42	-4.847E+01
42 - 43	-4.413E+01
43 - 44	-3.976E+01
44 - 45	-3.536E+01
45 - 46	-3.094E+01
46 - 47	-2.648E+01
47 - 48	-2.200E+01
48 - 49	-1.749E+01

49 - 50	-1.295E+01
50 - 51	-8.377E+00
51 - 52	-3.780E+00
52 - 53	8.473E-01
53 - 54	5.501E+00
54 - 55	1.018E+01
55 - 56	1.489E+01
56 - 57	1.963E+01
57 - 58	2.440E+01
58 - 59	2.920E+01
59 - 60	3.403E+01
60 - 61	3.888E+01
61 - 62	4.376E+01
62 - 63	4.867E+01
63 - 64	5.361E+01
64 - 65	5.858E+01
65 - 66	6.358E+01
66 - 67	6.861E+01
67 - 68	7.366E+01
68 - 69	7.874E+01
69 - 70	8.385E+01
70 - 71	8.899E+01
71 - 72	9.416E+01
72 - 73	9.935E+01
73 - 74	1.046E+02
74 - 75	1.098E+02
75 - 76	1.151E+02
76 - 77	1.123E+02

Final shear flows Qs in cell-3

1 - 2	3.118E+01
2 - 3	2.707E+01
3 - 4	2.301E+01
4 - 5	1.900E+01
5 - 6	1.503E+01
6 - 7	1.111E+01
7 - 8	7.234E+00
8 - 9	3.405E+00
9 - 10	-3.775E-01
10 - 11	-4.116E+00
11 - 12	-7.808E+00
12 - 13	-1.145E+01

13 - 14	-1.505E+01
14 - 15	-1.861E+01
15 - 16	-2.212E+01
16 - 17	-2.558E+01
17 - 18	-2.899E+01
18 - 19	-3.236E+01
19 - 20	-3.569E+01
20 - 21	-3.896E+01
21 - 22	-4.220E+01
22 - 23	-4.538E+01
23 - 24	-4.852E+01
24 - 25	-5.162E+01
25 - 26	-5.466E+01
26 - 27	-6.067E+01
27 - 28	-5.437E+01
28 - 29	-5.118E+01
29 - 30	-4.794E+01
30 - 31	-4.466E+01
31 - 32	-4.133E+01
32 - 33	-3.797E+01
33 - 34	-3.455E+01
34 - 35	-3.109E+01
35 - 36	-2.759E+01
36 - 37	-2.404E+01
37 - 38	-2.045E+01
38 - 39	-1.682E+01
39 - 40	-1.314E+01
40 - 41	-9.413E+00
41 - 42	-5.643E+00
42 - 43	-1.831E+00
43 - 44	2.026E+00
44 - 45	5.928E+00
45 - 46	9.872E+00
46 - 47	1.386E+01
47 - 48	1.790E+01
48 - 49	2.198E+01
49 - 50	2.610E+01
50 - 51	3.026E+01
51 - 52	3.448E+01
52 - 53	3.118E+01

Final shear flows Qs in mid-wall-1 and 2

-1.881E+02 -9.676E+01

----- Shear Flows and Shear Stress in Skins of the 3-cell box -----

Skin Panel No.	Shear Flows (N/mm)	Shear Stress (MPa)
1 - 2	1.872E+02	1.872E+01
2 - 3	1.885E+02	1.885E+01
3 - 4	1.893E+02	1.893E+01
4 - 5	1.897E+02	1.897E+01
5 - 6	1.895E+02	1.895E+01
6 - 7	1.889E+02	1.889E+01
7 - 8	1.878E+02	1.878E+01
8 - 9	1.863E+02	1.863E+01
9 - 10	1.843E+02	1.843E+01
10 - 11	1.818E+02	1.818E+01
11 - 12	1.792E+02	1.792E+01
12 - 13	1.764E+02	1.764E+01
13 - 14	1.736E+02	1.736E+01
14 - 15	1.707E+02	1.707E+01
15 - 16	1.676E+02	1.676E+01
16 - 17	1.645E+02	1.645E+01
17 - 18	1.612E+02	1.612E+01
18 - 19	1.578E+02	1.578E+01
19 - 20	1.543E+02	1.543E+01
20 - 21	1.507E+02	1.507E+01
21 - 22	1.470E+02	1.470E+01
22 - 23	1.432E+02	1.432E+01
23 - 24	1.393E+02	1.393E+01
24 - 25	1.353E+02	1.353E+01
25 - 26	1.312E+02	1.312E+01
26 - 27	1.271E+02	1.271E+01
27 - 28	1.230E+02	1.230E+01
28 - 29	1.147E+02	1.147E+01
29 - 30	1.106E+02	1.106E+01
30 - 31	1.064E+02	1.064E+01
31 - 32	1.021E+02	1.021E+01
32 - 33	9.786E+01	9.786E+00
33 - 34	9.356E+01	9.356E+00
34 - 35	8.924E+01	8.924E+00
35 - 36	8.488E+01	8.488E+00
36 - 37	8.049E+01	8.049E+00

37 - 38	7.607E+01	7.607E+00
38 - 39	7.163E+01	7.163E+00
39 - 40	6.715E+01	6.715E+00
40 - 41	6.264E+01	6.264E+00
41 - 42	5.810E+01	5.810E+00
42 - 43	5.353E+01	5.353E+00
43 - 44	4.893E+01	4.893E+00
44 - 45	4.430E+01	4.430E+00
45 - 46	3.964E+01	3.964E+00
46 - 47	3.495E+01	3.495E+00
47 - 48	3.023E+01	3.023E+00
48 - 49	2.548E+01	2.548E+00
49 - 50	2.070E+01	2.070E+00
50 - 51	1.588E+01	1.588E+00
51 - 52	1.104E+01	1.104E+00
52 - 53	6.169E+00	6.169E-01
53 - 54	1.265E+00	1.265E-01
54 - 55	-3.669E+00	-3.669E-01
55 - 56	-8.633E+00	-8.633E-01
56 - 57	-1.363E+01	-1.363E+00
57 - 58	-1.865E+01	-1.865E+00
58 - 59	-2.371E+01	-2.371E+00
59 - 60	-2.880E+01	-2.880E+00
60 - 61	-3.391E+01	-3.391E+00
61 - 62	-3.906E+01	-3.906E+00
62 - 63	-4.423E+01	-4.423E+00
63 - 64	-4.944E+01	-4.944E+00
64 - 65	-5.468E+01	-5.468E+00
65 - 66	-5.995E+01	-5.995E+00
66 - 67	-6.525E+01	-6.525E+00
67 - 68	1.123E+02	1.123E+01
68 - 69	1.070E+02	1.070E+01
69 - 70	1.018E+02	1.018E+01
70 - 71	9.665E+01	9.665E+00
71 - 72	9.150E+01	9.150E+00
72 - 73	8.639E+01	8.639E+00
73 - 74	8.130E+01	8.130E+00
74 - 75	7.624E+01	7.624E+00
75 - 76	7.121E+01	7.121E+00
76 - 77	6.622E+01	6.622E+00
77 - 78	6.125E+01	6.125E+00
78 - 79	5.632E+01	5.632E+00

79 - 80	5.141E+01	5.141E+00
80 - 81	4.653E+01	4.653E+00
81 - 82	4.169E+01	4.169E+00
82 - 83	3.687E+01	3.687E+00
83 - 84	3.209E+01	3.209E+00
84 - 85	2.733E+01	2.733E+00
85 - 86	2.261E+01	2.261E+00
86 - 87	1.791E+01	1.791E+00
87 - 88	1.325E+01	1.325E+00
88 - 89	8.614E+00	8.614E-01
89 - 90	4.008E+00	4.008E-01
90 - 91	-5.655E-01	-5.655E-02
91 - 92	-5.108E+00	-5.108E-01
92 - 93	-9.622E+00	-9.622E-01
93 - 94	-1.410E+01	-1.410E+00
94 - 95	-1.856E+01	-1.856E+00
95 - 96	-2.298E+01	-2.298E+00
96 - 97	-2.737E+01	-2.737E+00
97 - 98	-3.174E+01	-3.174E+00
98 - 99	-3.607E+01	-3.607E+00
99 - 100	-4.037E+01	-4.037E+00
100 - 101	-4.464E+01	-4.464E+00
101 - 102	-4.888E+01	-4.888E+00
102 - 103	-5.309E+01	-5.309E+00
103 - 104	-5.728E+01	-5.728E+00
104 - 105	3.118E+01	3.118E+00
105 - 106	2.707E+01	2.707E+00
106 - 107	2.301E+01	2.301E+00
107 - 108	1.900E+01	1.900E+00
108 - 109	1.503E+01	1.503E+00
109 - 110	1.111E+01	1.111E+00
110 - 111	7.234E+00	7.234E-01
111 - 112	3.405E+00	3.405E-01
112 - 113	-3.775E-01	-3.775E-02
113 - 114	-4.116E+00	-4.116E-01
114 - 115	-7.808E+00	-7.808E-01
115 - 116	-1.145E+01	-1.145E+00
116 - 117	-1.505E+01	-1.505E+00
117 - 118	-1.861E+01	-1.861E+00
118 - 119	-2.212E+01	-2.212E+00
119 - 120	-2.558E+01	-2.558E+00
120 - 121	-2.899E+01	-2.899E+00

121 - 122	-3.236E+01	-3.236E+00
122 - 123	-3.569E+01	-3.569E+00
123 - 124	-3.896E+01	-3.896E+00
124 - 125	-4.220E+01	-4.220E+00
125 - 126	-4.538E+01	-4.538E+00
126 - 127	-4.852E+01	-4.852E+00
127 - 128	-5.162E+01	-5.162E+00
128 - 129	-5.466E+01	-5.466E+00
129 - 130	-6.067E+01	-6.067E+00
130 - 131	-5.437E+01	-5.437E+00
131 - 132	-5.118E+01	-5.118E+00
132 - 133	-4.794E+01	-4.794E+00
133 - 134	-4.466E+01	-4.466E+00
134 - 135	-4.133E+01	-4.133E+00
135 - 136	-3.797E+01	-3.797E+00
136 - 137	-3.455E+01	-3.455E+00
137 - 138	-3.109E+01	-3.109E+00
138 - 139	-2.759E+01	-2.759E+00
139 - 140	-2.404E+01	-2.404E+00
140 - 141	-2.045E+01	-2.045E+00
141 - 142	-1.682E+01	-1.682E+00
142 - 143	-1.314E+01	-1.314E+00
143 - 144	-9.413E+00	-9.413E-01
144 - 145	-5.643E+00	-5.643E-01
145 - 146	-1.831E+00	-1.831E-01
146 - 147	2.026E+00	2.026E-01
147 - 148	5.928E+00	5.928E-01
148 - 149	9.872E+00	9.872E-01
149 - 150	1.386E+01	1.386E+00
150 - 151	1.790E+01	1.790E+00
151 - 152	2.198E+01	2.198E+00
152 - 153	2.610E+01	2.610E+00
153 - 154	3.026E+01	3.026E+00
154 - 155	3.448E+01	3.448E+00
155 - 156	-5.707E+01	-5.707E+00
156 - 157	-5.279E+01	-5.279E+00
157 - 158	-4.847E+01	-4.847E+00
158 - 159	-4.413E+01	-4.413E+00
159 - 160	-3.976E+01	-3.976E+00
160 - 161	-3.536E+01	-3.536E+00
161 - 162	-3.094E+01	-3.094E+00
162 - 163	-2.648E+01	-2.648E+00

163 - 164	-2.200E+01	-2.200E+00
164 - 165	-1.749E+01	-1.749E+00
165 - 166	-1.295E+01	-1.295E+00
166 - 167	-8.377E+00	-8.377E-01
167 - 168	-3.780E+00	-3.780E-01
168 - 169	8.473E-01	8.473E-02
169 - 170	5.501E+00	5.501E-01
170 - 171	1.018E+01	1.018E+00
171 - 172	1.489E+01	1.489E+00
172 - 173	1.963E+01	1.963E+00
173 - 174	2.440E+01	2.440E+00
174 - 175	2.920E+01	2.920E+00
175 - 176	3.403E+01	3.403E+00
176 - 177	3.888E+01	3.888E+00
177 - 178	4.376E+01	4.376E+00
178 - 179	4.867E+01	4.867E+00
179 - 180	5.361E+01	5.361E+00
180 - 181	5.858E+01	5.858E+00
181 - 182	6.358E+01	6.358E+00
182 - 183	6.861E+01	6.861E+00
183 - 184	7.366E+01	7.366E+00
184 - 185	7.874E+01	7.874E+00
185 - 186	8.385E+01	8.385E+00
186 - 187	8.899E+01	8.899E+00
187 - 188	9.416E+01	9.416E+00
188 - 189	9.935E+01	9.935E+00
189 - 190	1.046E+02	1.046E+01
190 - 191	1.098E+02	1.098E+01
191 - 192	1.151E+02	1.151E+01
192 - 193	-6.516E+01	-6.516E+00
193 - 194	-5.989E+01	-5.989E+00
194 - 195	-5.464E+01	-5.464E+00
195 - 196	-4.943E+01	-4.943E+00
196 - 197	-4.424E+01	-4.424E+00
197 - 198	-3.910E+01	-3.910E+00
198 - 199	-3.398E+01	-3.398E+00
199 - 200	-2.889E+01	-2.889E+00
200 - 201	-2.384E+01	-2.384E+00
201 - 202	-1.882E+01	-1.882E+00
202 - 203	-1.383E+01	-1.383E+00
203 - 204	-8.874E+00	-8.874E-01
204 - 205	-3.949E+00	-3.949E-01

205 - 206	9.442E-01	9.442E-02
206 - 207	5.806E+00	5.806E-01
207 - 208	1.064E+01	1.064E+00
208 - 209	1.543E+01	1.543E+00
209 - 210	2.020E+01	2.020E+00
210 - 211	2.493E+01	2.493E+00
211 - 212	2.963E+01	2.963E+00
212 - 213	3.430E+01	3.430E+00
213 - 214	3.894E+01	3.894E+00
214 - 215	4.354E+01	4.354E+00
215 - 216	4.811E+01	4.811E+00
216 - 217	5.265E+01	5.265E+00
217 - 218	5.716E+01	5.716E+00
218 - 219	6.164E+01	6.164E+00
219 - 220	6.608E+01	6.608E+00
220 - 221	7.049E+01	7.049E+00
221 - 222	7.487E+01	7.487E+00
222 - 223	7.922E+01	7.922E+00
223 - 224	8.354E+01	8.354E+00
224 - 225	8.782E+01	8.782E+00
225 - 226	9.207E+01	9.207E+00
226 - 227	9.629E+01	9.629E+00
227 - 228	1.005E+02	1.005E+01
228 - 229	1.046E+02	1.046E+01
229 - 230	1.129E+02	1.129E+01
230 - 231	1.170E+02	1.170E+01
231 - 232	1.210E+02	1.210E+01
232 - 233	1.249E+02	1.249E+01
233 - 234	1.288E+02	1.288E+01
234 - 235	1.327E+02	1.327E+01
235 - 236	1.365E+02	1.365E+01
236 - 237	1.402E+02	1.402E+01
237 - 238	1.439E+02	1.439E+01
238 - 239	1.475E+02	1.475E+01
239 - 240	1.509E+02	1.509E+01
240 - 241	1.542E+02	1.542E+01
241 - 242	1.573E+02	1.573E+01
242 - 243	1.603E+02	1.603E+01
243 - 244	1.632E+02	1.632E+01
244 - 245	1.659E+02	1.659E+01
245 - 246	1.685E+02	1.685E+01
246 - 247	1.709E+02	1.709E+01

247 - 248	1.732E+02	1.732E+01
248 - 249	1.754E+02	1.754E+01
249 - 250	1.775E+02	1.775E+01
250 - 1	1.793E+02	1.793E+01

Mid-Wall 67 - 192	-1.881E+02	-1.881E+01
Mid-Wall 104 - 155	-9.676E+01	-9.676E+00

C-S Area at root section = 4.872E+05 mm^2
C-S Area at tip section = 4.872E+05 mm^2
Reduced C-S Area at tip = 4.872E+05 mm^2
Skin-Stringer Volume (upper bound) = 4.872E+08 mm^3
Skin-Stringer Volume (lower bound) = 4.872E+08 mm^3

---------- End of Result Output ----------

APPENDIX F

Table F.1 Determination of β for stiffened panel with mid bay crack

h/b = 1/6 = 0.166667						h/b = 1/12 = 0.083333						h/b = 0.1558282209	
0.111		s = 0.316		0.428		0.111		s = 0.316		0.428		s = 0.316	
a/b	K1/K0	a/b	K1/K0	a/b	K1/K0	a/b	K1/K0	a/b	K1/K0	a/b	K1/K0	a/b	K1/K0
0.02	0.998	0.02	0.998964	0.02	1.000	0.02	0.995	0.02	0.9948092	0.02	0.995	0.02	0.9984237
0.06	0.998	0.06	0.9978	0.06	0.998	0.06	0.995	0.06	0.992414	0.06	0.991	0.06	0.9970995
0.11	0.998	0.11	0.9954073	0.11	0.994	0.11	0.993	0.11	0.9884834	0.11	0.986	0.11	0.9945067
0.15	0.996	0.15	0.9901427	0.15	0.987	0.15	0.990	0.15	0.9829343	0.15	0.979	0.15	0.9892052
0.18	0.992	0.18	0.9849363	0.18	0.981	0.18	0.987	0.18	0.9772303	0.18	0.972	0.18	0.983934
0.21	0.989	0.21	0.9814057	0.21	0.978	0.21	0.984	0.21	0.9718912	0.21	0.965	0.21	0.9801683
0.25	0.985	0.25	0.974278	0.25	0.968	0.25	0.980	0.25	0.9657687	0.25	0.958	0.25	0.9731713
0.28	0.981	0.28	0.964441	0.28	0.955	0.28	0.975	0.28	0.9582502	0.28	0.949	0.28	0.9636358
0.31	0.975	0.31	0.9586863	0.31	0.950	0.31	0.968	0.31	0.9476022	0.31	0.937	0.31	0.9572446
0.33	0.970	0.33	0.9439333	0.33	0.930	0.33	0.961	0.33	0.9368866	0.33	0.924	0.33	0.9430168
0.35	0.964	0.35	0.9356871	0.35	0.920	0.35	0.951	0.35	0.9234376	0.35	0.908	0.35	0.9340939
0.38	0.951	0.38	0.9204645	0.38	0.904	0.38	0.942	0.38	0.9067292	0.38	0.887	0.38	0.9186781
0.40	0.942	0.40	0.9043214	0.40	0.884	0.40	0.932	0.40	0.8872254	0.40	0.863	0.40	0.9020979
0.41	0.935	0.41	0.8909959	0.41	0.867	0.41	0.921	0.41	0.8730684	0.41	0.847	0.41	0.8886642
0.44	0.919	0.44	0.869744	0.44	0.843	0.44	0.904	0.44	0.8270276	0.44	0.785	0.44	0.8641882
0.44	0.917	0.44	0.8558114	0.44	0.823	0.44	0.898	0.44	0.8191962	0.44	0.776	0.44	0.8510491
0.46	0.900	0.46	0.8368186	0.46	0.802	0.46	0.865	0.46	0.7839091	0.46	0.740	0.46	0.8299371
0.47	0.893	0.47	0.8166312	0.47	0.775	0.47	0.851	0.47	0.7581858	0.47	0.707	0.47	0.8090297
0.48	0.869	0.48	0.7923647	0.48	0.751	0.48	0.799	0.48	0.6892061	0.48	0.629	0.48	0.7789478

h/b = 1/6 = 0.166667						h/b = 1/12 = 0.083333						h/b = 0.1558282209	
0.111		s = 0.316		0.428		0.111		s = 0.316		0.428		s = 0.316	
a/b	K1/K0	a/b	K1/K0	a/b	K1/K0	a/b	K1/K0	a/b	K1/K0	a/b	K1/K0	a/b	K1/K0
0.49	0.856	0.49	0.7760664	0.49	0.732	0.49	0.769	0.49	0.662653	0.49	0.604	0.49	0.7613157
0.50	0.841	0.50	0.7540558	0.50	0.707	0.50	0.745	0.50	0.6212646	0.50	0.554	0.50	0.7367848
0.51	0.827	0.51	0.7372143	0.51	0.688	0.51	0.711	0.51	0.5755736	0.51	0.502	0.51	0.7161911
0.52	0.794	0.52	0.6945571	0.52	0.640	0.52	0.651	0.52	0.5225539	0.52	0.452	0.52	0.6721861
0.54	0.777	0.54	0.674	0.54	0.618	0.54	0.614	0.54	0.4843221	0.54	0.413	0.54	0.6493302
0.55	0.768	0.55	0.6459081	0.55	0.579	0.55	0.596	0.55	0.4588379	0.55	0.384	0.55	0.6215775
0.57	0.751	0.57	0.6255013	0.57	0.557	0.57	0.573	0.57	0.4281482	0.57	0.349	0.57	0.5998333
0.58	0.740	0.58	0.606159	0.58	0.533	0.58	0.564	0.58	0.4228247	0.58	0.346	0.58	0.5823143
0.59	0.733	0.59	0.5883596	0.59	0.509	0.59	0.559	0.59	0.4207812	0.59	0.346	0.59	0.5665641
0.62	0.719	0.62	0.5713089	0.62	0.491	0.62	0.556	0.62	0.4271862	0.62	0.357	0.62	0.5525641
0.64	0.709	0.64	0.559717	0.64	0.478	0.64	0.559	0.64	0.4373362	0.64	0.371	0.64	0.5438
0.68	0.697	0.68	0.5540025	0.68	0.476	0.68	0.566	0.68	0.4516796	0.68	0.389	0.68	0.5406943
0.72	0.692	0.72	0.5536566	0.72	0.478	0.72	0.574	0.72	0.4649197	0.72	0.405	0.72	0.5421154
0.76	0.690	0.76	0.5577189	0.76	0.485	0.76	0.582	0.76	0.4776716	0.76	0.420	0.76	0.5473079
0.80	0.688	0.80	0.56403	0.80	0.496	0.80	0.592	0.80	0.490036	0.80	0.434	0.80	0.5544062
0.84	0.688	0.84	0.5723722	0.84	0.509	0.84	0.598	0.84	0.5017969	0.84	0.449	0.84	0.5631931
0.89	0.692	0.89	0.5809198	0.89	0.520	0.89	0.608	0.89	0.5122594	0.89	0.460	0.89	0.5719897
0.93	0.694	0.93	0.5851396	0.93	0.526	0.93	0.612	0.93	0.5204446	0.93	0.470	0.93	0.5767253
0.96	0.695	0.96	0.5916175	0.96	0.535	0.96	0.617	0.96	0.5273271	0.96	0.478	0.96	0.5832558
1.00	0.697	1.00	0.594675	1.00	0.539	1.00	0.622	1.00	0.5343018	1.00	0.486	1.00	0.5868228
1.05	0.701	1.05	0.5972734	1.05	0.541	1.05	0.627	1.05	0.5424871	1.05	0.496	1.05	0.5901478
1.09	0.703	1.09	0.601464	1.09	0.546	1.09	0.632	1.09	0.5493289	1.09	0.504	1.09	0.5946833

h/b = 1/6 = 0.166667						h/b = 1/12 = 0.083333						h/b = 0.1558282209	
0.111		s = 0.316		0.428		0.111		s = 0.316		0.428		s = 0.316	
a/b	K1/K0	a/b	K1/K0	a/b	K1/K0	a/b	K1/K0	a/b	K1/K0	a/b	K1/K0	a/b	K1/K0
1.13	0.704	1.13	0.6031686	1.13	0.548	1.13	0.636	1.13	0.553518	1.13	0.508	1.13	0.596711
1.16	0.706	1.16	0.6025739	1.16	0.546	1.16	0.636	1.16	0.555494	1.16	0.511	1.16	0.5964506
1.21	0.706	1.21	0.6026559	1.21	0.546	1.21	0.640	1.21	0.5583536	1.21	0.514	1.21	0.5968939
1.25	0.703	1.25	0.5979073	1.25	0.541	1.25	0.641	1.25	0.5588309	1.25	0.514	1.25	0.5928249
1.29	0.702	1.29	0.5951612	1.29	0.537	1.29	0.642	1.29	0.558273	1.29	0.513	1.29	0.5903635
1.32	0.697	1.32	0.5876215	1.32	0.528	1.32	0.640	1.32	0.5561876	1.32	0.510	1.32	0.5835332
1.36	0.693	1.36	0.5799423	1.36	0.518	1.36	0.635	1.36	0.5505552	1.36	0.504	1.36	0.5761202
1.40	0.685	1.40	0.5700234	1.40	0.507	1.40	0.629	1.40	0.5363385	1.40	0.486	1.40	0.5656423
1.43	0.676	1.43	0.5563028	1.43	0.491	1.43	0.614	1.43	0.5151628	1.43	0.461	1.43	0.5509521
1.46	0.660	1.46	0.5411508	1.46	0.476	1.46	0.588	1.46	0.4815899	1.46	0.423	1.46	0.5334042
1.48	0.645	1.48	0.5226127	1.48	0.456	1.48	0.552	1.48	0.4389191	1.48	0.377	1.48	0.5117274
1.50	0.629	1.50	0.5002445	1.50	0.430	1.50	0.507	1.50	0.3710048	1.50	0.296	1.50	0.4834354
1.50	0.622	1.50	0.4833574	1.50	0.408	1.50	0.489	1.50	0.3563085	1.50	0.284	1.50	0.4668333
1.52	0.601	1.52	0.4628462	1.52	0.388	1.52	0.452	1.52	0.3184198	1.52	0.246	1.52	0.4440619
1.53	0.593	1.53	0.4457125	1.53	0.365	1.53	0.436	1.53	0.300761	1.53	0.227	1.53	0.4268599
1.55	0.570	1.55	0.4256756	1.55	0.347	1.55	0.398	1.55	0.2711545	1.55	0.202	1.55	0.4055784
1.57	0.556	1.57	0.4101208	1.57	0.330	1.57	0.383	1.57	0.2586033	1.57	0.191	1.57	0.3904143
1.61	0.543	1.61	0.3958176	1.61	0.316	1.61	0.371	1.61	0.2543729	1.61	0.191	1.61	0.3774211
1.64	0.532	1.64	0.3813051	1.64	0.299	1.64	0.371	1.64	0.2591073	1.64	0.198	1.64	0.3654119
1.66	0.527	1.66	0.3770858	1.66	0.295	1.66	0.377	1.66	0.2696578	1.66	0.211	1.66	0.3631136
1.70	0.522	1.70	0.3754959	1.70	0.295	1.70	0.386	1.70	0.286527	1.70	0.232	1.70	0.3639245
1.74	0.522	1.74	0.3790527	1.74	0.301	1.74	0.402	1.74	0.3056554	1.74	0.253	1.74	0.3695065

h/b = 1/6 = 0.166667						h/b = 1/12 = 0.083333						h/b = 0.1558282209	
0.111		s = 0.316		0.428		0.111		s = 0.316		0.428		s = 0.316	
a/b	K1/K0	a/b	K1/K0	a/b	K1/K0	a/b	K1/K0	a/b	K1/K0	a/b	K1/K0	a/b	K1/K0
1.78	0.522	1.78	0.387395	1.78	0.314	1.78	0.411	1.78	0.3208667	1.78	0.272	1.78	0.3787422
1.82	0.522	1.82	0.3933445	1.82	0.323	1.82	0.421	1.82	0.3317841	1.82	0.283	1.82	0.3853379
1.84	0.523	1.84	0.4007821	1.84	0.334	1.84	0.428	1.84	0.338316	1.84	0.290	1.84	0.3926577
1.88	0.525	1.88	0.4050659	1.88	0.340	1.88	0.435	1.88	0.3490069	1.88	0.302	1.88	0.3977748
1.92	0.532	1.92	0.4148438	1.92	0.351	1.92	0.444	1.92	0.3578025	1.92	0.311	1.92	0.407425
1.95	0.536	1.95	0.4232143	1.95	0.362	1.95	0.449	1.95	0.3652089	1.95	0.319	1.95	0.4156701
2.00	0.539	2.00	0.426735	2.00	0.365	2.00	0.459	2.00	0.3761296	2.00	0.331	2.00	0.4201532
2.04	0.544	2.04	0.4333463	2.04	0.373	2.04	0.467	2.04	0.3828315	2.04	0.337	2.04	0.4267763
2.07	0.548	2.07	0.4371726	2.07	0.377	2.07	0.472	2.07	0.3887083	2.07	0.343	2.07	0.4308692
2.10	0.552	2.10	0.4430858	2.10	0.384	2.10	0.477	2.10	0.3954034	2.10	0.351	2.10	0.4368842
2.14	0.554	2.14	0.4449973	2.14	0.386	2.14	0.482	2.14	0.4009459	2.14	0.357	2.14	0.4392679
2.18	0.558	2.18	0.4501774	2.18	0.391	2.18	0.485	2.18	0.4048458	2.18	0.361	2.18	0.4442815
2.22	0.559	2.22	0.4504858	2.22	0.391	2.22	0.488	2.22	0.4084375	2.22	0.365	2.22	0.4450169
2.25	0.559	2.25	0.4516233	2.25	0.393	2.25	0.490	2.25	0.4108748	2.25	0.368	2.25	0.4463235
2.30	0.555	2.30	0.4480145	2.30	0.389	2.30	0.490	2.30	0.4108748	2.30	0.368	2.30	0.4431841
2.33	0.555	2.33	0.4443931	2.33	0.384	2.33	0.490	2.33	0.410331	2.33	0.367	2.33	0.4399629
2.37	0.555	2.37	0.4408363	2.37	0.378	2.37	0.485	2.37	0.4059461	2.37	0.363	2.37	0.4362984
2.41	0.540	2.41	0.430661	2.41	0.371	2.41	0.480	2.41	0.3948712	2.41	0.349	2.41	0.4260061
2.44	0.533	2.44	0.4199003	2.44	0.358	2.44	0.465	2.44	0.3770555	2.44	0.329	2.44	0.4143279
2.48	0.521	2.48	0.4084092	2.48	0.347	2.48	0.431	2.48	0.337283	2.48	0.286	2.48	0.3991584
2.50	0.509	2.50	0.3923435	2.50	0.329	2.50	0.392	2.50	0.2856671	2.50	0.228	2.50	0.3784691
2.52	0.497	2.52	0.376289	2.52	0.310	2.52	0.368	2.52	0.2566665	2.52	0.196	2.52	0.3607307

h/b = 1/6 = 0.166667						h/b = 1/12 = 0.083333						h/b = 0.1558282209	
0.111		s = 0.316		0.428		0.111		s = 0.316		0.428		s = 0.316	
a/b	K1/K0	a/b	K1/K0	a/b	K1/K0	a/b	K1/K0	a/b	K1/K0	a/b	K1/K0	a/b	K1/K0
2.52	0.494	2.52	0.3728404	2.52	0.306	2.52	0.361	2.52	0.2484891	2.52	0.187	2.52	0.3566671
2.54	0.486	2.54	0.3581116	2.54	0.288	2.54	0.343	2.54	0.2202169	2.54	0.153	2.54	0.3401768
2.55	0.478	2.55	0.3409959	2.55	0.266	2.55	0.331	2.55	0.2106149	2.55	0.145	2.55	0.3240383
2.57	0.464	2.57	0.3227222	2.57	0.246	2.57	0.308	2.57	0.196237	2.57	0.135	2.57	0.3062713
2.60	0.443	2.60	0.30586	2.60	0.231	2.60	0.289	2.60	0.1876426	2.60	0.132	2.60	0.2904845
2.63	0.431	2.63	0.2943666	2.63	0.220	2.63	0.287	2.63	0.1906337	2.63	0.138	2.63	0.2808749
2.67	0.418	2.67	0.2886639	2.67	0.218	2.67	0.298	2.67	0.2037245	2.67	0.152	2.67	0.2776166
2.70	0.417	2.70	0.2918659	2.70	0.224	2.70	0.304	2.70	0.2137259	2.70	0.164	2.70	0.2817029
2.74	0.417	2.74	0.294194	2.74	0.227	2.74	0.315	2.74	0.2249331	2.74	0.176	2.74	0.2851858
2.76	0.418	2.76	0.2993863	2.76	0.235	2.76	0.323	2.76	0.2339132	2.76	0.185	2.76	0.2908708
2.80	0.421	2.80	0.3039259	2.80	0.240	2.80	0.332	2.80	0.2444233	2.80	0.197	2.80	0.2961869
2.82	0.423	2.82	0.30945	2.82	0.247	2.82	0.338	2.82	0.2518965	2.82	0.205	2.82	0.3019645
2.86	0.426	2.86	0.3153577	2.86	0.255	2.86	0.348	2.86	0.2620162	2.86	0.215	2.86	0.3084201
2.91	0.429	2.91	0.3212198	2.91	0.262	2.91	0.357	2.91	0.2752135	2.91	0.230	2.91	0.3152361
2.95	0.438	2.95	0.3302241	2.95	0.271	2.95	0.364	2.95	0.2844164	2.95	0.241	2.95	0.3242663
2.98	0.443	2.98	0.3369328	2.98	0.279	2.98	0.368	2.98	0.289782	2.98	0.247	2.98	0.3308003
3.00	0.447	3.00	0.3404432	3.00	0.283	3.00	0.372	3.00	0.2988172	3.00	0.259	3.00	0.3350293

Table F.2 Determination of β for cracked panel with intact stringer

h/b = 1/6 = 0.166667						h/b = 1/12 = 0.083333						h/b = 0.1558	
s = 0.111		s = 0.316		s = 0.428		s = 0.111		s = 0.316		s = 0.428		s = 0.316	
a/b	K1/K0	a/b	K1/K0	a/b	K1/K0	a/b	K1/K0	a/b	K1/K0	a/b	K1/K0	a/b	K1/K0
0	1	0	1	0	1	0	1	0	1	0	1	0	1
0.03	0.981	0.03	0.9661262	0.03	0.958	0.03	0.897	0.03	0.8633722	0.03	0.845	0.03	0.9527271
0.06	0.952	0.06	0.9261325	0.06	0.912	0.06	0.868	0.06	0.8259653	0.06	0.803	0.06	0.9130707
0.09	0.933	0.09	0.8922587	0.09	0.87	0.09	0.848	0.09	0.7943249	0.09	0.765	0.09	0.8794881
0.12	0.913	0.12	0.8690252	0.12	0.845	0.12	0.828	0.12	0.7743249	0.12	0.745	0.12	0.8566763
0.15	0.903	0.15	0.8519117	0.15	0.824	0.15	0.818	0.15	0.7643249	0.15	0.735	0.15	0.8404904
0.18	0.894	0.18	0.8370915	0.18	0.806	0.18	0.811	0.18	0.7534448	0.18	0.722	0.18	0.826184
0.21	0.886	0.21	0.8252114	0.21	0.792	0.21	0.81	0.21	0.749858	0.21	0.717	0.21	0.8153853
0.24	0.879	0.24	0.8149779	0.24	0.78	0.24	0.809	0.24	0.746918	0.24	0.713	0.24	0.8061029
0.27	0.872	0.27	0.8060379	0.27	0.77	0.27	0.803	0.27	0.7422114	0.27	0.709	0.27	0.7977149
0.3	0.867	0.3	0.8003912	0.3	0.764	0.3	0.8	0.3	0.739858	0.3	0.707	0.3	0.7924976
0.33	0.865	0.33	0.7977445	0.33	0.761	0.33	0.802	0.33	0.739918	0.33	0.706	0.33	0.7902039
0.36	0.862	0.36	0.7928044	0.36	0.755	0.36	0.803	0.36	0.7402713	0.36	0.706	0.36	0.7859541
0.39	0.859	0.39	0.7878644	0.39	0.749	0.39	0.803	0.39	0.7402713	0.39	0.706	0.39	0.7816582
0.42	0.856	0.42	0.783571	0.42	0.744	0.42	0.803	0.42	0.740918	0.42	0.707	0.42	0.778009
0.45	0.854	0.45	0.7809243	0.45	0.741	0.45	0.803	0.45	0.7402713	0.45	0.706	0.45	0.7756231
0.48	0.854	0.48	0.7796309	0.48	0.739	0.48	0.803	0.48	0.7396246	0.48	0.705	0.48	0.7744141
0.51	0.852	0.51	0.7782776	0.51	0.738	0.51	0.805	0.51	0.7416246	0.51	0.707	0.51	0.7734981
0.54	0.85	0.54	0.777571	0.54	0.738	0.54	0.804	0.54	0.7432114	0.54	0.71	0.54	0.7730905
0.57	0.85	0.57	0.777571	0.57	0.738	0.57	0.803	0.57	0.742858	0.57	0.71	0.57	0.7730444
0.6	0.849	0.6	0.7772177	0.6	0.738	0.6	0.803	0.6	0.742858	0.6	0.71	0.6	0.7727372
0.63	0.849	0.63	0.7778644	0.63	0.739	0.63	0.802	0.63	0.7425047	0.63	0.71	0.63	0.7732535

h/b = 1/6 = 0.166667						h/b = 1/12 = 0.083333						h/b = 0.1558	
s = 0.111		s = 0.316		s = 0.428		s = 0.111		s = 0.316		s = 0.428		s = 0.316	
a/b	K1/K0	a/b	K1/K0	a/b	K1/K0	a/b	K1/K0	a/b	K1/K0	a/b	K1/K0	a/b	K1/K0
0.66	0.849	0.66	0.7778644	0.66	0.739	0.66	0.801	0.66	0.7415047	0.66	0.709	0.66	0.7731231
0.69	0.849	0.69	0.776571	0.69	0.737	0.69	0.801	0.69	0.7402114	0.69	0.707	0.69	0.7718297
0.72	0.849	0.72	0.7739842	0.72	0.733	0.72	0.801	0.72	0.738918	0.72	0.705	0.72	0.7694116
0.75	0.847	0.75	0.7681041	0.75	0.725	0.75	0.802	0.75	0.7373312	0.75	0.702	0.75	0.7640913
0.78	0.842	0.78	0.7605174	0.78	0.716	0.78	0.798	0.78	0.7307445	0.78	0.694	0.78	0.756635
0.81	0.836	0.81	0.7499905	0.81	0.703	0.81	0.795	0.81	0.722571	0.81	0.683	0.81	0.746415
0.84	0.83	0.84	0.7381703	0.84	0.688	0.84	0.795	0.84	0.7128707	0.84	0.668	0.84	0.7348713
0.87	0.818	0.87	0.7242303	0.87	0.673	0.87	0.79	0.87	0.696877	0.87	0.646	0.87	0.7206634
0.9	0.808	0.9	0.7090568	0.9	0.655	0.9	0.782	0.9	0.6759432	0.9	0.618	0.9	0.7047388
0.93	0.795	0.93	0.6895899	0.93	0.632	0.93	0.763	0.93	0.6517697	0.93	0.591	0.93	0.6846582
0.96	0.767	0.96	0.6661167	0.96	0.611	0.96	0.735	0.96	0.6121293	0.96	0.545	0.96	0.6590768
0.99	0.742	0.99	0.6352965	0.99	0.577	0.99	0.685	0.99	0.5698896	0.99	0.507	0.99	0.6267675
1.02	0.709	1.02	0.6010032	1.02	0.542	1.02	0.598	1.02	0.4751293	1.02	0.408	1.02	0.5845892
1.05	0.681	1.05	0.5490757	1.05	0.477	1.05	0.534	1.05	0.4027224	1.05	0.331	1.05	0.5299912
1.08	0.662	1.08	0.5242555	1.08	0.449	1.08	0.506	1.08	0.3870095	1.08	0.322	1.08	0.5063586
1.11	0.654	1.11	0.5123754	1.11	0.435	1.11	0.495	1.11	0.3870032	1.11	0.328	1.11	0.4960269
1.14	0.648	1.14	0.5083155	1.14	0.432	1.14	0.505	1.14	0.3944164	1.14	0.334	1.14	0.493463
1.17	0.642	1.17	0.5068423	1.17	0.433	1.17	0.509	1.17	0.4042366	1.17	0.347	1.17	0.4934625
1.2	0.636	1.2	0.5066625	1.2	0.436	1.2	0.515	1.2	0.4147634	1.2	0.36	1.2	0.4946788
1.23	0.634	1.23	0.5072492	1.23	0.438	1.23	0.523	1.23	0.4253502	1.23	0.372	1.23	0.4965696
1.26	0.634	1.26	0.509836	1.26	0.442	1.26	0.532	1.26	0.4349968	1.26	0.382	1.26	0.5000769
1.29	0.633	1.29	0.5133628	1.29	0.448	1.29	0.54	1.29	0.4429968	1.29	0.39	1.29	0.5041871
1.32	0.634	1.32	0.5175962	1.32	0.454	1.32	0.548	1.32	0.4529369	1.32	0.401	1.32	0.5091646

h/b = 1/6 = 0.166667						h/b = 1/12 = 0.083333						h/b = 0.1558	
s = 0.111		s = 0.316		s = 0.428		s = 0.111		s = 0.316		s = 0.428		s = 0.316	
a/b	K1/K0	a/b	K1/K0	a/b	K1/K0	a/b	K1/K0	a/b	K1/K0	a/b	K1/K0	a/b	K1/K0
1.35	0.636	1.35	0.5208896	1.35	0.458	1.35	0.555	1.35	0.4625237	1.35	0.412	1.35	0.5132787
1.38	0.638	1.38	0.5254763	1.38	0.464	1.38	0.561	1.38	0.469817	1.38	0.42	1.38	0.5182184
1.41	0.64	1.41	0.5307098	1.41	0.471	1.41	0.564	1.41	0.4766972	1.41	0.429	1.41	0.5236665
1.44	0.641	1.44	0.5355899	1.44	0.478	1.44	0.569	1.44	0.4855773	1.44	0.44	1.44	0.5290683
1.47	0.644	1.47	0.5411767	1.47	0.485	1.47	0.578	1.47	0.4945773	1.47	0.449	1.47	0.5351001
1.5	0.649	1.5	0.5461767	1.5	0.49	1.5	0.584	1.5	0.4992839	1.5	0.453	1.5	0.5400618
1.53	0.653	1.53	0.5488833	1.53	0.492	1.53	0.586	1.53	0.5038707	1.53	0.459	1.53	0.5430136
1.56	0.654	1.56	0.55247	1.56	0.497	1.56	0.588	1.56	0.5091041	1.56	0.466	1.56	0.5468151
1.59	0.655	1.59	0.5567035	1.59	0.503	1.59	0.593	1.59	0.512164	1.59	0.468	1.59	0.5508955
1.62	0.657	1.62	0.5599968	1.62	0.507	1.62	0.599	1.62	0.518164	1.62	0.474	1.62	0.5545418
1.65	0.658	1.65	0.5603502	1.65	0.507	1.65	0.603	1.65	0.5228107	1.65	0.479	1.65	0.555455
1.68	0.657	1.68	0.5599968	1.68	0.507	1.68	0.606	1.68	0.5258107	1.68	0.482	1.68	0.555539
1.71	0.657	1.71	0.5606435	1.71	0.508	1.71	0.606	1.71	0.5277508	1.71	0.485	1.71	0.5563543
1.74	0.66	1.74	0.5623502	1.74	0.509	1.74	0.604	1.74	0.5270442	1.74	0.485	1.74	0.5577463
1.77	0.662	1.77	0.5630568	1.77	0.509	1.77	0.603	1.77	0.5273375	1.77	0.486	1.77	0.558399
1.8	0.66	1.8	0.5597634	1.8	0.505	1.8	0.604	1.8	0.5276909	1.8	0.486	1.8	0.5555811
1.83	0.657	1.83	0.5541767	1.83	0.498	1.83	0.605	1.83	0.5261041	1.83	0.483	1.83	0.550516
1.86	0.653	1.86	0.5475899	1.86	0.49	1.86	0.603	1.86	0.5228107	1.86	0.479	1.86	0.5443587
1.89	0.647	1.89	0.5396498	1.89	0.481	1.89	0.597	1.89	0.5155174	1.89	0.471	1.89	0.536503
1.92	0.639	1.92	0.5277697	1.92	0.467	1.92	0.59	1.92	0.5014038	1.92	0.453	1.92	0.5243316
1.95	0.627	1.95	0.5099495	1.95	0.446	1.95	0.572	1.95	0.4827571	1.95	0.434	1.95	0.5064036
1.98	0.61	1.98	0.4897161	1.98	0.424	1.98	0.551	1.98	0.4501167	1.98	0.395	1.98	0.4845523
2.01	0.587	2.01	0.4667161	2.01	0.401	2.01	0.496	2.01	0.3996435	2.01	0.347	2.01	0.4579698

h/b = 1/6 = 0.166667						h/b = 1/12 = 0.083333						h/b = 0.1558	
s = 0.111		s = 0.316		s = 0.428		s = 0.111		s = 0.316		s = 0.428		s = 0.316	
a/b	K1/K0	a/b	K1/K0	a/b	K1/K0	a/b	K1/K0	a/b	K1/K0	a/b	K1/K0	a/b	K1/K0
2.04	0.564	2.04	0.4359558	2.04	0.366	2.04	0.445	2.04	0.3512303	2.04	0.3	2.04	0.4249076
2.07	0.549	2.07	0.4216025	2.07	0.352	2.07	0.401	2.07	0.29947	2.07	0.244	2.07	0.4056764
2.1	0.54	2.1	0.4113091	2.1	0.341	2.1	0.393	2.1	0.2966435	2.1	0.244	2.1	0.3963568
2.13	0.533	2.13	0.4062492	2.13	0.337	2.13	0.4	2.13	0.3075237	2.13	0.257	2.13	0.3933754
2.16	0.525	2.16	0.4040694	2.16	0.338	2.16	0.404	2.16	0.3160505	2.16	0.268	2.16	0.3925917
2.19	0.518	2.19	0.4022429	2.19	0.339	2.19	0.411	2.19	0.3230505	2.19	0.275	2.19	0.3919162
2.22	0.517	2.22	0.4025363	2.22	0.34	2.22	0.417	2.22	0.3329306	2.22	0.287	2.22	0.3934597
2.25	0.518	2.25	0.4054763	2.25	0.344	2.25	0.423	2.25	0.3434574	2.25	0.3	2.25	0.3973891
2.28	0.519	2.28	0.4084164	2.28	0.348	2.28	0.43	2.28	0.3504574	2.28	0.307	2.28	0.4008586
2.31	0.519	2.31	0.4103565	2.31	0.351	2.31	0.435	2.31	0.3561041	2.31	0.313	2.31	0.403282
2.34	0.52	2.34	0.4126498	2.34	0.354	2.34	0.443	2.34	0.3647508	2.34	0.322	2.34	0.4064038
2.37	0.524	2.37	0.4172965	2.37	0.359	2.37	0.451	2.37	0.3727508	2.37	0.33	2.37	0.4114878
2.4	0.527	2.4	0.4209432	2.4	0.363	2.4	0.455	2.4	0.3786909	2.4	0.337	2.4	0.4154335
2.43	0.53	2.43	0.4245899	2.43	0.367	2.43	0.462	2.43	0.3856909	2.43	0.344	2.43	0.4195175
2.46	0.534	2.46	0.4292366	2.46	0.372	2.46	0.467	2.46	0.3926309	2.46	0.352	2.46	0.4244632
2.49	0.536	2.49	0.4331767	2.49	0.377	2.49	0.473	2.49	0.3999243	2.49	0.36	2.49	0.4288405
2.52	0.54	2.52	0.4378233	2.52	0.382	2.52	0.479	2.52	0.4072177	2.52	0.368	2.52	0.4338324
2.55	0.548	2.55	0.4438833	2.55	0.387	2.55	0.482	2.55	0.4121577	2.55	0.374	2.55	0.4397463
2.58	0.553	2.58	0.44953	2.58	0.393	2.58	0.486	2.58	0.4161577	2.58	0.378	2.58	0.4451782
2.61	0.555	2.61	0.45347	2.61	0.398	2.61	0.492	2.61	0.421511	2.61	0.383	2.61	0.4493026
2.64	0.558	2.64	0.4571167	2.64	0.402	2.64	0.498	2.64	0.4281577	2.64	0.39	2.64	0.4533405
2.67	0.563	2.67	0.4621167	2.67	0.407	2.67	0.499	2.67	0.4310978	2.67	0.394	2.67	0.4580719
2.7	0.567	2.7	0.4667634	2.7	0.412	2.7	0.501	2.7	0.4324511	2.7	0.395	2.7	0.4622891

h/b = 1/6 = 0.166667						h/b = 1/12 = 0.083333						h/b = 0.1558	
s = 0.111		s = 0.316		s = 0.428		s = 0.111		s = 0.316		s = 0.428		s = 0.316	
a/b	K1/K0	a/b	K1/K0	a/b	K1/K0	a/b	K1/K0	a/b	K1/K0	a/b	K1/K0	a/b	K1/K0
2.73	0.568	2.73	0.4684101	2.73	0.414	2.73	0.505	2.73	0.4338644	2.73	0.395	2.73	0.4639053
2.76	0.568	2.76	0.4684101	2.76	0.414	2.76	0.511	2.76	0.4366309	2.76	0.396	2.76	0.4642661
2.79	0.564	2.79	0.4669968	2.79	0.414	2.79	0.512	2.79	0.4382776	2.79	0.398	2.79	0.4632519
2.82	0.559	2.82	0.4632902	2.82	0.411	2.82	0.509	2.82	0.4372177	2.82	0.398	2.82	0.4598904
2.85	0.553	2.85	0.4572902	2.85	0.405	2.85	0.508	2.85	0.4368644	2.85	0.398	2.85	0.4546267
2.88	0.544	2.88	0.4495836	2.88	0.398	2.88	0.506	2.88	0.435511	2.88	0.397	2.88	0.4477485
2.91	0.539	2.91	0.4439369	2.91	0.392	2.91	0.502	2.91	0.4269842	2.91	0.386	2.91	0.4417263
2.94	0.531	2.94	0.4339968	2.94	0.381	2.94	0.487	2.94	0.4210379	2.94	0.385	2.94	0.432307
2.97	0.518	2.97	0.4177634	2.97	0.363	2.97	0.46	2.97	0.3901577	2.97	0.352	2.97	0.4141636
3	0.511	3	0.4023565	3	0.343	3	0.423	3	0.3344038	3	0.286	3	0.3934954